TARGETING CELL INVASION SIGNALING TO IMPEDE BREAST CANCER METASTASIS

Dissertation

for the award of the degree

"Doctor Rerum Naturalium"

of the Georg-August-Universität Göttingen

within the doctoral program *Molecular Medicine*

of the Georg-August University School of Science (GAUSS)

submitted by

Johanna W. Hellinger

from Jena

Göttingen 2019

Members of the Thesis Committee

Prof. Dr. Hubertus Jarry, Department of Clinical and Experimental Endocrinology; University Medical Center Göttingen (UMG)

Prof. Dr. Heidi Hahn, Department of Human Genetics, University Medical Center Göttingen (UMG)

Prof. Dr. Dieter Kube, Department of Hematology and Oncology, University Medical Center Göttingen (UMG)

Members of the Examination Board

Reviewer: Prof. Dr. Hubertus Jarry, Department of Clinical and Experimental Endocrinology; University Medical Center Göttingen (UMG)

Second Reviewer: Prof. Dr. Heidi Hahn, Department of Human Genetics, University Medical Center Göttingen (UMG)

Prof. Dr. Dieter Kube, Department of Hematology and Oncology, University Medical Center Göttingen (UMG)

Further members of the Examination Board

Prof. Dr. mult. Thomas Meyer, Department of Psychosomatic Medicine and Psychotherapy, University Medical Center Göttingen (UMG); and German Centre for Cardiovascular Research, University of Göttingen

Prof. Dr. Ralf Dressel, Institute of Cellular and Molecular Immunology, University Medical Center Göttingen (UMG)

Prof. Dr. Peter Burfeind, Institute of Human Genetics, University Medical Center Göttingen (UMG)

Date of the oral examination: 30.01.2020

AFFIDATIV

Here I declare that my doctoral thesis entitled “Targeting cell invasion signaling to impede breast cancer metastasis” has been written independently with no other sources and aids than quoted.

Göttingen, December 2019 _____

Johanna W. Hellinger

TABLE OF CONTENT

1. ABSTRACT

Breast cancer cell invasion is the initial step of the invasion-metastatic cascade, and approximately 90 % of all cancer-related deaths are due to currently incurable cancer metastasis (1). Unique features of tumor microenvironment such as growth factors, cytokines, and extracellular matrix (ECM) composition modify tumor behavior and drive tumor progression (2). Matricellular protein, e.g. Cysteine- Rich Angiogenic Inducer 61 (CYR61), Connective Tissue Growth Factor (CTGF), exert their function by altering cell-ECM interactions, extracellular signaling, and were reported to facilitate angiogenesis, tumor initiation, invasion and progression (3-7).

The tumor microenvironment (TME) is crucial for tumor progression, drug delivery, therapy outcome, and drug efficacy. Identifying drivers that modify TME thereby supporting tumor initiation, invasion and progression would be of benefit to design new treatment options for metastatic breast cancer.

We aimed to identify molecular mechanisms underlying reduced breast cancer invasiveness due to reduced CYR61 expression. Using 2D transwell invasion and 3D spheroid invasion assays to evaluate the effect of CYR61 and downstream targets on the invasiveness of breast cancer cell. Furthermore, we wanted to shed light on the unique interaction between breast cancer cells and osteosarcoma cells. Combining this co-culture model with mass spectrometry–based secretome analysis, we identified potential extracellular secreted drivers of breast cancer invasion. Additionally, we wanted to identify molecular mechanisms underlying reduced breast cancer invasiveness due to reduced CTGF expression by assessing cell–ECM adhesion and proteolytic activity of breast cancer cells and identifying possible treatment options targeting CTGF.

Reduced CYR61 expression led to dephosphorylated ERK1/2 and lower S100A4 expression, thereby decreasing 3D spheroid invaded area growth. These results suggest that CYR61 and S100A4 are predictive markers and therapeutic targets for advanced breast cancer. Targeting CTGF, one potential driver of breast cancer bone-directed invasion, led to reduced proteolytic activity, decreased 2D transwell invasion and 3D spheroid invaded area growth, and increased cell-ECM invasion. Our results demonstrated a RhoA dependent- CTGF regulation, which can be impaired by GnRH agonist treatment.

2. INTRODUCTION

2.1. BREAST CANCER

Breast cancer is the most prominent cancer found in women. In 2018, every 18 seconds a patient was diagnosed with breast cancer. Breast cancer accounts for 626,679 death per year worldwide with a predicted annual increase of 3.1% (1). Due to advances in multimodal therapy, early-stage breast cancer, defined as cancer that is contained in the breast or has only spread to axillary lymph nodes, is curable in 70–80% of all cases (8). Currently, advanced breast cancer—cancer with distant metastasis—is not curable, but treatment is available to prolong survival and relieve symptoms (8). Treatment strategies differ depending on histological subtypes and molecular alterations of this heterogeneous disease (8). Two histological subtypes can be distinguished according to carcinoma invasiveness. The pre-invasive subtype includes ductal carcinoma *in situ* (DCIS), wherein the tumor spreads through the duct, distorts duct architecture, and can progress to invasive disease; and lobular carcinoma *in situ*, wherein lobe architecture is not altered (8). Invasive subtype comprises invasive ductal carcinoma (IDC), which develops from DCIS and can metastasize through vascular and lymphatic system, and invasive lobular carcinoma, which is an isolated tumor mass and metastasizes through viscera (8).

Molecular alterations in breast cancer led to classification of different subtypes (Figure 1). Originally, breast cancer molecular subtypes were classified through gene expression studies using isolated RNA from frozen tissue (9). Six intrinsic subtypes were classified through qPCR array (PAM50) using isolated RNA from formalin-fixed and paraffin embedded tissue (Figure 1) (10-12):

- Luminal A. Activation of estrogen receptor 1 (ESR1).
- Luminal B. Mutations in phosphatidylinositol-4, 5-bisphosphate-3 kinase catalytic subunit α (PI3KCA), ESR1, erb-B2 receptor tyrosine kinase 2 (ERBB2/HER2), and erb-B2 receptor tyrosine kinase 3 (ERBB3) genes; amplification of HER2, growth factor receptor bound protein 7 (GRB7), DNA topoisomerase 2 A (TOP2A), and/or MYC proto-oncogene (MYC) and mutations in the PI3KCA gene.
- Basal-like. Mutations in tumor suppressor P53 (TP53) and breast cancer 1 early onset (BRCA) genes.
- Claudine-low. No expression of estrogen receptor (ER) or progesterone receptor (PR) and no overexpression of HER2 (triple-negative breast cancer [TNBC]).
- Normal-like (8).

In current clinical practice, breast cancer is classified according to surrogated immunohistochemistry (IHC)–based subtypes (Figure 1) (8). Surrogated IHC-based subtype classification contains five subtypes based on the histological and immuno-histochemical expression of ER, PR, HER2, and Ki-67 as markers for proliferation:

- TNBC. No expression of ER and PR; no amplification of HER2; high Ki-67 expression; high histology score of special types including metaplastic, adenoid cystic, medullary-like, or secretory. Marked by poor prognosis.
- HER2-enriched (non-luminal). No expression of ER and PR; HER2 amplification; high Ki-67 expression. Marked by intermediate prognosis.
- Luminal A-like. Expression of ER and PR; no amplification of HER2; low Ki-67 expression. Marked by good prognosis (8).
- Luminal B-like. Lower expression of ER and PR than luminal A-like; high Ki-67 expression. May or may not have HER2 amplification. Marked by intermediate prognosis.

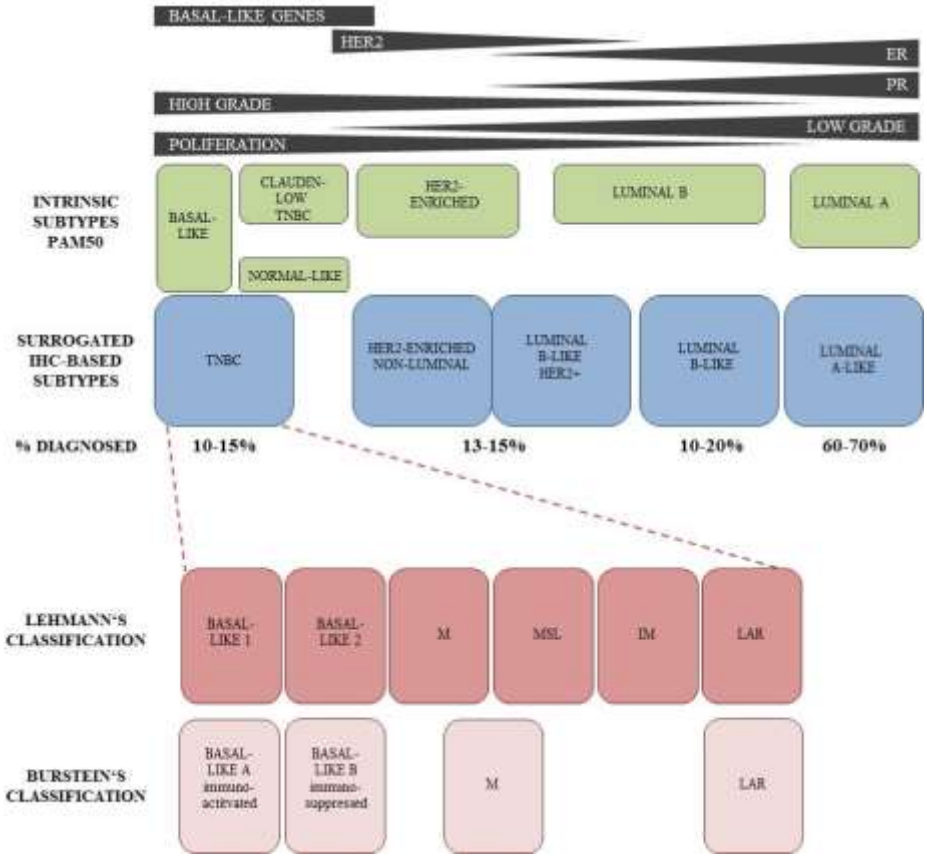

Figure 1 Characteristics and classification of breast cancer subtypes. Breast cancer can be classified according to intrinsic subtypes and PAM50 gene expression signature or surrogated immune-histochemical-based subtypes. Furthermore, TNBC can be classified according to Lehmann's (13) and Burstein's (14). Scheme illustrates proliferation, tumor grading, ER expression, PR expression, HER2 amplification, and expression of basal-like genes. Scheme modified regarding to (8, 15,

16). IM immunomodulatory, LAR luminal androgen receptor, M mesenchymal, MSL mesenchymal/ stem-like, TNBC triple negative breast cancer

Prevailing studies have demonstrated discordance of intrinsic subtypes and surrogated IHC-based subtypes, concluding that IHC-based classification could lead to suboptimal treatment discussions and poor outcomes (17). Treatment of heterogeneous TNBC is far behind other subtypes and, thus, is associated with the worst prognosis (8). Two different classifications were proposed for further classification of TNBC. The first classification was proposed by Lehmann et al. with the following six subtypes:

- Basal-like 1. Molecular alterations in cell cycle and DNA repair signaling, such as TP53, BRCA, mitogen-activated protein kinase kinase kinase 1 (MAP3K1/MEKK1), and PIK3CA (16).
- Basal-like 2. Molecular alterations in growth factor and metabolism signaling (13).
- Mesenchymal. Molecular alterations in cell motility, extracellular matrix (ECM) receptor, and cell differentiation signaling (e.g., Rho pathway, TGFβ signaling) (13).
- Mesenchymal/stem-like (MSL). Low expression of claudins. Molecular alterations are versatile and include, but are not limited to, extracellular signaling–related kinase 1/2 (ERK1/2 or MAPK1), G-protein coupled receptor, and calcium signaling (13).
- Immunomodulatory (IM). Molecular alteration in cellular immune process (13).
- Luminal androgen receptor (LAR). Overexpression of LAR. Molecular alterations in, but not restricted to, androgen/estrogen metabolism signaling (13).

Refinement of this classification led to four subtypes with implications for neoadjuvant therapy response (18). A similar classification was reported by Burstein et al. with RNA and DNA approaches (14). These subtypes are basal-like A (immune-activated), basal-like B (immunosuppressed), mesenchymal (mesenchymal and MSL are merged here), and LAR (14). Currently, no diagnostic test is routinely used in clinical practice (8).

Of all patients diagnosed with breast cancer, those with TNBC account for 10–15% of all cases. Thus, we want to investigate the drivers of this heterogeneous breast cancer subtype with special focus on mesenchymal molecular alterations. Understanding what drives tumor progression and advanced breast cancer could lead to the development of specific treatments to be able to prolong patient survival, impede metastasis, and cure this specific subtype.

2.2. METASTATIC CASCADE

To date, advanced cancer with distant metastases is not curable and is the cause of approximately 90% of cancer-related deaths (8). The invasion-metastatic cascade leading to cancer metastasis is a multistep-process (Figure 2) (19-22).

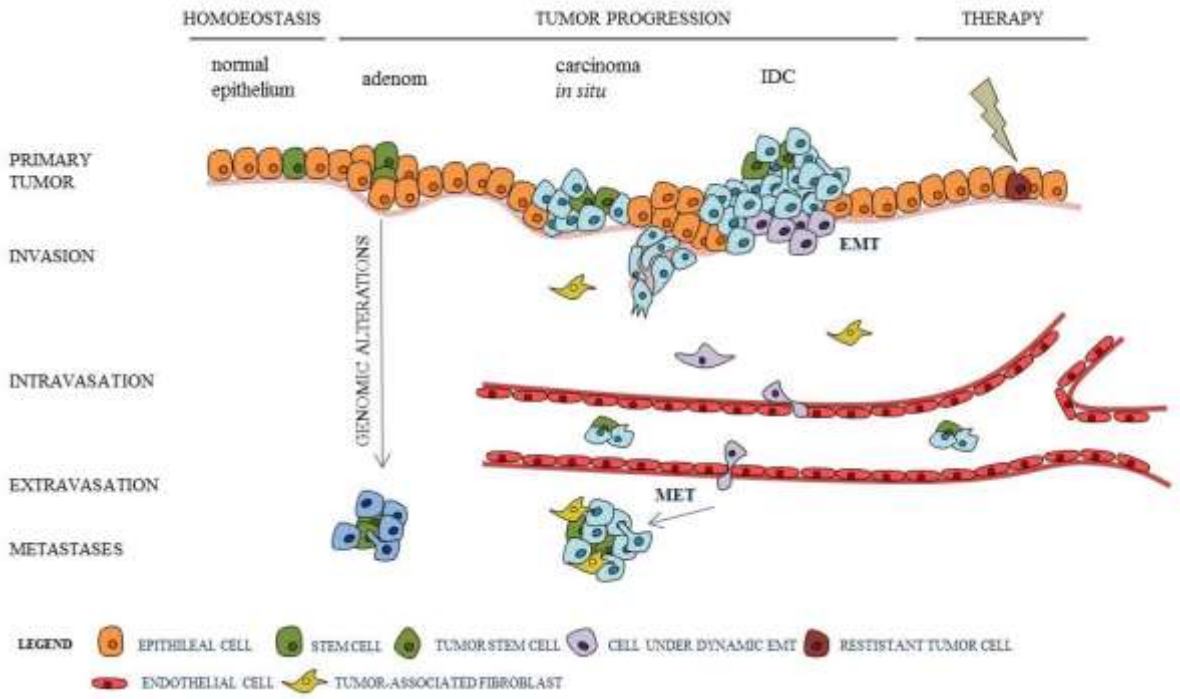

Figure 2 The Invasion-metastatic cascade. Scheme illustrating progress from tissue homoeostasis towards tumor progression and metastasis. Multistage invasion-metastatic cascade comprises dissemination of tumor cell from primary tumor site (invasion), migration through extracellular matrix (ECM), intravasation into vascular system, extravasation into parenchyma of distant site, colonization at metastatic niche. To proceed, metastatic tumor cells might hijack developmental processes like epithelial-mesenchymal transition (EMT) and mesenchymal-epithelial transition (MET). Scheme modified regarding to (23-25).

This process is initiated by local invasion of cancer cells from the primary tumor (carcinoma *in situ*) into the surrounding tissue (IDC). Due to gained motile and invasive properties, tumor cells move through the extracellular matrix (ECM) and intravasate into the vascular system. However, they need to survive during hematogenous non-adhesive transit. To exit hematogenous transit, tumor cells need adhesive properties to extravasate through the vascular walls into distant site tissue. Having unique microenvironmental features at the distant site, tumor cells need adhesive properties to form micrometastases and induce angiogenesis. Tumor metastasis is an inefficient process and needs special cellular features to proliferate, invade, intravasate, survive, extravasate, and proliferate again in different microenvironments (26). Evaluating which molecular alterations appear during the invasion-metastatic cascade could help to design treatment options to impede this process.

2.2.1. Invasion

Tumor initiation is a complex biological event. It starts with molecular alterations in normal cells, leading to uncontrolled proliferation, resistance to cell death signaling, and hyperplasia (27, 28). The tumor mass consists of heterogeneous tumor cells and the tumor microenvironment (TME). The TME comprises cancer-associated fibroblasts, immune and inflammatory cells, lymphatic vascular and blood networks, adipose cells, neuroendocrine cells, and the ECM. This composition has a critical role in malignancy evolution and varies depending on tissue site (29, 30). Regarding prognosis of a given tumor, the composition of the ECM is of great importance (30, 31). Three-dimensional structure of the ECM contains a reservoir of growth factors, collagens, elastin, fibronectin, hyaluronic acid, proteoglycans, and glycoproteins; it provides hydration and facilitates pH homeostasis (32-34). Due to continuous proliferation, the TME is constantly remodeled, leading to altered paracrine and autocrine communication between different cell types, increased interstitial fluid pressure, increased ECM stiffness, increased vascular network formation, and tumor progression (27, 35). Identifying the drivers within the TME, specifically the ECM, that alter tumor cell behavior toward invasion could help to design new therapeutic treatments targeting tumor progression and tracking tumor stage (30). Adhesion receptors (e.g., integrins, cadherins) transform stimuli by extracellular ligands from microenvironment into intracellular signals, thereby leading to cellular transformational processes, invasion, proliferation, or survival (36). Likewise, cells use adhesion receptors to sense, adapt, and respond to mechanical or biophysical signals from the ECM. They interact with the ECM through focal adhesions and hemidesmosomes (cell-ECM adhesions) (29). Understanding differences in physiological processes such as wound healing regarding adhesion receptor binding and alterations in cell-ECM adhesion compared to pathological processes such as fibrosis or tumor cell invasion could help specify targeted therapy to impede tumor cell invasion.

To be able to invade into surrounding tissue, molecular alterations are essential for cancer cells to drive proteolytic degradation of ECM and alter in cell-cell and cell-ECM adhesion (37). Different processes can enable the dissemination of primary tumor cells. Of these, collective invasion has been well described (25). In this process, invading cells keep their epithelial traits (cell-cell junctions) and disseminate as a collective cohesive cohort (Figure 2) (19, 25). Additionally, cells can invade by different types of single-cell invasion. First: in a mesenchymal manner, wherein cells are elongated and cell-ECM adhesion remains (25). Second: in an amoeboid manner, wherein cells are in rounded shape and rely on the contractility of cortical actomyosin (38). And third: cells using intermediate behaviors of the

former mentioned single cell invasion types, which were already reported before (38-41). Another possible invasion process is the epithelial-mesenchymal transition (EMT). In this process, cells invade by gaining mesenchymal traits and losing epithelial traits due to higher cellular plasticity.

2.2.2. EMT during invasion-metastatic cascade

The EMT is a group of dynamic biological programs employed under physiological conditions during embryogenesis and wound healing. These programs are dynamic with different intermediated states contributing to cellular plasticity. They are orchestrated through a set of transcription factors (EMT-TFs) (23, 42, 43) but are triggered by heterotypic signals (19, 23, 42, 43). Tumor cells hijack such physiologic dynamic programs to acquire mesenchymal traits and reduce epithelial traits (19, 44). Furthermore, it was suggested that the acquisition of mesenchymal traits led to resistance to common cytotoxic therapies and tumor initiation (19, 45-47). Currently, the contribution of the EMT to cell dissemination and metastasis is highly debated (43). One recent study indicated that acquiring a fully mesenchymal state resulted in cells unable to metastasize (48, 49). Cancer cell dissemination and intravasation could also be observed by collective invasion. It remains elusive if cells at the leading edge of invasive cohorts are in an intermediate state of the EMT due to acquired invasive properties (43). Recent studies suggested that cancer-associated fibroblasts or cancer cells at the leading edge under dynamic EMT programs led to collective invasion (25, 50). Interestingly, remodeling of the ECM during wound healing due to upregulation of Transforming Growth Factor β (TGFβ), interleukins, and growth factors results in comparable ECM composition (19). It was demonstrated that non-invasive breast cancer cells under dynamic EMT programs are able to form distant metastases *in vivo* and are more invasive in a 2D transwell invasion assay *in vitro* (51). Nevertheless, fundamental issues regarding EMT contribution to tumor invasion and metastasis remain elusive.

Regarding tumor initiation, two models currently exist. First clonal evolution: where cells gain tumorigenic properties due to molecular alterations leading to tumor initiation. Second: the cancer stem cell model, where cancer stem cells are considered as the precursor to initiate tumor growth and progression (8, 52). Growing evidence demonstrates that the EMT is able to induce stemness in cancer cells. Additionally, stem cells might evolve from clonal evolution, which could explain the polyclonal appearance of metastatic colonies (53). Further research should aim to reveal intracellular and extracellular signals that can activate, sustain, and reverse EMT. Reversion of EMT is also referred as mesenchymal-epithelial transition.

Distinguishing between different states could help to track tumor progression. Thus, we want to investigate the effect of EMT on breast cancer invasion by identifying intracellular and extracellular targets leading to altered EMT-TFs expression and acquired invasive traits. Furthermore, we want to target these intracellular and extracellular drivers to impede dynamic EMT programs and investigate whether this leads to reduced invasive capacities.

2.2.3. Breast cancer metastasis

Currently, metastatic breast cancer is incurable with a median overall survival of less than three years (54). *De novo* breast cancer accounts for more than 25% of all diagnosed metastatic breast cancers (8, 55, 56). The most common metastatic sites for breast cancer (ranked from highest to lowest percentage) are bone, axillary lymph nodes, liver, lung, and brain (Figure 3) (8).

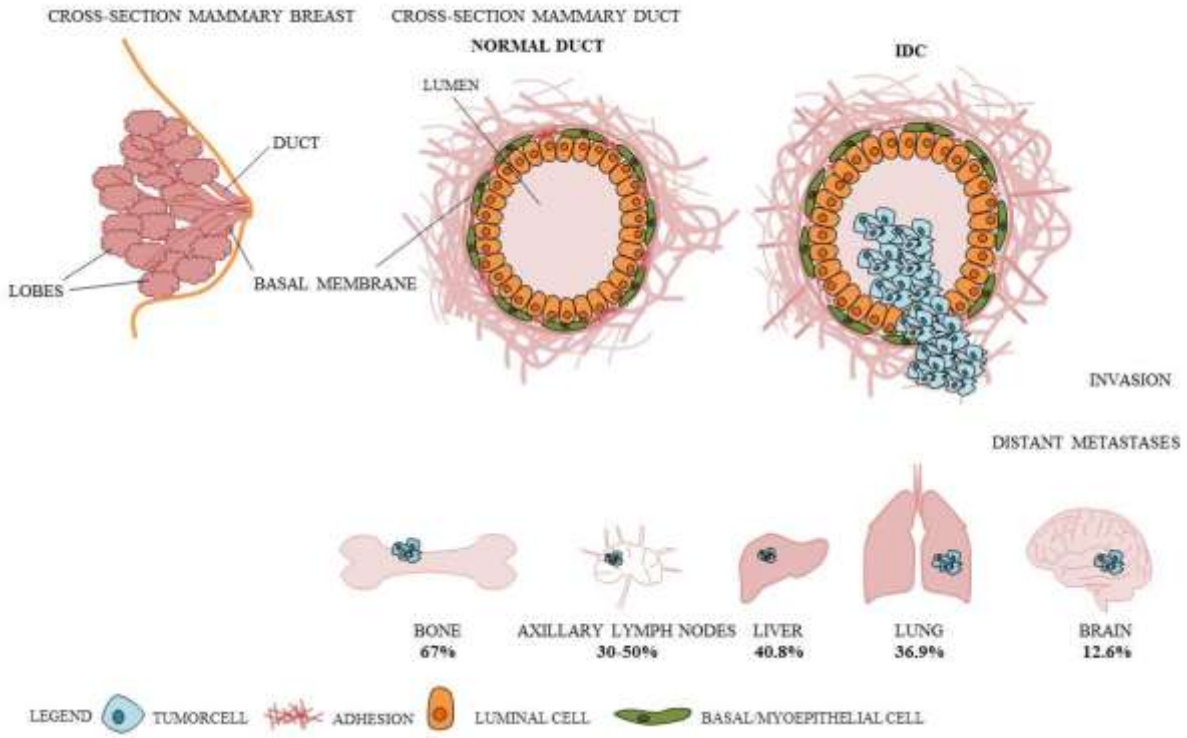

Figure 3 Metastatic sites of breast cancer. Anatomy of mammary duct and lobes in cross-section and cross-section of normal mammary duct vs. invasive ductal carcinoma (IDC). Most prominent site for distant metastases drom breast cancer is bone, counting for 67 % of all breast cancer metastases.

Tropism to specific metastatic sites depend on the intrinsic subtype (8).The intrinsic subtypes luminal A and B (no HER2 amplification) have a tropism for bone and lymph node metastases. TNBC have tropism for lung and brain metastases. Additionally, breast cancers with an amplification of HER2 have tropism for brain metastases (8, 57). Molecular alterations at the primary tumor site driving tumor progression and metastasis are up to 80% conserved at the metastatic site (8). Subclonal diversity differs by intrinsic subtypes of breast

cancer when comparing the primary site with the metastatic site. The highest subclonal diversity could be detected at PR-expressing tumors (~33%), followed by ER-expressing tumors (~20%), and HER2-amplified tumors (~8%). Differences between microenvironmental components of the primary site and unique features at the distant metastatic site can lead to discordance (8, 58, 59). Despite these findings, specific features that lead to metastases remain elusive (8). Bone is the most frequent site for metastases of breast cancer, accounting for 67% of all breast cancer-derived metastases (Figure 3) (8). Of these, 79% are classified as luminal B subtype, 60% as luminal A subtype, and 40% as HER2-amplified basal-like subtype (57). Due to unique physical properties, colonization in bone only appears in 24% of patients with detected circulating tumor cells (CTC) (60). Even when detected in bone marrow, outgrowth of metastatic tumor is not guaranteed (60-62). Bone is 100,000 times more rigid than soft tissue (58). Previous studies have suggested that rigidity facilitates cell transformational processes, leading to osteolytic gene expression in breast cancer cells and induced TGFβ signaling (63-66). It remains elusive which specific features of disseminated breast cancer cells are indispensable to colonize at the metastatic site.

Bones are continuously resorbed by osteoclast activity. These multinucleated cells are formed upon receptor activator of nuclear factor-κB ligand (RANKL) and the activity of macrophage colony-stimulating factor (M-CFS). Due to bone resorption, growth factors are released. Recent studies have reported that tumor cells express receptors to facilitate invasion and chemotaxis in different metastatic niches such as bone, lymph nodes, and the lungs. One of these specific receptors is C-X-C motif chemokine receptor 4 (CXCR4), which is able to bind to mesenchymal stem cells close to bone surface with CXCL12 receptors (67-72). Engineered bone structures with mesenchymal stem cells deficient of expressing CXCL12 are resistant to tumor cell invasion (71). Specific knowledge of bone environmental components and cellular interactions of cells that are specific to that location with disseminating tumor cells could help impede colonization and tumor cell attraction. However, it remains unclear why luminal cancer cells preferentially metastasize to bone and if specific paracrine signals or ECM components have an effect on relapse. Thus, we analyzed breast cancer bone-directed invasion with cell lines that harbor specific characteristics, including expression of CXCR4 or the luminal subtype, that make them preferentially metastasize to bone.

2.3. MATRICELLULAR PROTEINS

Unique features of TME such as growth factors, cytokines, chemotactic stimuli, and ECM composition modify tumor behavior and drive tumor progression (2). It remains unclear

which TME and ECM components alter tumor behavior toward invasion and metastasis. Additionally, it is not clear which interactions can be diminished to impede cell invasion without impeding physiological processes. Regulation of ECM composition is critical during development and fulfills versatile functions, including maintaining tissue homeostasis, regulating proliferation and survival signaling, scaffolding cell-cell-interactions, establishing ECM- growth factor interactions, and associating with proteins (73, 74). During physiological processes such as wound healing, stroma is modulated through TGFβ, interleukins, colony-stimulating factor 1 (CSF-1), tumor necrosis factor α (TNFα), and ligands of epithelial growth factor receptor (EGFR) (75). The basal membrane is the boundary between the duct and the adjacent tissue, which can be degraded by proteases (e.g., MMPs) and cause invasive programs to be initiated. The deposition of ECM components (e.g., collagens, fibronectin, matricellular proteins) leads to matrix remodeling and the release of proteases (76). In 1995, Bornstein described for the first time a group of secreted proteins within the ECM that facilitate wound healing and inflammation, naming them as matricellular proteins (3, 77). These proteins are non- structural components of the ECM; they exert functions on cell-ECM interaction, regulatory function of the cell, and act highly tissue and context specific (78). More specifically, they form scaffolds by binding to the ECM or cell surface receptors. These scaffolds trigger different extracellular signaling pathways to increase growth factors and inflammatory cytokines (79). Characteristics of matricellular proteins include: secretion by different cell types, counter-adhesiveness, and association with insoluble parts of the ECM (80). Originally defined as modulators of cell-ECM interactions, members of the family of matricellular proteins were secreted protein acidic and rich in cysteine (SPARC), thrombospondine-1 (TSP-1), and tenascin C (TN-C) (3, 4). The expanded family includes members of the CCN family, such as Cysteine-Rich Angiogenic Inducer 61 (CYR61) and Connective Tissue Growth Factor (CTGF) (80). Several proteins of this family have been proposed as therapeutic targets or predictive markers for a variety of pathological incidents including cardiovascular diseases, fibrosis, and different cancer entities (81-83).

2.3.1. CCN Family

The CCN family contains six homologues proteins, all of which are found in the ECM: CYR61, CTGF, nephroblastoma overexpressed (NOV), Wnt-1 induced secreted protein (WISP) 1, WISP-2, and WISP-3 (84-86). Each protein constitutes four main domains: homologies to insulin-like growth factor binding proteins, Von Willebrand factor type C (VWC) repeat, TSP-1 repeat, and carboxyl-terminal domain (CT) (84). Members of this

family are reported to be involved in versatile cellular processes, including regulation of inflammatory regulators (e.g., TGFβ, prostaglandins), angiogenesis, signal modulation of proteins involved in tumor growth, tumor initiation, and tumor progression (e.g., integrins, Wnt) (5, 6, 87-91).

2.3.1.1.CYR61 and cancer invasion

As a member of the matricellular family, CYR61 is associated with ECM and exerts its functions in matrix signaling by binding to integrin receptors ($\alpha_V\beta_3$, $\alpha_V\beta_3$, $\alpha_6\beta_1$, $\alpha_M\beta_2$), syndecan 4 (SDC4), and heparan sulfate proteoglycans (HSPGs) (77, 80, 92, 93). CYR61 exerts its funtion in cell type and tissue specific manner (94). While it acts as a tumor suppressor in human hepatocellular carcinoma and non–small cell lung cancer (NSCLC) (95, 96), CYR61 also acts as an oncogene in the cancers of the breast, ovaries, stomach, and pancreas, as well as glioblastoma (97-101). In physiological events, CYR61 exerts functions in cardiovascular development during embryogenesis (77). Its binding to integrin $\alpha v\beta_3$ facilitates proliferation, survival, and angiogenesis (73, 77, 102). Additionally, it was proposed that CYR61 induces vascular endothelial growth factor A (VEGF-A) and VEGF-C expression, which are known angiogenic factors (90, 91). Furthermore, its binding to integrin $\alpha_6\beta_1$ and HSPGs induces apoptosis and senescence (77). Diverse signaling pathways induced transcriptional activation of CYR61 including TGFβ signaling, growth factors stimulation, cytokine stimulation, estrogen signaling, and tamoxifen signaling, as well as bacterial and viral infections (77, 87, 103-106). Through the transcriptional activation of yes-associated protein (YAP), CYR61 is part of the Hippo signaling pathway (107). Previous studies have demonstrated that CYR61 can affect estrogen resistance and resistance to chemotherapy, as well as facilitate breast cancer tumor growth, tumor progression, and metastasis, thereby leading to poor prognosis (97, 108-111).

Regarding breast cancer, growing evidence demonstrates that increased CYR61 expression led to tumor growth *in vivo* and poor prognosis (109). Decreased CYR61 expression reduced invasion and transendothelial migration in TNBC cells and reduced lung metastasis (112-114). Additionally, it was proposed that breast cancer cells under dynamic EMT programs exhibit increased CYR61 expression, metastasis, and tumor cell invasion (7). Using neutralizing CYR61 antibodies, breast cancer invasion and metastasis could be diminished *in vitro* and *in vivo* (7, 115). Thus, we investigated breast cancer bone-directed invasion and reveal the underlying mechanism that led to reduced breast cancer cell invasion due to reduced CYR61 expression. Furthermore, we wanted to evaluate whether CYR61 can be used as a prognostic marker and therapeutic target for advanced breast cancer.

2.3.1.2.CTGF and cancer invasion

Under physiological incident, CTGF is upregulated during embryogenesis and facilitates renal, skeletal, and cardiovascular development (116). CTGF exerts its function context and tissue specific. Previous studies have demonstrated that CTGF acts as a tumor suppressor regarding advanced colon cancer but acts as a oncogene in other tumor entities (116-120). CTGF binding is reported with following receptors: $\alpha_M\beta_2$, $\alpha_v\beta_3$, $\alpha_4\beta_1$, $\alpha_5\beta_1$, $\alpha_5\beta_3$, tropomyosin-related kinase A, tyrosine kinases, low-density receptor-related proteins (LRPs), and HSPGs (80, 116, 121-126). Additionally, CTGF binds to cytokines and ECM proteins, thereby regulating matrix turnover, cell adhesion, and motility (116). Versatile stimuli lead to transcriptional induction of CTGF (e.g., mechanical stress, cytokines, growth factors, and oxygen deprivation) (127). Furthermore, CTGF is transcriptionally induced by key regulators of the Hippo pathway, which are YAP, transcriptional coactivator with PDZ-binding motif (TAZ), and transcriptional enhancer factor TEF-1 (TEAD) (116). Stimulation of ETS proto-oncogene 1 (ETS1) leads to the induction of CTGF and was reported to remodel the ECM in cancer cells, fibroblasts, and endothelial cells (116, 128, 129). Regarding breast cancer, CTGF induced motility by binding to integrin $\alpha_5\beta_3$ and ERK1/2 phosphorylation; it also correlates with poor prognosis and facilitates osteolytic metastasis (116, 129, 130). Likewise, CTGF upregulation led to invasion, migration, and mammosphere formation through the EMT (111). It was proposed that CTGF regulation and regulation of other CCN protein or TME components result in synergistic effects (131).

Both CYR61 and CTGF have the ability to interact with different cell types and the ECM, making them valuable targets for localized drug delivery (81). Thus, we investigated the molecular mechanisms of CYR61 and CTGF with regards to TNBC, cells with high cellular plasticity, and breast cancer bone-directed invasion. Identifying prognostic markers and therapeutic targets could help to improve the treatment of currently incurable metastatic breast cancer.

2.4. AIM OF THE THESIS

The aim of this thesis was to elucidate the mechanism of breast cancer cell invasion to impede metastasis. To achieve this aim, the following three tasks were implemented:

1. **Identification of molecular mechanisms underlying reduced breast cancer invasiveness due to reduced CYR61 expression.** The task was to evaluate whether CYR61 could be of value as a prognostic marker and therapeutic target for advanced breast cancer. It was demonstrated that CYR61 is upregulated in mesenchymal-transformed breast cancer cells and that reducing extracellular CYR61 led to reduced 2D transwell invasion in a co-culture model with osteosarcoma cells (7). In this study, transient RNA silencing was used to reduce CYR61 expression and reveal the effects on cell signaling.
2. **Identification of the extracellular drivers of invasion to better understand the unique interaction between breast cancer cells and osteosarcoma cells.** Von Alten et al. demonstrated that co-culturing non-invasive breast cancer cells with primary osteoblast and osteosarcoma cells led to increased 2D transwell invasion (132). In this study, we combined this co-culture model with mass spectrometry based secretome analysis to identify potential extracellular secreted drivers of breast cancer invasion.
3. **Identification of molecular mechanisms underlying reduced breast cancer invasiveness due to reduced CTGF expression.** CTGF expression is induced when breast cancer cells are mesenchymal transformed, facilitating invasiveness and metastasis (51). In this study, transient RNA silencing was used to reduce CTGF expression thereby assessing the effect on invasion by 3D spheroid invasion assay. Additionally, cell-ECM adhesion and proteolytic activity of breast cancer cells were assessed. Furthermore, possible treatment options targeting CTGF were identified.

3. RESULTS

3.1. MANUSCRIPT A

Inhibition of CYR61-S100A4 Axis Limits Breast Cancer Invasion

Citation

Hellinger, J. W., Hüchel, S., Goetz, L., Bauerschmitz, G., Emons, G., & Gründker, C. (2019). Inhibition of CYR61-S100A4 Axis Limits Breast Cancer Invasion. *Front Oncol, 9*(1074). doi: 10.3389/fonc.2019.01074

Own contribution: Conducted experiments and analyzed data for figures 1- 6 and supplemental material. Shared contribution for experiments presented in figures 1 C, 2 C, and 4 C-E. Contribution to: method design, figure arrangement, manuscript writing, and manuscript revision.

frontiers in Oncology

ORIGINAL RESEARCH
published: 23 October 2019
doi: 10.3389/fonc.2019.01074

Inhibition of CYR61-S100A4 Axis Limits Breast Cancer Invasion

*Johanna W. Hellinger, Silke Hüchel, Lena Goetz, Gerd Bauerschmitz, Günter Emons and Carsten Gründker**

Department of Gynecology and Obstetrics, University Medicine Göttingen, Göttingen, Germany

Background and Objective: Matricellular proteins modulate the micro environment of tumors and are recognized to contribute to tumor cell invasion and dissemination. The cysteine-rich angiogenic inducer 61 (CYR61) is upregulated in mesenchymal transformed and invasive breast cancer cells. CYR61 correlates with poor prognosis of breast cancer patients. The signaling mechanism that causes invasive properties of cancer cells regarding to epithelial-mesenchymal transition (EMT) needs further research. In this study, we investigated the signaling mechanism, which is responsible for reduced cell invasion after suppression of CYR61 in mesenchymal transformed breast cancer cells and in triple negative breast cancer cells.

Methods: We addressed this issue by generating a mesenchymal transformed breast cancer cell line using prolonged mammosphere cultivation. Western blotting and quantitative PCR were used to analyze gene expression alterations. Transient gene silencing was conducted using RNA interference. Proliferation was assessed using AlamarBlue assay. Invasiveness was analyzed using 2D and 3D invasion assays. Immune-histochemical analysis of patient tissue samples was performed to examine the prognostic value of CYR61 expression.

Results: In this study, we investigated whether CYR61 could be used as therapeutic target and prognostic marker for invasive breast cancer. We discovered an interaction of CYR61 with metastasis-associated protein S100A4. Suppression of CYR61 by RNA interference reduced the expression of S100A4 dependent on ERK1/2 activity regulation. Non-invasive breast cancer cells became invasive due to extracellular CYR61 supplement. Immune-histochemical analysis of 239 patient tissue samples revealed a correlation of higher CYR61 and S100A4 expression with invasive breast cancer and metastasis.

Conclusion: Our data suggest that suppression of CYR61 impedes the formation of an invasive cancer cell phenotype by reducing ERK1/2 phosphorylation thereby suppressing S100A4. These findings identify mechanisms by which CYR61 suppresses cell invasion and suggest it to be a potential therapeutic target and prognostic marker for invasive breast cancer and metastasis.

Keywords: breast cancer, CYR61, invasion, EMT, triple negative breast cancer

OPEN ACCESS

Edited by:
Mohit Kumar Jolly,
Indian Institute of Science (IISc), India

Reviewed by:
Saurav Kumar,
Indian Institute of Science (IISc), India
Daniele Vergara,
University of Salento, Italy
Bisrat G. Debeb,
University of Texas MD Anderson Cancer Center, United States

****Correspondence:***
Carsten Gründker
grundker@med.uni-goettingen.de

Specialty section:
This article was submitted to Molecular and Cellular Oncology, a section of the journal Frontiers in Oncology

Received: *22 July 2019*
Accepted: *30 September 2019*
Published: *23 October 2019*

Citation:
Hellinger JW, Hüchel S, Goetz L, Bauerschmitz G, Emons G and Gründker C (2019) Inhibition of CYR61-S100A4 Axis Limits Breast Cancer Invasion. Front. Oncol. 9:1074. doi: 10.3389/fonc.2019.01074

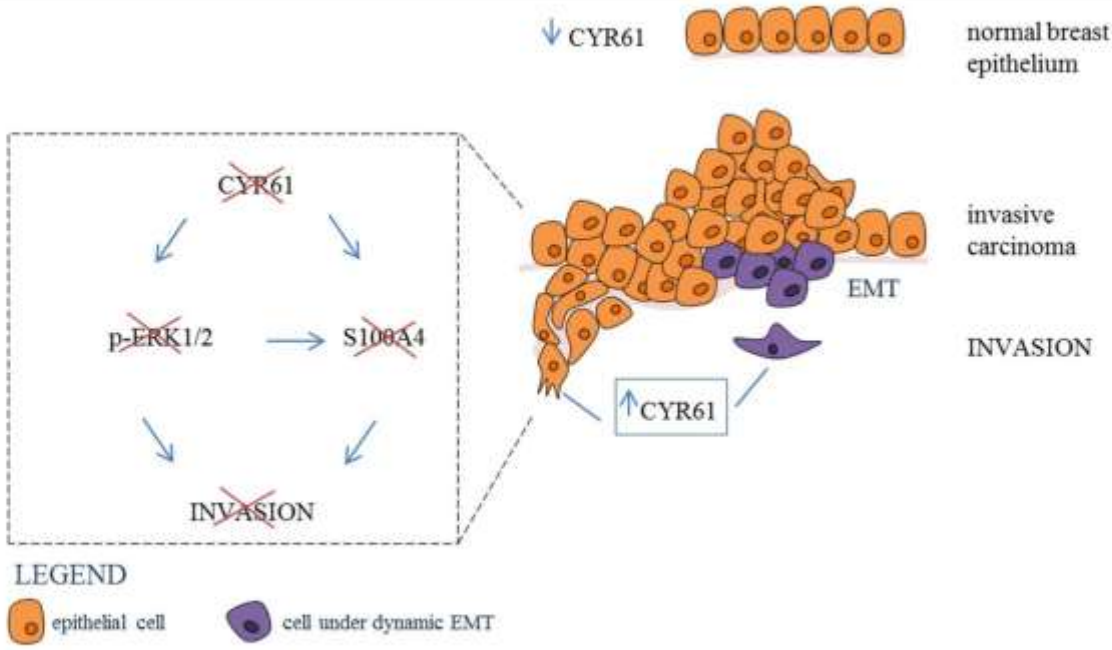

GRAPHICAL ABSTRACT | Inhibtion of CYR61-S100A4 axis limitis breast cancer Invasion. CYR61 expression is low in normal breast epithelium, while expression is increased in invasive breast carcinoma. Suppression of CYR61 leads to reduced ERK1/2 phosphorylation and S100A4 expression thereby reducing breast cancer invasion. EMT, epithelial-mesenchymal transition.

INTRODUCTION

In 2019, approximately 271270 woman and men in the United States will be diagnosed with breast cancer. Due to improved early detection techniques and treatment options 5-year-survival rates for local and regional breast cancer are 84–99 %. However, only 27of patients diagnosed with distant metastasis survive a period of 5 years (1). Consequently it is necessary to identify prognostic markers for the early detection of breast cancer metastasis and new treatment options for this indications which accounts for more than 90% of cancer related death (2).

The first key event in the multi-step process of metastasis is the separation of tumor cells from the primary tumor and the dissemination into the surrounding tissue. Cells gain the ability to migrate and invade by altering their cytoskeletal organization, cell-cell-contacts, contacts with the extracellular matrix (ECM) and surrounding stroma (3). Epithelial-mesenchymal transition (EMT) is a transient dynamic program induced by different transcription factors (TFs). EMT-TFs orchestrate tumor-promoting micro environmental changes, cancer cell stemness, and chemo resistance (4, 5). The contribution of EMT programs to the metastatic cascade regarding breast cancer is supported by several publications (6–8). However, it is still under debate if an involvement of EMT programs is indispensable for creating an invasive phenotype (4). Therefore it is necessary to study cancer cell invasion with regards to EMT complexity (9, 10).

The cysteine rich angiogenic inducer (CYR61) belongs to the CCN family (CYR61, CTGF /CCN12, NOV/CCN3, WISP-1/CCN4, WISP-2/CCN5, WISP-3/CCN6) of matricellular proteins and is localized on cell surface, cytoplasm and as a secreted protein in the extracellular matrix. The functions of CYR61 are cell type and context-dependent (11). They are transmitted through binding to integrin and heparin sulfate proteoglycans (HSPGs). CYR61 was shown to be involved in facilitating EMT programs in different cancer entities (12–14). It is known that elevated CYR61 expression promotes tumor progression, proliferation, migration and invasion of breast cancer (15, 16), whereas the role of CYR61 in breast cancer EMT programs remains elusive. Otherwise, CYR61 can act as a tumor suppressor in non-small cell lung cancer (17) and in fibroblasts by inducing apoptosis and senescence during wound healing (18, 19). The role of CYR61 signaling in cancer invasion and EMT programs regarding to a potential use as therapeutic target and prognostic marker needs further evaluation.

We hypothesize that CYR61 is a key regulator of breast cancer invasion. We want to identify the mechanisms by which CYR61 facilitates an invasive phenotype. Furthermore, we want to investigate the value of CYR61 as a therapeutic target and prognostic marker for invasive and metastatic breast cancer.

MATERIALS AND METHODS

Cell Lines and Cell Culture

Human breast cancer cell lines MCF-7, T47D, MDA-MB-231, and HCC1806 were obtained from American Type Cell Collection (ATCC; Manassas, VA, USA) and cultured in minimum essential medium (MEM; biowest, Nuaillé, France) supplemented with 10% fetal bovine serum (FBS; biochrom, Berlin, Germany), 1% Penicillin/Streptomycin (P/S; Gibco, Carlsbad, CA, USA), 0,1% Transferrin (Sigma, St. Louis, USA) and 26 IU Insulin (Sanofi, Frankfurt, Germany). Human osteosarcoma cell line MG-63 was purchased from ATCC and cultured Dulbecco's modified eagle medium (DMEM; Gibco) supplemented with 10% FBS (biochrom) and 1% Penicillin/Streptomycin (Gibco). To retain identity of cell lines, purchased cells were expanded and aliquots were frozen in liquid nitrogen. A new frozen stock was used every half year and Mycoplasma testing of cultured cell lines was performed routinely using PCR Mycoplasma Test Kit I/C (PromoCell GmbH, Heidelberg, Germany). All cells were cultured in a humidified atmosphere with 5% CO_2 at 37°C.

Generation of Mesenchymal Transformed MCF-7 Cells

Mesenchymal transformed MCF-7 breast cancer cells (MCF-7-EMT) were generated as described earlier (20). Briefly, 4×10^4 cells/ml were cultured in prolonged mammosphere culture (5–6 weeks) in ultralow adherence six well plates (Corning, Lowell, MA, USA) in DMEM/F12 (Gibco) supplemented with 10% charcoal-stripped fetal calf serum (cs-FCS;PAN-biotech, Aiden Bach, Germany), 2% B27 supplement (Invitrogen, Darmstadt, Germany), 1% penicillin/streptomycin, 0.5 mg/ml hydrocortisone (Sigma, St. Louis, MO, USA), 5 µg/ml insulin, 20 ng/ml epidermal growth factor (EGF; Sigma, St. Louis, MO, USA).

Treatment With rhCYR61 and U0126

Human breast cancer cells were seeded at 5×10^5 cells/ml in MEM supplemented with 10% FB, 1% P/S, 0,1% Transferrin 26 IU Insulin. Cells treated with 1 µg/ml rhCYR61 (recombinant human CYR61; C-63398; PromoKine; Heidelberg; Germany) were serum-deprived 24 h prior to treatment and lysed 24 h after treatment. Cells treated with 10 µM U0126 (#tlrl-u0126; InvivoGen; San Diego; USA) were lysed 24 h after treatment.

Transwell Invasion Assay

Using co-culture transwell assay as described earlier (21), 1×10^4 breast cancer cells were seeded in DMEM w/o phenol red (Gibco), supplemented with 10% cs-FCS into a cell cultural insert (upper well) with a polycarbonate membrane (8 µm pore diameter, Merck Millipore, Cork, Ireland) coated with 30 µL of a Matrigel® (BD Bioscience, Bedford, MA, USA) solution (1:2 in serum-free DMEM). The osteosarcoma cells were seeded (2.5×10^4) in DMEM supplemented with 10% cs-FCS into the lower well (24-well-plate). After 24 h cells were co-cultured for 48 h or 96 h. Stably transfected cells (overexpressing CYR61 or S100A4) were seeded at a density of 1×10^4 per well in DMEM w/o phenol red cell cultural insert (upper well, Matrigel-coated with a polycarbonate membrane), with the lower well containing DMEM w/o phenol red supplemented with 10% cs-FBS and cultured for 96 h. Invaded cells on the lower side of the insert were stained with hematoxylin and the number of cells in four randomly selected fields of each insert was counted.

3D Spheroid Assay

Assessment of 3D cell invasion was pursued as describes earlier with minor changes (22). Briefly 1×10^3 breast cancer cells were seeded in 100 µL in a well of an ultra-low-adherence 96-well plate (ULA; Nexcelom, Cenibra GmbH, Bramsche, Germany). After 48 h spheroid formation was visually confirmed and 50 µL of media was removed. Thereafter 50 µL Matrigel were added to the spheroid wells. Central position of the spheroids was checked visually and Matrigel was allowed to solidify for 1 h at 37°C and 5% CO_2. Afterwards 50 µL media were added to each well and a picture was taken marking time point 0 (t0h). When indicated 1µg/ml rhCYR61 or 10µM U0126 were added. Spheroid growth area was analyzed using ImageJ polygonal selection and measurement. Mean values were calculated and compared to respective control.

Small Interfering RNA Transfection

Breast cancer cell lines MCF-7-EMT (5×10^5 cells/ml) and MDA-MB-231 (2.5×10^5 cells/ml) were seeded in 2 ml of MEM with 10% FBS (-P/S) in 25 cm^2 cell culture flask. The cells were transiently transfected with siRNA specific to S100A4 (sc-106781 pool of three S100A4-specific siRNAs; Santa Cruz Biotechnology, Dallas, USA), CYR61 (sc-39331 pool of three CYR61-specific siRNAs; Santa Cruz Biotechnology) or YAP1 (sc38637 pool of three YAP1 specific siRNAs; Santa Cruz Biotechnologies) in OPTI-MEM I medium (Gibco, Carlsbad, CA, USA) with siRNA transfection reagent (sc-29528; Santa Cruz Biotechnology, Dallas, USA). A non-targeting siRNA was used as control (sc-37007 control-A; Santa Cruz Biotechnology, Dallas, TX, USA). After an incubation period of 6 h, MEM supplemented with 20% FBS and 20% penicillin/streptomycin was added.

Immune-Histochemical Staining

Immune-histochemical staining of human tissue array slides (T087a; BR20837; BR248a; US Biomax, Derwood, MD, USA) was performed as described earlier (23). Sample sections were deparaffinized and rehydrated. Then antigens were retrieved by slide incubation in 0.01 M citrate buffer (pH 6.0) in microwave (700W) for 5 min. Using 3% hydrogen peroxidase solution for 6 min the endogenous peroxidase activity was quenched. Sample sections were incubated over night with primary labeled antibodies against S100A4 (NBP2-54580AF488; Alexa Fluor 488 labeled; 5 µg/ml; Novus Biologicals, Centennial, CO, USA) and CYR61 (NB100-356R; DyLight labeled; 5 µg/ml; Novus Biologicals) at 4°C. Staining was visualized using a Zeiss Scope A1 Axio microscope (ZEISS, Oberkochen, Germany) with an oil EC PLAN-NEOFLUAR 100x (ZEISS, Oberkochen, Germany) objective and the ZEN software (ZEISS, Oberkochen, Germany).

Real-Time Quantitative PCR Analysis

Total RNA was extracted using an RNeasy mini kit (Qiagen, Hilden, Germany) and 2 µg were reverse transcribed with

high capacity cDNA reverse transcription kit (Qiagen, Hilden, Germany). Real- time qPCR was performed using SYBR green PCR master mix kit (Qiagen, Hilden, Germany). Primer were, for S100A4 5′- GTACTCGGGCAAAGAGGGTG−3′ (forward) 5′- TTGTCCCTGTTGCTGTCCAA−3′ (reverse), for CYR61 5′-CTCCCTGTTTTTGGAATGGA−3′ (forward) 5′- TGGTCTTG CTGCATTTCTTG−3′ (reverse), for YAP1 5′- TCCCAGATG AACGTCACAGC−3′ (forward) 5′- TCATGGCAAAACGAGG GTCA−3′ (reverse), E-cadherin 5′-CCTCCTGAAAAGAGAG TGGA−3′ (forward) 5′-GTGTCCGGATTAATCTCCAG−3′ (reverse), Vimentin 5′-GCTGCTAACTACCAAGACAC−3′ (forward) 5′-TCAGGTTCAGGGAGGAAAAG−3′ (reverse), Zeb1 5′-AAGACAAACTGCATATTGTGGAAG−3′ (forward) 5′-CTGCTTCATCTGCCTGAGCTT−3′ (reverse), SNAI1 5′-GCCAAACTACAGCGAACTGG−3′ (forward) 5′- GAGA GAGGCCATTGGGTAGC-3′ (reverse), SNAI2 5′- AAGATGCA CATCCGAAGCCA-3′ (forward) 5′- CATTCGGGAGAAGGTC CGAG−3′ (reverse) and GAPDH 5′- GAAGGTCGGAGTCAAC GGAT−3′ (forward) 5′- TGGAATTTGCCATGGGTGGA−3′ (reverse). PCR conditions were: denaturing once at 95°C (2 min), 95°C (5 s), and 60°C (15 s) for 40 cycles.

Western Blot Analysis

Cells were lysed in cell lytic M buffer (Sigma, St. Louis, USA) supplemented with 0.1% phosphatase-inhibitor (Sigma, St. Louis, MO, USA) and 0.1% protease-inhibitor (Sigma, St. Louis, MO, USA). Isolated proteins (40 µg) were fractioned using 12% SDS gels and electro-transferred to a polyvinylidene difluoride membrane (Merck Millipore, Cork, Ireland). Primary antibodies against S100A4 1:250 (HPA007973; Sigma, St. Louis, USA), CYR61 1:250 (HPA029853; Sigma, St. Louis, MO, USA), YAP 1:250 (sc-398182; Santa Cruz Biotechnology, Dallas, TX, USA), ERK1/2 1:1000 (4695S;Cell Signaling Technologies Inc., Danvers, MA, USA), Phospho-ERK1/2(Thr202/Tyr204) 1:1000 (9101S; Cell Signaling Technologies Inc.), and GAPDH 1:2000 (5174; Cell Signaling Technologies Inc) were used. The membrane was washed and incubated in horseradish peroxidase-conjugated secondary antibodies (GE Healthcare, Buckinghamshire, UK). Antibody-bond protein bands were assayed using a chemiluminescent luminol enhancer solution (Cyanagen, Bologna, Italy).

ECM Degradation

Wells of a 96-well plate were coated at room temperature for 20 min with 0.05 mg/ml Poly-L-lysine in DPBS (Sigma) and 15 min with glutaraldehyde 0.5% in DPBS. Gelatin (2 mg/ml; G9391; Sigma) was FITC conjugated as recommend by manufacture (#343210; EMD Millipore Corp., Billeria, MA, USA). Wells were coated with 60 µL FITC-conjugated gelatin (2 mg/ml; Invitrogen, Milpitas, CA, USA) diluted 1:5 with unlabeled gelatin (Sigma) and incubated for 10 min at RT. Solution was discarded and wells were incubated for 30 min in 70% ethanol and afterwards free aldehydes were quenched with culture media for 30 min at room temperature before cells were seeded. Cells were seeded (4.4×10^3 cells per Well) and treated with rhCTGF (1 µg/ml; R&D systems). After 24 h proteolytic activity was detected by measuring fluorescence (extinction 490 nm/emission 520 nm) using Synergy (BioTek Instruments, Bad Friedrichshall, Germany). Each experiment was performed in duplicates for at least three times. Mean values were compared to the respective control.

AlamarBlue Assay

3D spheroids were grown as described above and 48 h after adding Matrigel AlamarBlue (BioRad, Hercules, USA) was added and incubated for 4 h at 37°C 5% CO_2. The colorimetric change of resazurin to resorufin upon cellular metabolic reduction was measured by absorbance reading at 540 nm and 630 nm, using Synergy (BioTek Instruments). Relative AlamarBlue Reduction was calculated as indicated by manufacturer.

KM Plotter Analysis

The database of the Kaplan-Meier plotter (www.kmplot.com) downloads information of gene expression and overall survival from Gene Expression Omnibus (GEO; only Affymetrix microarrays), the European Genome- Phenome Archive (EGA) and The Cancer Genome Atlas (TCGA). To be able to analyze the prognostic value (overall survival) of CYR61 in 1,402 patient samples, the samples were split into two cohorts according to the expression of quantiles of CYR61 where all possible cutoff values between the lower and the upper quantiles are computed and the best performing threshold is used as a cutoff. These groups are compared by a Kaplan-Meier survival plot and the hazard ratio with 95% confidence intervals. Redundant samples were removed, biased arrays excluded and the proportional hazard assumption was set to zero (24).

Statistical Analysis

All experiments were performed at least in three biological and technical replicates. Data were analyzed by GraphPad Prism (GraphPad software Inc., v. 7.03, La Jolla, Ca, USA) using unpaired, two-tailed, parametric *t*-test comparing two groups (treatment to respective control) by assuming both populations have the same standard derivation. $P < 0.05$ was considered statistically significant.

RESULTS

CYR61 Expression Correlates With Altered Breast Cancer Cell Invasion

Mesenchymal transformed breast cancer cells show a TGFβ-dependent increased invasive and metastatic potential (20). Despite, it is still under debate, if EMT programs are indispensable for cell invasion (4) and which key players are crucial for pathological EMT programs. We investigated whether within dynamic EMT programs or triple-negative breast cancer (TNBC; no expression of estrogen or progesterone and no overexpression of Her2neu) cells show changes in CYR61 expression. It was shown before that non-invasive breast cancer cells gain invasiveness when co-cultured with primary osteoblasts or osteosarcoma cells (21). Gründker et al. suggested that mesenchymal transformed non-invasive MCF-7 cells (MCF-7-EMT) show an increased invasiveness and elevated CYR61 expression (23). Increased invasiveness could be suppressed by reducing extracellular CYR61 using blocking antibodies. Despite, it remains elusive, if targeting intracellular CYR61

alters cell invasiveness in 2D transwell co-culture invasion assay. Two non-invasive estrogen positive cell lines (MCF-7, T47D) were mesenchymal transformed (MCF-7-EMT; T47D-EMT) and altered expression of EMT-Transcriptionfactors (EMT-TFs) was assessed. Mesenchymal transformation using prolonged mammosphere culture leads to a decreased E-cadherin expression (**Figure 1**, **Figure S1B**) in two different estrogen positive breast cancer cells lines. Transforming growth factor induced (TGFBI), Zinc Finger E-Box Binding Homeobox 1 (Zeb1) and Snail Family Transcriptional Repressor 2 (Snai2) expression was increased after mesenchymal transformation (**Figure 1**, **Figures S1A,D–F**), while vimentin expression was upregulated in MCF-7-EMT breast cancer cells (**Figure 1**, **Figure S1C**) and Snail Family Transcriptional Repressor 1 (Snai1) was upregulated in T47D-EMT cells. In addition CYR61 expression is upregulated in mesenchymal transformed breast cancer cells (**Figure 1A**; MCF-7-EMT: 2.18 ± 0.2 SEM relative expression compared to MCF-7; $n = 5$; T47D-EMT: 3.04 ± 0.62 SEM relative expression compared to T47D) and in TNBC cells (**Figure 1A**; MDA-MB-231: 68.67±11.27 SEM relative expression compared to MCF-7; $n = 4$; HCC1806: 1.3 ± 0.09 SEM relative expression compared to MCF-7; $n = 3$). Moreover, mesenchymal transformed and TNBC cell lines show increased invasiveness in a 2D transwell co-culture invasion assay (**Figure 1B**; MCF-7-EMT: 683.9 ± 53.25 SEM invaded cells in % to MCF-7; $n = 36$; $P < 0.0001$; T47D-EMT: 11881 ± 155.8 SEM invaded cells in % to T47D; $n = 36$; $P = 0.0022$; MDA-MB-231: 466.7 ± 58.52 SEM invaded cells in % to MCF-7; $n = 24$; $P < 0.0001$; HCC1806: 2277 ± 237.4 SEM invaded cells in % to MCF-7; $n = 54$; $P < 0.0001$). To determine whether intracellular suppressed CYR61 regulates breast cancer cell invasion, we transiently reduced CYR61 (see verification of CYR61 suppression **Figure 1**, **Figure S2A**) in different invasive breast cancer cell lines and analyzed invasiveness using 2D invasion co-culture assay. Reducing CYR61 results in decreases cell invasion (**Figure 1C**; MCF-7-EMT CYR61$^-$: 59.01 ± 4.34 SEM invaded cells in % to MCF-7-EMT control; $n = 36$; $P < 0.0001$; T47D-EMT CYR61$^-$: 50.73 ± 8.71 SEM invaded cells in % to T47D-EMT control; $n = 36$; $P = 0.002$; MDA-MB-231 CYR61$^-$: 31.44 ± 4.22 SEM invaded cells in % to MDA-MB-231 control; $n = 18$; $P < 0.0001$; HCC1806 CYR61$^-$:18.51 ± 2.96; $n = 18$; $P < 0.0001$). To confirm the impact of CYR61 suppression on breast cancer cell invasion, we assessed whether CYR61 suppression leads to a reduced 3D spheroid invasion growth. Reducing CYR61 results in a decreased 3D spheroid invasion area (**Figure 1D**; MCF-7-EMT CYR61$^-$: 87.93 ± 2.54 SEM invaded area in % to MCF-7-EMT control; $n = 5$; $P = 0.0014$; T47D-EMT CYR61$^-$: 61.56 ± 4.3 SEM invaded area in % to T47D-EMT control; $n = 6$; $P < 0.0001$; MDA-MB-231 CYR61$^-$:50.37 ± 13.29; $n = 5$; $P = 0.006$; HCC1806 CYR61$^-$:82.24 ± 4.81 SEM invaded area in % to HCC1806 control; $n = 6$; $P = 0.004$). To determine whether decreased 3D spheroid invaded area is due to altered proliferation AlamarBlue Assay was conducted. Transient reduces CYR61 does not alter proliferation in 3D breast cancer cell spheroids after 96 h (**Figure 1**, **Figure S2B**). Furthermore, increased extracellular CYR61 expression increases 3D spheroid invaded area of non-invasive estrogen positive breast cancer cells (**Figure 1E**; MCF-7 rhCYR61: 119.7 ± 2.93 SEM invaded area in % to MCF-7 control; $n = 5$; $P = 0.001$; T47D rhCYR61: 128.6 ± 4.38 SEM invaded area in % to T47D control; $n = 4$; $P = 0.0006$). The underlying mechanism of cell invasion into the surrounding tissue evolve different processes including altered cell-cell adhesion, cell-ECM adhesion and ECM degradation (3). Proteolytic activity of estrogen positive breast cancer cells treated with extracellular CYR61 was increased (**Figure 1F**; MCF-7 rhCYR61: 110.8 ± 2.65 SEM relative proteolytic activity in % compared to MCF-7 control; $n = 3$; $P = 0.015$; T47D rhCYR61: 106.2 ± 1.806 SEM relative proteolytic activity compared to T47D control; $n = 3$; $P = 0.026$), while proliferation was not altered (**Figure 1**, **Figure S2C**). Collectively, these data indicate that suppression CYR61 decreases invasiveness in mesenchymal transformed and TNBC cells. Furthermore, increased extracellular CYR61 expression increases invasiveness of non-invasive estrogen positive breast cancer cells.

Suppression of CYR61 Reduces S100A4 Expression

Identically to CYR61, S100A4 is upregulated during EMT programs in breast cancer and correlates with bone metastasis (23, 25). Blocking extracellular signaling of S100A4 reduced invasiveness of breast cancer cells in a 2D transwell invasion assay (23). Both CYR61 and S100A4 alter breast cancer invasiveness but the underlying molecular mechanisms remain elusive. Chen et al. suggested that CTGF regulates S100A4 through regulation of extracellular regulated kinases ERK1 and ERK2 (26). CYR61 and CTGF both bind to integrinαV (12, 26, 27). We wanted to elucidate, whether suppression of CYR61 decreases S100A4 expression (**Figure 2A**). S100A4 was upregulated in mesenchymal transformed and TNBC cells (**Figure 2B**; MCF-7-EMT: 1.84 ± 0.27 SEM relative expression compared to MCF-7;$n = 5$; $P = 0.014$; T47D-EMT: 1.47 ± 0.16 SEM relative expression compared to T47D;$n = 5$; $P = 0.0185$; HCC1806: 1.89 ± 0.38 relative expression compared to MCF-7; $n = 6$; $P = 0.0403$; MDA-MB-231: 90.31 ± 13.3 SEM relative expression compared to MCF-7; $n = 4$; $P = 0.0005$). To elucidate the impact of CYR61 expression on S100A4, relative S100A4 expression was assessed after transient CYR61 suppression. Decreased CYR61 expression resulted in decreased S100A4 expression (**Figure 2C**; MCF-7-EMT CYR61$^-$:0.64 ± 0.05 SEM relative S100A4 expression compared to MCF-7-EMT control; $n = 4$; $P = 0.0002$; T47D-EMT CYR61$^-$: 0.79 ± 0.04 SEM relative S100A4 expression compared to T47D-EMT control; $n = 3$; $P = 0.0078$; MDA-MB-231 CYR61$^-$:0.78 ± 0.08 SEM relative S100A4 expression compared to MDA-MB-231 control; $n = 4$; $P = 0.0297$; HCC1806 CYR61-: 0.63 ± 0.07 SEM relative S100A4 expression compared to HCC1806 control; $n = 3$; $P = 0.0066$), while suppresses S100A4 had no impact on CYR61 expression (**Figure 2**, **Figure S3D**). We investigated whether decreased S100A4 suppresses cell invasion in a 2D transwell co-culture assay. Decreased S100A4 expression (verification **Figure 2**, **Figures S1–S3**) suppressed the invasiveness of mesenchymal transformed und TNBC cells (**Figure 2D**; MCF-7-EMT S100A4$^-$: 83.81 ± 4.9 SEM invaded

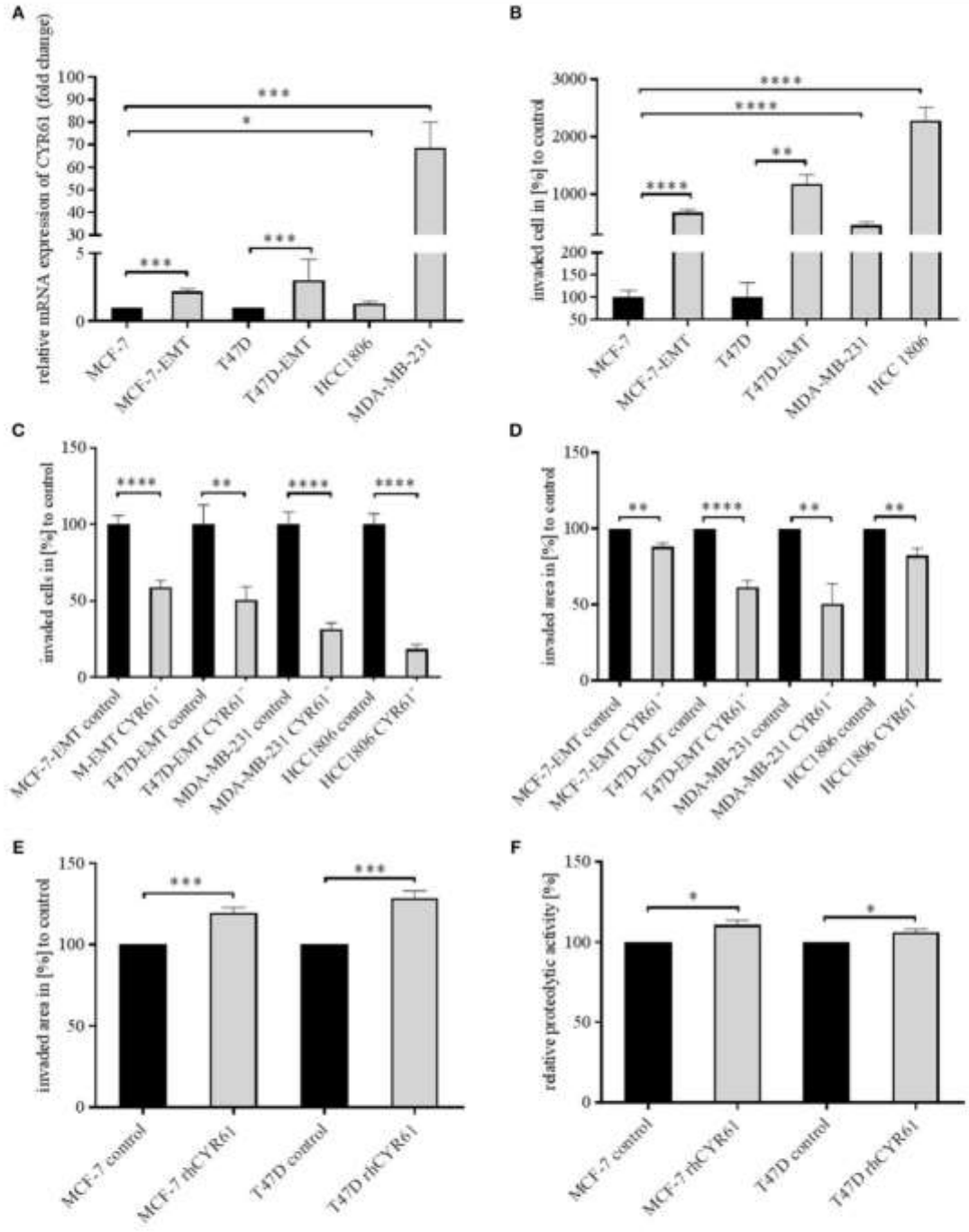

FIGURE 1 | CYR61 expression correlates with breast cancer cell invasiveness. **(A)** Relative CYR61 expression of invasive breast cancer cell lines compared to non-invasive controls. Data represent mean ± SEM. Using unpaired, two-tailed *t*-test analysis. MCF-7-EMT n = 5; T47D-EMT *n* = 6; MDA-MB-231 *n* = 4; HCC1806 *n* = 3; $^{*}P < 0.05$; $^{***}P < 0.005$ **(B)** 2D Invasion analysis of co-cultured (MG-63, osteosarcoma cells) breast cancer cells for 96 h. Percentage of cell invasion compared to controls was assessed by counting invaded cells under the filter in 4 random filter regions. Data represent mean ± SEM. Using unpaired, two-tailed *t*-test analysis. MCF-7-EMT *n* = 36; T47D-EMT *n* = 36; MDA-MB-231 *n* = 24; HCC1806 *n* = 54; $^{**}P < 0.01$; $^{****}P < 0.0001$ **(C)** 2D Invasion analysis of co-cultured (MG-63, osteosarcoma cells) breast cancer cells transient transfected with CYR61 siRNA for 96 h. Percentage of cell invasion compared to controls was assessed by counting invaded cells under the filter in 4 random filter regions. Data represent mean ± SEM. MCF-7-EMT *n* = 36; T47D-EMT *n* = 18; MDA-MB-231 *n* = 18;

(Continued)

FIGURE 1 | HCC1806 $n = 36$; $^{**}P < 0.01$; $^{****}P < 0.0001$ **(D)** 3D invasion analysis of breast cancer spheroids seeded after transient siRNA transfection. Spheroid area was assessed 48 h after adding Matrigel using polygonal selection and compared to spheroid area at time point 0 (adding of Matrigel). Area growth was compared to area growth of control spheroids. Data represent mean ± SEM. Using unpaired, two-tailed *t*-test analysis. MCF-7-EMT $n = 5$; T47D-EMT $n = 6$; MDA-MB-231 $n = 5$; HCC1806 $n = 6$; $^{**}P < 0.01$; $^{***}P < 0.005$ **(E)** 3D invasion analysis of breast cancer spheroids treated with recombinant human CYR61 (rhCYR61). Spheroid area was assessed 48 h after adding Matrigel and rhCYR61 using polygonal selection and compared to spheroid area at time point 0 (adding of Matrigel+ rhCYR61). Area growth was compared to area growth of control spheroids. Data represent mean ± SEM. Using unpaired, two-tailed *t*-test analysis. MCF-7 $n = 3$; T47D $n = 3$; $^{***}P < 0.005$ **(F)** Proteolytic activity of non-invasive breast cancer cells treated with rhCYR61 was asses by measurement of fluorescence 24 h after seeding cells on wells coated with FITC-labeled gelatin. Relative proteolytic activity of rhCYR61 treated cells was compared to proteolytic activity of control cells. Data represent mean ± SEM. Using unpaired, two-tailed *t*-test analysis. MCF-7 $n = 3$; T47D $n = 3$ $^{*}P < 0.05$.

cell in % compared to MCF-7-EMT control; $n = 36$; $P = 0.0321$; T47D-EMT S100A4$^-$:66.29 ± 8.52 SEM invaded cells in % to T47D-EMT control; $n = 36$; $P = 0.0303$; MDA-MB-231 S100A4$^-$:65.02 ± 5.58 SEM invaded cells in % to MDA-MB-231 control; $n = 24$; $P = 0.0003$; HCC1806 S100A4$^-$: 51.84 ± 4.62 invaded cells in % to HCC1806 control; $n = 36$; $P < 0.0001$). Furthermore, decreased S100A4 expression reduces 3D spheroid invasion area of mesenchymal transformed and TNBC cells (**Figure 2E**; MCF-7-EMT S100A4$^-$: 82.77 ± 2.82 SEM invaded area in % compared to MCF-7-EMT control; $n = 6$; $P = 0.0001$; T47D-EMT S100A4$^-$: 78.24 ± 4.17 SEM invaded area in % to T47D-EMT control; $n = 6$; $P = 0.0004$; MDA-MB-231 S100A4$^-$: 47.93 ± 7.95 SEM invaded area in % to MDA-MB-231 control; $n = 12$; $P < 0.0001$; HCC1806 S100A4$^-$: 67.97 ± 5.46 invaded area in % to HCC1806 control; $n = 6$; $P = 0.0002$), while proliferation was not altered (**Figure 2**, **Figure S3E**). To assess whether extracellular CYR61 can counteract the S100A4 suppressive effect on 3D spheroid invaded area, spheroids with suppressed S100A4 were treated with rhCYR61. Decreased S100A4 expression and additional increased extracellular CYR61 expression lead to an increased spheroid invaded area (**Figure 2F**; MCF-7-EMT S100A4$^-$+rhCYR61: 112.8 ± 4.97 SEM invaded area in % compared to MCF-7-EMT S100A4$^-$; $n = 4$; $P = 0.0415$; T47D-EMT S100A4$^-$+rhCYR61: 118.9 ± 4.36 SEM invaded area in % compared to T47D-EMT S100A4$^-$; $n = 6$; $P = 0.0015$; MDA-MB-231 S100A4$^-$+rhCYR61: 174.2 ± 33.83 invaded area in % compared to MDA-MB-231 S100A4$^-$; $n = 5$; $P = 0.0596$; HCC1806 S100A4$^-$+rhCYR61: 116.3 ± 6.85 invaded area in % compared to HCC1806 S100A4$^-$; $n = 6$; $P = 0.0383$). These data indicate a close correlation between CYR61 and S100A4 expression and the invasiveness of mesenchymal transformed and TNBC cells *in vitro*.

ERK1/2 Activity Is Transducer of CYR61 Mediated S100A4 Regulation

We found that decreased CYR61 resulted in a decreased S100A4 expression. Despite it remains elusive how CYR61 regulates S100A4 expression. To elucidate underlying intracellular mechanism we tested, whether decreased CYR61 expression reduces the phosphorylation of ERK1/2 thereby regulating S100A4 expression (**Figure 3A**). Mesenchymal transformed and TNBC cells shows a decreased ERK1/2 expression, while ERK1/2 phosphorylation was increased compared to non-invasive estrogen positive breast cancer cells (**Figure 3B**). Reducing CYR61 expression led to a decreased ERK1/2 phosphorylation (**Figure 3C**). MEK1 and MEK2 are upstream regulators of ERK1/2 activity (28) By using U0126 inhibitor, ERK phosphorylation can be diminished (29). Blocking ERK1/2 phosphorylation due to an MEK1 and MEK2 specific inhibitor U0126 (verification of U0126 induced blocking of ERK1/2 phosphorylation **Figure 3**, **Figure S4A**) resulted in a decreased S100A4 expression (**Figure 3D**; MCF-7-EMT U0126: 0.89 ± 0.02 SEM relative S100A4 expression compared to MCF-7-EMT DMSO; $n = 3$; $P = 0.0114$; T47D-EMT U0126: 0.38 ± 0.07 SEM relative S100A4 expression compared to T47D-EMT DMSO control; $n = 3$; $P = 0.0009$; MDA-MB-231 U0126: 0.85 ±0.02 SEM relative S100A4 expression compared to MDA-MB-231 DMSO; $n = 3$; $P = 0.0026$; HCC1806 U0126: 0.71 ± 0.06 SEM relative S100A4 expression compared to HCC1806 DMSO; $n = 3$; $P = 0.0076$). Furthermore, U0126 treatment reduced 3 D spheroid invaded area (**Figure 3E**; MCF-7-EMR U0126: 47.52 ± 5.77 SEM invaded area in % compared to MCF-7-EMT DMSO; $n = 6$; $P < 0.0001$; T47D-EMT U0126: 71.51 ± 2.61 SEM invaded area in % compared to T47D-EMT DMSO; $n = 5$; $P < 0.0001$; MDA-MB-231 U0126: 35.31 ± 10.91 SEM invaded area in % compared to MDA-MB-231 DMSO; $n = 6$; $P = 0.0002$; HCC1806 U0126: 85.01 ± 4.05 SEM invaded area in % compared to HCC1806 DMSO; $n = 5$; $P = 0.006$). Treatment with U0126 reduced proliferation in 3D spheroids (**Figure 3F**; MCF-7-EMT U0126: 86.57 ± 2.11 SEM relative AlamarBlue reduction in % compared to MCF-7-EMT DMSO; $n = 3$; $P = 0.0031$; T47D-EMT U0126: 67.53 ± 8.61 SEM relative AlamarBlue reduction compared to T47D-EMT DMSO; $n = 4$; $P = 0.0093$; MDA-MB-231 U0126:52.23 ± 13.32 SEM relative AlamarBlue reduction in % compared to MDA-MB-231 DMSO; $n = 3$; $P = 0.023$; HCC1806 U0126: 70.37 ± 9.29 SEM relative AlamarBlue reduction in % compared to HCC1806 DMSO; $n = 3$; $P = 0.0332$). Moreover, treating non-invasive estrogen positive breast cancer cell spheroids with rhCYR61 lead to increased ERK1/2 phosphorylation (**Figure 3**, **Figure S4B**). These results suggest that decreased ERK1/2 phosphorylation suppresses S100A4 expression. Moreover, ERK1/2 phosphorylation is reduced by decreased CYR61 expression.

Suppression of YAP1 Reduces Invasiveness Through Altering CYR61-S100A4-pERK1/2 Signaling

Yes-associated protein (YAP) is a known upstream target of CYR61 in breast cancer (30). Validating that the observed results can be reproduced by altering YAP expression (**Figure 4A**), YAP was transiently decreased (verification **Figure 4**, **Figure S5A**). Decreased YAP expression reduced invaded area of 3 D spheroids

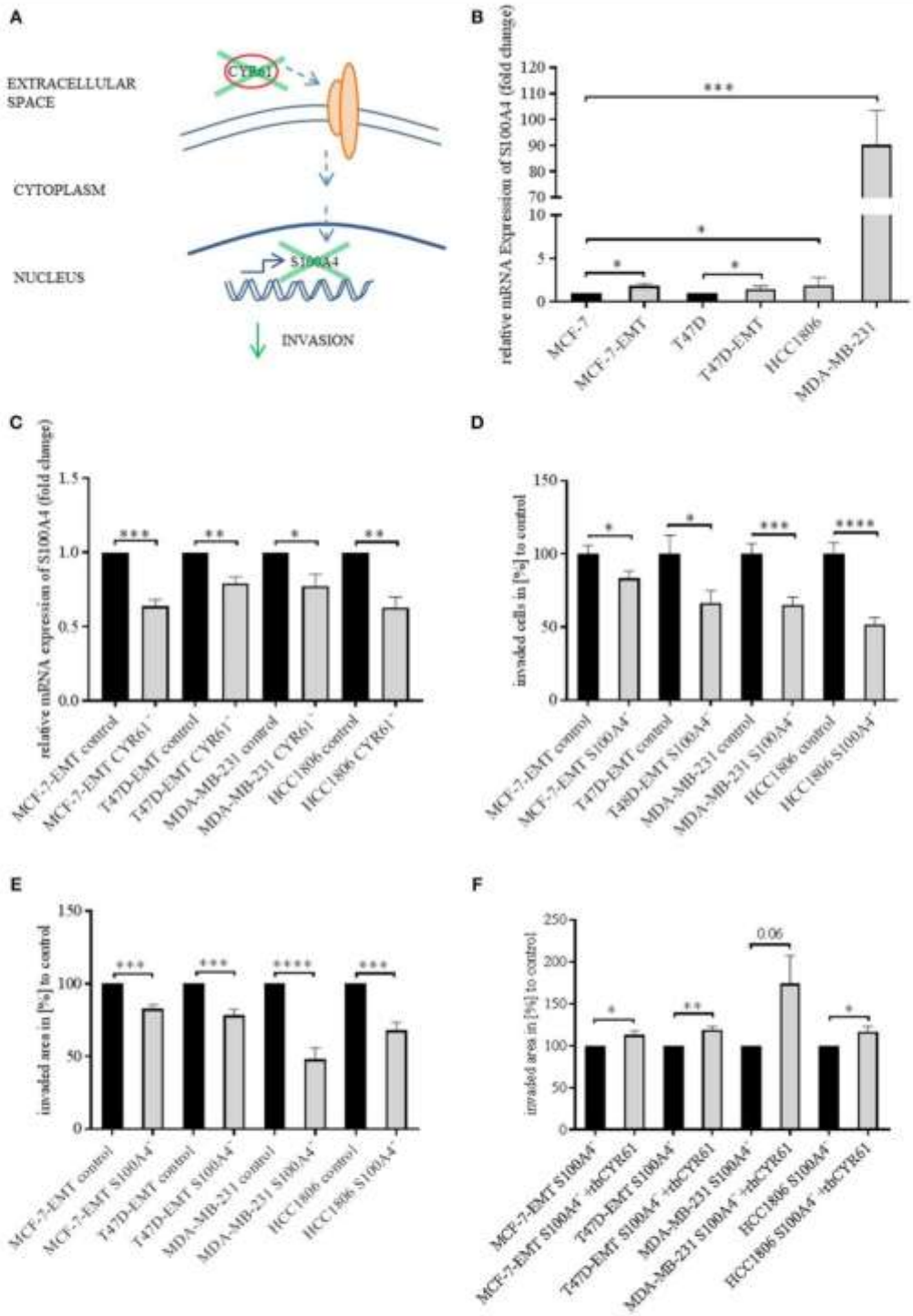

FIGURE 2 | Suppression of CYR61 reduces S100A4 expression. **(A)** Scheme illustrating hypothesis of CYR61-dependent cell invasion regulation. **(B)** Relative S100A4 expression of invasive breast cancer cell lines compared to non-invasive controls. Data represent mean ± SEM. Using unpaired, two-tailed *t*-test analysis. MCF-7-EMT $n = 5$; T47D-EMT $n = 5$; MDA-MB-231 $n = 4$; HCC1806 $n = 6$; $^{*}P < 0.05$; $^{***}P < 0.005$ **(C)** Relative S100A4 expression of invasive breast cancer cell lines 96 h after transient CYR61 transfection compared to non-invasive controls. Data represent mean ± SEM. Using unpaired, two-tailed *t*-test analysis. MCF-7-EMT

(Continued)

FIGURE 2 | $n = 4$; T47D-EMT $n = 3$; MDA-MB-231 $n = 4$; HCC1806 $n = 3$; $^*P < 0.05$; $^{**}P < 0.01$; $^{***}P < 0.005$ **(D)** 2D Invasion analysis of co-cultured (MG-63, osteosarcoma cells) breast cancer cells transient transfected with S100A4 siRNA for 96 h. Percentage of cell invasion compared to controls was assessed by counting invaded cells under the filter in 4 random filter regions. Data represent mean ± SEM. MCF-7-EMT $n = 36$; T47D-EMT $n = 36$; MDA-MB-231 $n = 24$; HCC1806 $n = 36$; $^*P < 0.05$; $^{***}P < 0.005$; $^{****}P < 0.0001$ **(E)** 3D invasion analysis of breast cancer spheroids seeded after transient siRNA transfection. Spheroid area was assessed 48 h after adding Matrigel using polygonal selection and compared to spheroid area at time point 0 (adding of Matrigel). Area growth was compared to area growth of control spheroids. Data represent mean ± SEM. Using unpaired, two-tailed *t*-test analysis. MCF-7-EMT $n = 6$; T47D-EMT $n = 6$; MDA-MB-231 $n = 12$; HCC1806 $n = 6$; $^{***}P < 0.005$; $^{****}P < 0.0001$ **(F)** 3D invasion analysis of breast cancer spheroids seeded after transient S100A4 siRNA transfection and treated with rhCYR61. Spheroid area was assessed 48 h after adding Matrigel and rhCYR61 using polygonal selection and compared to spheroid area at time point 0 (adding of Matrigel + rhCYR61). Area growth was compared to area growth of S100A4- spheroids. Data represent mean ± SEM. Using unpaired, two-tailed *t*-test analysis. MCF-7-EMT $n = 4$; T47D-EMT $n = 4$; MDA-MB-231 $n = 5$; HCC1806 $n = 6$; $^*P < 0.05$; $^{**}P < 0.001$.

(**Figure 4B**; MCF-7-EMT YAP$^-$:87.48 ± 3.84 SEM invaded area in % compared to MCF-7-EMT control; $n = 4$; $P = 0.0172$; T47D-EMT YAP$^-$: 76.23 ± 5.1 SEM invaded area in % compared to T47D-EMT control; $n = 5$; $P = 0.0016$; MDA-MB-231 YAP$^-$: 47 ± 12.39 SEM invaded area in % compared to MDA-MB-231 control; $n = 12$; $P = 0.0003$; HCC1806 YAP$^-$: 60.67 ± 7.38 SEM invaded area in % compared to HCC1806 control), while proliferation was not altered (**Figure 4**, **Figure S5B**). Decreased YAP expression reduces CYR61 expression (**Figure 4C**; MCF-7-EMT YAP$^-$: 0.79 ± 0.05 SEM relative CYR61 expression compared to MCF-7-EMT control; $n = 3$; $P = 0.01$; T47D-EMT YAP$^-$: 0.82 ± 0.05 SEM relative CYR61 expression compared to T47D-EMT control; $n = 3$; $P = 0.0269$; MDA-MB-231 YAP$^-$: 0.74 ± 0.03 SEM relative CYR61 expression compared to MDA-MB-231 control; $n = 3$; $P = 0.0008$; HCC1806 YAP$^-$: 0.54 ± 0.12 SEM relative CYR61 expression compared to HCC1806 control; $n = 3$; $P = 0.0198$) and S100A4 expression (**Figure 4D**; MCF-7-EMT YAP$^-$: 0.86 ± 0.04 SEM relative S100A4 expression compared to MCF-7-EMT control; $n = 3$; $P = 0.0362$; T47D-EMT YAP$^-$: 0.72 ± 0.08 SEM relative S100A4 expression compared to T47D-EMT control; $n = 3$; $P = 0.0289$; MDA-MB-231 YAP$^-$: 0.88 ± 0.03 SEM relative S100A4 expression compared to MDA-MB-231 control; $n = 3$; $P = 0.0179$; HCC1806 YAP$^-$: 0.78 ± 0.04 SEM relative S100A4 expression compared to HCC1806 control; $n = 3$; $P = 0.0067$). Furthermore, decreased YAP expression reduces ERK1/2 phosphorylation (**Figure 4E**). Transient decreased YAP expression in mesenchymal transformed and TNBC cells treated with rhCYR61 show no impact on spheroid invaded area (**Figure 4F**). Collectively, these data suggest that decreased YAP expression leads to a CYR61, pERK1/2 and S100A4 suppression. The effect of decreased YAP expression on spheroid invaded area can be restored be supplemented extracellular CYR61.

CYR61 and S100A4 as Prognostic Markers for Invasive and Metastatic Breast Cancer

To assess the value of CYR61 and S100A4 as prognostic marker meta-analysis were conducted. Reduced CYR61 expression increases the probability of distant-metastasis free survival (DMFS) of breast cancer patients with a lymph node positive status (**Figure 5A**; dataset 213226_at; $n = 382$; FDR 1%; $P = 2.8\ e^{-07}$). Reduced S100A4 expression increases the probability of DMFS of breast cancer patients with a lymph node positive status but shows a higher FDR (**Figure 5B**; dataset 203186_s_at; $n = 382$; FDR > 50%; $P = 0.024$, cut-off values see **Figure 5**, **Figure S6**). Analyzing the effects of decreases CYR61 or S100A4 expression with regards to the relapse free survival (RFS) shows comparable results (**Figures 5C,D**; CYR61: dataset 213226_at; $n = 1133$; FDR 1%; $P = 6.8\ e^{-09}$; S100A4: dataset 203186_s_at; FDR > 50%; $P = 0.0012$, cut-off values see **Figure 5**, **Figure S6**). These data demonstrate that CYR61 could act as a prognostic marker in breast cancer.

CYR61 and S100A4 as Therapeutic Target for Invasive and Metastatic Breast Cancer

CYR61 and S100A4 are drivers for breast cancer cell invasion *in vitro*. Consequently, we examined the value of CYR61 and/or S100A4 as a potential therapeutic target for advanced breast cancer. Analyzing the expression in 239 paraffin-fixed patient breast tissue sections (104 invasive breast cancer sections with corresponding metastatic lymph node section and progesterone receptor-, estrogen receptor- and Her2neu expression, BR20837; 17 invasive ductal,1 medullary carcinoma and 6 normal breast tissue sections, BR248a; 2 invasive ductal carcinomas, 1 invasive lobular carcinoma and 2 normal breast tissue section, T087a). Analyzing if expression was detected (immunofluorescence signal for CYR61 and/or S100A4 1-5 spots +; 5-10 spots ++; >10 spots + + +) or not (−), we find the following pattern: 90.2% of invasive ductal carcinomas were positive for CYR61 expression, 82% were positive for S100A4 expression and 78% showed both CYR61 and S100A4 expression (**Figure 6A** and **Figure S7**). Corresponding metastatic lymph node sections were in 96% positive for CYR61, in 75% positive for S100A4 and in 74% for both CYR61 and S100A4. TNBC tissue sections were in 97% positive for CYR61, in 75.8% positive for S100A4, and in 75.8% expressing both CYR61 and S100A4. Interestingly, CYR61 expression was only detected in 12.5% of normal breast tissue samples and S100A4 expression in none (**Figure 6D**, detailed list **Figure S7**). Visual expression of CYR61 and S100A4 in blood vessels (**Figure 6D**) could be found throughout all tissue sections. We find that the CYR61 and S100A4 expression appeared in very close localization to each other (**Figure 6**, white arrows) or even co-localized (**Figure 6**, white stars). These studies demonstrate that CYR61 and S100A4 could be valuable therapeutic targets and prognostic marker for invasive breast cancer and metastasis.

DISCUSSION

CYR61 is best recognized as regulator of inflammation and wound healing (31, 32). Several studies indicate that CYR61 can facilitate invasion and is crucial for EMT programs regarding

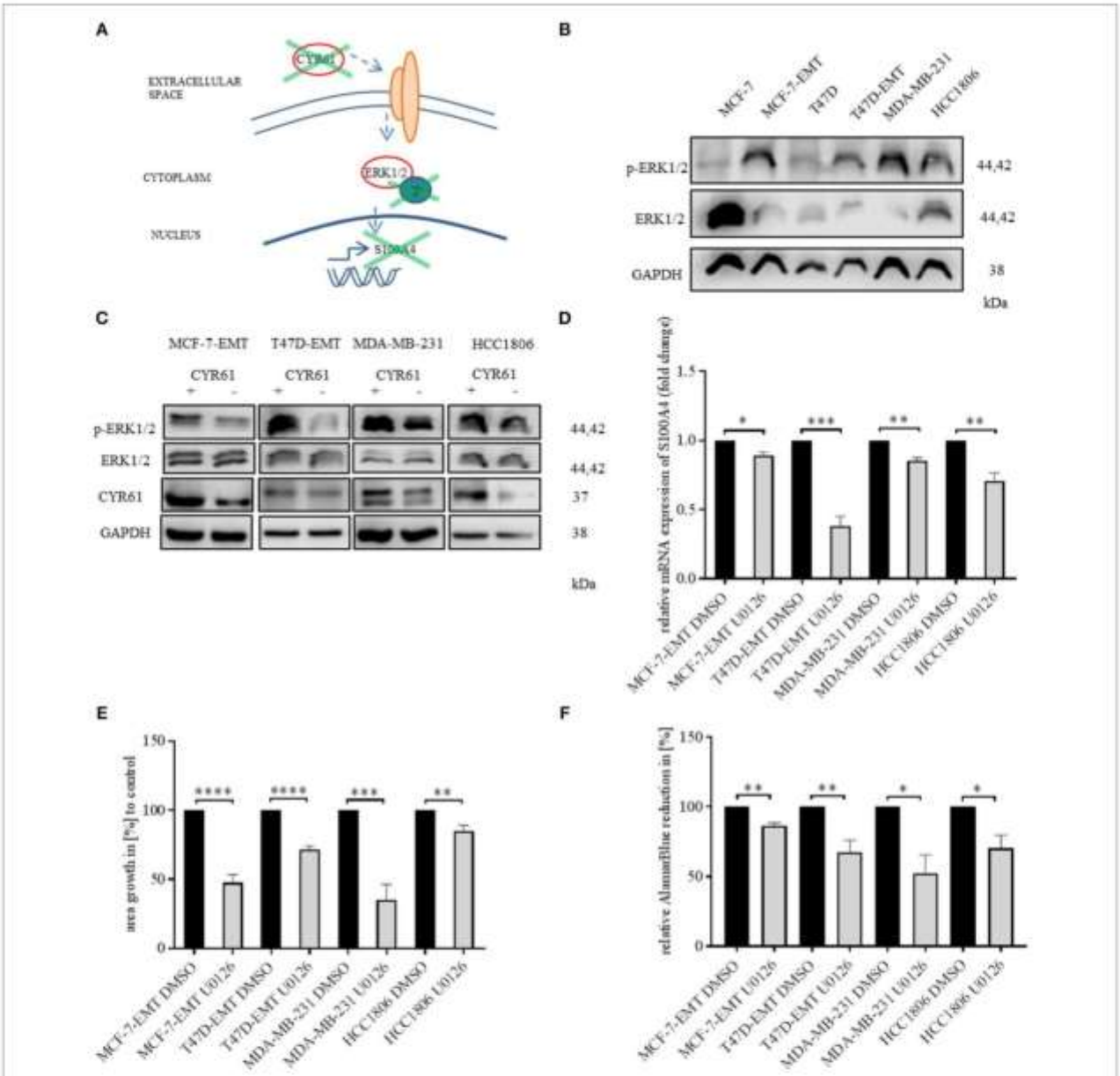

FIGURE 3 | ERK1/2 activity is transducer of CYR61 mediated S100A4 regulation. **(A)** Scheme illustrating hypothesis of CYR61 regulating S100A4 in a p-ERK1/2 dependent manner. **(B)** ERK1/2 and p-Erk1/2 (Thr202/Tyr204) expression in different breast cancer cell lines detected by western blotting. **(C)** ERK1/2 and p-Erk1/2 (Thr202/Tyr204) and CYR61 expression in different breast cancer cell lines after transient CYR61 transfection detected by western blotting. **(D)** Relative S100A4 expression of invasive breast cancer cell lines treated with 10 μM U0126 compared to DMSO controls. Data represent mean ± SEM. Using unpaired, two-tailed *t*-test analysis. $n = 3$; $^{*}P < 0.05$; $^{**}P < 0.01$; $^{***}P < 0.005$ **(E)** 3D invasion analysis of breast cancer spheroids seeded after U0126 treatment. Spheroid area was assessed 48 h after adding Matrigel using polygonal selection and compared to spheroid area at time point 0 (adding of Matrigel + 10 μM U0126). Area growth was compared to area growth of control spheroids. Data represent mean ± SEM. Using unpaired, two-tailed *t*-test analysis. MCF-7-EMT $n = 6$; T47D-EMT $n = 5$; MDA-MB-231 $n = 6$; HCC1806 $n = 5$; $^{**}P < 0.01$; $^{***}P < 0.005$; $^{****}P < 0.0001$ **(F)** Analysis of relative AlamarBlue reduction as indicator for cell viability. Breast cancer cell spheroids were grown and AlamarBlue reduction was assessed 48 h after adding Matrigel and 10 μM U0126 at 4 h incubation. Relative AlamarBlue reduction was calculated compared to DMSO control spheroids. Data represent mean ± SEM. MCF-7-EMT $n = 3$; T47D-EMT $n = 4$; MDA-MB-231 $n = 3$; HCC1806 $n = 3$; $^{*}P < 0.05$; $^{**}P < 0.01$.

cancer progression (12, 15, 16, 23). The question remains how CYR61 facilitates invasion in breast cancer and which role it possesses regarding EMT complexity (4). Since CYR61 has known oncogenic functions in serval tumor entities (12, 13), including breast cancer (15, 16), the question appeared if CYR61 might be a valuable therapeutic target in aggressive breast cancer

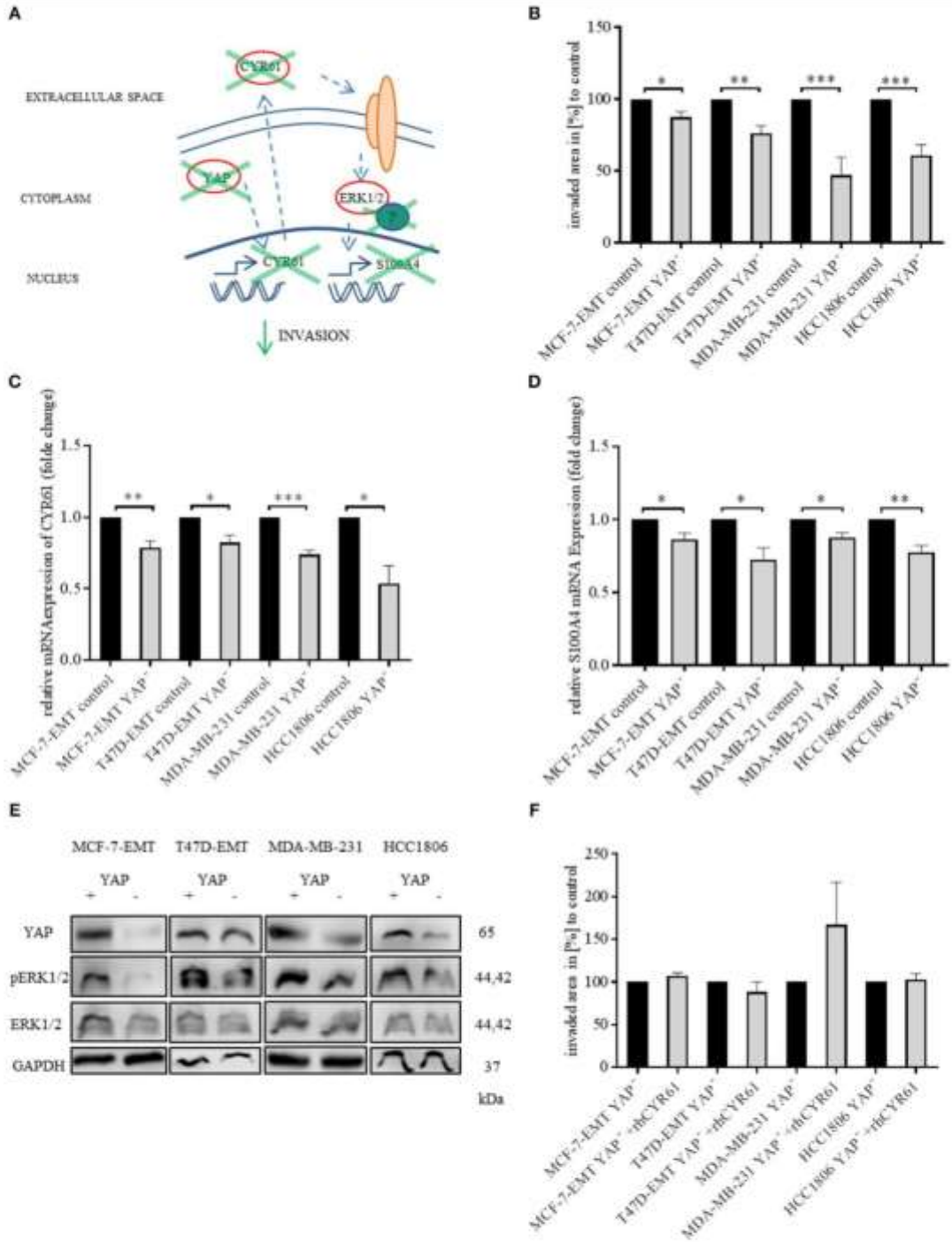

FIGURE 4 | Suppression of YAP reduces invasiveness through blocking CYR61-S100A4-pERK1/2 signaling. **(A)** Scheme illustrating hypothesis of YAP regulating S100A4 in a CYR61 - p-ERK1/2 dependent manner. **(B)** 3D invasion analysis of breast cancer spheroids seeded after transient YAP siRNA transfection. Spheroid area was assessed 48 h after adding Matrigel using polygonal selection and compared to spheroid area at time point 0 (adding of Matrigel). Area growth was compared to area growth of control spheroids. Data represent mean ± SEM. Using unpaired, two-tailed *t*-test analysis. MCF-7-EMT $n = 4$; T47D-EMT $n = 5$; MDA-MB-231 $n = 12$; HCC1806 $n = 8$; $^*P < 0.05$; $^{**}P < 0.01$; $^{***}P < 0.005$ **(C)** Relative CYR61 expression of invasive breast cancer cell lines 48 h after transient YAP siRNA compared to controls. Data represent mean ± SEM. Using unpaired, two-tailed *t*-test analysis. $n = 3$;$^*P < 0.05$; $^{**}P < 0.01$; $^{***}P < 0.005$ **(D)** Relative S100A4 expression of invasive breast cancer cell lines 48 h after transient YAP siRNA compared to controls. Data represent mean ± SEM. Using unpaired, two-tailed *t*-test analysis.

(Continued)

FIGURE 4 | $n = 3$; $^*P < 0.05$; $^{**}P < 0.01$; **(E)** ERK1/2, p-Erk1/2 (Thr202/Tyr204) and YAP expression in different breast cancer cell lines after transient YAP siRNA transfection detected by western blotting. **(F)** 3D invasion analysis of breast cancer spheroids seeded after transient YAP siRNA transfection and treated with rhCYR61. Spheroid area was assessed 48 h after adding Matrigel and rhCYR61 using polygonal selection and compared to spheroid area at time point 0 (adding of Matrigel + rhCYR61). Area growth was compared to area growth of YAP- spheroids. Data represent mean ± SEM. Using unpaired, two-tailed *t*-test analysis. MCF-7-EMT $n = 6$; T47D-EMT $n = 6$; MDA-MB-231 $n = 4$; HCC1806 $n = 6$.

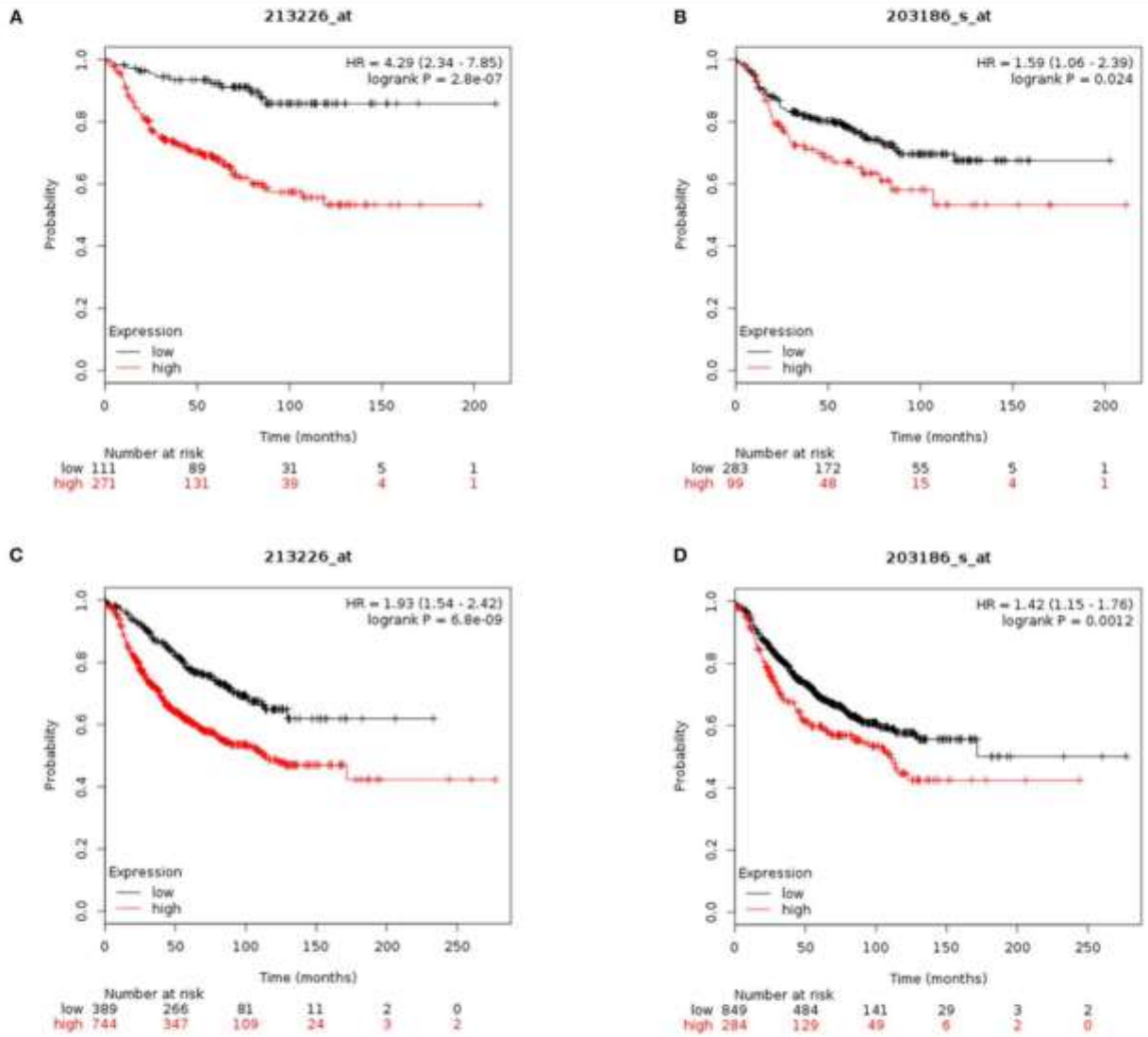

FIGURE 5 | CYR61 and S100A4 as prognostic marker for breast cancer progression. **(A)** Probability of distant metastasis free survival (DMFS) in 382 breast cancer patients with lymph node positive status according to CYR61expression level. Kaplan–Meier plots were generated using Kaplan–Meier plotter (www.kmplot.com) data set 213226_at with a false-discovery rate (FDR) of 1%. Black line illustrates high CYR61 expression group and red line illustrates low CYR61 expression group. **(B)** Probability of DMFS in 382 breast cancer patients with lymph node positive status according to S100A4 expression level. Kaplan–Meier plots were generated using Kaplan–Meier plotter (www.kmplot.com) data set 203186_at with a false-discovery rate (FDR) over 50%. Black line illustrates high S100A4 expression group and red line illustrates low S100A4 expression group. **(C)** Probability of remission free survival (RFS) in 1133 breast cancer patients with lymph node positive status according to CYR61 expression level. Kaplan–Meier plots were generated using Kaplan–Meier plotter (www.kmplot.com) data set 213226_at with a false-discovery rate (FDR) of 1%. Black line illustrates high CYR61 expression group and red line illustrates low CYR61 expression group. **(D)** Probability of RFS in 1133 breast cancer patients with lymph node positive status according to CYR61 expression level. Kaplan–Meier plots were generated using Kaplan–Meier plotter (www.kmplot.com) data set 203186_at with a false-discovery rate (FDR) over 50 %. Black line illustrates high S100A4 expression group and red line illustrates low S100A4 expression group. HR, hazard ratio.

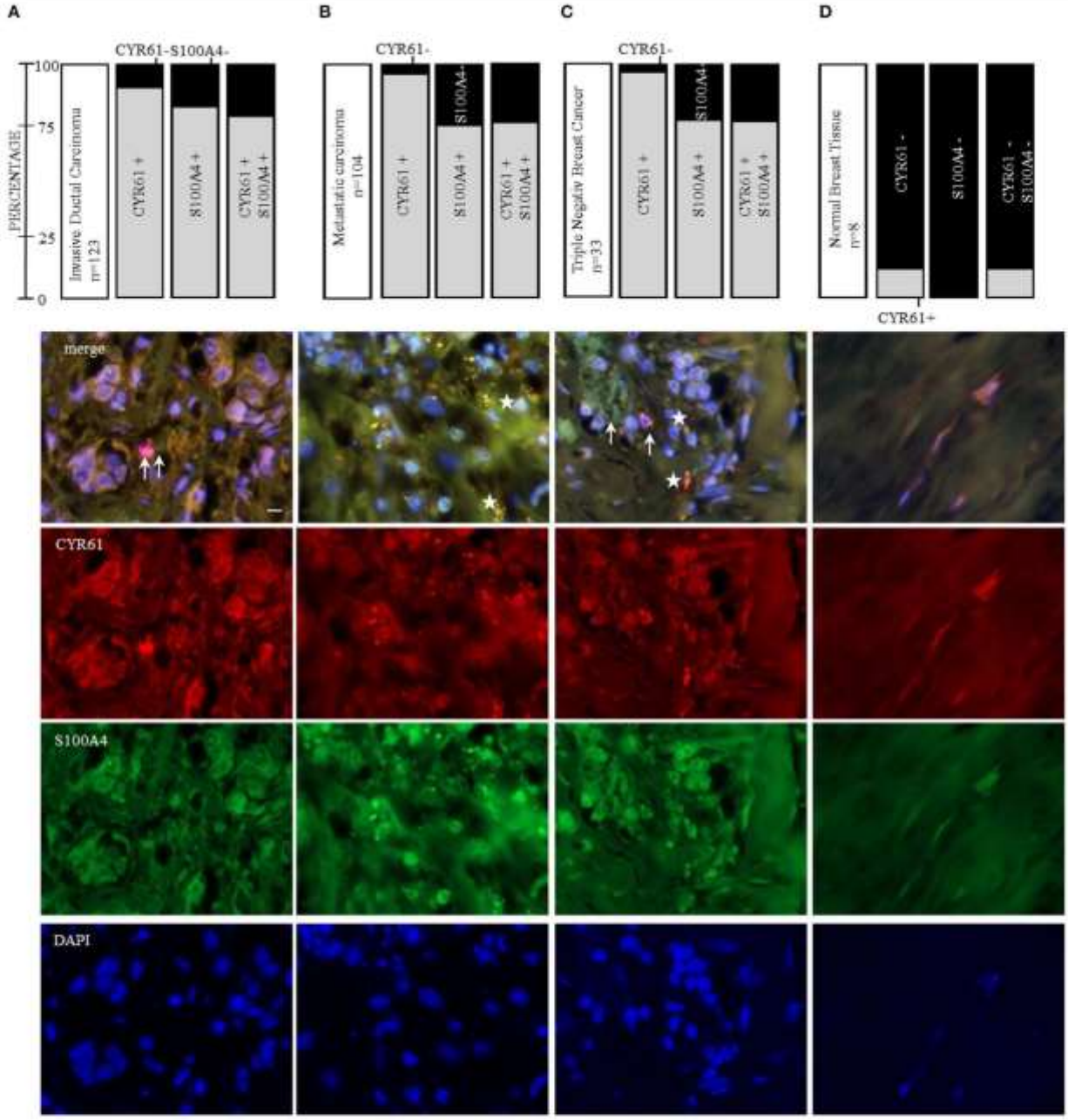

FIGURE 6 | CYR61 and S100A4 as therapeutic target for invasive and metastatic breast cancer. Immunofluorescence staining of three tissue arrays (biomax) containing 104 invasive ductal carcinoma tissue sections with corresponding metastatic carcinomas, further 21 invasive ductal carcinoma tissue sections and 8 normal breast tissue sections. With 33 of the carcinoma tissue sections being negative for the estrogen receptor and progesterone receptor and do not overexpress the Her2neu receptor (triple negative breast cancer, TNBC). **(A)** CYR61 and/or S100A4 expression analysis in 123 invasive ductal carcinoma tissue sections and corresponding lymph node sections from 104 patients **(B)** and representative immunofluorescence staining analyzed with a 100x oil objective (Axio ZEISS). **(C)** Within the 123 invasive ductal carcinomas patient tissue sections 33 were stated as being TNBC. **(D)** Normal breast tissue sections ($n = 8$) were analyzed for their CYR61 and/ or S100A4 expression using immunofluorescence staining. Scale bar gauges 20 μm.

and if it could be a prognostic marker for these indications. We report that a higher CYR61 expression correlates with a poor prognosis of breast cancer patients. Moreover, we found that reducing the CYR61 expression leads to a decreased invasion in 2D and 3D invasion analysis setups, showing comparable results. Suggesting that reduced invasion upon CYR61 suppression is

due to reduces ERK1/2 phosphorylation and S100A4 expression. CYR61 might be a valuable therapeutic target and prognostic marker for invasive and metastatic breast cancer.

Triple negative breast cancers (TNBC) account for 15–20% of all breast cancer incidents and there is no specific targeted therapy available (33). There is a need for identifying new targets for future therapy options. Consistent with previous published results we could demonstrate that CYR61 expression is increased in TNBC cell line MDA-MB-231 (34) and further more in the TNBC cell line HCC1806. The contribution of EMT-induced expression changes to the invasion and metastatic cascade regarding cancer progression is highly debated and needs to be interpreted cell and tissue specific (4, 8, 35). Mesenchymal transformed breast cancer cells show an increased expression of CYR61 and S100A4 (23), which we could reproduce in our setting. It was shown that S100A4 facilitates breast cancer invasion (36). Gründker et al. demonstrated that suppressing extracellular signaling of CYR61 and S100A4 decreased the ability of breast cancer cell invasion in a co-cultural setting mimicking bone metastasis (23). It was not tested how the intracellular signaling is affected when CYR61 or S100A4 expression is reduced. We report here that transient gene silencing of either CYR61 or S100A4 can reduce invasiveness in mesenchymal transformed and TNBC cells. To further assess the impact of CYR61 on breast cancer cell invasion we increased extracellular CYR61 expression in non-invasive breast cancer cells and could show that this led to an increased invasive behavior. These findings indicate that CYR61 could be a regulator of breast cancer cells invasion. We showed that reversing EMT-induced upregulation of CYR61 and S100A4 leads to reduced invasive behavior in breast cancer cells in different invasion setups. This could indicate a role of EMT within this process. Further research is necessary to assess, if modulating CYR61 regulates EMT-TFs and thereby facilitates cellular plasticity. It has been suggested that targeting EMT-TFs could help to overcome chemo resistance and recent findings suggest an involvement of CYR61 in resistance to certain therapies in different tumor entities (5, 37, 38).

Despite, it was unclear how CYR61 regulates invasiveness of breast cancer cells. We suggest that CYR61 regulates S100A4 expression in mesenchymal transformed and TNBC cells through regulating ERK1/2 phosphorylation. Reducing S100A4 expression leads to decreased 3 D spheroid invasion and invasiveness of breast cancer cells in co-culture with osteosarcoma cells. Adding extracellular CYR61 to breast cancer spheroids with transient decreased S100A4 expression could restore the effect und led to a slightly increased invaded area. Hou et al. suggested that regulating CYR61 in osteosarcoma cells targets the MEK-ERK pathway (12). ERK1/2 signaling is gaining higher interest since the unique ERK1/2 position within cellular signaling. Targeting ERK1/2 could be valuable for therapy-resistant cancer to known clinically used BRAF and MEK inhibitors (39). We could show that inhibition of ERK1/2 phosphorylation led to decreased 3D spheroid invasion and reduced spheroid proliferation. Inhibition of ERK1/2 phosphorylation led to decreased S100A4 expression. But S100A4 decreased expression by itself had no impact on spheroid proliferation, neither had CYR61 or YAP transient suppression.

YAP is regulated negatively through the Hippo-Pathway, which regulates key events of organ size, development and angiogenesis (40–42). Regarding breast cancer YAP is reported to have dual function as oncogene and tumor suppressor (43). Higher YAP expression correlates with increased EMT marker expression (44). We suggest that reduced YAP expression leads to decreased 3D spheroid invasion by suppression of CYR61, p-ERK1/2 and S100A4. The effect of reduced YAP expression on 3D invasion could be restored by extracellular CYR61 addition.

CYR61 or S100A4 are suggested to be valuable prognostic markers regarding several tumor entities (45–48). Egeland et al. suggested the use of S100A4 as a prognostic marker for early-stage breast cancer (49). We examined whether CYR61 and S100A4 could be valuable prognostic marker for invasive and metastatic breast cancer. CYR61 and S100A4 are highly expressed in invasive-ductal carcinomas, including TNBC, and both are expressed in metastatic lymph node sections. Of all analyzed tissue sections 82.2% expressing CYR61 did express S100A4, respectively, which lead to the conclusion, that CYR61 together with S100A4 would be valuable prognostic marker for breast cancer and breast cancer metastasis. Moreover, we found that expression of CYR61 and S100A4 is closely located (**Figure 6**, indicated by arrow) or even co-localized (**Figure 6**, indicated by star). Considering that CYR61 regulates cancer invasion and the findings, that it may be a valuable prognostic marker in different cancer entities (45, 46, 50, 51), It was suggested before, that CYR61 regulates E-cadherin, N-cadherin and Twist in osteosarcoma cells (12). Further investigations should clarify if CYR61 suppression regulates EMT-TFs in breast cancer and facilitates invasion by altering ECM degradation and adhesion. Secretome analysis of co-cultured cancer cells could identify secreted proteins, like matricellular proteins, that are drivers for invasion and promote metastasis.

Our findings suggest that CYR61 plays a major role in breast cancer invasion. This impact is facilitated through the regulation of ERK phosphorylation and S100A4 expression. Moreover, targeting YAP, a CYR61 upstream regulator, regulates CYR61, ERK phosphorylation and S100A4. We could identify a close correlation between CYR61 and S100A4 expression and breast cancer invasion and metastasis in breast cancer patients. CYR61 together with S100A4 might be utilized as therapeutic target and prognostic marker for invasive breast cancer and metastasis.

DATA AVAILABILITY STATEMENT

The datasets used and/or analyzed during the current study are available from the corresponding author on reasonable request.

AUTHOR CONTRIBUTIONS

Conception and design of the reported work was done by JH and CG. JH, GB, and CG did the development of methodology used. JH and SH performed invasion assays. JH and LG

contributed to protein expression analysis. JH contributed to immune histochemical staining, gene expression analysis, proliferation analysis, *in silico* and network analysis. Analysis and interpretation of data was performed by JH, SH, LG, GB, GE, and CG. All authors read and approved the final manuscript.

FUNDING

Research reported in this publication was supported, by the Deutsche Krebshilfe grant 70112534.

ACKNOWLEDGMENTS

We would like to thank Sonja Blume for her excellent technical assistance. The group of Dr. Florian Wegwitz for fruitful discussions. Moreover, we appreciate the valuable suggestions of the reviewers.

SUPPLEMENTARY MATERIAL

The Supplementary Material for this article can be found online at: https://www.frontiersin.org/articles/10.3389/fonc.2019.01074/full#supplementary-material

Figure S1 | CYR61 expression correlates with breast cancer cell invasiveness. **(A)** Relative transforming growth factor beta induced (TGFBI) expression of mesenchymal transformed breast cancer cell lines compared to non-invasive controls was assessed using real-time quantitative PCR. Data represent mean ± SEM. Using unpaired, two-tailed *t*-test analysis. MCF-7-EMT $n = 3$; T47D-EMT $n = 6$; $^{***}P < 0.0005$; $^{****}P < 0.0001$ **(B)** Relative E-cadherin expression of mesenchymal transformed breast cancer cell lines compared to non-invasive controls was assessed using real-time quantitative PCR. Data represent mean ± SEM. Using unpaired, two-tailed *t*-test analysis. MCF-7-EMT $n = 4$; T47D-EMT $n = 3$; $^{*}P < 0.05$; $^{****}P < 0.0001$ **(C)** Relative Vimentin expression of mesenchymal transformed breast cancer cell lines compared to non-invasive controls was assessed using real-time quantitative PCR. Data represent mean ± SEM. Using unpaired, two-tailed *t*-test analysis. MCF-7-EMT $n = 5$; T47D-EMT $n = 3$; $^{*}P < 0.05$ **(D)** Relative Zeb1 expression of mesenchymal transformed breast cancer cell lines compared to non-invasive controls was assessed using real-time quantitative PCR. Data represent mean ± SEM. Using unpaired, two-tailed *t*-test analysis. MCF-7-EMT $n = 4$; T47D-EMT $n = 3$; $^{*}P < 0.05$ **(E)** Relative SNAI1 expression of mesenchymal transformed breast cancer cell lines compared to non-invasive controls was assessed using real-time quantitative PCR. Data represent mean ± SEM. Using unpaired, two-tailed *t*-test analysis. MCF-7-EMT $n = 4$; T47D-EMT $n = 5$; $^{***}P < 0.0005$ **(F)** Relative SNAI2 expression of mesenchymal transformed breast cancer cell lines compared to non-invasive controls was assessed using real-time quantitative PCR. Data represent mean ± SEM. Using unpaired, two-tailed *t*-test analysis. MCF-7-EMT $n = 3$; T47D-EMT $n = 4$; $^{*}P < 0.05$.

Figure S2 | CYR61 expression correlates with breast cancer cell invasiveness. **(A)** Relative CYR61 expression 96 h after transient CYR61 siRNA transfection compared to control was assessed using real-time quantitative PCR. Data represent mean ± SEM. Using unpaired, two-tailed *t*-test analysis. MCF-7-EMT $n = 8$; T47D-EMT $n = 7$; MDA-MB-231 $n = 3$; HCC1806 $n = 4$; $^{**}P < 0.01$; $^{***}P < 0.0001$ **(B)** Analysis of relative AlamarBlue reduction as indicator for cell viability. Transient transfected breast cancer cell spheroids were grown and AlamarBlue reduction was assessed 48 hours after adding Matrigel at 4 h incubation. Relative AlamarBlue reduction was calculated compared to control spheroids. Data represent mean ± SEM. $n = 3$ **(C)** Analysis of relative AlamarBlue reduction as indicator for cell viability. Breast cancer cell spheroids were grown and AlamarBlue reduction was assessed 48 h after adding Matrigel and 1 µg/ml rhCYR61 at 4 h incubation. Relative AlamarBlue reduction was calculated compared to control spheroids. Data represent mean ± SEM. $n = 3$.

Figure S3 | Suppression of CYR61 reduces S100A4 expression. **(A)** Immunoblot analysis of S100A4 mRNA expression levels in different breast cancer cell lines 96 h after S100A4 siRNA transfection was detected using western blotting. Date represent mean ± SEM. Using unpaired, two-tailed *t*-test analysis. MCF-7-EMT $n = 4$; T47D-EMT $n = 4$; MDA-MB-231 $n = 3$; HCC1806 $n = 3$; $^{*}P < 0.05$; $^{**}P < 0.01$; $^{***}P < 0.005$ **(B)** Representative experiments of S100A4 protein expression quantification corresponding to **(A)**. **(C)** S100A4 mRNA expression analysis 96 h after siRNA transfection using quantitative PCR. Date represent mean ± SEM. Using unpaired, two-tailed *t*-test analysis. MCF-7-EMT $n = 4$; T47D-EMT $n = 4$; MDA-MB-231 $n = 3$; HCC1806 $n = 3$; $^{***}P<0.005$; $^{****}P<0.0001$ **(D)** CYR61 mRNA expression analysis 96 h after S100A4 siRNA transfection using quantitative PCR. Date represent mean ± SEM. MCF-7-EMT $n = 5$; T47D-EMT $n = 6$; MDA-MB-231 $n = 3$; HCC1806 $n = 3$ **(E)** Analysis of relative AlamarBlue reduction as indicator for cell viability. Breast cancer cell spheroids transient transfected with S100A4 siRNA were grown and AlamarBlue reduction was assessed 48 h after adding Matrigel at 4 h incubation. Relative AlamarBlue reduction was calculated compared to control spheroids. Data represent mean ± SEM. $n = 3$.

Figure S4 | ERK1/2 activity is transducer of CYR61 mediated S100A4 regulation. **(A)** ERK1/2 and p-Erk1/2 (Thr202/Tyr204) expression in different breast cancer cell lines with or without 10µM U0126 treatment detected by western blotting. **(B)** ERK1/2 and p-Erk1/2 (Thr202/Tyr204) expression in non-invasive breast cancer cell lines with or without 1µg/ml rhCYR61 treatment detected by western blotting.

Figure S5 | Suppression of YAP reduces invasiveness through blocking CYR61-S100A4-pERK1/2 signaling. **(A)** Relative YAP expression 96 h after transient YAP siRNA transfection compared to control was assessed using real-time quantitative PCR. Data represent mean ± SEM. Using unpaired, two-tailed *t*-test analysis. MCF-7-EMT $n = 5$; T47D-EMT $n = 3$; MDA-MB-231 $n = 3$; HCC1806 $n = 3$; $^{*}P < 0.05$; $^{**}P < 0.01$; $^{****}P < 0.001$ **(B)** Analysis of relative AlamarBlue reduction as indicator for cell viability. Breast cancer cell spheroids were grown and AlamarBlue reduction was assessed 48 hours after adding Matrigel at 4 h incubation. Relative AlamarBlue reduction was calculated compared to control spheroids. Data represent mean ± SEM. $n = 3$.

Figure S6 | CYR61 and S100A4 as prognostic marker for breast cancer progression. Cut-off values were downloaded from kmplot.com after target (dataset 213226_at = CYR61; dataset 203186_s_at = S100A4) specific analysis. RFS, relapse free survival; DMFS, distant metastasis free survival.

Figure S7 | CYR61 and S100A4 are highly expressed in invasive and metastatic B cancer patient tissue samples. Expression analysis of CYR61 and S100A4 via fluorescence staining using biomax tissue arrays (BR 20837,BR 248a, T087a) with paraffin-embedded patient samples. Table shows Arraytyp of analyzed samples, patients age, sex, the organic tissue site, pathology diagnosis, classification of M tumors (TNM), grading, stage, typ, tisse ID and for most analyzed tised the xpression of estrogen(ER), progesteron (PR) and Herceptinreceptor2 (Her2). Expression of CYR61 and S100A4 was assessed as (–) not expressed, (+) low expression, (++) medium expression, (+ + +) high expression.

REFERENCES

1. Noone AM, Howlader N, Krapcho M, Miller D, Brest A, Yu M, et al. (eds.). *SEER Cancer Statistics Review, 1975-2015*. Bethesda, MD: National Cancer Institute. Available online at: https://seer.cancer.gov/csr/1975_2015/ (accessed September 10, 2018).
2. Gupta GP, Massague J. Cancer metastasis: building a framework. *Cell.* (2006) 127:679–95. doi: 10.1016/j.cell.2006.11.001
3. Hanahan D, Weinberg RA. Hallmarks of cancer: the next generation. *Cell.* (2011) 144:646–74. doi: 10.1016/j.cell.2011.02.013
4. Brabletz T, Kalluri R, Nieto MA, Weinberg RA. Emt in cancer. *Nat Rev Cancer.* (2018) 18:128–34. doi: 10.1038/nrc.2017.118

5. Van Staalduinen J, Baker D, Ten Dijke P, Van Dam H. Epithelial–mesenchymal-transition-inducing transcription factors: new targets for tackling chemoresistance in cancer? *Oncogene.* (2018) 37:6195–211. doi: 10.1038/s41388-018-0378-x
6. Fischer KR, Durrans A, Lee S, Sheng J, Li F, Wong ST, et al. Epithelial-to-mesenchymal transition is not required for lung metastasis but contributes to chemoresistance. *Nature.* (2015) 527:472–6. doi: 10.1038/nature15748
7. Tran HD, Luitel K, Kim M, Zhang K, Longmore GD, Tran DD. Transient snail1 expression is necessary for metastatic competence in breast cancer. *Cancer Res.* (2014) 74:6330–40. doi: 10.1158/0008-5472.CAN-14-0923
8. Ye X, Brabletz T, Kang Y, Longmore GD, Nieto MA, Stanger BZ, et al. Upholding A role for emt in breast cancer metastasis. *Nature.* (2017) 547:E1–E3. doi: 10.1038/nature22816
9. Garg M. Epithelial, mesenchymal and hybrid epithelial/mesenchymal phenotypes and their clinical relevance in cancer metastasis. *Expert Rev Mol Med.* (2017) 19:E3. doi: 10.1017/erm.2017.6
10. Simeone P, Trerotola M, Franck J, Tristan C, Fournier I, Salzet M, et al. The multiverse nature of epithelial to mesenchymal transition. In: Vincent T, editor. *Seminars in Cancer Biology.* London: Academic Press Ltd-Elsevier Science Ltd (2018).
11. Kim YN, Choe SR, Cho KH, Cho DY, Kang J, Park CG, et al. Resveratrol suppresses breast cancer cell invasion by inactivating A Rhoa/yap signaling axis. *Exp Mol Med.* (2017) 49:E296. doi: 10.1038/emm.2016.151
12. Hou CH, Lin LL, Hou SM, Liu LF. Cyr61 promotes epithelial-mesenchymal transitionand tumor metastasis of osteosarcoma byraf-1/Mek/Erk/Elk-1/Twist-1 signaling pathway. *Mol Cancer.* (2014) 13:13. doi: 10.1186/1476-4598-13-236
13. Haque I, Mehta S, Majumder M, Dhar K, De A, Mcgregor D, et al. Cyr61/Ccn1 signaling is critical for epithelial-mesenchymal transition and stemness and promotes pancreatic carcinogenesis. *Mol Cancer.* (2011) 10:8. doi: 10.1186/1476-4598-10-8
14. Huang X, Xiang L, Li Y, Zhao Y, Zhu H, Xiao Y, et al. Snail/Foxk1/Cyr61 signaling axis regulates the epithelial-mesenchymal transition and metastasis in colorectal cancer. *Cell Physiol Biochem.* (2018) 47:590–603. doi: 10.1159/000490015
15. Tsai M-S, Bogart DF, Castañeda JM, Li P, Lupu R. Cyr61 promotes breast tumorigenesis and cancer progression. *Oncogene.* (2002) 21:8178. doi: 10.1038/sj.onc.1205682
16. Huang HT, Lan Q, Lorusso G, Duffey N, Rugg C. The matricellular protein Cyr61 promotes breast cancer lung metastasis by facilitating tumor cell extravasation and suppressing anoikis. *Oncotarget.* (2017) 8:16. doi: 10.18632/oncotarget.13677
17. Tong X, Xie D, O'kelly J, Miller CW, Muller-Tidow C, Koeffler HP. Cyr61, A member of Ccn family, is A tumor suppressor in non-small cell lung cancer. *J Biol Chem.* (2001) 276c47709–14. doi: 10.1074/jbc.M107878200
18. Jun JI, Lau LF. The matricellular protein Ccn1 induces fibroblast senescence and restricts fibrosis in cutaneous wound healing. *Nat Cell Biol.* (2010) 12:676–85. doi: 10.1038/ncb2070
19. Todorovic V, Chen CC, Hay N, Lau LF. The matrix protein Ccn1 (Cyr61) induces apoptosis in fibroblasts. *J Cell Biol.* (2005) 171:559–68. doi: 10.1083/jcb.200504015
20. Ziegler E, Hansen MT, Haase M, Emons G, Grundker C. Generation of Mcf-7 cells with aggressive metastatic potential *in vitro* and *in vivo*. *Breast Cancer Res Treat.* (2014) 148:269–77. doi: 10.1007/s10549-014-3159-4
21. Von Alten J, Fister S, Schulz H, Viereck V, Frosch KH, Emons G, et al. Gnrh analogs reduce invasiveness of human breast cancer cells. *Breast Cancer Res Treat.* (2006) 100:13–21. doi: 10.1007/s10549-006-9222-z
22. Vinci M, Box C, Eccles SA. Three-dimensional (3D) tumor spheroid invasion assay. *J Vis Exp.* (2015) e52686. doi: 10.3791/52686
23. Grundker C, Bauerschmitz G, Schubert A, Emons G. Invasion and increased expression of S100a4 and Cyr61 in mesenchymal transformed breast cancer cells is downregulated By Gnrh. *Int J Oncol.* (2016) 48:2713–21. doi: 10.3892/ijo.2016.3491
24. Gyorffy B, Lanczky A, Eklund AC, Denkert C, Budczies J, Li Q, et al. An online survival analysis tool to rapidly assess the effect of 22,277 genes on breast cancer prognosis using microarray data Of 1,809 patients. *Breast Cancer Res Treat.* (2010) 123:725–31. doi: 10.1007/s10549-009-0674-9
25. Chen A, Wang L, Li BY, Sherman J, Ryu JE, Hamamura K, et al. Reduction in migratory phenotype in a metastasized breast cancer cell line via downregulation of S100a4 and Grm3. *Sci Rep.* (2017) 7:3459. doi: 10.1038/s41598-017-03811-9
26. Chen PS, Wang MY, Wu SN, Su JL, Hong CC, Chuang SE, et al. Ctgf enhances the motility of breast cancer cells via an integrin-α vβ3–Erk1/2-dependent S100a4-upregulated pathway. *J Cell Sci.* (2007) 120:2053–65. doi: 10.1242/jcs.03460
27. Jim Leu S-J, Sung J-S, Huang M-L, Chen M-Y, Tsai T-W. A novel anti-Ccn1 monoclonal antibody suppresses Rac-dependent cytoskeletal reorganization and migratory activities in breast cancer cells. *Biochem Biophy Res Commun.* (2013) 434:885–91. doi: 10.1016/j.bbrc.2013.04.045
28. Shaul YD, Seger R. The Mek/Erk cascade: from signaling specificity to diverse functions. *Biochim et Biophys Acta Mol Cell Res.* (2007) 1773:1213–26. doi: 10.1016/j.bbamcr.2006.10.005
29. Favata MF, Horiuchi KY, Manos EJ, Daulerio AJ, Stradley DA, Feeser WS, et al. Identification of A novel inhibitor of mitogen-activated protein kinase kinase. *J Biol Chem.* (1998) 273:18623–32. doi: 10.1074/jbc.273.29.18623
30. Shen J, Cao B, Wang Y, Ma C, Zeng Z, Liu L, et al. Hippo component yap promotes focal adhesion and tumour aggressiveness via transcriptionally activating Thbs1/fak signalling in breast cancer. *J Exp Clin Cancer Res Cr.* (2018) 37:175–175. doi: 10.1186/s13046-018-0850-z
31. Emre Y, Imhof BA. Matricellular protein Ccn1/Cyr61: a new player in inflammation and leukocyte trafficking. *Semin Immunopathol.* (2014) 36:253–9. doi: 10.1007/s00281-014-0420-1
32. Bornstein P. Matricellular proteins: an overview. *J Cell Commun Signal.* (2009) 3:163–5. doi: 10.1007/s12079-009-0069-z
33. Yao H, Guangchun HE, Shichao Y, Chen C, Liujiang S, Thomas J, et al. Triple-negative breast cancer: is there a treatment on the horizon? *Oncotarget.* (2016) 8:12. doi: 10.18632/oncotarget.12284
34. Xie D, Nakachi K, Wang H, Elashoff R, Koeffler HP. Elevated levels of connective tissue growth factor, WISP-1, and CYR61 in primary breast cancers associated with more advanced features. *Cancer Res.* (2001) 61:8917–23.
35. Nieto MA. Context-specific roles of emt programmes in cancer cell dissemination. *Nat Cell Biol.* (2017) 19:416–8. doi: 10.1038/ncb3520
36. Jenkinson SR, Barraclough R, West CR, Rudland PS. S100a4 regulates cell motility and invasion in an in vitro model for breast cancer metastasis. *Br J Cancer.* (2004) 90:253–62. doi: 10.1038/sj.bjc.6601483
37. Maity G, Ghosh A, Gupta VG, Haque I, Sarkar S, Das A, et al. Cyr61/Ccn1 regulates Dck And Ctgf and causes gemcitabine resistant phenotype in pancreatic ductal adenocarcinoma. *Mol Cancer Therapeut Molcanther.* (2019) 0899:2018. doi: 10.1158/1535-7163.MCT-18-0899
38. Long X, Yu Y, Perlaky L, Man T-K, Redell MS. Stromal Cyr61 confers resistance to mitoxantrone via spleen tyrosine kinase activation in human acute myeloid leukaemia. *Br J Haematol.* (2015) 170:704–18. doi: 10.1111/bjh.13492
39. Liu F, Yang X, Geng M, Huang M. Targeting Erk, an achilles' heel of the mapk pathway, in cancer therapy. *Acta Pharmaceut Sin B.* (2018) 8:552–62. doi: 10.1016/j.apsb.2018.01.008
40. Boopathy GTK, Hong W. Role of hippo pathway-Yap/Taz signaling in angiogenesis. *Front Cell Dev Biol.* (2019) 7:49 doi: 10.3389/fcell.2019.00049
41. Halder G, Johnson RL. Hippo signaling: growth control and beyond. *Development.* (2011) 138:9–22. doi: 10.1242/dev.045500
42. Pan D. The hippo signaling pathway in development and cancer. *Dev Cell.* (2010) 19:491–505. doi: 10.1016/j.devcel.2010.09.011
43. Cao L, Sun PL, Yao M, Jia M, Gao H. Expression of yes-associated protein (Yap) and its clinical significance in breast cancer tissues. *Hum Pathol.* (2017) 68:166–74. doi: 10.1016/j.humpath.2017.08.032
44. Warren JSA, Xiao Y, Lamar JM. Yap/Taz activation as a target for treating metastatic cancer. *Cancers.* (2018) 10:E115. doi: 10.3390/cancers10040115
45. Mayer S, Gabriel B, Erbes T, Timme-Bronsert S, Jager M, Rucker G, et al. Cyr61 expression pattern and association with clinicopathological factors in patients with cervical cancer. *Anticancer Res.* (2017) 37:2451–6. doi: 10.21873/anticanres.11585

46. Wei J, Yu G, Shao G, Sun A, Chen M, Yang W, et al. Cyr61 (Ccn1) is a metastatic biomarker of gastric cardia adenocarcinoma. *Oncotarget.* (2016) 7:31067–78. doi: 10.18632/oncotarget.8845
47. Destek S, Gul VO. S100a4 may be a good prognostic marker and a therapeutic target for colon cancer. *J Oncol.* (2018) 2018:1828791. doi: 10.1155/2018/1828791
48. Ai KX, Lu LY, Huang XY, Chen W, Zhang HZ. Prognostic significance of S100a4 and vascular endothelial growth factor expression in pancreatic cancer. *World J Gastroenterol.* (2008) 14:1931–5. doi: 10.3748/wjg.14.1931
49. Egeland EV, Boye K, Park D, Synnestvedt M, Sauer T, Oslo Breast Cancer C, et al. Prognostic significance of S100a4-expression and subcellular localization in early-stage breast cancer. *Breast Cancer Res Treat.* (2017) 162:127–37. doi: 10.1007/s10549-016-4096-1
50. Monnier Y, Farmer P, Bieler G, Imaizumi N, Sengstag T, Alghisi GC, et al. Cyr61 and alphavbeta5 integrin cooperate to promote invasion and metastasis of tumors growing in preirradiated stroma. *Cancer Res.* (2008) 68:7323–31. doi: 10.1158/0008-5472.CAN-08-0841
51. Kassis JN, Virador VM, Guancial EA, Kimm D, Ho AS, Mishra M, et al. Genomic and phenotypic analysis reveals A key role for Ccn1 (Cyr61) In bag3-modulated adhesion and invasion. *J Pathol.* (2009) 218:495–504. doi: 10.1002/path.2557

Conflict of Interest: The authors declare that the research was conducted in the absence of any commercial or financial relationships that could be construed as a potential conflict of interest.

Supplementary Material

The Supplementary Material for this article can be found online at:
https://www.frontiersin.org/articles/10.3389/fonc.2019.01074/full#supplementary-material

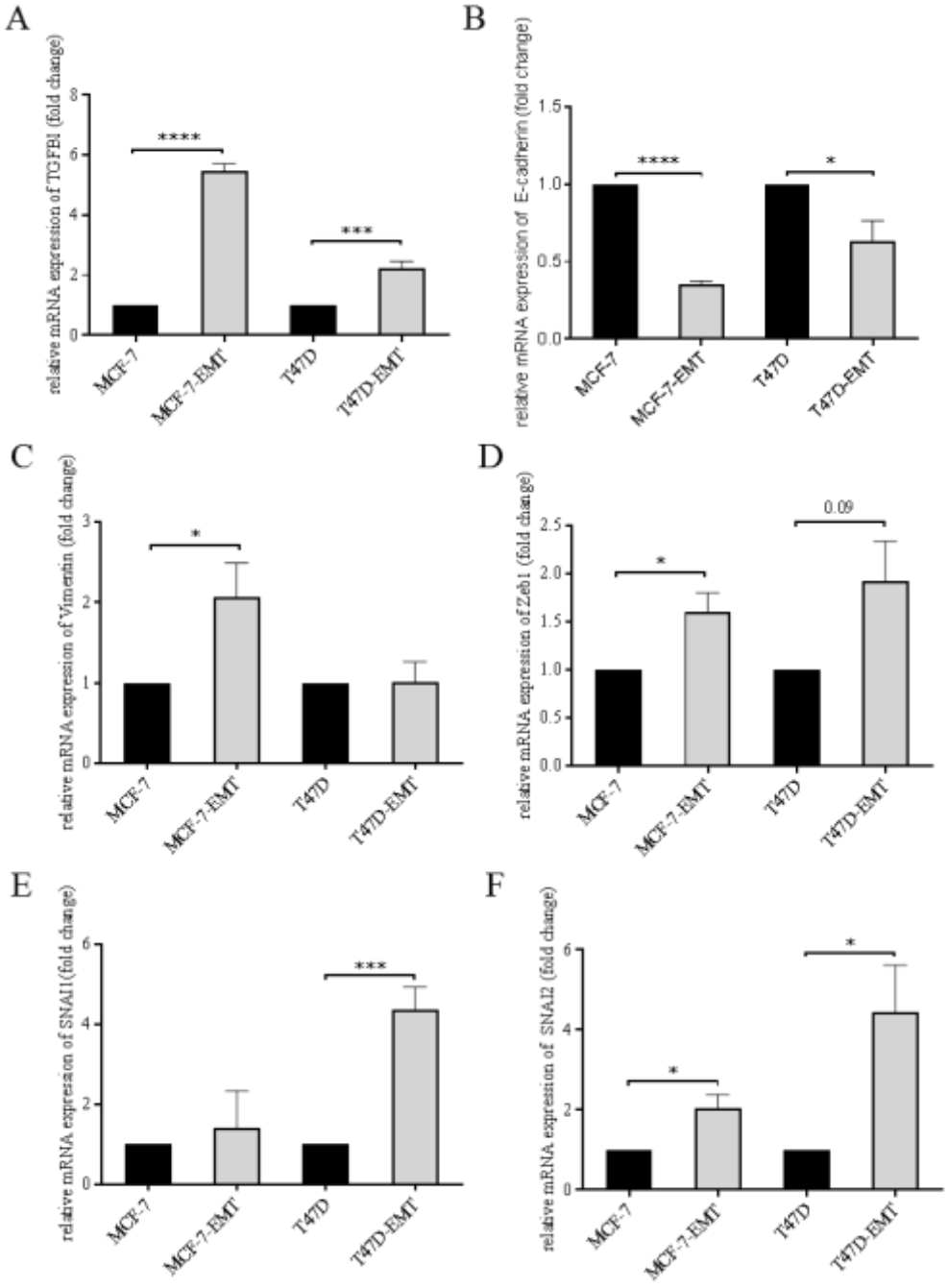

Figure S1. CYR61 expression correlates with breast cancer cell invasiveness. **(A)** Relative transforming growth factor beta induced (TGFBI) expression of mesenchymal transformed breast cancer cell lines compared to non-invasive controls was assessed using real-time quantitative PCR. Data represent mean ± SEM. Using unpaired, two-tailed *t*-test analysis. MCF-7-EMT $n = 3$; T47D-EMT $n = 6$; $^{***}P < 0.0005$; $^{****}P < 0.0001$ **(B)** Relative E-cadherin expression of mesenchymal transformed breast cancer cell lines compared to non-invasive controls was assessed using real-time quantitative PCR. Data represent mean ± SEM. Using unpaired, two-tailed *t*-test analysis. MCF-7-EMT $n = 4$; T47D-EMT $n = 3$; $^{*}P < 0.05$; $^{****}P < 0.0001$ **(C)** Relative Vimentin expression of mesenchymal transformed breast cancer cell lines compared to non-invasive controls was assessed using real-time quantitative PCR. Data represent mean ± SEM. Using unpaired, two-tailed *t*-test analysis. MCF-7-EMT $n = 5$; T47D-EMT $n = 3$; $^{*}P < 0.05$ **(D)** Relative Zeb1 expression of mesenchymal transformed breast cancer cell lines compared to non-invasive controls was assessed using real-time quantitative PCR. Data represent mean ± SEM. Using unpaired, two-tailed *t*-test analysis. MCF-7-EMT $n = 4$; T47D-EMT $n = 3$; $^{*}P < 0.05$ **(E)** Relative SNAI1 expression of mesenchymal transformed breast cancer cell lines compared to non-invasive

controls was assessed using real-time quantitative PCR. Data represent mean ± SEM. Using unpaired, two-tailed *t*-test analysis. MCF-7-EMT $n = 4$; T47D-EMT $n = 5$; $^{***}P < 0.0005$ **(F)** Relative SNAI2 expression of mesenchymal transformed breast cancer cell lines compared to non-invasive controls was assessed using real-time quantitative PCR. Data represent mean ± SEM. Using unpaired, two-tailed *t*-test analysis. MCF-7-EMT $n = 3$; T47D-EMT $n = 4$; $^{*}P < 0.05$.

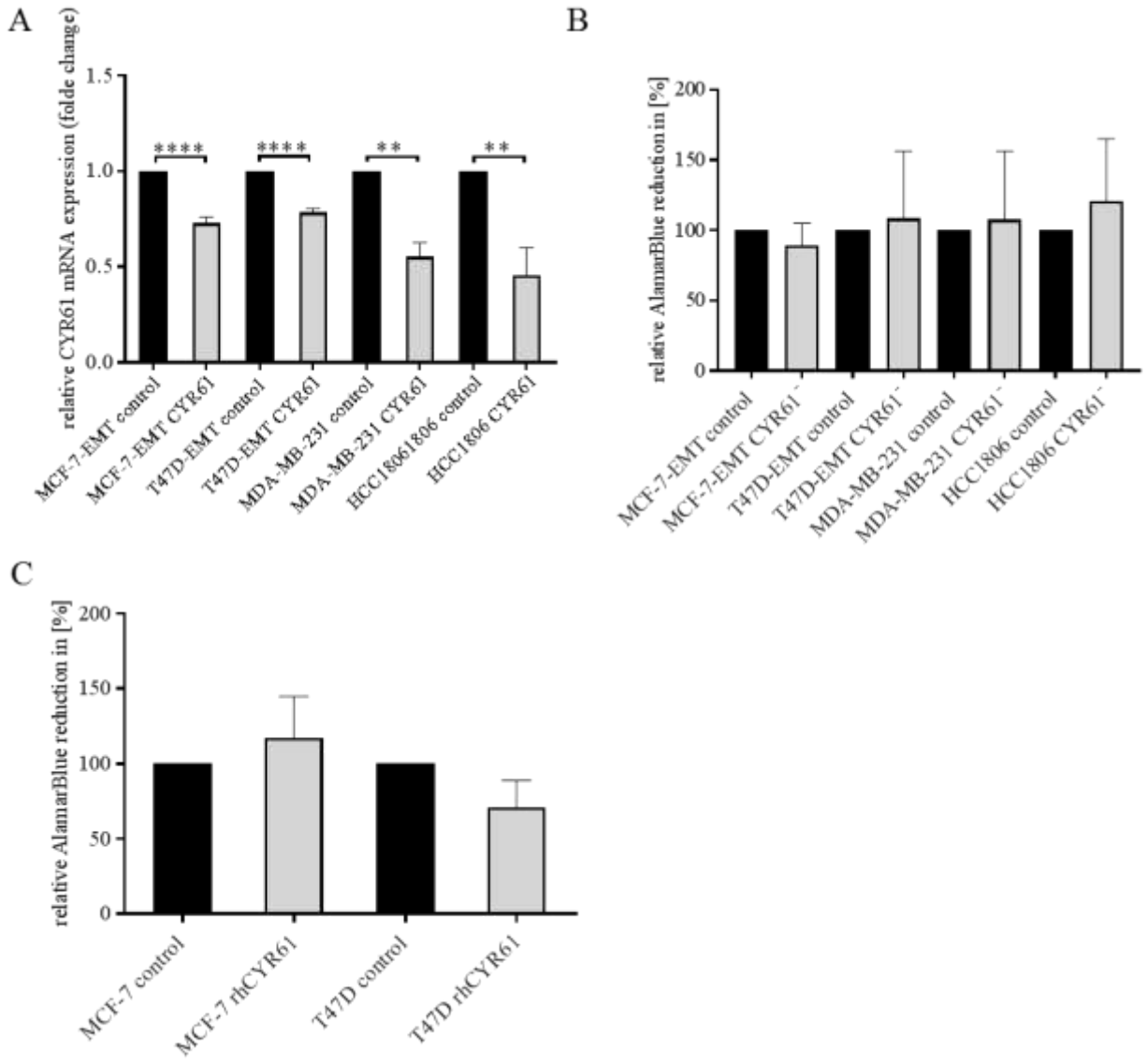

Figure S2. CYR61 expression correlates with breast cancer cell invasiveness. **(A)** Relative CYR61 expression 96 h after transient CYR61 siRNA transfection compared to control was assessed using real-time quantitative PCR. Data represent mean ± SEM. Using unpaired, two-tailed *t*-test analysis. MCF-7-EMT $n = 8$; T47D-EMT $n = 7$; MDA-MB-231 $n = 3$; HCC1806 $n = 4$; $^{**}P < 0.01$; $^{***}P < 0.0001$ **(B)** Analysis of relative AlamarBlue reduction as indicator for cell viability. Transient transfected breast cancer cell spheroids were grown and AlamarBlue reduction was assessed 48 hours after adding Matrigel at 4 h incubation. Relative AlamarBlue reduction was calculated compared to control spheroids. Data represent mean ± SEM. $n = 3$ **(C)** Analysis of relative AlamarBlue reduction as indicator for cell viability. Breast cancer cell spheroids were grown and AlamarBlue reduction was assessed 48 h after adding Matrigel and 1µg/ml rhCYR61 at 4 h incubation. Relative AlamarBlue reduction was calculated compared to control spheroids. Data represent mean ± SEM. $n = 3$.

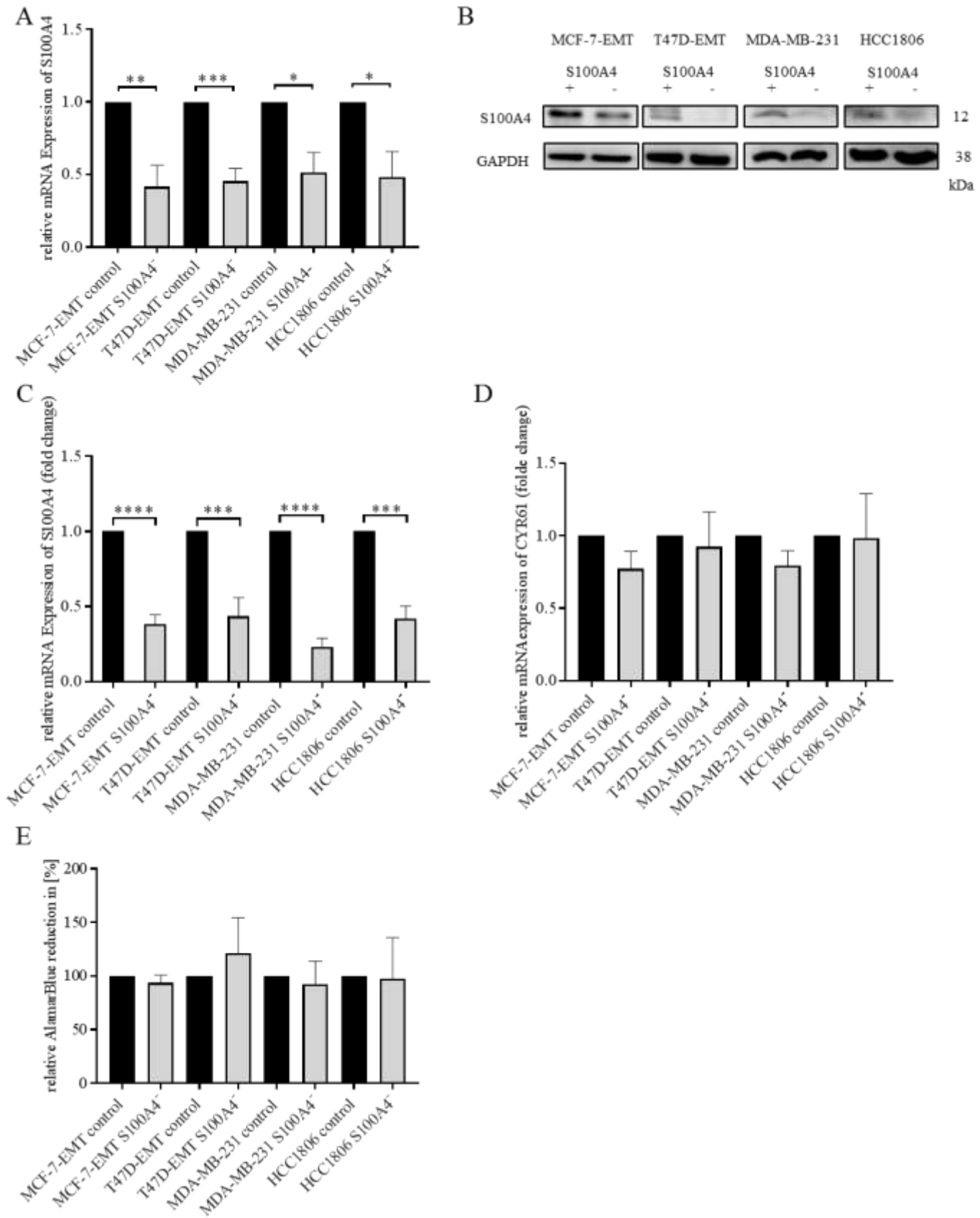

Figure S3. Suppression of CYR61 reduces S100A4 expression. **(A)** Immunoblot analysis of S100A4 mRNA expression levels in different breast cancer cell lines 96 h after S100A4 siRNA transfection was detected using western blotting. Date represent mean ± SEM. Using unpaired, two-tailed *t*-test analysis. MCF-7-EMT $n = 4$; T47D-EMT $n = 4$; MDA-MB-231 $n = 3$; HCC1806 $n = 3$; $^{*}P < 0.05$; $^{**}P < 0.01$; $^{***}P < 0.005$ **(B)** Representative experiments of S100A4 protein expression quantification corresponding to **(A). (C)** S100A4 mRNA expression analysis 96 h after siRNA transfection using quantitative PCR. Date represent mean ± SEM. Using unpaired, two-tailed *t*-test analysis. MCF-7-EMT $n = 4$; T47D-EMT $n = 4$; MDA-MB-231 $n = 3$; HCC1806 $n = 3$; $^{***}P < 0.005$; $^{****}P < 0.0001$ **(D)** CYR61 mRNA expression analysis 96 h after

S100A4 siRNA transfection using quantitative PCR. Date represent mean ± SEM. MCF-7-EMT $n = 5$; T47D-EMT $n = 6$; MDA-MB-231 $n = 3$; HCC1806 $n = 3$ **(E)** Analysis of relative AlamarBlue reduction as indicator for cell viability. Breast cancer cell spheroids transient transfected with S100A4 siRNA were grown and AlamarBlue reduction was assessed 48 h after adding Matrigel at 4 h incubation. Relative AlamarBlue reduction was calculated compared to control spheroids. Data represent mean ± SEM. $n = 3$.

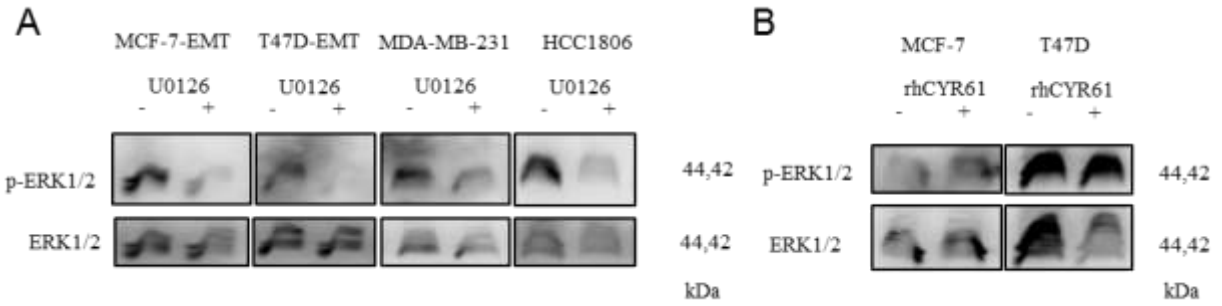

Figure S4. ERK1/2 activity is transducer of CYR61 mediated S100A4 regulation. **(A)** ERK1/2 and p-Erk1/2 (Thr202/Tyr204) expression in different breast cancer cell lines with or without 10μM U0126 treatment detected by western blotting. **(B)** ERK1/2 and p-Erk1/2 (Thr202/Tyr204) expression in non-invasive breast cancer cell lines with or without 1μg/ml rhCYR61 treatment detected by western blotting.

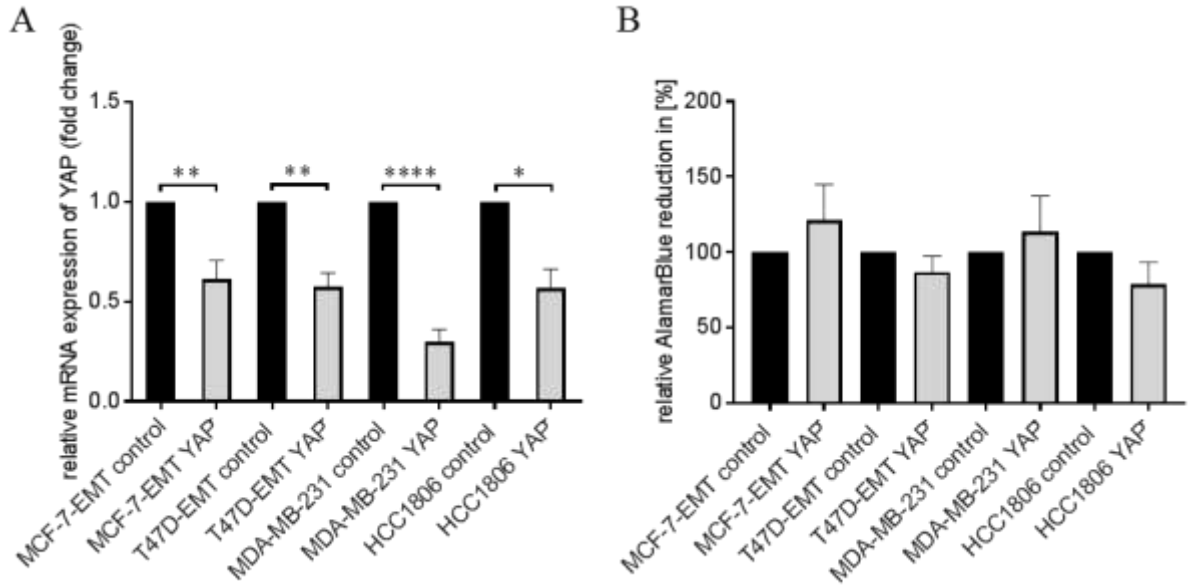

Figure S5. Suppression of YAP reduces invasiveness through blocking CYR61-S100A4-pERK1/2 signaling. **(A)** Relative YAP expression 96 h after transient YAP siRNA transfection compared to control was assessed using real-time quantitative PCR. Data represent mean ± SEM. Using unpaired, two-tailed *t*-test analysis. MCF-7-EMT $n = 5$; T47D-EMT $n = 3$; MDA-MB-231 $n = 3$; HCC1806 $n = 3$; $^{*}P < 0.05$; $^{**}P < 0.01$; $^{****}P < 0.001$ **(B)** Analysis of relative AlamarBlue reduction as indicator for cell viability. Breast cancer cell spheroids were grown and AlamarBlue reduction was assessed 48 hours after adding Matrigel at 4 h incubation. Relative AlamarBlue reduction was calculated compared to control spheroids. Data represent mean ± SEM. $n = 3$.

Table S6. CYR61 and S100A4 as prognostic markers for breast cancer progression. Cut-off values were downloaded from kmplot.com after target (dataset 213226_at = CYR61; dataset 203186_s_at = S100A4) specific analysis. RFS, relapse free survival; DMFS, distant metastasis free survival.

RFS, 213226_at	**RFS,203186_s_at**	**DMFS, 213226_at**	**DMFS,203186_s_at**
"cutoff value" "p value"	"cutoff value" "p value"	"cutoff value" "p value"	"cutoff value" "p value"
236 1.19562075974189e-05	1724 0.215266077871679	241 5.66603372054164e-06	1720 0.0851389129703291
237 9.16064789491244e-06	1726 0.191509442365171	243 4.29158303050237e-06	1730 0.0762015647592793
237 1.31517158498129e-05	1730 0.215326922690825	244 3.03409633506391e-06	1737 0.0673434160590155
237 1.03268303958126e-05	1733 0.199535025397062	245 2.20617246315946e-06	1747 0.0556060355003921
237 1.00797209752201e-05	1737 0.186083604474143	246 4.43337966471447e-06	1748 0.087933906857383

238 1.57871180219704e-05	1738 0.165469954866447	247 1.00878139384086e-05	1756 0.0752060763965201
239 1.3133087896966e-05	1743 0.196401432280997	249 7.66093542547974e-06	1760 0.0684295279604519
240 2.04982598729364e-05	1744 0.229162350068697	249 5.8403632995363e-06	1761 0.058187868026223
240 1.82132154802339e-05	1746 0.271702917719659	250 4.06173852962599e-06	1777 0.0513550586893096
241 2.92356093257728e-05	1747 0.306719419607372	251 3.25679224266739e-06	1789 0.0416604122418941
241 2.31493902208557e-05	1748 0.359338656499993	251 2.44171086549727e-06	1790 0.0363794114545782
241 1.76178184373432e-05	1754 0.33247013388508	251 1.70432254920083e-06	1792 0.0292419343852079
243 1.33655356101547e-05	1756 0.30867274953045	252 1.23662871620578e-06	1799 0.0429254824133023
243 1.01074182558003e-05	1759 0.297076013999274	252 8.20637044318673e-07	1811 0.0366056590849839
244 8.05231597533762e-06	1760 0.282453439032526	257 5.63565007549727e-07	1819 0.0604947658664786
244 6.40227151926798e-06	1760 0.259763610817575	260 3.78015050594982e-07	1839 0.0814051076668032
245 8.94217762414939e-06	1761 0.295737208212877	260 2.78867625880252e-07	1840 0.0725683150354628
245 7.10601420161883e-06	1761 0.276436035709882	262 6.62580763810539e-07	1862 0.107455633487161
245 5.2466149349506e-06	1765 0.262381467087415	267 1.43703413579832e-06	1887 0.0977158797816955
245 6.92955615444468e-06	1765 0.23526798320554	268 1.03511381610577e-06	1901 0.0849816218819209
245 5.35539351897985e-06	1765 0.208769914409052	268 7.34527087598025e-07	1912 0.0758511612442003
246 4.07384862899374e-06	1769 0.236957978028407	269 1.73399462544133e-06	1918 0.104776762227724
246 3.17352482592792e-06	1772 0.216103513770683	272 3.7616837191834e-06	1921 0.0939248047300196
246 4.83428874564762e-06	1772 0.198984416826844	272 9.3088758236215e-06	1922 0.128904150968058
246 6.51540647678139e-06	1777 0.237961479866444	272 1.98618701841013e-05	1942 0.172333234285498
246 9.60522328286029e-06	1777 0.216140569100701	273 1.39090123512098e-05	1947 0.147449458900218
246 7.60227337093244e-06	1779 0.196004566051068	273 2.90651110483875e-05	1960 0.131128731953917
248 6.11384563808937e-06	1779 0.183960951153308	273 2.1610279594908e-05	1970 0.112497065151357
249 5.52392967401172e-06	1785 0.212511725412508	273 1.48060434349562e-05	1987 0.0956183630635912
249 4.50373640015211e-06	1786 0.25270823918695	275 1.21762063713948e-05	1992 0.0794500645492436
249 3.42171236322741e-06	1789 0.23112027846647	275 8.57026095868463e-06	1994 0.106254306905796
250 2.77973353690619e-06	1789 0.214447470846727	275 5.99395959210991e-06	1999 0.0901955813852092
250 2.76598099768766e-06	1789 0.194359112734678	277 1.37382970206712e-05	1999 0.0748279991348035
250 2.02198567778034e-06	1790 0.186889836352773	277 1.15386745084267e-05	2008 0.0617007183075305
250 1.68050999171943e-06	1790 0.218133359598657	279 2.5296652380713e-05	2011 0.090045061272588
251 1.40629752065635e-06	1799 0.19392212993269	281 2.05543480013004e-05	2015 0.0760836642596744
251 1.24119074640383e-06	1800 0.178129139124167	285 4.86238237439318e-05	2015 0.106782995278059
251 1.70597296855757e-06	1811 0.199602294170614	285 4.09335500751729e-05	2044 0.0891305277018941
251 1.31653941659593e-06	1811 0.191793866795494	287 7.37085799374926e-05	2063 0.0775417186529733
252 1.20379161649975e-06	1812 0.231110558427013	289 0.000130883380082825	2095 0.0703899398757712
252 1.69670519156728e-06	1814 0.211299491514386	291 0.00010703511141319	2100 0.066121449983751
252 1.25655580240913e-06	1817 0.188598316049836	292 9.25938850192543e-05	2101 0.0584410377368827
252 9.79088268016071e-07	1819 0.222863161545062	292 6.47255128320978e-05	2102 0.0897470557658191
252 1.62115713453481e-06	1820 0.250822080526413	293 0.000116182583821955	2122 0.0744985900059224
253 2.32017150858521e-06	1826 0.229714663031805	294 9.54973299709394e-05	2123 0.0626274422039131
253 2.30573700354952e-06	1827 0.208763457277195	295 0.000208139612756675	2128 0.0523805135143922
253 1.82940585258251e-06	1831 0.189273427256919	295 0.000174334483184824	2128 0.0475036128885575
254 1.43772194205471e-06	1834 0.171195510768562	296 0.000360834213675276	2157 0.0386292387616045
255 1.00990012930069e-06	1839 0.163869501705034	298 0.000343339337023463	2170 0.0610571335943456
255 7.67022996450706e-07	1840 0.15194307716761	303 0.000280923155394741	2176 0.0868137561902532
256 5.72842213331093e-07	1846 0.180511260025027	308 0.000579316402860686	2181 0.0719782664801982
256 5.12077636849462e-07	1849 0.166161704496115	308 0.00108472383027114	2185 0.10865715156357

256 4.18382948619289e-07	1858 0.153668285590497	309 0.000795639197176734	2185 0.14245627598121
256 3.76138022839534e-07	1859 0.171849271687902	315 0.00118424622265356	2186 0.120210191385983
256 2.71179761202056e-07	1862 0.203201790486923	317 0.000966155129936141	2217 0.164789660012147
257 2.08668260892608e-07	1862 0.231961198310353	318 0.000704898666113674	2223 0.143921673503251
258 1.4838685036267e-07	1865 0.221095888409517	319 0.000647468397959816	2230 0.20275136250539
259 1.40405063353555e-07	1865 0.255831811329815	320 0.000509583008150516	2234 0.275634979398276
259 1.2914549019083e-07	1866 0.254123071669478	324 0.0004358655842579	2239 0.345404787345011
260 1.00031872896089e-07	1874 0.237474329558779	324 0.000370063021993161	2249 0.442542517710701
260 7.91898819851866e-08	1875 0.222836880414222	325 0.000313584378086373	2254 0.396778781473283
260 1.19628971284591e-07	1875 0.259743649781649	326 0.000622992311550719	2262 0.366538337268565
261 9.57591369532551e-08	1878 0.23859204708506	326 0.000457498193164985	2264 0.337220912257099
261 9.49707348318896e-08	1882 0.22478029135448	330 0.000885063518853757	2279 0.314798263683163
261 7.36233095599559e-08	1883 0.264621565762214	330 0.000760368780494458	2287 0.284916304363587
261 1.07718611697116e-07	1886 0.236600847775659	331 0.00140324914659562	2296 0.247357485139009
262 8.11910031428553e-08	1886 0.236160079816392	331 0.00246679287864937	2303 0.230725590598424
262 6.10481789564687e-08	1887 0.275324204482123	331 0.00188831275111445	2310 0.223438557821734
263 4.12928825577197e-08	1888 0.302749313427006	331 0.00158440892511735	2321 0.191954709102051
263 6.71643917149467e-08	1899 0.340276754214218	332 0.00147475979578715	2326 0.255484682851482
263 5.88748279017892e-08	1900 0.306940775781175	336 0.00123685500726878	2333 0.229125617947425
264 1.04193878636138e-07	1901 0.348872456969976	338 0.00220124492747253	2338 0.203003645668535
264 1.71846160967881e-07	1902 0.328574041869557	338 0.00371272359011954	2341 0.185117873391642
264 1.32262361285385e-07	1902 0.376916141761159	339 0.00314243956006788	2344 0.159245678113497
266 9.98524761763875e-08	1904 0.347784490224784	341 0.00462758843392508	2352 0.141132228404744
266 7.4513990977465e-08	1904 0.317635339967506	341 0.00388676501701501	2354 0.13279180502925
266 1.21466082303456e-07	1908 0.299826002515624	344 0.00337118731305097	2355 0.119638440562708
267 1.88390779531922e-07	1916 0.269408317383367	345 0.00256075742349082	2360 0.101254839079628
267 1.61634415296597e-07	1916 0.314871422095889	345 0.00411263470286305	2367 0.0842681749327846
267 1.34563795550768e-07	1916 0.289128432144377	348 0.00348007049785326	2371 0.0794864608093663
268 1.04411183698971e-07	1917 0.319093473252659	349 0.00347445429704873	2372 0.116586066077033
268 1.65843934030185e-07	1918 0.297618971055644	349 0.00553500357650694	2378 0.103477588588751
268 1.65023602893832e-07	1919 0.280250300628833	350 0.00897944104750537	2383 0.150449947990125
269 1.27184828779825e-07	1922 0.258193523198209	354 0.00773100382998504	2392 0.137103793667081
269 1.1517759490598e-07	1925 0.28610286180373	356 0.0124958659493957	2395 0.19055322547557
269 1.67981362486636e-07	1935 0.284500175566847	356 0.0104990814929842	2405 0.174812188761902
269 1.19196918446664e-07	1937 0.326019134433791	359 0.0150389947418161	2415 0.15282904391052
269 9.0107305950049e-08	1939 0.379820256832246	360 0.0119737554915491	2436 0.13654510473774
270 6.67132945553206e-08	1942 0.407659741183885	361 0.010255961062127	2442 0.125119126299403
270 5.82980838048641e-08	1944 0.370533469916463	368 0.0088350470522196	2466 0.110025709304274
270 8.88747224703224e-08	1947 0.347634265643376	370 0.00674829354262729	2470 0.0988178801976953
270 7.16454489069207e-08	1948 0.325119523274265	371 0.00524697388947692	2485 0.0835739556345095
270 5.6170264661759e-08	1950 0.300132013482624	371 0.00861791575945847	2494 0.0689423806353213
271 4.26608740555778e-08	1953 0.271680666266674	373 0.00656273931468387	2498 0.0677467263103555
272 3.23272231206317e-08	1954 0.310860984912757	374 0.00640647469531253	2505 0.0592582853170343
273 2.27221484960793e-08	1955 0.294206314642646	374 0.00537889077755083	2507 0.0532352116546972
273 1.81173992475081e-08	1964 0.285472328965033	378 0.00421284049805404	2513 0.0461494252525911
273 2.87305753632339e-08	1965 0.275800091017399	379 0.00325155254065601	2516 0.0380401133620312
273 2.29393376516285e-08	1970 0.257589142035339	379 0.00239805229412238	2525 0.034214588174705

273 3.6288547944352e-08	1972 0.235463643431292	380 0.00430273655416247	2527 0.0545472026566984
273 3.27387702503401e-08	1973 0.272223516723934	385 0.00374941568100984	2545 0.0447863305895111
273 2.5119030411247e-08	1975 0.250524999762855	387 0.00314541229009513	2552 0.0393087404175503
273 2.22065582589082e-08	1979 0.285998768656639	387 0.00235196251809966	2553 0.0571978312041423
274 1.87687883013155e-08	1985 0.321910692963709	388 0.0042084260996017	2555 0.0534174179934813
274 1.69538635352851e-08	1987 0.371934370143207	390 0.00338688030159739	2582 0.0761005491107757
275 1.27514775405402e-08	1987 0.427020288476206	390 0.00264773961984399	2589 0.0649045385775959
275 9.37434208037047e-09	1990 0.390679006151845	391 0.0019896076297633	2597 0.0587391725181905
275 6.82632494974911e-09	1992 0.420094001485059	393 0.00163430741441306	2601 0.0518004672962135
276 1.16068509248279e-08	1993 0.453378553118673	393 0.00280016003421213	2609 0.0462461735235759
276 1.81584434155724e-08	1994 0.419582528326454	393 0.00456514074505066	2617 0.0699139415927424
277 1.46770273712349e-08	1995 0.387723377817179	398 0.00698094011181394	2624 0.0698332569322473
277 1.22636260035947e-08	1997 0.443010880839524	399 0.0057353698952054	2640 0.101246664631641
277 2.04465617770211e-08	1999 0.503988575557351	399 0.00561091308056894	2641 0.128997252013429
278 1.5458386903866e-08	2000 0.462307852074369	401 0.00416367708329823	2642 0.182110690382545
278 2.20976346110291e-08	2008 0.492053878562571	403 0.00345325539946129	2644 0.165447853529337
279 3.35019040287321e-08	2011 0.548027596120278	403 0.00251829979113749	2646 0.232405307020051
279 2.7753825126986e-08	2011 0.597503604961244	404 0.0042743888810074	2673 0.200912759040937
279 4.33388500642451e-08	2014 0.554620059815944	405 0.00627680803791797	2675 0.178629389453745
279 3.07350176420584e-08	2015 0.600402996216928	407 0.00530522849531012	2704 0.24527543966663
280 4.61425662123816e-08	2015 0.656365576982325	408 0.00425243634028116	2717 0.213715935925123
280 7.6995421927073e-08	2021 0.622168570833772	409 0.00310478760628996	2728 0.182237125038688
280 1.20988626006735e-07	2022 0.590462571278286	409 0.0022397738795944	2729 0.165695060835247
280 1.00273684133789e-07	2024 0.636788944501883	411 0.00159572693627053	2755 0.152624439741069
281 7.39575423125416e-08	2024 0.613033005589626	412 0.00112224333580269	2768 0.137611575420534
281 6.55825826978429e-08	2026 0.576122889153891	413 0.000935693375710089	2776 0.124638967108924
282 1.13656968170339e-07	2039 0.540066615992411	413 0.00189531492152339	2779 0.103671327307853
282 8.70573739764069e-08	2041 0.512767860010821	414 0.00133560496850971	2783 0.0935876621967305
283 6.86509733505147e-08	2044 0.470971143388139	423 0.00113160029658199	2792 0.0850157191357667
283 6.22386341353476e-08	2049 0.453977649444532	425 0.000975109435587762	2807 0.125953733682631
286 1.06038442249101e-07	2054 0.429119949133783	428 0.00175124837988438	2817 0.111870405951665
286 1.76753272906893e-07	2056 0.467999511097211	431 0.00142608167910296	2836 0.150267611241634
286 1.25325452904335e-07	2056 0.531966784577156	432 0.00126054041139456	2840 0.148254781114133
287 1.0584352627685e-07	2061 0.495744072867847	432 0.00100564457554897	2846 0.132821882521155
287 1.46456968219688e-07	2063 0.45720374724927	433 0.000991115121332764	2846 0.186734138291301
287 1.98223909175788e-07	2064 0.441357235782128	437 0.00158321354894209	2848 0.243251896880292
287 1.42623854171298e-07	2071 0.487829301255586	437 0.00283170716413961	2849 0.309360698619301
287 1.20510533219154e-07	2072 0.456850796266864	437 0.00207470401516052	2869 0.277674085018493
288 9.07188849597063e-08	2073 0.498638809802843	439 0.00148052541997956	2890 0.246034185434486
288 7.30139807503249e-08	2076 0.557910858378448	444 0.00267885790881428	2907 0.212182802812189
289 1.04844137482907e-07	2077 0.543993881598222	447 0.00433381606036698	2910 0.190903806408577
289 1.56868317113812e-07	2086 0.541175598385868	452 0.00331472177865177	2920 0.163762639877945
289 1.29013594141192e-07	2095 0.50774505900349	452 0.00526404147870352	2920 0.143454884186663
289 9.176287052437e-08	2095 0.498181442621935	455 0.00920380689482192	2925 0.120593543009316
289 7.04673652762722e-08	2097 0.533717647396442	458 0.0160618210534534	2951 0.101358604870804
290 1.00755291665422e-07	2098 0.515607733546018	460 0.0119958935819044	2952 0.0875619860742392
290 1.46371683218405e-07	2101 0.473938001168804	465 0.0202823747237908	2967 0.0776047290755741

290 1.35039699977746e-07	2114 0.537245505172286	465 0.0171370570894152	2979 0.110239215506483
291 2.29879716928671e-07	2123 0.506195550453999	466 0.0127866434355218	3009 0.0903739953954005
291 2.08308547300362e-07	2127 0.472546686639048	466 0.00940685821381715	3022 0.0795062886969751
291 1.63744850789627e-07	2128 0.524587096468455	468 0.014739215951181	3034 0.0716117004809856
292 1.37104937070198e-07	2128 0.50899846632858	471 0.0224264017550586	3045 0.108641115050008
292 1.05029175023752e-07	2129 0.467704322326176	472 0.0168089763934393	3055 0.0898641763468526
292 7.53991763469131e-08	2143 0.437418267890435	473 0.0286855948032703	3068 0.0743141656131258
292 6.30710489391006e-08	2144 0.411224934581717	475 0.0249866081719786	3072 0.106914612636845
293 8.74374301851333e-08	2147 0.388109318823133	476 0.0211654895773197	3084 0.087158828203676
293 7.26779884052675e-08	2148 0.365708059157096	477 0.0181584613585305	3107 0.120696801649496
294 5.13157436543565e-08	2151 0.344251868288328	477 0.0138343460534508	3109 0.107232571749157
294 8.77429109369388e-08	2154 0.363163607594829	477 0.0119036337577698	3123 0.106348004865172
294 1.49547734196176e-07	2155 0.401521648128648	481 0.0201941241871229	3123 0.0958182733410868
294 2.23924790709873e-07	2162 0.454621306627265	482 0.016901717305413	3150 0.0808487141957904
294 1.5877542047793e-07	2162 0.512750594460228	486 0.0252462582282001	3169 0.0785618145011202
295 2.47502582206849e-07	2162 0.565349790397007	487 0.041102024890602	3176 0.108964137429538
295 2.11965944796333e-07	2163 0.536892071834426	488 0.0658712354984232	3186 0.0936881637696263
295 3.5108045004506e-07	2165 0.507559034551738	488 0.097055966957743	3206 0.125970352907788
296 2.64067238631149e-07	2166 0.549637615819215	492 0.0870424308456467	3207 0.10290043621273
296 2.55138578597602e-07	2169 0.514645790294705	494 0.0839581527225681	3223 0.0831360318383928
296 2.09823680097365e-07	2175 0.473288096501925	506 0.118130218938485	3255 0.127811843937393
297 3.17168378005661e-07	2176 0.441088421928376	511 0.179776480337608	3256 0.113797112567825
297 4.78409231341459e-07	2181 0.404866351470378	512 0.161318915894916	3276 0.0961454833849308
298 6.79045897511443e-07	2184 0.462794625768934	516 0.146335059435057	3284 0.078884458552078
298 5.30389107633589e-07	2185 0.525609394566797	523 0.201768263133772	3298 0.0641012916527399
298 4.33109593189762e-07	2186 0.483819200848602	524 0.289142068203547	3302 0.053795670075411
298 3.44355362669191e-07	2187 0.537307022040612	525 0.243153260512366	3311 0.0502627549129147
300 4.63454157717536e-07	2188 0.502103131252314	525 0.218640055843596	3318 0.0717846178995084
300 4.384678022884e-07	2189 0.54498907422458	526 0.180358577027205	3324 0.0601269881928223
301 3.52417529270177e-07	2189 0.606247485777509	526 0.161634022812842	3398 0.0522202566408647
303 3.47003545231317e-07	2192 0.570175904721589	528 0.132286250713154	3399 0.0714642218668313
303 2.74958287027616e-07	2192 0.62776154074037	528 0.112399527702889	3407 0.0574588969108735
303 2.07984688804785e-07	2194 0.590535260697454	530 0.172129427675998	3411 0.0501003375143075
304 1.57607281892069e-07	2196 0.63963083243406	531 0.147711879810305	3422 0.0710371837046017
304 1.26565121272293e-07	2198 0.600070296777585	532 0.196645048097449	3441 0.056344796844109
304 1.25032323161633e-07	2202 0.586404402896709	537 0.276069411934701	3445 0.0446062286379904
305 8.96853348253401e-08	2204 0.553505186049998	537 0.384689933780886	3448 0.0677357403108566
305 6.4082170236901e-08	2206 0.533588655143947	546 0.335092745753487	3490 0.0583655196928524
306 5.02250703249274e-08	2208 0.596051458434985	547 0.434304481518211	3533 0.0511817881007089
306 4.38862803875395e-08	2208 0.567740770636341	548 0.518296247814666	3575 0.0401680320256471
306 7.68637227199775e-08	2217 0.601276964383235	553 0.647690853284132	3578 0.0318241662094364
306 6.32590616556072e-08	2222 0.567187422638689	555 0.793981065922219	3599 0.0289617067421652
306 5.70253781972951e-08	2223 0.539982545143818	556 0.744255490380291	3639 0.0244057288016714
307 8.56718763708741e-08	2225 0.604953848523326	561 0.849725158350464	3663 0.0392570967679895
307 5.99269678325243e-08	2230 0.667247971409584	565 0.972093727935338	3675 0.0662750534480202
308 4.59227142979302e-08	2230 0.736464654299698		
308 7.47291720726295e-08	2230 0.699584054191313		

309 5.65291037313287e-08	2231 0.663188674451532		
309 9.07394995808275e-08	2232 0.645589006889933		
309 7.10460850150696e-08	2234 0.684114866949018		
311 6.01161453950283e-08	2239 0.732161251268197		
311 4.56429243289591e-08	2239 0.683646504857333		
312 5.72943568144524e-08	2243 0.75096668357643		
312 4.32039538589279e-08	2249 0.731358874882108		
313 6.75223349455578e-08	2251 0.69186958870717		
313 1.12353625958406e-07	2254 0.660148259307044		
313 1.01405392527454e-07	2254 0.714045036190564		
313 1.36244042603373e-07	2255 0.683994188475823		
314 2.33684312123117e-07	2259 0.72518080470681		
314 1.84152153970274e-07	2259 0.692567985488717		
314 1.54729476675719e-07	2262 0.660185406223942		
314 1.16062666366545e-07	2263 0.630193639076053		
315 8.50892014625515e-08	2270 0.62755544713205		
316 1.23521481376621e-07	2273 0.604524919778917		
316 1.11480768172356e-07	2278 0.559930789453068		
317 8.22646908371638e-08	2279 0.518815502657734		
317 1.22693164739118e-07	2281 0.488071334816708		
318 1.99079530971424e-07	2287 0.536859824981744		
318 1.68211424678155e-07	2290 0.494898263287402		
318 2.44498355894684e-07	2295 0.464011224416034		
318 2.29231242210304e-07	2296 0.440605533199355		
319 1.72403442966207e-07	2296 0.426142303837692		
320 1.35358748210024e-07	2300 0.472426069796172		
320 1.18875449262035e-07	2303 0.438806943395914		
320 1.06330925064846e-07	2306 0.433564859825019		
321 8.10611031631936e-08	2309 0.415248557884492		
321 6.81133814905976e-08	2309 0.400099298004771		
322 5.65821922648979e-08	2311 0.36556404117383		
322 4.41349441437922e-08	2312 0.415190059012866		
323 3.93829590050743e-08	2321 0.388339084126502		
324 3.27519225074013e-08	2326 0.442415241394388		
324 2.59044924399987e-08	2333 0.407027322133589		
324 2.22408637062799e-08	2337 0.380504173299217		
325 1.63850699674839e-08	2337 0.409462651656763		
326 2.7946178482452e-08	2338 0.384034702047868		
326 2.02253007675068e-08	2341 0.36439551730728		
328 3.43350168297007e-08	2344 0.334670987671008		
328 2.36352508675708e-08	2345 0.31327258480046		
328 4.02548763211996e-08	2352 0.304349781838656		
328 2.97139928218115e-08	2353 0.296374611934045		
330 2.23606082538907e-08	2354 0.330480205148936		
330 1.94272375964033e-08	2355 0.31135763067887		
331 3.20113309193459e-08	2358 0.285531735555039		
331 5.13132922819182e-08	2358 0.275140198222341		

331 3.79362735669631e-08	2358 0.307479745222018		
331 3.09147509813812e-08	2360 0.280927089706003		
331 2.04100456535627e-08	2367 0.25301681451987		
332 1.33721669293152e-08	2371 0.232716410197453		
333 1.0846007980625e-08	2378 0.271873747514953		
333 1.90146637324418e-08	2381 0.316623056794478		
333 3.10021524008164e-08	2383 0.293523461856302		
333 4.86731800419804e-08	2388 0.278927647920909		
333 3.56942257973003e-08	2391 0.256185006881525		
334 2.54956171730214e-08	2392 0.238359290194269		
334 1.90846992653704e-08	2393 0.276972743879207		
336 2.88975652296131e-08	2394 0.264012632129704		
336 2.23459492021405e-08	2395 0.291954118003007		
336 3.64128782681661e-08	2405 0.277672001487392		
338 2.3925822212334e-08	2405 0.256547099512873		
338 3.81719051922857e-08	2407 0.230932296391167		
338 3.09308159085475e-08	2420 0.206647846862706		
338 4.72052519295829e-08	2420 0.192482585401954		
339 3.49388125098216e-08	2424 0.177995324025048		
339 3.01293968663074e-08	2426 0.165558714149107		
339 2.13365038970181e-08	2430 0.184928473923862		
339 1.38700426699501e-08	2436 0.174676161727893		
339 1.84938654390621e-08	2437 0.166454066322091		
339 2.56776936380376e-08	2442 0.197595488939309		
340 3.98218016339769e-08	2442 0.182657615452784		
341 6.52504876796911e-08	2443 0.207571928744931		
341 5.16134306405291e-08	2445 0.242230548379286		
341 7.79366653436142e-08	2455 0.221614733882098		
342 6.40309406607642e-08	2466 0.213178900453134		
342 1.10458597601948e-07	2467 0.20026651348789		
342 8.76807536576152e-08	2470 0.178377094848959		
342 7.15139368834272e-08	2474 0.161923306960064		
342 5.8415000503409e-08	2479 0.147298206369622		
343 1.01744852099017e-07	2485 0.133195775620466		
344 7.03043091521138e-08	2487 0.11809515034508		
344 4.83289859243285e-08	2493 0.106144369419761		
344 3.59914612557688e-08	2494 0.121150106664243		
345 5.5783032526513e-08	2498 0.120150753423883		
347 8.05548171500803e-08	2505 0.110395571528574		
349 1.13800004752918e-07	2507 0.104176140162844		
349 1.77433540082816e-07	2511 0.0952456085541571		
349 2.5836314487826e-07	2512 0.114239758038072		
349 3.99356818281404e-07	2514 0.103440648780117		
350 2.68259859437237e-07	2515 0.0906267254202576		
350 2.22143570760558e-07	2516 0.089938331762951		
352 3.08259164860658e-07	2525 0.0855114670825262		
353 2.3069734178538e-07	2525 0.104349957112358		

353 1.89704727593387e-07	2545 0.127171228625458		
353 2.97430264195597e-07	2552 0.11757695126655		
353 2.52648758580776e-07	2553 0.138011150606725		
353 1.75802860935548e-07	2555 0.133958142126466		
354 1.16216920309498e-07	2561 0.156075612710348		
355 1.77642821674873e-07	2565 0.179954411898895		
356 2.5906512490792e-07	2566 0.157456814464866		
356 2.0370457531893e-07	2570 0.175856502283501		
356 1.87826449393746e-07	2574 0.160625683771714		
356 1.84053501328663e-07	2574 0.153021834201184		
356 2.43992912984936e-07	2581 0.135105007710892		
357 3.48782989600949e-07	2582 0.155096921397809		
357 2.82442746080136e-07	2582 0.141643681009105		
358 4.55670136290109e-07	2583 0.140586217138475		
358 3.18620546835291e-07	2585 0.127309971357685		
358 2.38913614447611e-07	2587 0.149589367243812		
359 3.42340824133203e-07	2589 0.175734747243897		
360 2.58473610736942e-07	2589 0.167908958332189		
360 2.07528594642348e-07	2590 0.148628871341165		
360 1.81247771791071e-07	2591 0.173776376780992		
361 2.97175950292328e-07	2593 0.15864242519535		
361 2.45493689376985e-07	2594 0.143488998405173		
362 3.3418609857172e-07	2597 0.127091608522214		
363 4.16410951054047e-07	2601 0.117496398534827		
365 3.08379391356084e-07	2602 0.110430132710181		
365 5.19411752719634e-07	2609 0.0997189949606494		
366 8.18469549246359e-07	2619 0.120253042483915		
366 1.18320187025844e-06	2624 0.117357500740943		
367 1.86077980912636e-06	2625 0.139762632952047		
368 2.48575271910578e-06	2625 0.130503600419885		
368 1.81529677723002e-06	2626 0.11460501993032		
369 1.28769833984688e-06	2634 0.135737723442596		
369 9.08450879633094e-07	2635 0.130732117013202		
370 6.09206813440011e-07	2640 0.11821958461168		
371 4.338419201666e-07	2641 0.130518110914243		
371 3.83080439481098e-07	2642 0.156186111200466		
371 5.93192188147462e-07	2646 0.14584260326519		
371 4.13068204752065e-07	2646 0.137012211079479		
372 3.05688533264181e-07	2650 0.120452353401661		
373 4.52339418699488e-07	2657 0.146303217841463		
374 4.42188237137486e-07	2659 0.130693239183727		
374 3.51985138480337e-07	2659 0.116895596835257		
374 2.65427686496622e-07	2663 0.106263614741468		
375 1.96837363408697e-07	2663 0.123885675415464		
376 2.60846072075438e-07	2673 0.144149482775821		
377 3.60485223005469e-07	2674 0.132215898368639		
378 5.82092544165747e-07	2675 0.131938455670894		

379 4.38855400908267e-07	2677 0.157746404679655		
379 3.0800121819663e-07	2677 0.170961318980758		
379 4.48662816565637e-07	2678 0.154783729770627		
380 6.57538526738222e-07	2678 0.145371429607057		
380 5.7044755019664e-07	2679 0.175207066227995		
383 8.51558786929552e-07	2690 0.158961183640501		
383 1.30396045450176e-06	2700 0.147393054686733		
383 1.20892472044165e-06	2702 0.171668013673267		
385 1.89036186026836e-06	2704 0.202987078188986		
385 2.81477348740289e-06	2708 0.184828569511644		
386 2.30851696991774e-06	2713 0.171138513951824		
387 3.72984915952834e-06	2715 0.149152496214251		
387 5.21664959041157e-06	2717 0.138110056605818		
387 3.56755015462618e-06	2724 0.121311852569788		
387 2.58398565833318e-06	2725 0.106997467537576		
387 4.07830092652439e-06	2726 0.100716739128256		
388 5.81186833925607e-06	2728 0.0876290092768094		
390 4.63416563956098e-06	2729 0.081155526706262		
390 6.56492596606828e-06	2734 0.0769512888192267		
390 5.11291060756314e-06	2736 0.0737256583132326		
390 3.90159089513897e-06	2737 0.0697342535592513		
391 2.93546538376876e-06	2737 0.0600363609887522		
391 2.54252834253066e-06	2749 0.0540349430200893		
391 2.27542612563081e-06	2751 0.0516217143236055		
391 1.83573647194457e-06	2755 0.0432595874878264		
392 1.28591070991391e-06	2756 0.0395631318204946		
392 1.1610491108538e-06	2760 0.0343507162247524		
392 8.07061853458357e-07	2763 0.0284318453792395		
393 1.19738626447319e-06	2763 0.0261456782135656		
393 1.81900462870033e-06	2764 0.0336004499497536		
393 2.20395898986592e-06	2765 0.0295954901986812		
394 3.18533569043655e-06	2767 0.0353554767872047		
396 4.96838458874382e-06	2768 0.0337205937930475		
398 3.52274038917244e-06	2768 0.0309813635699269		
398 2.79851489159988e-06	2773 0.0377885160911141		
399 4.22737456240441e-06	2776 0.0334246635026586		
399 6.69742075776192e-06	2779 0.0281890346855138		
401 4.80248439960196e-06	2782 0.0259093662749652		
403 3.8906256347726e-06	2783 0.0224748243569224		
403 2.78299586997655e-06	2783 0.0285939163837601		
404 4.18603279594976e-06	2783 0.0254064997853127		
405 5.35853219052473e-06	2792 0.0237494019751421		
405 4.81834853149898e-06	2793 0.0305358253854715		
405 3.89954706803142e-06	2793 0.0371117553250881		
406 3.23571771321252e-06	2797 0.0439296680537168		
407 4.13963203604872e-06	2798 0.041743071305032		
408 3.35359728598217e-06	2799 0.0365043679532935		

408 3.02831261933534e-06	2807 0.0449832174695154		
408 2.11928360427383e-06	2809 0.040518832620009		
409 1.68985239890063e-06	2823 0.0459254425879849		
409 1.18051225828086e-06	2836 0.0416077939583002		
409 9.78439551158061e-07	2837 0.0521960300771332		
410 7.93503633245152e-07	2840 0.0641267228871966		
411 1.0637751380882e-06	2846 0.0583823615410862		
411 7.30205872101486e-07	2846 0.0720870571444369		
411 6.38480485148918e-07	2847 0.084876920561774		
412 4.94469533318664e-07	2847 0.0984632110145943		
412 4.22393433896495e-07	2848 0.114222075838437		
413 5.07908493485587e-07	2849 0.131062656777136		
413 8.6587823100448e-07	2869 0.119104706615886		
414 5.90840973369033e-07	2870 0.107485652220362		
414 5.41811650101032e-07	2882 0.123082463789777		
414 4.08267156415398e-07	2883 0.11674202161663		
414 3.14585413829782e-07	2888 0.110840589814175		
414 2.73919274373924e-07	2890 0.106931279544851		
415 2.10125320032617e-07	2894 0.0936831633031918		
415 1.72023891464868e-07	2894 0.0914831948329905		
415 2.6958821230938e-07	2898 0.0870058829244083		
416 4.20867752981557e-07	2901 0.0753628802374946		
416 3.48384792348e-07	2901 0.0677793422479258		
416 2.57747543086495e-07	2902 0.060977834849636		
417 3.50267451820763e-07	2907 0.0585564701204656		
418 4.77067994997249e-07	2914 0.0529097455535787		
420 6.52123258282344e-07	2915 0.0500412186263294		
421 4.1828480046302e-07	2917 0.0448588632221144		
422 6.69574322431643e-07	2919 0.0413961938705086		
422 5.42589326690823e-07	2920 0.0394685889926969		
422 3.64763202087559e-07	2920 0.0351350286352026		
423 4.55363584839219e-07	2924 0.0298633472453669		
423 4.06790322426964e-07	2924 0.0283831362129172		
423 6.69073861980785e-07	2928 0.0275465484021028		
424 5.99434676895605e-07	2933 0.0249817006678249		
425 5.25355287606111e-07	2939 0.0293994803233697		
426 8.20425003045244e-07	2944 0.0365634691015512		
428 5.98809094976005e-07	2946 0.0317880507669215		
428 9.53245049895024e-07	2950 0.0275498944570661		
431 7.65128088775491e-07	2951 0.0338738889289903		
432 6.94182653249165e-07	2952 0.0300859492441451		
432 5.42735652864224e-07	2967 0.0273036476285383		
432 4.24236229701336e-07	2974 0.0338432322094088		
432 4.1812868245561e-07	2979 0.0425431821430295		
432 6.79983070184242e-07	2980 0.0360554111178653		
433 5.0240575200089e-07	2983 0.0316248293906922		
434 8.45060478704696e-07	2994 0.0381021460855113		

437 1.33628874532388e-06	2994 0.0340568294670234		
437 2.20554520102834e-06	2997 0.0297749791962197		
439 1.50697324108329e-06	3007 0.0356873437622215		
441 2.35986364072183e-06	3009 0.0310659345845803		
441 1.7676356133256e-06	3015 0.0278336850306085		
442 2.57994822283614e-06	3016 0.0336555514761016		
442 2.24084846078831e-06	3017 0.03128092513164		
444 2.18020194386881e-06	3022 0.0261488545470606		
445 1.89139002138017e-06	3023 0.0243446660261168		
445 2.30621395369557e-06	3028 0.0315914033890958		
446 1.77746246787791e-06	3034 0.035027754089937		
447 1.40390687830561e-06	3039 0.0447254568300698		
447 1.05377018744246e-06	3045 0.0385952097016012		
448 7.63781869972391e-07	3048 0.0327599083253273		
448 6.79633996081286e-07	3052 0.0283645057331173		
450 1.02443503080529e-06	3053 0.0338526439384651		
450 1.42401070335474e-06	3058 0.0436364520888933		
450 2.38086570669704e-06	3063 0.0507513051850758		
452 1.78229586045298e-06	3077 0.0443007599709992		
452 2.4151651781823e-06	3078 0.0545639814078858		
452 3.85850291328982e-06	3080 0.0524733768793391		
453 2.98113086205642e-06	3081 0.0448504623044268		
453 2.54446485059567e-06	3082 0.0380550981116599		
454 1.91669952442908e-06	3083 0.0328295297320348		
454 3.07200818794318e-06	3084 0.0280694972539014		
455 2.55572710528007e-06	3085 0.034148507068445		
455 4.20582297055994e-06	3085 0.0295430871974027		
457 5.50325520221051e-06	3088 0.026309446462693		
457 4.63689776852849e-06	3089 0.0281258009721693		
458 6.44741232447288e-06	3089 0.0266666188029576		
459 4.43439808162083e-06	3091 0.0225686205553298		
459 3.52750712462324e-06	3100 0.0273832792763703		
459 3.01802932101136e-06	3107 0.0249709959688152		
462 2.2538142496753e-06	3108 0.0224169837440361		
462 1.79454027948722e-06	3108 0.0277655167253323		
465 2.30439025017404e-06	3109 0.0240148921647898		
465 1.81931132636759e-06	3109 0.0238469621100117		
465 1.21801826935553e-06	3122 0.022353117163246		
466 8.54885460865873e-07	3123 0.0220992809297211		
466 6.30646759147702e-07	3124 0.0204646377927258		
467 9.22904924816059e-07	3129 0.0265177968512536		
468 6.51944110141578e-07	3132 0.0227441923503642		
468 9.36415973762372e-07	3132 0.0210135486648917		
468 1.46452023941368e-06	3136 0.0263118690309897		
468 1.10825225818623e-06	3138 0.0237402456050828		
469 1.22139535674304e-06	3139 0.0209456416976599		
470 1.92905667961707e-06	3146 0.0174126011365295		

470 3.07589339165748e-06	3148 0.0162421629812356		
471 2.41848218196505e-06	3150 0.0200433633244118		
472 1.77868351403099e-06	3152 0.0197203652615867		
473 2.98788538954931e-06	3158 0.0178311965405292		
473 2.55373095936484e-06	3158 0.0146422812063609		
475 3.90923359239181e-06	3161 0.0123115196521252		
475 3.12625525056287e-06	3166 0.0111663316519693		
477 4.91246222633634e-06	3169 0.014362480219796		
477 3.99327824263107e-06	3173 0.0176194436966183		
477 2.89377626450094e-06	3176 0.0210014465153892		
477 2.48573348748948e-06	3179 0.0183710096760276		
479 4.02198093329975e-06	3183 0.0231355167664156		
479 2.69607035885411e-06	3186 0.0211613953278679		
481 3.74616510889769e-06	3188 0.0248488338679287		
482 2.94263772138148e-06	3199 0.0315791613932749		
482 2.37923849433219e-06	3204 0.0285316181802018		
482 3.22223182946946e-06	3207 0.0368243181233796		
482 2.47810390674452e-06	3209 0.0309690266676365		
483 3.76147279090855e-06	3213 0.0274374128692462		
483 2.55063187748483e-06	3218 0.0238271029915824		
483 2.03587067171274e-06	3220 0.0211464842907252		
483 1.3379205766606e-06	3223 0.0180578067955731		
484 9.51595257259186e-07	3224 0.0240226441329758		
484 1.53541525660383e-06	3235 0.02138792386523		
486 1.10452282253704e-06	3236 0.0283125690437035		
487 1.8441151941051e-06	3248 0.032087070838088		
488 3.10052543761596e-06	3255 0.0303562446996953		
488 4.82909582233404e-06	3262 0.0273476164917753		
490 4.1748886412396e-06	3262 0.0219735389584517		
490 5.93146355931662e-06	3265 0.0189127700971208		
490 4.50591551304225e-06	3276 0.0232423571430063		
490 7.41542043947163e-06	3279 0.0197524516662876		
490 1.25926767852169e-05	3281 0.0162258484680616		
491 1.77088219948107e-05	3284 0.013759681591574		
493 1.5681667309253e-05	3286 0.0115465795246071		
493 2.56122996248331e-05	3289 0.00934258489148776		
494 3.75401112677753e-05	3291 0.0128325904642822		
496 5.9260619468926e-05	3296 0.012192379776463		
497 4.13369381165873e-05	3298 0.0121164066180595		
498 3.23892200873033e-05	3301 0.0104433445013234		
498 2.59573938685698e-05	3302 0.00933384755035493		
498 2.22634706525948e-05	3303 0.00894338476901857		
499 1.5164013719926e-05	3310 0.00764334957045698		
501 1.12517480259644e-05	3311 0.00712768145654885		
502 1.67058997547764e-05	3311 0.00884626003382905		
502 2.6264583367297e-05	3324 0.00757400036203193		
503 3.91425310902749e-05	3341 0.00667723478027027		

504 3.01474402267798e-05	3367 0.0055112606928982		
504 2.55510527249481e-05	3380 0.00457477573101339		
506 2.29140019107898e-05	3388 0.00567940249481291		
509 3.63711989486148e-05	3389 0.00510286625340406		
511 2.51295739103208e-05	3392 0.00430857276404784		
512 2.07482391663127e-05	3398 0.00581729278311882		
512 1.803060302219e-05	3399 0.00542447684003655		
513 1.21312787535466e-05	3402 0.00445658194649412		
513 8.9354650950711e-06	3407 0.00554439286643127		
515 6.40075939706275e-06	3407 0.00491889679883606		
516 1.05396751678422e-05	3411 0.0068700150076918		
517 1.60022517499137e-05	3422 0.00834661926488389		
519 2.13254293540688e-05	3422 0.00676435991108115		
520 2.66584207552212e-05	3429 0.00560571337056226		
520 3.60407500527016e-05	3430 0.00527255476922495		
521 2.70550873184838e-05	3441 0.00430523039580788		
522 1.99550698772866e-05	3445 0.00375343344246593		
523 1.35714935742826e-05	3445 0.00502395762633323		
523 1.02529671112128e-05	3448 0.00394695391569322		
523 1.76662492615831e-05	3450 0.00340647827852902		
524 2.96331739882971e-05	3452 0.00275114819240196		
525 4.07232818112613e-05	3454 0.00366745288618542		
525 6.71281342009555e-05	3457 0.00310923673987218		
526 5.46262432739031e-05	3459 0.00386694668610088		
526 4.5419182932549e-05	3469 0.00308202320303874		
528 3.2149499740175e-05	3470 0.00247890702657549		
528 2.459735312621e-05	3475 0.00218831881809878		
528 1.74703023302358e-05	3479 0.00285581454564698		
529 2.93823590109543e-05	3480 0.00399224132836917		
529 3.61337837074815e-05	3490 0.00329392030980191		
529 3.07035068973782e-05	3495 0.00295126330397522		
530 2.77190147841555e-05	3501 0.00234469012535543		
531 2.10934529629725e-05	3508 0.001910459828949		
531 2.8878690430445e-05	3512 0.00145542558859091		
532 1.92034224550941e-05	3521 0.00178884549399505		
532 1.71638105597172e-05	3521 0.0016646858206798		
534 2.74951081968844e-05	3525 0.00246544469265153		
535 4.18276171800791e-05	3533 0.00210652284582258		
536 6.2955951193433e-05	3538 0.00167279423678346		
537 6.04540846810275e-05	3548 0.00246757435312339		
537 9.44288307078711e-05	3552 0.00199139215797062		
537 0.0001419551258387	3558 0.00281666551468129		
537 0.000225614593863055	3575 0.0021329800298584		
539 0.000171363500064858	3578 0.00171660343457436		
541 0.000137714467283723	3581 0.00160703440560628		
542 9.44683286101533e-05	3585 0.00119697306081723		

Table S7. CYR61 and S100A4 are highly expressed in invasive and metastatic Breast cancer patient tissue samples. Expression analysis of CYR61 and S100A4 via fluorescence staining using biomax tissue arrays (BR 20837, BR 248a, and T 087a) with paraffin- embedded patient samples. Table indicate Array type of analyzed samples, patients age, sex, the organic tissue site, pathology diagnosis, classification of M tumors (TNM), grading, stage, type, tissue ID and for most analyzed samples the expression of estrogen (ER), progesterone (PR) and Herceptinreceptor2 (Her2). Expression of CYR61 and S100A4 was assessed as (−) not expressed, (+) low expression, (++) medium expression, (+++) high expression. B, breast; LN, lymph node.

Array type	Age	Sex	Organ/ Anatomic Site	Pathology diagnosis	TNM	Grade	Stage	Type	Tissue ID.	ER	PR	HER2	S100A4	CYR61
BR 20837	45	F	B	IDC	T1N1 M0	1	IIA	M	Fmg 100017	-	-	0	+	+
BR 20837	45	F	LN	MET CA from No.1	-	-	-	MET.	Fmg 100017	-	-	0	-	+
BR 20837	45	F	B	IDC	T2N2 M0	1	IIIA	M	Fmg 100096	+	-	0	++	+
BR 20837	45	F	LN	MET CA from No.3	-	-	-	MET.	Fmg 100096	-	+	0	+	++
BR 20837	40	F	B	IDC	T2N1 M0	1	IIB	M	Fmg 100153	-	-	0	+	+
BR 20837	40	F	LN	MET CA from No.5 (LN tissue)	-	-	-	MET.	Fmg 100153	-	-	0	+	++
BR 20837	50	F	B	IDC	T2N1 M0	1	IIB	M	Fmg 070169	-	-	1+	+	++
BR 20837	50	F	LN	MET CA from No.7	-	-	-	MET.	Fmg 070169	-	-	0	+	+
BR 20837	49	F	B	IDC	T3N1 M0	1	IIIA	M	Fmg 080061	+++	-	0	+	+
BR 20837	49	F	LN	MET CA from No.9	-	-	-	MET.	Fmg 080061	+++	-	0	++	++
BR 20837	55	F	B	IDC	T4N1 M0	1	IIIB	M	Fmg 080090	+	-	0	+	+
BR 20837	55	F	LN	MET CA from No.11	-	-	-	MET.	Fmg 080090	+++	+	0	+	+
BR 20837	66	F	B	IDC	T2N1 M0	1	IIB	M	Fmg 050800	+	++	3+	+++	+++
BR 20837	66	F	LN	MET CA from No.13	-	-	-	MET.	Fmg 050800	-	-	3+	+	+
BR 20837	54	F	B	IDC	T2N1 M0	1	IIB	M	Fmg 060589	-	-	3+	+	+
BR 20837	54	F	LN	MET CA from No.15	-	-	-	MET.	Fmg 060589	-	-	3+	+	++
BR 20837	46	F	B	IDC	T2N1 M0	2	IIB	M	Fmg 060130	-	-	0	+	++
BR 20837	46	F	LN	MET CA from No.17	-	-	-	MET.	Fmg 060130	-	-	2+	+++	++
BR 20837	48	F	B	IDC	T2N1 M0	2	IIB	M	Fmg 100135	-	-	3+	+++	+++
BR 20837	48	F	LN	MET CA from No.19	-	-	-	MET.	Fmg 100135	-	-	3+	+	+
BR 20837	55	F	B	IDC	T2N2 M0	2	IIIA	M	Fmg 100230	-	-	3+	-	+
BR 20837	55	F	LN	MET CA from No.21	-	-	-	MET.	Fmg 100230	-	-	3+	+	+
BR 20837	59	F	B	IDC (fiBR fatty tissue and blood vessel)	T2N1 M0	-	IIB	M	Fmg 060965	-	-	*	+	+
BR 20837	59	F	LN	MET CA from No.23	-	-	-	MET.	Fmg 060965	-	-	3+	+	++
BR 20837	50	F	B	IDC	T2N2 M0	2	IIIA	M	Fmg 060049	++	-	1+	+	+
BR 20837	50	F	LN	MET CA	-	-	-	MET	Fmg 060049	++	-	1+	+	+

				from No.25				.					
BR 20837	48	F	B	IDC	T1N1 M0	2	IIA	M	Fmg 100062	++	-	0	++	++
BR 20837	48	F	LN	MET CA from No.27	-	-	-	MET .	Fmg 100062	-	-	0	+	+
BR 20837	45	F	B	IDC	T2N1 M0	2	IIB	M	Fmg 100181	-	-	3+	+++	+++
BR 20837	45	F	LN	MET CA from No.29	-	-	-	MET .	Fmg 100181	-	-	3+	+	+
BR 20837	55	F	B	IDC	T2N2 M0	2	IIIA	M	Fmg 100167	-	-	3+	+	+
BR 20837	55	F	LN	MET CA from No.31	-	-	-	MET .	Fmg 100167	-	++	0	+	+
BR 20837	39	F	B	IDC	T3N2 M0	2	IIIA	M	Fmg 060256	-	+	0	+	+++
BR 20837	39	F	LN	MET CA from No.33	-	-	-	MET .	Fmg 060256	+	++	0	+	+
BR 20837	54	F	B	IDC	T2N2 M0	2	IIIA	M	Fmg 100101	+	-	0	+	+
BR 20837	54	F	LN	MET CA from No.35	-	-	-	MET .	Fmg 100101	-	-	0	++	++
BR 20837	38	F	B	IDC (tumor necrosis)	T3N1 M0	-	IIB	M	Fmg 100103	-	-	*	+	+++
BR 20837	38	F	LN	MET CA from No.37	-	-	-	MET .	Fmg 100103	-	-	0	++	+++
BR 20837	49	F	B	IDC	T2N1 M0	2	IIB	M	Fmg 060127	+	-	3+	++	+
BR 20837	49	F	LN	MET CA from No.39	-	-	-	MET .	Fmg 060127	-	-	3+	+++	+
BR 20837	56	F	B	IDC	T2N1 M0	2	IIB	M	Fmg 060146	-	-	1+	++	+
BR 20837	56	F	LN	MET CA from No.41	-	-	-	MET .	Fmg 060146	-	-	0	+	+
BR 20837	39	F	B	IDC	T4N2 M0	2	IIIB	M	Fmg 060154	-	-	0	+	+
BR 20837	39	F	LN	MET CA from No.43	-	-	-	MET .	Fmg 060154	-	-	0	-	+
BR 20837	52	F	B	IDC	T2N1 M0	2	IIB	M	Fmg 060191	-	-	0	+	+
BR 20837	52	F	LN	MET CA from No.45	-	-	-	MET .	Fmg 060191	-	-	0	+	+
BR 20837	41	F	B	IDC	T2N2 M0	2	IIIA	M	Fmg 060033	+	++	0	+	++
BR 20837	41	F	LN	MET CA from No.47	-	-	-	MET .	Fmg 060033	++	++	0	-	++
BR 20837	69	F	B	IDC	T4N1 M0	2	IIIB	M	Fmg 050767	+++	-	2+	++	++
BR 20837	69	F	LN	MET CA from No.49	-	-	-	MET .	Fmg 050767	+++	-	2+	++	+
BR 20837	53	F	B	IDC	T2N2 M0	2	IIIA	M	Fmg 060601	-	-	3+	+	+
BR 20837	53	F	LN	MET CA from No.51	-	-	-	MET .	Fmg 060601	-	-	3+	+++	++
BR 20837	54	F	B	IDC	T2N2 M0	2	IIIA	M	Fmg 100105	-	-	0	+++	+
BR 20837	54	F	LN	MET CA from No.53 (sparse carcinoma tissue)	-	-	-	MET .	Fmg 100105	-	-	0	+	+
BR 20837	49	F	B	IDC	T2N2	2	IIIA	M	Fmg 060741	+	+	2+	+	+++

					M0									
BR 20837	49	F	LN	MET CA from No.55	-	-	-	MET.	Fmg 060741	-	-	0	+++	+
BR 20837	60	F	B	IDC	T1N1 M0	2	IIA	M	Fmg 060771	++	+	1+	-	+
BR 20837	60	F	LN	MET CA from No.57	-	-	-	MET.	Fmg 060771	++	++	1+	-	-
BR 20837	50	F	B	IDC	T2N1 M0	2	IIB	M	Fmg 100224	-	-	0	+	+++
BR 20837	50	F	LN	MET CA from No.59	-	-	-	MET.	Fmg 100224	-	-	0	+	++
BR 20837	54	F	B	IDC	T2N2 M0	2	IIIA	M	Fmg 100104	-	-	3+	++	++
BR 20837	54	F	LN	MET CA from No.61	-	-	-	MET.	Fmg 100104	-	-	0	+	+
BR 20837	42	F	B	IDC	T2N1 M0	2	IIB	M	Fmg 100279	*	-	3+	+	+
BR 20837	42	F	LN	MET CA from No.63	-	-	-	MET.	Fmg 100279	*	-	3+	+	+
BR 20837	52	F	B	IDC	T2N1 M0	3	IIB	M	Fmg 060773	+++	+	1+	++	++
BR 20837	52	F	LN	MET CA from No.65	-	-	-	MET.	Fmg 060773	+++	+	1+	+++	+
BR 20837	39	F	B	IDC	T2N1 M0	3	IIB	M	Fmg 060781	-	-	3+	+	+
BR 20837	39	F	LN	MET CA from No.67	-	-	-	MET.	Fmg 060781	-	-	3+	++	+
BR 20837	35	F	B	IDC	T1N1 M0	3	IIA	M	Fmg 060782	+	-	3+	++	++
BR 20837	35	F	LN	MET CA from No.69	-	-	-	MET.	Fmg 060782	++	-	3+	+	+
BR 20837	51	F	B	IDC	T2N0 M0	3	IIA	M	Fmg 061010	+	+	1+	++	+++
BR 20837	51	F	LN	MET CA from No.71	-	-	-	MET.	Fmg 061010	+	+	1+	+++	++
BR 20837	50	F	B	IDC	T4N1 M0	3	IIIB	M	Fmg 070122	-	*	*	-	++
BR 20837	50	F	LN	MET CA from No.73	-	-	-	MET.	Fmg 070122	-	-	1+	-	+
BR 20837	48	F	B	IDC	T2N1 M0	3	IIB	M	Fmg 050797	+	+++	2+	-	+++
BR 20837	48	F	LN	MET CA from No.75	-	-	-	MET.	Fmg 050797	+	+++	2+	-	++
BR 20837	55	F	B	IDC	T2N1 M0	3	IIB	M	Fmg 060821	+	+	0	++	++
BR 20837	55	F	LN	MET CA from No.77	-	-	-	MET.	Fmg 060821	+	+	0	-	+
BR 20837	48	F	B	IDC	T2N2 M0	3	IIIA	M	Fmg 060999	+	++	0	-	+
BR 20837	48	F	LN	MET CA from No.79	-	-	-	MET.	Fmg 060999	+	+	0	-	+
BR 20837	34	F	B	IDC	T2N1 M0	3	IIB	M	Fmg 070242	+++	-	1+	+	++
BR 20837	34	F	LN	MET CA from No.81	-	-	-	MET.	Fmg 070242	+++	-	1+	+	+
BR 20837	50	F	B	IDC	T2N1 M0	3	IIB	M	Fmg 080055	+++	-	0	+	++
BR 20837	50	F	LN	MET CA from No.83	-	-	-	MET.	Fmg 080055	+++	-	0	+	++
BR 20837	32	F	B	IDC	T2N1 M0	3	IIB	M	Fmg 050793	-	-	0	++	+
BR 20837	32	F	LN	MET CA	-	-	-	MET	Fmg 050793	-	-	0	+	++

				from No.85				.						
BR 20837	87	F	B	IDC	T2N1 M0	3	IIB	M	Fmg 050794	-	-	0	-	+
BR 20837	87	F	LN	MET CA from No.87	-	-	-	MET .	Fmg 050794	-	-	1+	-	+
BR 20837	50	F	B	IDC (degenerat ion tissue)	T2N1 M0	-	IIB	M	Fmg 070167	-	-	0	-	+
BR 20837	50	F	LN	MET CA from No.89 (degenerat ion tissue)	-	-	-	MET .	Fmg 070167	-	-	0	-	+
BR 20837	47	F	B	IDC	T2N1 M0	3	IIB	M	Fmg 061126	-	-	3+	+	++
BR 20837	47	F	LN	MET CA from No.91	-	-	-	MET .	Fmg 061126	-	-	3+	-	+
BR 20837	52	F	B	IDC	T2N1 M0	3	IIB	M	Fmg 070124	-	-	2+	-	++
BR 20837	52	F	LN	MET CA from No.93	-	-	-	MET .	Fmg 070124	-	-	2+	-	+++
BR 20837	68	F	B	IDC	T2N1 M0	3	IIB	M	Fmg 060779	-	-	0	+	+
BR 20837	68	F	LN	MET CA from No.95	-	-	-	MET .	Fmg 060779	-	-	0	-	++
BR 20837	37	F	B	IDC	T3N1 M0	3	IIIA	M	Fmg 050765	-	-	3+	+	++
BR 20837	37	F	LN	MET CA from No.97	-	-	-	MET .	Fmg 050765	-	-	3+	++	+
BR 20837	52	F	B	IDC	T2N1 M0	3	IIB	M	Fmg 100132	-	-	3+	+	++
BR 20837	52	F	LN	MET CA from No.99	-	-	-	MET .	Fmg 100132	-	-	3+	++	+++
BR 20837	33	F	B	IDC	T3N3 M0	3	IIIC	M	Fmg 060568	-	-	1+	+	++
BR 20837	33	F	LN	MET CA from No.101	-	-	-	MET .	Fmg 060568	+	+	1+	+	+
BR 20837	47	F	B	IDC	T2N1 M0	3	IIB	M	Fmg 060588	-	+	2+	+	+
BR 20837	47	F	LN	MET CA from No.103	-	-	-	MET .	Fmg 060588	++	+++	2+	+	+
BR 20837	56	F	B	IDC	T2N1 M0	3	IIB	M	Fmg 110095	-	-	0	+	++
BR 20837	56	F	LN	MET CA from No.105	-	-	-	MET .	Fmg 110095	-	-	0	+	++
BR 20837	42	F	B	IDC	T2N1 M0	3	IIB	M	Fmg 120083	-	-	0	+	++
BR 20837	42	F	LN	MET CA from No.107	-	-	-	MET .	Fmg 120083	-	-	0	+	+
BR 20837	54	F	B	IDC	T2N1 M0	3	IIB	M	Fmg 060784	-	-	3+	+	++
BR 20837	54	F	LN	MET CA from No.109	-	-	-	MET .	Fmg 060784	-	-	3+	+	+
BR 20837	42	F	B	IDC	T2N2 M0	3	IIIA	M	Fmg 060787	-	-	3+	+	++
BR 20837	42	F	LN	MET CA from No.111	-	-	-	MET .	Fmg 060787	-	-	3+	+	++
BR 20837	31	F	B	IDC	T3N1 M0	3	IIIA	M	Fmg 050134	++	++	0	++	++
BR 20837	31	F	LN	MET CA from No.113 (chronic inflammat	-	-	-	MET .	Fmg 050134	-	-	0	+	+

				ion with fiBR ous tissue and blood vessel)										
BR 20837	40	F	B	IDC	T2N1 M0	3	IIB	M	Fmg 060963	+++	++	2+	++	++
BR 20837	40	F	LN	MET CA from No.115	-	-	-	MET.	Fmg 060963	-	-	0	+	+
BR 20837	50	F	B	IDC	T2N1 M0	3	IIB	M	Fmg 120115	++	-	0	+	+
BR 20837	50	F	LN	MET CA from No.117	-	-	-	MET.	Fmg 120115	++	-	0	+	+
BR 20837	37	F	B	IDC	T2N1 M0	3	IIB	M	Fmg 080106	-	-	1+	-	+
BR 20837	37	F	LN	MET CA from No.119	-	-	-	MET.	Fmg 080106	-	-	1+	-	+
BR 20837	32	F	B	IDC	T2N1 M0	3	IIB	M	Fmg 060594	+	++	0	+++	++
BR 20837	32	F	LN	MET CA from No.121	-	-	-	MET.	Fmg 060594	-	++	0	++	+
BR 20837	51	F	B	IDC	T2N1 M0	3	IIB	M	Fmg 060597	-	-	3+	+	++
BR 20837	51	F	LN	MET CA from No.123	-	-	-	MET.	Fmg 060597	+	-	3+	+	+++
BR 20837	52	F	B	IDC	T1N1 M0	3	IIA	M	Fmg 100020	+++	-	0	+	+
BR 20837	52	F	LN	MET CA from No.125 (LN tissue)	-	-	-	MET.	Fmg 100020	-	-	0	++	+
BR 20837	45	F	B	IDC	T2N1 M0	3	IIB	M	Fmg 100235	-	-	1+	-	++
BR 20837	45	F	LN	MET CA from No.127	-	-	-	MET.	Fmg 100235	-	-	1+	-	+
BR 20837	49	F	B	IDC	T2N2 M0	3	IIIA	M	Fmg 100041	-	-	0	+	+
BR 20837	49	F	LN	MET CA from No.129	-	-	-	MET.	Fmg 100041	-	-	0	-	+
BR 20837	32	F	B	IDC	T2N2 M0	3	IIIA	M	Fmg 060426	-	-	1+	+	+
BR 20837	32	F	LN	MET CA from No.131 (LN tissue)	-	-	-	MET.	Fmg 060426	+	-	1+	++	++
BR 20837	46	F	B	IDC (B tissue)	T2N1 M0	-	IIB	M	Fmg 060211	-	-	*	-	+
BR 20837	46	F	LN	MET CA from No.133	-	-	-	MET.	Fmg 060211	-	-	3+	+	++
BR 20837	44	F	B	IDC	T2N2 M0	3	IIIA	M	Fmg 060391	-	-	3+	-	+
BR 20837	44	F	LN	MET CA from No.135	-	-	-	MET.	Fmg 060391	+++	++	2+	-	+
BR 20837	45	F	B	IDC	T2N1 M0	1	IIB	M	Fmg 100069	-	-	3+	+	+
BR 20837	45	F	LN	MET CA from No.137	-	-	-	MET.	Fmg 100069	-	-	3+	-	+
BR 20837	45	F	B	IDC	T2N2 M0	3	IIIA	M	Fmg 120025	+	-	0	-	+
BR 20837	45	F	LN	MET CA from No.139	-	-	-	MET.	Fmg 120025	++	-	0	-	+
BR 20837	48	F	B	IDC	T2N1 M0	3	IIB	M	Fmg 110034	-	-	0	+++	++
BR 20837	48	F	LN	MET CA	-	-	-	MET	Fmg 110034	-	-	0	++	+

				from No.141				.						
BR 20837	48	F	B	IDC	T2N1 M0	3	IIB	M	Fmg 100217	-	-	3+	-	+
BR 20837	48	F	LN	MET CA from No.143 (necrosis tissue)	-	-	-	MET .	Fmg 100217	*	-	*	-	++
BR 20837	35	F	B	IDC	T2N2 M0	3	IIIA	M	Fmg 090034	-	-	0	++	+++
BR 20837	35	F	LN	MET CA from No.145	-	-	-	MET .	Fmg 090034	-	-	1+	+++	+++
BR 20837	43	F	B	IDC	T2N1 M0	3	IIB	M	Fmg 080053	-	-	1+	++	+++
BR 20837	43	F	LN	MET CA from No.147	-	-	-	MET .	Fmg 080053	-	-	2+	++	++
BR 20837	51	F	B	IDC	T3N2 M0	3	IIIA	M	Fmg 070120	-	*	*	-	-
BR 20837	51	F	LN	MET CA from No.149	-	-	-	MET .	Fmg 070120	-	*	*	-	-
BR 20837	50	F	B	IDC	T3N1 M0	3	IIIA	M	Fmg 100292	++	+	1+	++	++
BR 20837	50	F	LN	MET CA from No.151	-	-	-	MET .	Fmg 100292	+	-	1+	+++	+++
BR 20837	42	F	B	IDC	T2N1 M0	3	IIB	M	Fmg 100148	-	-	2+	+	+
BR 20837	42	F	LN	MET CA from No.153	-	-	-	MET .	Fmg 100148	-	++	0	+	+
BR 20837	72	F	B	IDC (sparse)	T2N1 M0	3	IIB	M	Fmg 080070	-	-	0	+	+
BR 20837	72	F	LN	MET CA from No.155	-	-	-	MET .	Fmg 080070	-	-	3+	+	+
BR 20837	79	F	B	IDC	T2N1 M0	3	IIB	M	Fmg 060580	-	-	0	+	++
BR 20837	79	F	LN	MET CA from No.157	-	-	-	MET .	Fmg 060580	-	-	0	++	+
BR 20837	50	F	B	IDC	T2N1 M0	3	IIA	M	Fmg 100164	-	-	0	+	+
BR 20837	50	F	LN	MET CA from No.159	-	-	-	MET .	Fmg 100164	-	-	0	+	+
BR 20837	48	F	B	IDC	T2N1 M0	3	IIB	M	Fmg 100067	+++	-	0	+	+
BR 20837	48	F	LN	MET CA from No.161 (MET CA of fiBR ofatty tissue)	-	-	-	MET .	Fmg 100067	+++	-	0	+	+
BR 20837	47	F	B	IDC	T4N1 M0	3	IIIB	M	Fmg 060077	++	+	0	+	++
BR 20837	47	F	LN	MET CA from No.163	-	-	-	MET .	Fmg 060077	+++	+++	0	+	-
BR 20837	54	F	B	IDC	T2N1 M0	3	IIB	M	Fmg 100244	-	-	2+	+++	+++
BR 20837	54	F	LN	MET CA from No.165	-	-	-	MET .	Fmg 100244	-	-	0	-	+++
BR 20837	54	F	B	IDC	T2N2 M0	3	IIIA	M	Fmg 100245	+++	+	1+	+	+++
BR 20837	54	F	LN	MET CA from No.167	-	-	-	MET .	Fmg 100245	+++	+	1+	+	+
BR 20837	43	F	B	IDC	T1N1 M0	3	IIA	M	Fmg 100066	+++	-	0	-	-
BR 20837	43	F	LN	MET CA from	-	-	-	MET .	Fmg 100066	+++	-	0	+	+

				No.169										
BR 20837	42	F	B	IDC	T2N1 M0	3	IIB	M	Fmg 120054	-	-	0	-	++
BR 20837	42	F	LN	MET CA from No.171	-	-	-	MET.	Fmg 120054	-	-	0	+	+
BR 20837	50	F	B	ILC	T2N1 M0	-	IIB	M	Fmg 070246	-	-	0	-	+
BR 20837	50	F	LN	MET CA from No.173	-	-	-	MET.	Fmg 070246	-	-	0	-	++
BR 20837	19	F	B	ILC	T2N1 M0	-	IIB	M	Fmg 070179	+	-	2+	-	++
BR 20837	19	F	LN	MET CA from No.175	-	-	-	MET.	Fmg 070179	+	-	2+	-	+
BR 20837	55	F	B	ILC	T2N2 M0	-	IIIA	M	Fmg 100027	-	-	3+	+	++
BR 20837	55	F	LN	MET CA from No.177	-	-	-	MET.	Fmg 100027	-	-	3+	+	+++
BR 20837	45	F	B	ILC	T2N1 M0	-	IIB	M	Fmg 100047	-	-	0	+	++
BR 20837	45	F	LN	MET CA from No.179	-	-	-	MET.	Fmg 100047	-	-	0	+	++
BR 20837	55	F	B	ILC	T2N1 M0	-	IIB	M	Fmg 110031	+	-	0	+	+++
BR 20837	55	F	LN	MET CA from No.181	-	-	-	MET.	Fmg 110031	++	-	0	+	++
BR 20837	54	F	B	ILC	T2N1 M0	-	IIB	M	Fmg 100044	-	-	0	+	+
BR 20837	54	F	LN	MET CA from No.183	-	-	-	MET.	Fmg 100044	-	-	0	-	+
BR 20837	74	F	B	ILC	T2N1 M0	-	IIB	M	Fmg 060128	-	-	0	+	++
BR 20837	74	F	LN	MET CA from No.185	-	-	-	MET.	Fmg 060128	-	-	0	+	+
BR 20837	51	F	B	ILC (fiBR ofatty tissue and blood vessel)	T2N1 M0	-	IIB	M	Fmg 100212	-	-	*	+	+
BR 20837	51	F	LN	MET CA from No.187	-	-	-	MET.	Fmg 100212	-	-	0	+	-
BR 20837	50	F	B	Medullary carcinoma	T3N1 M0	-	IIIA	M	Fmg 080030	-	-	0	+	+
BR 20837	50	F	LN	MET CA from No.189	-	-	-	MET.	Fmg 080030	-	-	0	+	+
BR 20837	48	F	B	Invasive micro papillary carcinoma	T2N1 M0	-	IIB	M	Fmg 120067	++	+	2+	+	+
BR 20837	48	F	LN	MET CA from No.191	-	-	-	MET.	Fmg 120067	++	+	2+	-	+
BR 20837	50	F	B	Mixed carcinoma (IDC and ILC)	T3N2 M0	-	IIIA	M	Fmg 060600	++	-	2+	+	+
BR 20837	50	F	LN	MET CA from No.193	-	-	-	MET.	Fmg 060600	++	-	2+	+	++
BR 20837	65	F	B	Mixed carcinoma (IDC and ILC)	T1N1 M0	-	IIA	M	Fmg 060775	++	+++	2+	+++	+
BR 20837	65	F	LN	MET CA from No.195	-	-	-	MET.	Fmg 060775	++	+++	2+	+++	+
BR 20837	54	F	B	Mixed carcinoma	T2N1 M0	-	IIB	M	Fmg 100221	+	-	3+	+	+

				(IDC and ILC)									
BR 20837	54	F	LN	MET CA from No.197	-	-	-	MET.	Fmg 100221	-	-	3+	-	+
BR 20837	43	F	B	Mixed carcinoma (IDC and ILC)	T2N1 M0	-	IIB	M	Fmg 070244	++	-	2+	+	+
BR 20837	43	F	LN	MET CA from No.199	-	-	-	MET.	Fmg 070244	++	-	2+	+	+
BR 20837	48	F	B	Mixed carcinoma (IDC and ILC)	T2N2 M0	-	IIIA	M	Fmg 110129	-	-	3+	-	+
BR 20837	48	F	LN	MET CA from No.201	-	-	-	MET.	Fmg 110129	-	-	3+	+	+
BR 20837	45	F	B	Mixed carcinoma (IDC and ILC)	T2N1 M0	-	IIB	M	Fmg 100054	-	-	0	+	+
BR 20837	45	F	LN	MET CA from No.203	-	-	-	MET.	Fmg 100054	-	-	0	+	+
BR 20837	43	F	B	Mixed carcinoma (IDC and ILC)	T2N2 M0	-	IIIA	M	Fmg 100273	++	++	0	+	++
BR 20837	43	F	LN	MET CA from No.205	-	-	-	MET.	Fmg 100273	++	++	0	+	++
BR 20837	49	F	B	Mixed carcinoma (sparse IDC and ILC)	T2N2 M0	-	IIIA	M	Fmg 060250	-	-	*	-	+++
BR 20837	49	F	LN	MET CA from No.207	-	-	-	MET.	Fmg 060250	-	-	3+	+	+
BR 248a	34	F	B	IDC	T3N0 M0	1--2	IIB	M	Fmg 040048				+++	+
BR 248a	37	F	B	IDC	T2N0 M0	1--2	IIA	M	Fmg 020357				+++	++
BR 248a	60	F	B	IDC	T2N0 M0	2	IIA	M	Fmg 040031				++	-
BR 248a	57	F	B	IDC	T2N0 M0	2	IIA	M	Fmg 040001				+	-
BR 248a	38	F	B	IDC	T1N0 M0	2	I	M	Fmg 040052				+++	+
BR 248a	55	F	B	IDC	T2N0 M0	2	IIA	M	Fmg 040104				+++	++
BR 248a	45	F	B	IDC	T2N0 M0	2	IIA	M	Fmg 040113				+++	-
BR 248a	48	F	B	IDC	T2N0 M0	2	IIA	M	Fmg 040118				++	-
BR 248a	58	F	B	IDC	T2N0 M0	2	IIA	M	Fmg 040120				++	+
BR 248a	34	F	B	IDC	T2N0 M0	2	IIA	M	Fmg 040123				++	++
BR 248a	49	F	B	IDC	T2N0 M0	2	IIA	M	Fmg 040125				++	++
BR 248a	58	F	B	IDC	T2N0 M0	2	IIA	M	Fmg 040130				+	++
BR 248a	38	F	B	IDC	T2N1 M0	2	IIB	M	Fmg 040131				++	+++
BR 248a	79	F	B	IDC	T2N1 M0	3	IIB	M	Fmg 010491				+	-
BR 248a	43	F	B	IDC	T2N0 M0	3	IIA	M	Fmg 040004				-	-
BR 248a	46	F	B	IDC	T3N0 M0	3	IIB	M	Fmg 040074				++	++
BR 248a	76	F	B	IDC	T4N0 M0	3	IIIB	M	Fmg 010789				+	+
BR 248a	47	F	B	Medullary carcinoma	T2N0 M0	-	IIA	M	Fmg 040016				++	++

BR 248a	21	F	B	Adenosis	-	-	-	N	Fmg 06N024				-	-
BR 248a	28	F	B	NBT (fiBR ofatty tissue and blood vessel)	-	-	-	N	Fmg 11N017				-	-
BR 248a	21	F	B	NBT	-	-	-	N	Fmg 12N001				-	+
BR 248a	50	F	B	Adenosis	-	-	-	N	Fmg 08N034				-	-
BR 248a	50	F	B	NBT	-	-	-	N	Fmg 12N002				-	-
BR 248a	19	F	B	NBT	-	-	-	N	Fmg 07N013				-	-
T087a	57	F	B	IDC	T2N1 M0	2	IIb	M	183742				++	+
T087a	49	F	B	IDC	T2N0 M0	3	IIa	M	Fmg 040987				+	-
T087a	40	F	B	ILC	T2N1 M0	-	IIb	M	Fmg 060878				+	+
T087a	42	F	B	Apocrine carcinoma	T2N0 M0	-	IIa	M	Fmg 070034				+	+
T087a	27	F	B	NBT	-	-	-	N	Fmg 07N025				-	+
T087a	19	F	B	Adenosis	-	-	-	N	Fmg 07N013				-	-

3.2. MANUSCRIPT B

Identification of drivers of breast cancer invasion by secretome analysis: insight into CTGF signaling

Citation

Hellinger, J. W., Schömel, F., Lenz, C., Bauerschmitz, G., Emons, G., & Gründker, C. Identification of drivers of breast cancer invasion by secretome analysis: insight into CTGF signaling. *(under revision at Communications Biology)*

Own contribution: Conducted experiments and analyzed data for figures 1- 7 and supplemental material. Shared contribution for experiments presented in figures 6 G and 6 H. Contribution to: method design, figure arrangement, manuscript writing, and manuscript revision.

Abstract

Altered tumor micro environmental consistency facilitates tumor progression toward metastasis. Here, we combine data from secretome and proteome analysis using mass spectrometry with microarray data from mesenchymal transformed breast cancer cells (MCF-7-EMT) to elucidate drivers of epithelial-mesenchymal transition and cell invasion. Suppression of growth factor CTGF reduced invasion in 2D and 3D invasion assays and expression of TGFBI, ZEB1 and LOX, while cell-extracellular matrix (ECM) adhesion is increased in mesenchymal transformed breast cancer cells. Increased expression of CTGF leads to an increased 3D invasion, expression of FN1, SPARC and CD44, and decreased cell-ECM adhesion. GnRH agonist Triptorelin reduces CTGF expression in a RhoA-dependent manner. Our results suggest, that CTGF drives breast cancer cell invasion and therefore represents an attractive therapeutic target for drug development to prevent breast cancer dissemination.

Introduction

Metastasis is second leading cause of cancer-related death in the US. Barely 27 % of breast cancer patients diagnosed with distant metastasis survive a period of 5 years (133). Breast cancer mortality will increase by 46.5% until 2040 to almost 1 million deaths worldwide (134). Single most frequent site for breast cancer metastasis is bone, which accounts for 70% of all metastatic breast cancer (135). Elucidation of drivers of cancer metastasis is therefore pivotal. The metastatic cascade is initiated by dissemination of cancer cells into surrounding tissue (136). Micro environments of primary tumor and metastatic niche have shared communication networks. Tumor stroma stiffness facilitates deposition and remodeling of extracellular matrix (ECM) in breast cancer (2, 63, 64). Cancer cells, cancer associated fibroblast, and immune cells modulate ECM by deposition of structural components like collagens or fibronectin (FN1), secretion of growth factors (e.g. Transforming growth factor-beta-induced protein ig-h3, connective tissue growth factor) and ECM-transforming enzymes (e.g. Lysyl oxidase) (2). Gene expression studies identified a bone metastatic signature which includes expression of connective tissue growth factor (CTGF) and is associated with poor patient outcome and metastasis (58, 137). Cancer cells can embrace developmental processes like epithelial-mesenchymal transition (EMT) to gain invasive properties and stemness, which could help them to disseminate, intravasate, circulate, extravasate and retain during dormancy but are in need of mesenchymal-epithelial transition (MET) to reactivate upon cues from metastatic niche and outgrow (138). This theory is consistent with observations that clinical

samples of human metastasis resemble epithelial phenotype of primary tumors (139). There is an urgent need to identify potential drivers of cell invasion, the initial step within metastatic cascade, at the primary site and colonization at distant sites. A better understanding of transient dynamic processes of high cellular plasticity could help to intercept the metastatic cascade, which could in turn lead to identification of targets for new treatment options to prevent cancer cell dissemination and metastatic outgrowth. We aim to identify secreted proteins priming micro environment resulting in increased cancer cell dissemination and driving epithelial-mesenchymal transition.

We combined co-culture model for bone-directed breast cancer cell invasion with mass spectrometry based secretome analysis and identified secreted CTGF is a potential driver for breast cancer cell invasion. In this system, CTGF was found to regulate cell-ECM adhesion, proteolytic activity and expression of EMT inducing genes. Moreover, CTGF expression is dependent on RhoA activity and that treatment of invasive breast cancer cells with gonadotropin releasing hormone (GnRH) agonist Triptorelin could increase RhoA activity. These data indicate, that CTGF is a promising target to inhibit invasion in highly plastic breast cancer cells and aggressive triple negative breast cancer (TNBC) cells.

Results

Identifying potential drivers of breast cancer cell invasion

Up to 13.6% of breast cancer patients (diagnosed in stage I-III) will develop bone metastasis within 15 years of follow-up (140). Previous studies demonstrate that co-culture of breast cancer cells with osteosarcoma cells (MG-63) or osteoblast-like cells increased invasiveness (132). However, mechanisms by which breast cancer cells metastasize to bone remain elusive. To shed light on drivers for bone-directed breast cancer invasion, we decided to investigate if identified potential drivers by analyzing secretome of co-culture media using mass spectrometry. Excluding serum from media and analyzing only secreted proteins, we first tested if non-invasive MCF-7 breast cancer cells gain invasive properties when co-cultured with osteosarcoma cells without adding serum to media (fig.1 A). Indeed, invasiveness of MCF-7 breast cancer cells increased more than 4-fold, when using Matrigel in a transwell co-culture invasion assay (fig. 1A; co-culture matrigel: 413.7 ± 83.07 % vs. MCF-7 matrigel; $P = 0.0021$, $n = 12$) and a more than 7-fold increase of invasiveness, when using gelatin (fig. 1A; co-culture gelatin: 737.5 ± 250.9 % vs. MCF-7 gelatin; $P = 0.0316$, $n = 6$). We next co-cultured MCF-7 cells with MG-63 cells and analyzed co-culture media using mass spectrometry

secretome analysis to identify proteins that drive bone-directed metastasis. We could identify 28 secreted potential drivers for bone-directed breast cancer cell invasion (fig. 1 B, C, and S1). Gene ontology (GO) enrichment analysis elucidated that observed secreted proteins play most prominently roles in extracellular matrix organization (fig. 1 S2, FDR 3.26 x 10^{-15}; 50% of detected proteins), extracellular structure organization (fig. 1 S2, FDR 1.52 x 10^{-14}; 50% of detected proteins) and wound healing (fig. 1 S2, FDR 8.92 x 10^{-9}; 39% of detected proteins). Further classification of observed proteins using Shiny GO indicated that 39% of detected proteins are categorized within locomotion and cell motility and 36 % within cell adhesion (fig. 1 S3, S4A). Additionally, we could detect that co-culture media in comparison to MG-63 media a decreases MMP2 protein expression and an increased SPARC expression was detected (fig.1 S 4B). To further examine underlying molecular mechanism of breast cancer cell invasion we analyzed lysates of co-cultured MCF-7 cells compared to untreated MCF-7 cells (fig.1 S4 and S5). GO enrichment analysis elucidated that observed regulated proteins play most prominently roles in protein folding (fig.1 S6, FDR 7.55 x10 $^{-6}$; 33% of detected proteins), programmed cell death (fig. 1 S6, FDR 1.34 x10 $^{-5}$; 61% of detected proteins) and cellular response to cytokine stimulus (fig.1 S6, FDR 1.34 x10 $^{-5}$; 50% of detected proteins). Interestingly, cell death associated proteins seem to be regulated prominently, including HSPA9 (heat shock protein family A (Hsp70) member 9), HSP90B1 (heat shock protein 90 β family member 1), HSP90AB1 (heat shock protein 90 α family class B member 1), HSPD1 (heat shock protein family D (Hsp60) member), and HSPB1 (heat shock protein family B member 1) (fig. 1 S4D, S5 and S6). While detected findings from proteome analysis are different from detected secretome findings, GO grouping of proteome findings elucidated similar results compared to secretome findings. Proteome analysis findings where categorized (amongst others) in 33% locomotion, 33% cell motility and 27 % cell adhesion (fig.1 S7).

Cells undergoing dynamic EMT programs reveal an increased invasive behavior (51). Microarray analysis of MCF-7 breast cancer cells within a dynamic TGFβ-dependent EMT program exhibited an increased expression of CTGF, CD44 molecule (CD44), Sushi, von Willebrand factor type A, EGF and pentraxin domain containing 1 (SVEP1), Transforming growth factor-beta-induced protein ig-h3 (TGFBI), Secreted Protein Acidic And Cysteine Rich (SPARC), Lysyl oxidase (LOX), FN1 and Matrix Metallopeptidase 2 (MMP2) and Follistatin-like 1(FSTL1) (51). Interestingly, we found these proteins are highly secreted in co-culture medium of MCF-7 and MG-63 as elucidated by secretome analysis (fig. 1 D, and S1).

CTGF expression correlates with invasiveness of mesenchymal transformed and TNBC cells

One of the potential drivers of invasion is CTGF, which is upregulated during wound healing and has an impact on osteolytic breast cancer metastasis (111, 141). Using patient data from large public cancer genomic datasets CTGF expression was assessed in bone, lung, liver, and brain where breast cancer spreads most prominently (142). Expression of CTGF in bone and lung appeared to be close to expression in breast tissue, while expression in brain in liver is reduced compared to breast (fig. 2 S8). CTGF mRNA expression is upregulated in mesenchymal transformed (fig. 2A; MCF-7-EMT: 1.995 ± 0.4356 vs. MCF-7; P = 0.0454; n=6) and TNBC cells (fig. 2A; MDA-MB-231: 190.5 ± 45.81 fold change vs. MCF-7; P = 0.0061; n=4). Protein expression analysis gave similar results (fig. 2B; MCF-7-EMT: 321 ± 82.6 % vs. M; P=0.0233; n=6 and MDA-MB-231: 213 ± 27.17 %; P=0.002; n=6). To verify the potential use of CTGF as a therapeutic target for invasive breast cancer we analyzed 24 breast tissue sections. Of these, 18 were invasive ductal carcinomas and 88.9% exhibit a positive signal (fig. 2 C, D and S 8 indicated by + or ++) for CTGF while 80% of the 6 analyzed normal breast tissues were negative for CTGF (fig. 2 C, D and S 9 indicated by -).

Detection of mesenchymal transformed and aggressive breast cancer cells is a major requirement to select specific treatment options. Previously, it was demonstrated that cells in transient transitional stages express specific cell receptor markers (143). We found, that highly plastic breast cancer cells and TNBC do not only express more CTGF but co-express CD106 (Vascular cell adhesion molecule 1) and CD51 (Integrin subunit alpha V) in a higher probability than non-invasive MCF-7 cells (fig. 2 E and F; MCF-7-EMT 72.67 ± 18.21 counts $CD106^{high}$ $CD51^{high}$ vs. MCF-7; P=0.043; n=3; MDA-MB-231 197 ± 49 counts $CD106^{high}$ $CD51^{high}$ vs. MCF-7; P = 0.0217, n=3).

Findings from secretome and proteome analyses prominently grouped into locomotion and cell motility categories. Therefore, we assessed impact of CTGF expression on invasiveness of mesenchymal transformed and TNBC cells. Using RNA interference CTGF expression was transiently suppressed (fig. 3 S10 A and B). Suppression of CTGF leads to reduced invasion of mesenchymal transformed (fig. 3 A and B; MCF-7-EMT 61.41 ± 7.427 % vs control; P=0.0034; n=18) and TNBC (fig. 3B; MDA-MB-231 79.44 ±4.64 % vs control; P= 0.0258; n=17) cells in 2D transwell invasion co-culture assay. Recent reports suggested that YAP-activation appears differently dependent on dimension model used (144). CTGF is transcriptional expressed upon YAP translocation to nucleus. We therefore tested, if effects

were reproducible in 3D invasion assay setup (fig. 3 C). Reducing CTGF expression transiently reduced invaded area in 3D breast cancer spheroids of mesenchymal transformed (fig. 3D and E; MCF-7-EMT 94.25 ± 2.535 % vs control; P=0.032; n=15) and TNBC cells (fig. 3 D and E; MDA-MB-231 55.93 ± 13.3 % vs control; P= 0.0044; n=9) cells.

Upon co-culturing breast cancer cells with osteosarcoma cells, cells gain invasive potential and exhibit a specific expression profile. It was suggested earlier, that an increased CTGF expression alters expression of matrix metalloproteinases and MMP-2 promotes migration by cleaving fibronectin and CTGF (145-147). It remained unclear though, whether extracellular MMP2, CTGF and FN1 facilitate invasion in breast cancer interdependently. Consequently, we analyzed if spheroid invaded area and proliferation were altered when treated with human MMP2, CTGF and FN1. Furthermore, we analyzed if treatment with an MMP2 inhibitor (BB-94, Batimastat) reduces breast cancer invasiveness. We found that 3D spheroid area growth was increased when treated with recombinant human CTGF (rhCTGF; fig. 3F; rhCTGF: 135.5 ± 35.5 % mean difference vs. untreated; p=0.0006; F= 21.61; n=6), recombinant human MMP2 (rhMMP2, fig. 3F; rhMMP2: 137.8 ± 37.8 % mean difference vs. untreated; p=0.0003; F= 21.61; n=6), rhCTGF and human FN1 (hFN1) and recombinant human MMP2 (fig. 3F; rhCTGF+hFN1+rhMMP2: 137 ± 37 % mean difference vs. untreated; p=0.0003; F= 21.61; n=6), or rhCTGF and rhMMP2 (fig. 3F; rhCTGF+rhMMP2: 137.2 ± 37.2 % mean difference vs. untreated; p=0.0015; F= 21.61; n=4). Adding hFN1, combination of hFN1 with rhCTGF or rhMMP2 does not alter spheroid area growth (fig 3F). In contrast, combining hFN1 and BB-94 treatment (fig. 3F; hFN1+BB-94: 68.4 ± 31.6 % mean difference vs. untreated; p=0.0028; F= 21.61; n=4), or rhMMP2 and BB-94 (fig. 3F; rhMMP2+BB-94: 69.4 ± 30.1 % mean difference vs. untreated; p=0.0041; F= 21.61; n=6) or rhCTGF and hFN1 and rhMMP2 and BB-94 (fig. 3F; rhCTGF+hFN1+rhMMP2+BB-94: 75.66 ± 24.34 % mean difference vs. untreated control; p=0.0006; F= 21.61; n=6) results in decreased area growth. Combination of rhCTGF with BB-94 did not alter invasive area growth. While none of the settings altered proliferation (S10 D).

CTGF alters cell-ECM adhesion and proteolytic activity of breast cancer cells

Cell invasion as initial step of metastatic cascade results from suppression of cell-cell adhesion modulated by cadherin's and cell-ECM adhesion promoted through different receptors including integrins (148). Secretome- and proteome analysis elucidated that co-culturing non-invasive MCF-7 breast cancer cells with osteosarcoma cells led to an expression alteration of proteins involved in cell adhesion. We tested if cell-ECM adhesion

was altered in invasive breast cancer cells (MCF-7-EMT, MDA-MB-231) when intracellular CTGF was suppressed by RNA interference, extracellular CTGF was blocked using CTGF-specific antibodies or non-invasive MCF-7 breast cancer cells were treated with rhCTGF. CTGF suppression increased cell-ECM adhesion (fig. 4A, B; MCF-7-EMT: 146.3 ± 12.1 % vs. control; p=0.0185; n=3; MDA-MB-231: 168.3 ±14.3% vs. control; p=0.0083; n=3). Blocking extracellular CTGF increased cell-ECM adhesion (fig. 4C, D; MCF-7-EMT: 120.6 ± 5.724 % vs. IgG control; p=0.0071; n=5; MDA-MB-231: 110.5 ± 3.776 % vs. IgG control; p=0.0493; n=3). Adding rhCTGF to non-invasive MCF-7 breast cancer cells resulted in dose-dependent decreased cell-ECM adhesion (fig. 4E, F; MCF-7 1µg/ml rhCTGF: 94.2 ± 5.809 % mean difference vs. untreated; p=0.0459; F = 6.244; n=3).

Matrix metalloproteinases contribute to invadopodia formation and tissue invasion through proteolytic activity alteration of cells (149). We examined, whether suppression of CTGF or treatment with rhCTGF regulates relative proteolytic activity of breast cancer cells. Reduced CTGF expression decreased relative proteolytic activity of mesenchymal transformed breast cancer cells (fig. 4G; MDA-MB-231 $CTGF^-$: 117 ± 28.92 % vs. control; p=0.0205; n=3), while it did not alter relative proteolytic activity of TNBC cells (fig. 4G). Treatment with rhCTGF induced proteolytic activity in non-invasive MCF-7 breast cancer cells (fig. 4H; MCF-7 rhCTGF: 113.7 ± 4.229 % vs. untreated; p=0.0314; n=3).

CTGF differentially regulates potential drivers of invasion and EMT-markers in mesenchymal transformed and triple negative breast cancer cells

To further analyze underlying mechanisms of CTGF-induced invasion and suppressed adhesion we examined, if reduced CTGF expression alters expression of TGFBI, CD44, SPARC, FN1, LOX and FSTL1 which were all identified potential drivers for invasion by secretome analysis. We could detect, that reduced CTGF in mesenchymal transformed breast cancer cells suppressed expression of TGFBI (fig. 5A; TGFBI $CTGF^-$: 0.6474 ± 0.1107 FC vs. TGFBI control; p= 0.0052; n= 6) and LOX (fig. 5A; LOX $CTGF^-$: 0.7933 ± 0.043 FC vs. LOX control; p= 0.0088; n= 3), and increased expression of CD44 (fig. 5A; CD44 $CTGF^-$:1.21 ± 0.045 FC vs. CD44 control; p= 0.0096; n= 3), SPARC (fig. 5A; SPARC $CTGF^-$: 2.083 ± 0.2749 FC vs. SPARC control; p= 0.0169; n= 3) and FN1 (fig. 5A; FN1 $CTGF^-$: 1.41 ± 0.07234 FC vs. FN1 control; p= 0.0048; n= 3). Suppressed CTGF expression altered FN1 (fig. 5B; FN1 $CTGF^-$: 1.557 ± 0.1014 FC vs. FN1 control; p= 0.0054; n= 3) expression in TNBC cells.

We found that CTGF had in impact on TGFBI-expression, and further wanted to test, whether a reduced CTGF expression can regulate expression of EMT transcription factors. We examined expression of Cadherin 1 (CDH1), Vimentin (Vim), ZEB1 and SNAIl family transcriptional repressor 2 (SNAI2) after transient CTGF suppression in mesenchymal transformed and TNBC cells. We found that downregulation of CTGF led to reduced ZEB1 expression in mesenchymal transformed breast cancer cells (fig. 5C; 0.7767 ± 0.063 FC vs. control; p=0.0138; n=3). In contrast, suppressed CTGF resulted in downregulated Vimentin expression in TNBC cells (fig. 5D; 0.65 ± 0.0985; p=0.0237; n=3).

GnRH agonist regulates CTGF expression through altered RhoA activity in mesenchymal transformed breast cancer cells

Most luminal breast cancer will metastasize to bone (150). Suppression of ovarian function is part of therapy of endocrine-sensitive premenopausal early and advanced hormone breast cancer. Triptorelin, a GnRH agonist, revealed clinical benefit in high-risk patients by suppressing ovarian steroids and it has been investigated in attempt to preserve ovarian function during chemotherapy in young female patients (151). GnRH receptor is expressed in 50-64% of all human breast cancers (152-156). Around 15% of all human breast cancers are stated as TNBC, which is associated with high risk recurrence and metastasis (157, 158). Approximately 74 % of all TNBC express GnRH receptor (7, 132, 159). It was observed that GnRH agonist Triptorelin has in impact on breast cancer invasiveness (51, 132, 160). Accordingly, we wanted to assess whether, Triptorelin treatment suppresses CTGF expression. Mesenchymal transformed breast cancer cells were treated for 48 hours with 10^{-9} M or 10^{-7} M Triptorelin every 24 hours. We found that treatment with 10^{-7} M Triptorelin reduced CTGF expression (fig. 6A; Triptorelin 10^{-7} M: 0.435 ± 0.565 FC vs. untreated; p=0.0052; F= 8.366; n=3; and fig. 6B; 83.67 ± 3.383 % vs. untreated control; p=0.0085; n=3) which we could verify in TNBC cell as well (S11 A, B). Furthermore, we analyzed, whether Triptorelin treatment altered cell-ECM adhesion. We found that 10^{-7} M Triptorelin treatment increased cell-ECM adhesion (fig. 6 C, D; Triptorelin 10^{-7} M: 114.9 ± 3.861 % vs untreated; p=0.0049; n=5), which we found to be true for TNBC cells as well (fig. 6 S11 C, D).

It was suggested earlier that RhoA determines mesenchymal cell fate and regulates CTGF cleavage (161). We wanted to test, if GnRH agonist Triptorelin facilitates reduced invasiveness and increased adhesion by regulating RhoA activity. We found that Triptorelin regulates RhoA activity in a time-dependent manner. After 4 hours Triptorelin treatment (10^{-7} M) no increased RhoA activity could be detected by active RhoA pulldown. After 24 hours a

clear increased RhoA activity appeared (fig. 6E). Furthermore, we found that mesenchymal transformed breast cancer cells treated with a Rho activator exhibit a decreased invasive capacity (fig. 6F; RhoA activator II: 22.99 ± 9.922 % vs. untreated; p=0.0401; n=7), which could be verified for TNBC cells as well (fig. 6 S11 E). Besides, non-invasive MCF-7 breast cancer cells with transiently suppressed RhoA expression exhibit an increased invasiveness (fig. 6G; $RhoA^-$: 123.1± 7.73% vs. control; p= 0.0432; n=18). Furthermore, we tested if this increased invasiveness is due to an increased CTGF expression. We could observe that through reduction of RhoA expression (verification; fig. 6 S12 A and 6H; RhoA: $RhoA^-$: 0.7033 ± 0.04702 FC vs. control; p=0.0032; n=3) CTGF expression is increased (fig. 6H; CTGF $RhoA^-$: 2.88 ± 0.3143 FC vs. control; p=0.0039; n=3), while proliferation was not altered (fig. 6 S12 B).

Discussion

Tumor metastasis is highly regulated by micro environmental changes. Drugs are needed to modify breast micro environment were tumor cells gain ability to disseminate and bone micro environment, which is the niche where breast cancer cells preferentially colonize and remain in a state of survival and dormancy. Micro environmental modifications may be lethal for isolated, dormant cancer cells, reducing risk of reactivating dormant cells and growth of distant metastases over time is a high priority in preventing metastasis. Here we suggest potential drivers of initial dissemination of tumor cells with regards to bone-directed metastasis.

An increased CTGF expression in human breast cancer correlates with poor patient outcome and drug resistance (6). While it was suggested previously that downregulation of CTGF inhibits bone metastasis in a BMP9-dependent manner (162). A major question has remained: if targeting CTGF will help to prevent breast cancer cell dissemination into surrounding tissue, and which underlying molecular mechanisms are involved in breast cancer directed bone metastasis.

We found that CTGF is highly upregulated in invasive ductal carcinoma (fig. 2C) and during co-culture of breast cancer cells with osteosarcoma cells (fig. 1 C, D). Furthermore, CTGF expression is comparable in bone and mammary gland tissue (fig. 2 S8).

Consistent with recent findings we could assess that an elevated expression of CTGF led to increased cell invasiveness and correlated with bone-directed metastasis. Reducing CTGF expression resulted in a decreased invasion in 2D and 3D invasion assays. It was suggested

earlier, that FN1 has a protective function against metastasis when uncleaved (147) and that autocrine FN1 inhibits breast cancer metastasis (163). Additionally, it was proposed that CTGF is cleaved by MMPs to reactivate angiogenesis (145). Expression of MMP2 was upregulated when MCF-7 cells were co-cultured with osteosarcoma cells (fig. 1C, D). We tested if 3D MCF-7 spheroid area growth can be altered when CTGF and/or FN1 and/or MMP2 and /or a MMP inhibitor are added. Interestingly, we found that spheroid area growth was significantly increased when CTGF or MMP2, CTGF and MMP2, and CTGF with FN1 and MMP2 are added (fig. 3F). But there was no increased area growth when FN1 or FN1 with CTGF neither FN1 with MMP2 was added. Therefore we could assess that FN1 does not alter invasive behavior of breast cancer cells in 3D invasion setup. Also, treatment with CTGF and FN1 or MMP2 with FN1 did not alter invasive behavior as well (fig. 1G), which could be an indicator for a protective FN1 feature. Only treatment with CTGF, MMP2 and FN1 led to an increased area growth. This effect could be reversed by an additional treatment with an MMP inhibitor (BB-94). But surprisingly this inhibitor was not effective enough to reverse effect of CTGF treatment, which could be an indicator for a MMP2-independent mechanism.

Loss of intercellular and cell-ECM adhesion allows malignant cells to escape from their site of origin (164). To further analyze, why cancer cells treated with extracellular CTGF are highly invasive, we analyzed their cell-ECM adhesive and proteolytic abilities. We suggest that reduced CTGF increases cell-ECM adhesion (fig. 4-D), while ECM degradation was decreased (fig. 4G). Increased extracellular CTGF expression led to decreased cell-ECM adhesion (fig. 4E) and increased ECM degradation (fig. 4 H). This is supported by previous findings that CTGF induces expression of ECM degradations genes and fibronectin (165).

MCF-7-EMT cells exhibited increased expression of TGFBI, Twist, Vimentin and N-cadherin, while E-cadherin expression was reduced. Also MCF-7-EMT cells are more invasive (51). We could furthermore identify, that these mesenchymal transformed breast cancer cells revealed a high ITGαV (CD51) and VCAM-1 (CD106) co-expression compared to non- invasive MCF-7 breast cancer cells (fig. 2 E-F). Interestingly it was suggested, that CTGF stimulates osteosarcoma metastasis by upregulating VCAM-1 expression. Additionally, VCAM-1 may have a role in activation of dormant micro metastasis (58, 166, 167). CTGF enhances cell motility in breast cancer through integrinαVβ3-ERK1/2 dependent S100A4 upregulation (168). We analyzed impact of CTGF on other secretome analysis detected targets and could detect that reducing CTGF expression represses TGFBI, LOX and ZEB1 expression in mesenchymal transformed breast cancer cells (fig. 5 A, C). LOX was

demonstrated to be involved in collagen I stabilization leading to chemo resistance (169). It was proposed previously that EMT-TFs SNAI1 and SNAI2 activate TGBFI signaling in breast cancer and that CTGF and SPARC are upregulated as well (170). Reduced CTGF expression led to increased CD44, SPARC, and FN1 expression in mesenchymal transformed breast cancer cells (fig. 5A). CD44 is a stem cell marker and appears to have a dual nature regarding tumor progression and metastasis (171). SPARC has anticancer effects (172), inhibits bone metastasis (173) and was suggested to be involved in same biological pathways than CTGF (174). We could assess earlier in that study that an increased FN1 expression prevents 3D invasion, even when CTGF is added as well. This could indicate that downregulation of CTGF leads to an increased FN1 expression. We found that suppressed CTGF upregulated FN1 in TNBC cells, and downregulated Vimentin (fig. 5 B, D). Except for similar CTGF-dependent FN1 regulation, regulated targets are cell-type specific and could be related to expression of hormone- receptors or to MDA-MB-231 cell line specific mutations. These interesting observations need further evaluation by analyzing CTGF driven mechanism in another TNBC cell line and a hormone receptor positive mesenchymal transformed cell line.

Discovering the prominent role of CTGF during breast cancer invasion by modifying cell adhesion, ECM degradation and FN1 expression, we wanted to test if CTGF can be targeted and elucidated molecular mechanism by which CTGF can be repressed to suppress cell dissemination and colonization at distant sites. We found that GnRH agonist Triptorelin, which is in clinical use for ovarian function suppression of premenopausal breast cancer with high clinical risk of recurrence (151) and was demonstrated to reduce breast cancer invasion (7), reduced CTGF expression in mesenchymal transformed breast cancer in a dose-dependent manner (fig. 6A, B). Furthermore, we found that CTGF was downregulated by Triptorelin treatment in TNBC cells (fig. 6 S11 A, B). GnRH receptor is expressed in 50-60% of all human breast cancer and to a further extent in approximately 74 % of all TNBC (7, 132, 159). We could demonstrate that treatment with 10^{-7} M Triptorelin led to an increased cell-ECM adhesion in mesenchymal transformed breast cancer cells (fig. 6 C) and TNBC cells (fig. 6 S11 C) as it was detected by CTGF suppression as well.

It was suggested that RhoA determines lineage fate of mesenchymal stem cells in ECM and that RhoA activity controls CTGF cleavage (161). Beside, Arguilar-Rojas and colleagues found out that Busrelin, a GnRH agonist, regulates RhoA activity in MDA-MB-231 breast cancer cells thereby decreasing invasiveness (175). We wanted to examine, if Triptorelin

regulates RhoA activity and also if RhoA expression has an impact on CTGF expression. We could observe that Triptorelin induces RhoA activity in a time-dependent manner through in mesenchymal transformed breast cancer cells (fig. 6E). As expected, invasiveness of mesenchymal transformed breast cancer cells was reduced when RhoA was activated. Later we wanted to assess if reducing RhoA expression has an impact on invasiveness of non-invasive MCF-7 breast cancer. We found that transient RhoA suppression led to increased invasion (fig. 6G), which is facilitated through upregulation of CTGF (fig. 6H). This led to the conclusion that CTGF expression is dynamically regulated through RhoA activation and thereby regulates cell-ECM adhesion.

On molecular level it would be interesting to evaluate, if Triptorelin treatment has an impact on cell plasticity by regulating EMT-TF expression. CTGF activates ERK1/2 signaling through ITGαV cascade (168) and plastic breast cancer cell co-express higher ITGαV and VCAM-1 receptors and exhibit an increased CTGF expression. ERK1/2 appears to be a new treatment option with promising preclinical phase I trials (176, 177). Targeting CTGF when cancer cells gained drug resistance, could help to identify new treatment options. In addition, a new phase III trial study (HOrmonal BOne Effects-2, HOBOE-2) revealed interesting results using zoledronic acid which is approved to treat osteoporosis (178). In this context it may be worthwhile to examine if zoledronic acid reduces extracellular CTGF, which may open up possibilities for preventing bone metastasis.

Using proteome analysis it was detected, that heat shock proteins (HSP) are dysregulated when breast cancer cells are co-cultured with osteosarcoma cells (Supplement 4 C, D and Supplement 5). Nonetheless, further evaluation is necessary due to different basal expression of detected potential drivers within different cell lines. It was suggested previously, that cancer cells are more dependent on heat shock protein chaperonage due to an elevated level of misfolded onco-proteins (179, 180). Additionally, inhibiting HSP90 inhibits versatile pro-invasive and proangiogenic pathways (181). Inhibiting HSP90 led to LATS1 and LATS2 depletion, which led to reduced YAP phosphorylation and decreased CTGF expression (182). Targeting HSP90 could be of great interest to regulate CTGF expression and HSP90 inhibitors are currently under investigation for metastatic breast cancer (183-185) .

In summary, we identified a novel mechanism by which extracellular CTGF drives cell dissemination by regulating cell adhesion, ECM degradation and regulation of EMT inducing factor TGFBI. Furthermore, we propose that CTGF is a versatile regulator in breast cancer and facilitates SPARC, LOX, ZEB1, VIM and FN1 expression changes. Moreover, it was

assessed that CTGF expression is regulated by RhoA activity. Performed experiments support value of CTGF as therapeutic target for invasive breast cancer, and GnRH agonist Triptorelin could be of value in clinical applications.

Methods

Cell culture

Human breast cancer cell lines MCF-7, MDA-MB-231 were obtained from the American Type Cell Collection (ATCC; Manassas, VA, USA) and cultured in minimum essential medium (MEM; biowest, Nuaillé, France) supplemented with 10% fetal bovine serum (FBS; biochrom, Berlin, Germany), 1 % Penicillin/Streptomycin (P/S; Gibco, Carlsbad, CA, USA), 0,1 % Transferrin (Sigma, St. Louis, USA) and 26 IU Insulin (Sanofi, Frankfurt, Germany). Human osteosarcoma cell line MG-63 was purchased from ATCC and cultured Dulbecco's modified eagle medium (DMEM; Gibco) supplemented with 10% FBS (biochrom) and 1% Penicillin/Streptomycin (Gibco). To retain identity of cell lines, purchased cells were expanded and aliquots were frozen in liquid nitrogen. A new frozen stock was used every half year and mycoplasma testing of cultured cell lines was performed routinely using PCR Mycoplasma Test Kit I/C (PromoCell GmbH, Heidelberg, Germany). All cells were cultured in a humidified atmosphere with 5% CO_2 at 37 °C.

Generation of mesenchymal transformed MCF-7 cells

Mesenchymal transformed MCF-7 breast cancer cells (MCF-7-EMT) were generated as described earlier (51). Briefly, 4x 10^4 cells/ml were cultured in prolonged mammosphere culture (5-6 weeks) in ultralow adherence six well plates (Corning, Lowell, MA, USA) in DMEM/F12 supplemented with 10% charcoal-stripped fetal calf serum (cs-FCS;PAN-biotech, Aidenbach, Germany), 2% B27 supplement (Invitrogen, Darmstadt, Germany), 1% penicillin/streptomycin, 0.5 mg/ml hydrocortisone (Sigma, St. Louis, MO, USA), 5 µg/ml insulin, 20 ng/ml epidermal growth factor (EGF; Sigma, St. Louis, MO, USA).

Small interfering RNA transfection

Breast cancer cell lines MCF-7-EMT (5 x 10^5 cells/ml), MDA-MB-231 (2.5 x 10^5 cells/ml) were seeded in 2 ml of MEM with 10% FBS (-P/S) in 25 cm^2 cell culture flask. Cells were transiently transfected with siRNA specific to CTGF (sc-39329 pool of three specific siRNAs; Santa Cruz Biotechnology (SCBT), Dallas, USA) or RhoA (sc-44209 pool of three specific siRNAs; SCBT) in OPTI-MEM I medium (Gibco, Carlsbad, CA, USA) with siRNA

transfection reagent (sc-29528; Santa Cruz Biotechnology, Dallas, USA). A non-targeting control was used as control (sc-37007 control-A; Santa Cruz Biotechnology, Dallas, TX, USA). After an incubation period of 6 h, MEM supplemented with 20 % FBS and 20% penicillin/streptomycin was added.

Transwell co-culture invasion assay

Using co-culture transwell assay as describes earlier (132), 1 x 10^4 breast cancer cells were seeded in DMEM w/o phenol red, supplemented with 10% cs-FCS into a cell cultural insert (upper well) with a polycarbonate membrane (8 µm pore diameter, Merck Millipore, Cork, Ireland) coated with 30µL of a Matrigel® (BD Bioscience, Bedford, MA, USA) solution (1:2 in serum-free DMEM) or gelatin (1mg/ml in PBS, Sigma). Osteosarcoma cells were seeded (2.5 x 10^4) in DMEM supplemented with or without 10% cs-FCS into the lower well (24-well-plate). After 24 hours cells were co-cultured for 96 hours or 48 hours when treated with RhoA activator II. Invaded cells on lower side of inserts were stained with hematoxylin and number of cells in four randomly selected fields of each insert was counted.

3D spheroid assay

Assessment of 3D cell invasion was pursued as describes earlier with minor changes (186). Briefly 1x10^3 breast cancer cells were seeded in 100 µL in a well of an ultra-low-adherence 96-well plate (ULA; Nexcelom, Cenibra GmbH, Bramsche, Germany). After 48 hours spheroid formation was visually confirmed and 50 µL of media was removed. Thereafter, 50 µL Matrigel were added to wells with spheroids. Central position of spheroids was checked visually and Matrigel was allowed to solidify for 1 hour at 37°C and 5% CO^2. Afterwards 50 µL media were added to each well and a picture was taken marking time point 0 (t0h). When indicated rhCTGF (recombinant human connective tissue growth factor; 1 µg/ml; R&D systems), pdhFN1 (plasma-derived human fibronectin 1; 1 µg/ml; R&D systems), rhMMP2 (recombinant human matrix metalloproteinase 2; 0.01µg/ml; R&D systems, Minneapolis, MN, USA), Batimastat (BB-94, 4nM; Selleckchem, Munich, Germany) polyclonal rabbit IgG control (15µg/ml; R&D systems) or anti-CTGF (15 µg/ml; Novus Biologicals**).** Spheroid growth area was analyzed using ImageJ polygonal selection and measurement. Mean values were calculated and compared to respective control.

Adherence Assay

Cell-ECM adherence was examined by coating 96-well plates with bovine collagen I (30 µL; 0.04 mg/ml; BD Bioscience) for 12 hours at 4°C. Solution was aspirated and plate was left to dry under bench. Cells were washed 3 times with FBS-free DMEM and cultured for 8 hours in DMEM-FBS prior to adhesion assessment. Cells were detached using 10mM EDTA-PBS solution. Cells were pelleted (1300 rpm for 5 minutes) and washed twice with DMEM supplemented with 0.1% BSA. Cells were seeded ($2x10^4$) in DMEM supplemented with 0.1% BSA, when indicated treated with rhCTGF (1 µg/ml; R&D systems), Triptorelin (10^{-7} M), polyclonal rabbit IgG control (15µg/ml; R&D systems) or anti-CTGF (15 µg/ml; Novus Biologicals**),** and incubated at 37°C with 5% CO_2 for 20 min. Non-adherent cells were washed of by adding 100 µL of DMEM four times. Adherent cells were counter-stained with crystal violet solution (0.5%) for 20 min at RT shaking. Wells were washed four times with ddH_2O and dried for at least 2 hours. Pictures were taken and afterwards 200 µL Methanol were added to each well, incubated for 20 min shaking and absorbance was assessed at 570 nm using Synergy (BioTek Instruments, Bad Friedrichshall, Germany). Each experiment was performed in six replicates. Mean values were compared to respective control.

ECM degradation

Degradation of ECM was examined by depriving cell from FBS 12 hours prior to seeding. Wells of a 96-well plate were coated with 50 µL FITC-conjugated gelatin (2mg/ml; BioVision Inc, Milpitas, CA,USA) diluted 1:5 with unlabeled gelatin (Sigma) and incubated for 1 hour at 37°C and 5% CO_2. Solution was discarded and plate left to dry under bench. FBS deprived cells were seeded ($1x10^4$) on gelatin coated wells and when indicated treated with rhCTGF (1 µg/ml; R&D systems). After 24 hours proteolytic activity was detected by measuring fluorescence (extinction 490nm/emission 520nm) using Synergy (BioTek Instruments, Bad Friedrichshall, Germany). Each experiment was performed in three replicates. Mean values were compared to respective control.

AlamarBlue Assay

Transiently transfected breast cancer cells were seeded in 96- wells (1.25×10^3) in DMEM w/o phenol-red supplemented with 10% cs-FBS and relative AlamarBlue reduction (BioRad, Hercules, USA) was assessed at 48 hours and/or 120 hours. 3D spheroids were grown as described above and 48 hours after seeded in Matrigel AlamarBlue was added and incubated for 4 hours. Thereafter, relative AlamarBlue reduction was measured by absorbance reading

at 540 nm and 630 nm, using Synergy (BioTek Instruments). Relative AlamarBlue Reduction was calculated as indicated by manufacturer.

Immuno-histochemical staining

Immuno-histochemical staining of human tissue array slide (BR248a; US Biomax, Derwood, MD, USA) was performed as described earlier (7). Sections were deparaffinized and rehydrated. Thereafter, antigens were retrieved by slide incubation in 0.01 M citrate buffer (pH 6.0) in microwave (700W) for 5 minutes. Using 3% hydrogen peroxidase solution for 6 min endogenous peroxidase activity was quenched. Sections were incubated over night with primary labeled antibodies against CTGF (0.02 mg/ml; Novus Biologicals) in fluorescence staining solution (1% BSA + 0.4% TRITON X-100 in PBS) at 4°C. Labeling with secondary was performed by incubating slide with secondary rabbit antibody Alexa488 (Invitrogen) and DAPI (1µg/ml; Novus Biologicals) in fluorescence staining solution for 30 minutes at room temperature protected from light. Staining was visualized using a Zeiss Scope A1 Axio microscope (ZEISS, Oberkochen, Germany) with an oil EC PLAN-NEOFLUAR 100x (ZEISS, Oberkochen, Germany) objective and ZEN software (ZEISS, Oberkochen, Germany).

Flow Cytometry

Cells were detached from culture dish with trypsin for 5 min and washed once with PBS. $1x10^6$ were suspended in pre-cooled flow cytometry staining solution (PBS, 10% FCS, $1NaN_3$) and incubated with conjugated primary antibodies (CD51-FITC; CD-106-APC; eBioscience Inc., ThermoFisher Scientific, Waltham, MN, USA) for 20 minutes at 4 °C. Stained cells were washed twice with flow cytometry staining solution and analyzed immediately by BD CANTOII flow cytometer (BD Biosciences). Untreated cells and UltraComp compensations beads (Invitrogen) incubated with labeled antibodies were used as negative control for determining specificity of signal.

Western Blot analysis

In Western Blot analysis, cells were lysed in lyse buffer consisting of cell lytic M buffer (Sigma, St. Louis, USA) supplemented with 0.1% phosphatase-inhibitor (Sigma, St. Louis, MO, USA) and 0.1% protease-inhibitor (Sigma, St. Louis, MO, USA). Isolated proteins (40µg) were fractioned using 12 % SDS gels and electro-transferred to a polyvinylidene difluoride membrane (Merck Millipore, Cork, Ireland). Primary antibodies against CTGF

1:1000 (#NB100-724, Novus Biologicals), RhoA 1:500 (#ARH04, Cytoskeleton, Denver, CO, USA) and GAPDH 1:2000 (#5174S, Cell Signaling, Danvers, MA, USA) were used. Membrane was washed and incubated in horseradish peroxidase-conjugated secondary antibody (GE Healthcare, Buckinghamshire, UK). Antibody-bond protein bands were assayed using a chemiluminescent luminol enhancer solution (Cyanagen, Bologna, Italy).

RhoA pull-down

RhoA pulldown assay was examines using Rho activation assay biochem Kit as describes by the manufacturer (BK036-S; Cytoskeleton Inc.). Briefly, 300 µg proteins was loaded with 50 µg Rhotekin rho binding domain (RBD) glutathione agarose bound beads which binds/precipitates specifically active GTP-bond Rho proteins. To quantify active RhoA total RhoA protein was determined. A positive cellular control loaded with non-hydrolysable GTP analog (GTPγS) and a negative control loaded with GDP were determined from each examined sample. To assess functionality of assay one sample was treated with RhoA activator II (CN03, 1µg/ml, Cytoskeleton). As quantitation estimate for endogenous Rho, His-RhoA protein was run on gel together with examined samples.

Mass spectrometric secretome and proteome analysis

Sample preparation

Breast cancer cells were seeded (0.75×10^5) in Bio-one ThinCert (Greiner Bio-one, Kremsmünster, Austria) and Osteosarcoma cells were seeded ($1,3 \times 10^5$) in 6 wells. After 24 hours cells were deprived of FBS and co-cultured for 96 hours. Cell medium was precipitated with acetone. Medium was centrifuged for 10 minutes at 13300 rpm at 4°C and five times volume on pre-cooled (-20°C) was added to samples. Samples were vortexed and protein precipitation performed for 2 hours at -20°C. Protein was pelleted by centrifugation for 30 minutes at 13300 rpm at 4°C. Protein pellets were washed with ethanol (80%, pre-cooled at -20°C), centrifuged for 30 minutes at 13300 rpm at 4°C, and protein pellets were air dried.

Cell lysates were generated by cutting membranes from insert and recovering cells with Recovery solution (Corning, New York, NY, USA) for 1 hour at 4°C while shaking. Cells were pelleted and resuspended in 30 µL lysis buffer.

MS sample processing

For generation of a peptide library, equal amount aliquots from comparable samples were pooled to a total amount of 100 µg, and separated into eight fractions using a reversed phase

spin column (Pierce High pH Reversed-Phase Peptide Fractionation Kit, ThermoFisher Scientific). All samples were spiked with a synthetic peptide standard used for retention time alignment (iRT Standard, Schlieren, Schweiz).

Protein digests were analyzed on a nanoflow chromatography system (Eksigent nanoLC425) hyphenated to a hybrid triple quadrupole-TOF mass spectrometer (TripleTOF 5600+) equipped with a Nanospray III ion source (Ionspray Voltage 2400 V, Interface Heater Temperature 150°C, Sheath Gas Setting 12) and controlled by Analyst TF 1.7.1 software build 1163 (all AB Sciex). In brief, peptides were dissolved in loading buffer (2% acetonitrile, 0.1% formic acid in water) to a concentration of 0.42 µg/µl. For each analysis 2.1 µg of digested protein were enriched on a precolumn (0.18 mm ID x 20 mm, Symmetry C18, 5 µm, Waters, Milford/MA, U.S.A) and separated on an analytical RP-C18 column (0.075 mm ID x 250 mm, HSS T3, 1.8 µm, Waters) using a 90 min linear gradient of 5-35 % acetonitrile/0.1% formic acid (v: v) at 300 nl min^{-1}.

Qualitative LC/MS/MS analysis was performed using a Top25 data-dependent acquisition method with an MS survey scan of *m/z* 350–1250 accumulated for 350 ms at a resolution of 30,000 full width at half maximum (FWHM). MS/MS scans of *m/z* 180–1600 were accumulated for 100 ms at a resolution of 17,500 FWHM and a precursor isolation width of 0.7 FWHM, resulting in a total cycle time of 2.9 s. Precursors above a threshold MS intensity of 125 cps with charge states 2+, 3+, and 4+ were selected for MS/MS, the dynamic exclusion time was set to 30 s. MS/MS activation was achieved by CID using nitrogen as a collision gas and manufacturer's default rolling collision energy settings. Three technical replicates per reversed phase fraction were analyzed to construct a spectral library.

For quantitative SWATH analysis, MS/MS data were acquired using 65 variable size windows (187) across the 400-1,050 *m/z* range. Fragments were produced using rolling collision energy settings for charge state 2+, and fragments acquired over an *m/z* range of 350–1400 for 40 ms per segment. Including a 100 ms survey scan this resulted in an overall cycle time of 2.75 s. Two replicate injections were acquired for each biological sample.

Protein identification was achieved using ProteinPilot Software version 5.0 build 4769 (AB Sciex) at "thorough" settings. MS/MS spectra from combined qualitative analyses were searched against UniProtKB human reference proteome (revision 04-2018, 93.661 entries) augmented with a set of 52 known common laboratory contaminants to identify 217 proteins at a False Discovery Rate (FDR) of 5% in the secretome, and 2,033 proteins at an FDR of 1%

for whole proteome analysis. We consciously allowed for a larger FDR in the secretome analysis since identified candidate proteins were further validated during SWATH data extraction and by biochemical experimentation.

Spectral library generation and SWATH peak extraction were achieved in PeakView Software version 2.1 build 11041 (AB Sciex) using SWATH quantitation microApp version 2.0 build 2003. Following retention time correction using iRT standard, peak areas were extracted using information from MS/MS library at an FDR of 1% (188). Resulting peak areas were then summed to peptide and finally protein area values, which were used for further statistical analysis.

Real-time quantitative PCR analysis

Total RNA was extracted using an RNeasy mini kit (Qiagen, Hilden, Germany) and 2 µg were reverse transcribed with high capacity cDNA reverse transcription kit (Qiagen, Hilden, Germany). Real- time qPCR was performed using SYBR green PCR master mix kit (Qiagen, Hilden, Germany) and following Primers: CTGF (forward) 5'-CTTGCGAAGCTGACCTGGAA-3', CTGF (reverse) 5'- GTGCAGCCAGAAAGCTCAAA-3', TGFBI (forward) 5'- AGGCCTTCGAGAAGATCCCT -3', TGFBI (reverse) 5'-GAGATGATCGCCTTCCCGTT-3', CD44 (forward) 5'- CACACCCTCCCCTCATTCAC-3', CD44 (reverse) 5'- CAGCTGTCCCTGTTGTCGAA -3', SPARC (forward) 5'-GTGCGAGCTGGATGAGAACA-3', SPARC (reverse) 5'-TTGCAAGGCCCGATGTAGTC-3', FN1 (forward) 5'- GCTGCACATGTCTTGGGAAC-3', FN1 (reverse) 5'- CATGAAGCACTCAATTGGGCA-3', LOX (forward) 5'-GGGCGACGACCCTTACAAC-3', LOX (reverse) 5'- GCCCTGTATGCTGTACTGGC-3', FSTL1 (forward) 5'- TCTGCCAGCCCAGTTGTTTG-3', FSTL1 (reverse) 5'-GAGTCCAGGCGAGAATCACC-3', CDH1 (forward) 5'-CCTCCTGAAAAGAGAGTGGA -3', CDH1 (reverse) 5'- GTGTCCGGATTAATCTCCAG-3', VIM (forward) 5'-GCTGCTAACTACCAAGACAC-3', VIM (reverse) 5'-TCAGGTTCAGGGAGGAAAAG -3', ZEB1 (forward) 5'- AAGACAAACTGCATATTGTGGAAG-3', ZEB1 (reverse) 5'-CTGCTTCATCTGCCTGAGCTT-3', SNAI2 (forward) 5'-GCCAAACTACAGCGAACTGG -3', SNAI2 (reverse) 5'-GAGAGAGGCCATTGGGTAGC -3', RhoA (forward) 5'-CAAGGACCAGTTCCCAGAGG -3', RhoA (reverse) 5'-TGTCCCACAAAGCCAACTCT -3', and GAPDH (forward) 5'- GAAGGTCGGAGTCAACGGAT -3', GAPDH (reverse) 5'-TGGAATTTGCCATGGGTGGA -3' .PCR conditions were: denaturing once at 95°C (2 minutes), 95°C (5 seconds), 60°C (15 seconds) for 40 cycles.

Data analysis

Gene ontology enrichment analysis, networks summarizing overlapping terms and hierarchical lustering trees were conducted using Shiny GO v0.60 with a p-value cutoff (FDR) of 0.05 (189).

CTGF expression analysis in human tissues

Statistical analysis of tissue-specific CTGF expression was conducted using large public cancer genomics datasets (GTEX, TARGET, TCGA) as described previously (190).

Statistical analysis

All experiments were performed at least in three biological and technical replicates. Data were analyzed by GraphPad Prism Software version 7.03 (GraphPad Software Inc., La Jolla, CA/USA) using unpaired, two-tailed, parametric t-test comparing two groups (treatment to respective control) by assuming both populations have same standard derivation or ANOVA one-way analysis when more than two groups were compared. F-values were recorded and a Dunnett‘s multiple comparison test with no matching or pairing between groups was calculated. $P< 0.05$ was considered statistically significant.

Availability of data and material

The datasets used and/or analyzed during current study are available from the corresponding author on reasonable request.

Competing interests

The authors declare that they have no competing interests.

Figures and tables

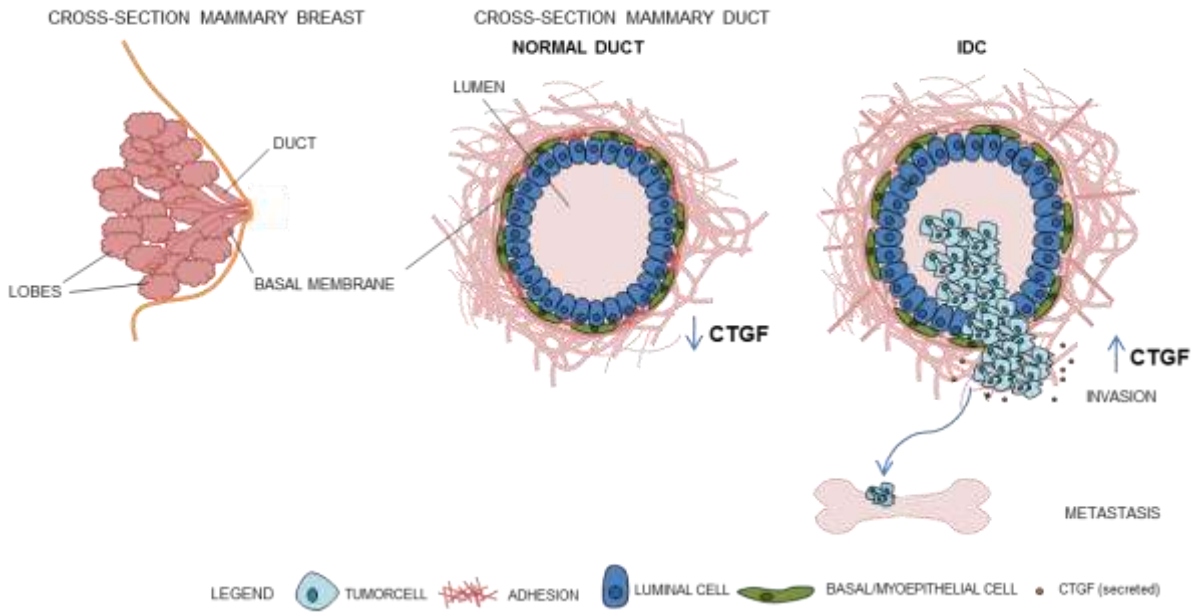

Graphical abstract Anatomy of mammary duct and lobes (cross-section) vs. anatomy of invasive ductal carcinoma (IDC). Connective tissue growth factor (CTGF) expression is downregulated in normal duct. Increased extracellular CTGF expression leads to breast cancer bone-directed invasiveness.

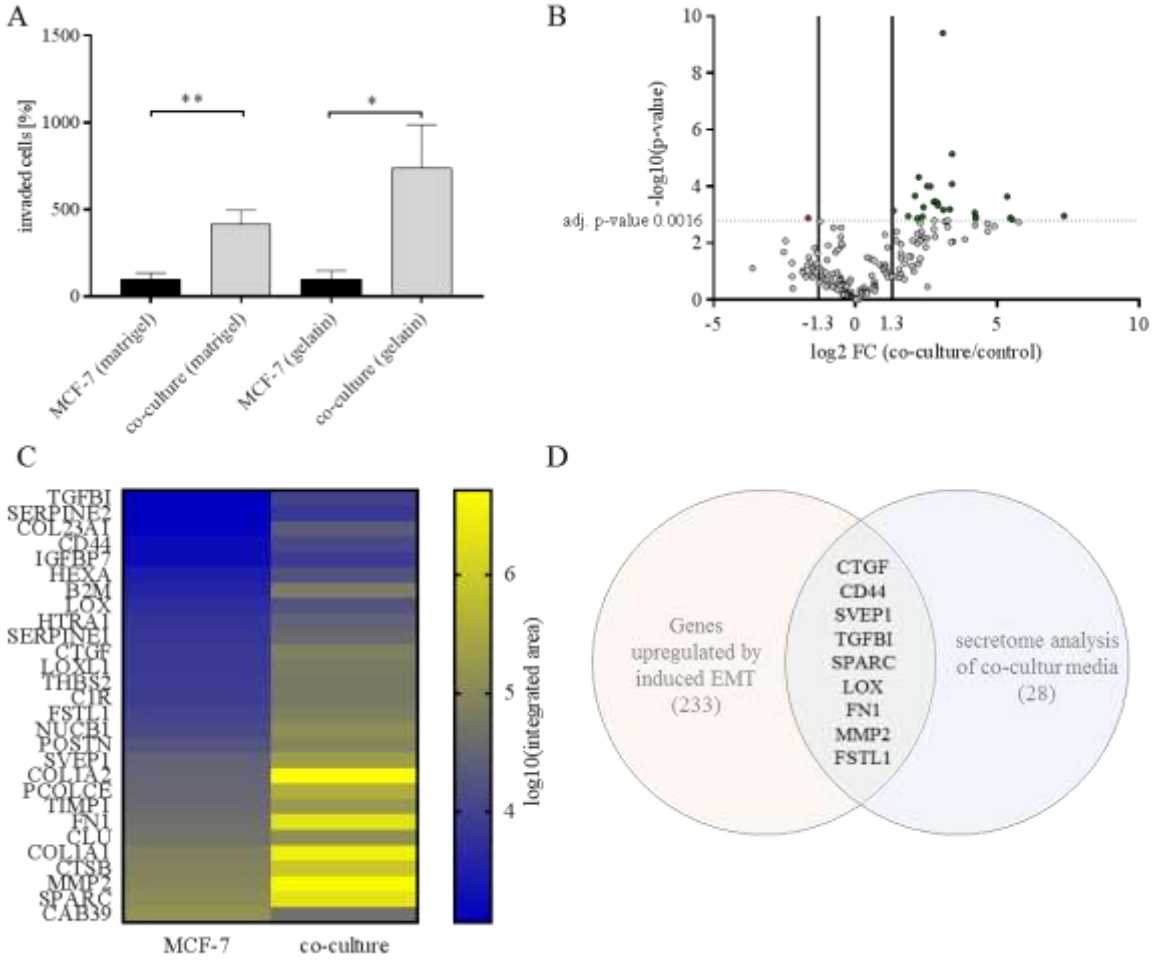

Figure 1 Identifying drivers of breast cancer cell invasion. A Transwell-invasion co-culture assay of MCF-7 breast cancer cells and MG-63 osteosarcoma cells without FBS addition and Matrigel or Collagen I coated insert. Invaded cells under the filter were stained and counted in four randomly selected regions after 96 hours in co-culture. Data represent mean ± SEM. MCF-7 (Matrigel) n=12, MCF-7 (gelatin) n=6, unpaired, two-sided t-test to respective control. * *P< 0.05;* ** *P<0.01* **B** Volcano plot demonstrating potential bone-directed breast cancer invasiveness related targets using secretome analysis. Detected target proteins were stated as discovery when adjusted p-value (adj. p-value) was below 0.0016 (dotted line) with a false-discovery rate (FDR) of 1% and a log 2 fold change (FC) higher 1.3 or lower -1.3. Every dot indicates one target, green dots indicate upregulated discoveries and red dot indicates downregulated discovery. n=6, discovery determined using the two-stage linear step-up procedure of Benjamini, Krieger and Yekutieli, with Q = 1%. Each row was analyzed individually, without assuming a consistent SD. **C** Heat map visualizing all discoveries with a color gradient of log10 integrated area of mean values of three biological and two technical replicates corresponding to B. **D** Scheme of overlapping targets from microarray analysis of MCF-7 cells under dynamic EMT program and secretome analysis of co-cultured MCF-7 cells with a fold change of higher 1.3 or lower -1.3 and FDR 5% (microarray) and FDR 1% (secretome analysis).

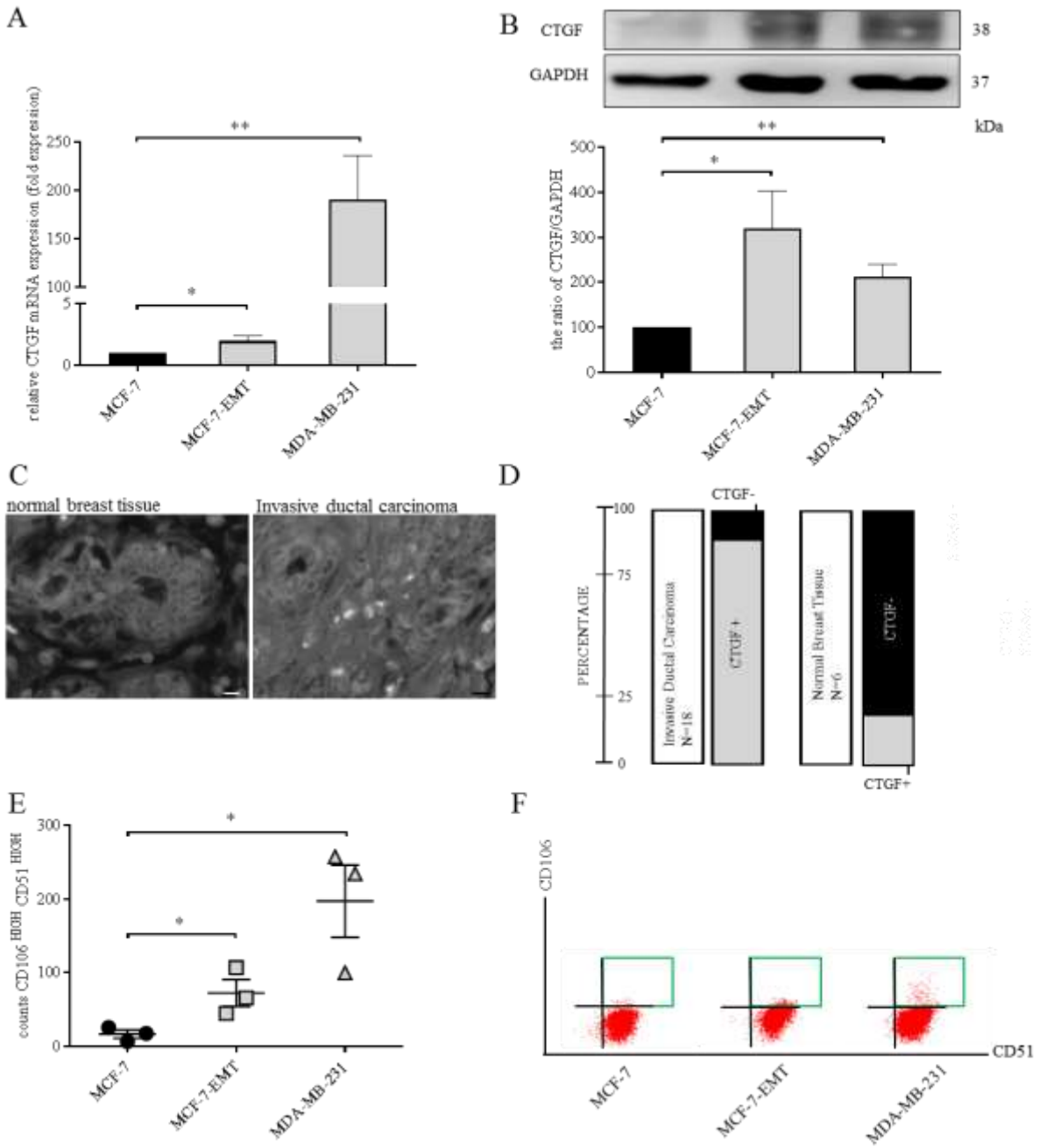

Figure 2 CTGF expression correlates with invasiveness of mesenchymal transformed and TNBC cells. A Assessment of CTGF mRNA expression in different breast cancer cell lines using quantitative real-time PCR. Data represent mean ± SEM. MCF-7-EMT n=6, MDA-MB-231 n=4 using unpaired, two-tailed t-test analysis to respective control (MCF-7). * *P< 0.05;* ** *P<0.01* **B** Quantification and representative experiments of CTGF protein expression in different breast cancer cell lines compared to non-invasive MCF-7 breast cancer cell line. CTGF band intensity was quantified by densitometry and normalized to GAPDH. Data represent mean ± SEM. n=6 using unpaired, two-tailed t-test analysis to respective control (MCF-7). * *P< 0.05;* ** *P<0.01* **C** Patient tissue sections (n=24) were analyzed for CTGF expression. Representative images of normal breast tissue (right panel) and IDC (invasive ductal carcinoma, left panel) are illustrated. **D** Graph illustrating distribution of CTGF expression within two different analyzed patient sample categories. **E** Results of three independent flow cytometry experiments of CD51 and CD106 co-expression in MCF-7 (circle), MCF-7-EMT (square) and MDA-MB-231 (triangle) breast cancer cell lines. Data represent mean ± SEM. MCF-7-EMT, MDA-MB-231 n=3 using unpaired, two-tailed t-test analysis to respective control (MCF-7). * *P< 0.05* **F** Proportion of CD51 to CD106 was asses using flow cytometry after staining with fluorescence-labeled antibodies. A representative experiment to E is illustrated.

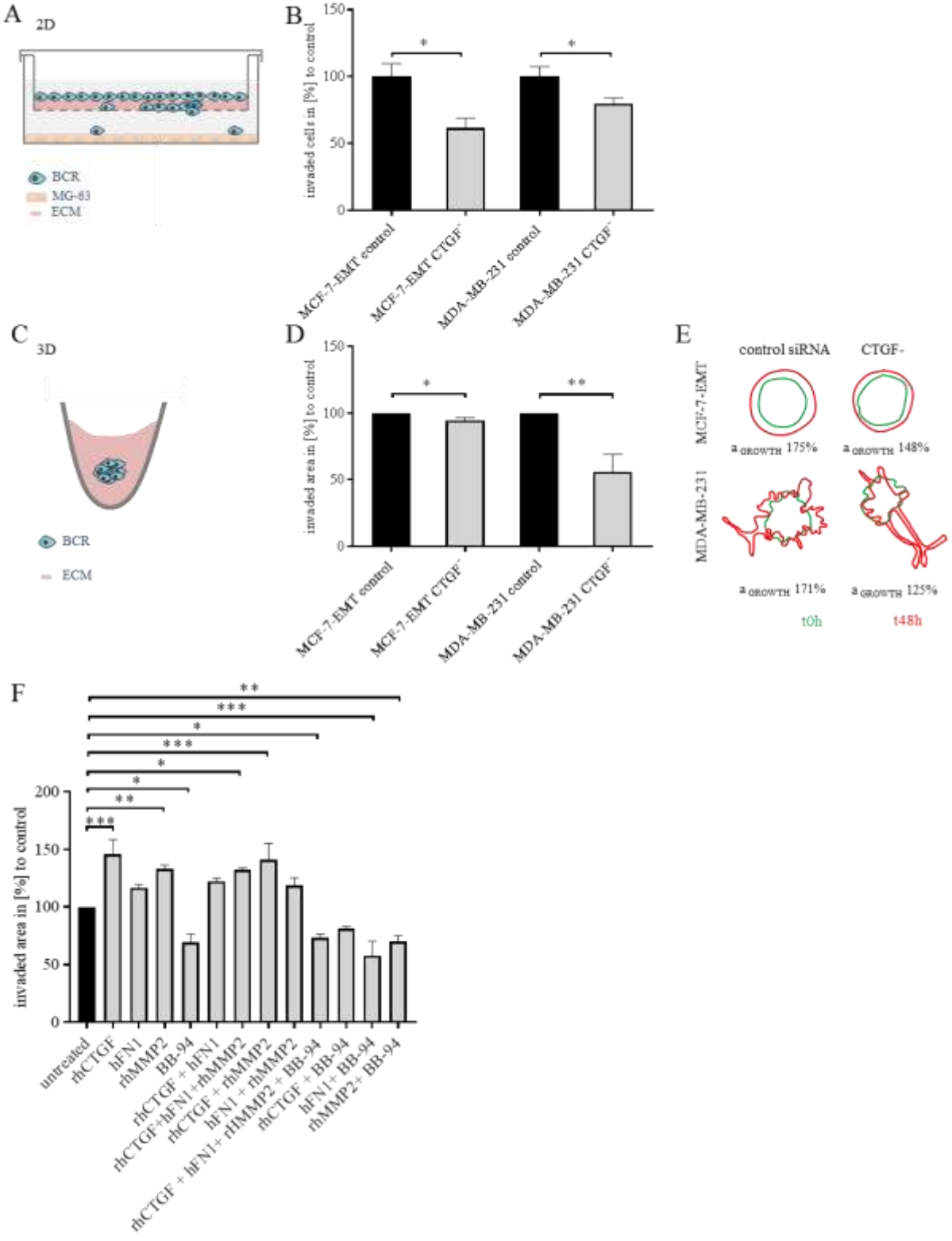

Figure 3 CTGF regulates invasiveness in breast cancer cells. A Scheme illustrating 2D invasion experiment using a co-culture transwell invasion assay. BCR = breast cancer cell, ECM = extracellular matrix **B** Following CTGF siRNA transfection invaded cells under filter were counted in four randomly selected regions, using a co-culture Matrigel invasion assay for 96 hours. Data represent mean ± SEM. MCF-7-EMT n=15, MDA-MB-231 n=9 using unpaired, two-tailed t-test analysis to respective control. * *P< 0.05* **C** Scheme illustrating 3D spheroid invasion assay. Cells were seeded in ultra-low attachment wells and after initial spheroid formation (48 hours), spheroids were surrounded by Matrigel matrix and further cultivated. **D** 3 D spheroid assay was performed after transient CTGF siRNA transfection. Invaded area was assessed using ImageJ software and relative area growth was calculated corresponding to respective control. Data represent mean ± SEM.MCF-7-EMT n=15, MDA-MB-231 n=9 using unpaired, two-tailed t-test analysis to respective control. * *P< 0.05;* ** *P*

<0.01 **E** Representative experiment illustrating area measurement of 3D spheroids. Green shape corresponding to initial spheroid size right after adding Matrigel and red shape corresponding to time point 48 hours after Matrigel adding. **F** 3 D spheroid assay of MCF-7 cells treated with different combinations of 1 µg/ml rhCTGF, 1µg/ml hFN1, 1µg/ml rhMMP2, and/or 4nM BB-94 (Batimastat) for 48 hours every 24 hours. Area growth of spheroids was assessed using ImageJ software and relative area growth was calculated corresponding to untreated control. Data represent mean ± SEM. n=4-6 using one-way ANOVA and a Dunnett's multiple comparison test with no matching or pairing between groups was calculated to assess significant differences compared to untreated control. **P<0.05; ** P <0.01; *** P <0.005*

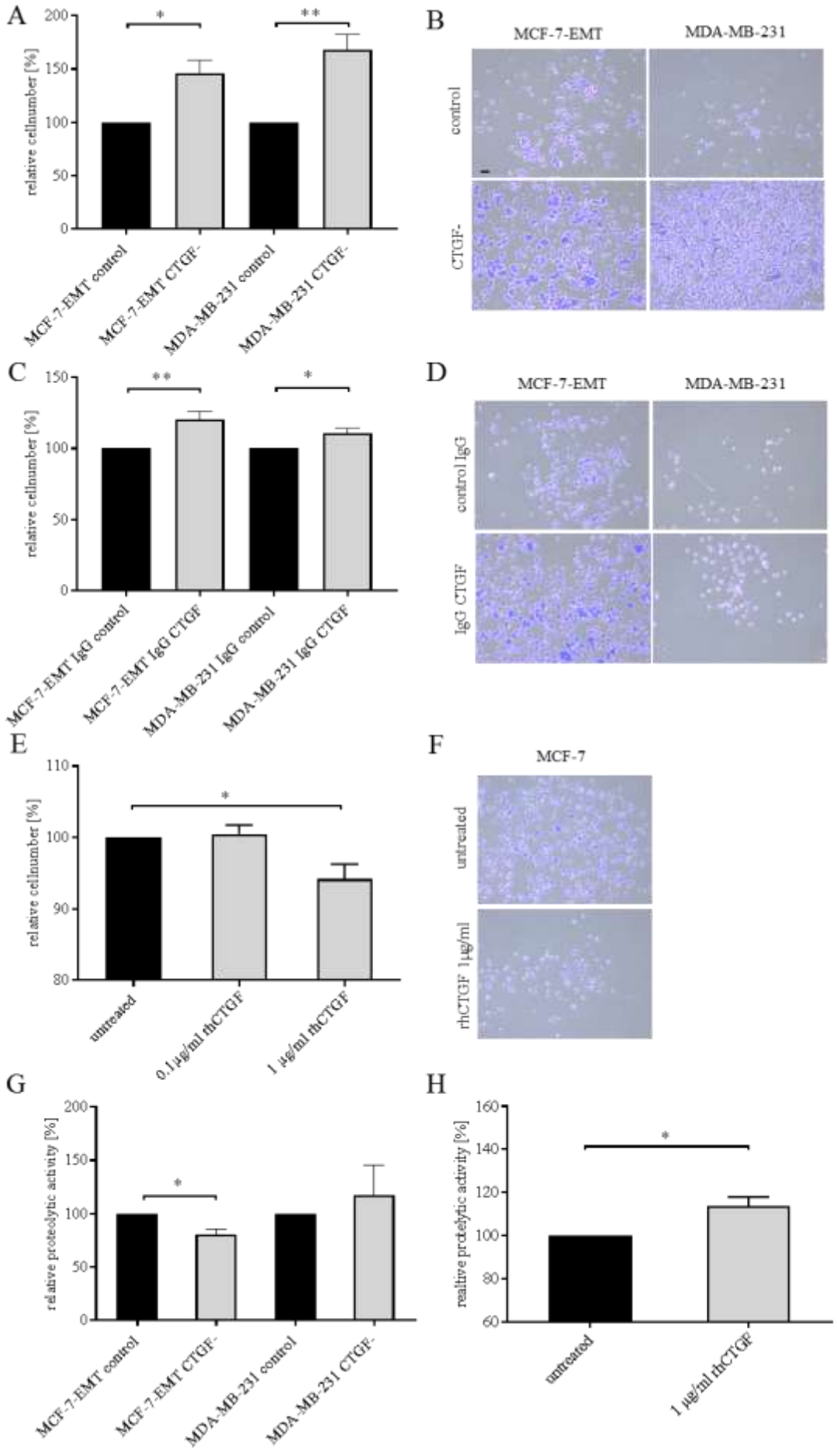
A
relative cellnumber [%]
200
150
100
50
0
*
**
MCF-7-EMT control
MCF-7-EMT CTGF-
MDA-MB-231 control
MDA-MB-231 CTGF-
B
MCF-7-EMT
MDA-MB-231
control
CTGF-
C
relative cellnumber [%]
150
100
50
0
**
*
MCF-7-EMT IgG control
MCF-7-EMT IgG CTGF
MDA-MB-231 IgG control
MDA-MB-231 IgG CTGF
D
MCF-7-EMT
MDA-MB-231
control IgG
IgG CTGF
E
relative cellnumber [%]
110
100
90
80
*
untreated
0.1 µg/ml rhCTGF
1 µg/ml rhCTGF
F
MCF-7
untreated
rhCTGF 1µg/ml
G
relative proteolytic activity [%]
200
150
100
50
0
*
MCF-7-EMT control
MCF-7-EMT CTGF-
MDA-MB-231 control
MDA-MB-231 CTGF-
H
realtive prteolytic activity [%]
160
140
120
100
80
60
*
untreated
1 µg/ml rhCTGF

Figure 4 CTGF alters cell-ECM adhesion and proteolytic activity of breast cancer cells. A Adhesion analysis of transiently transfected mesenchymal transformed and triple-negative breast cancer cells. Adhesive cells where counter-stained with crystal violet and absorption was measured at 570nm. Data represent mean ± SEM. MCF-7-EMT n=3, MDA-MB-231 n=3 using unpaired, two-tailed t-test analysis to respective control. * *P< 0.05;* ***P<0.01* **B** Representative images corresponding to A. **C** Extracellular CTGF was reduced using a blocking-antibody against CTGF and cell-ECM adhesion was assessed. Data represent mean ± SEM. MCF-7-EMT n=6, MDA-MB-231 n=3 using unpaired, two-tailed t-test analysis to respective control (IgG control). * *P< 0.05;* ***P<0.01* **D** Representative images corresponding to C. **E** MCF-7 cells where treated with recombinant human CTGF (rhCTGF) in different concentrations prior to assessing of cell-ECM adhesion. Data represent mean ± SEM. n=3 using one-way ANOVA with F= 6.244 and a Dunnett's multiple comparison test with no matching or pairing between groups. * *P< 0.05* **F** Representative images corresponding to E. **G** Following transient transfection mesenchymal transformed and triple negative breast cancer cells were seeded on FITC-conjugated gelatin (0.2%). Degradation of gelatin /proteolytic activity results in an increase of fluorescence. Data represent mean ± SEM. MCF-7-EMT n=3, MDA-MB-231 n=3 using unpaired, two-tailed t-test analysis to respective control. * *P< 0.05* **H** Assessment of proteolytic activity of MCF-7 breast cancer cells after treatment with rhCTGF. Data represent mean ± SEM. M n=3 using unpaired, two-tailed t-test analysis to respective control (untreated).* *P< 0.05.* Scale bar gauges 200 µm.

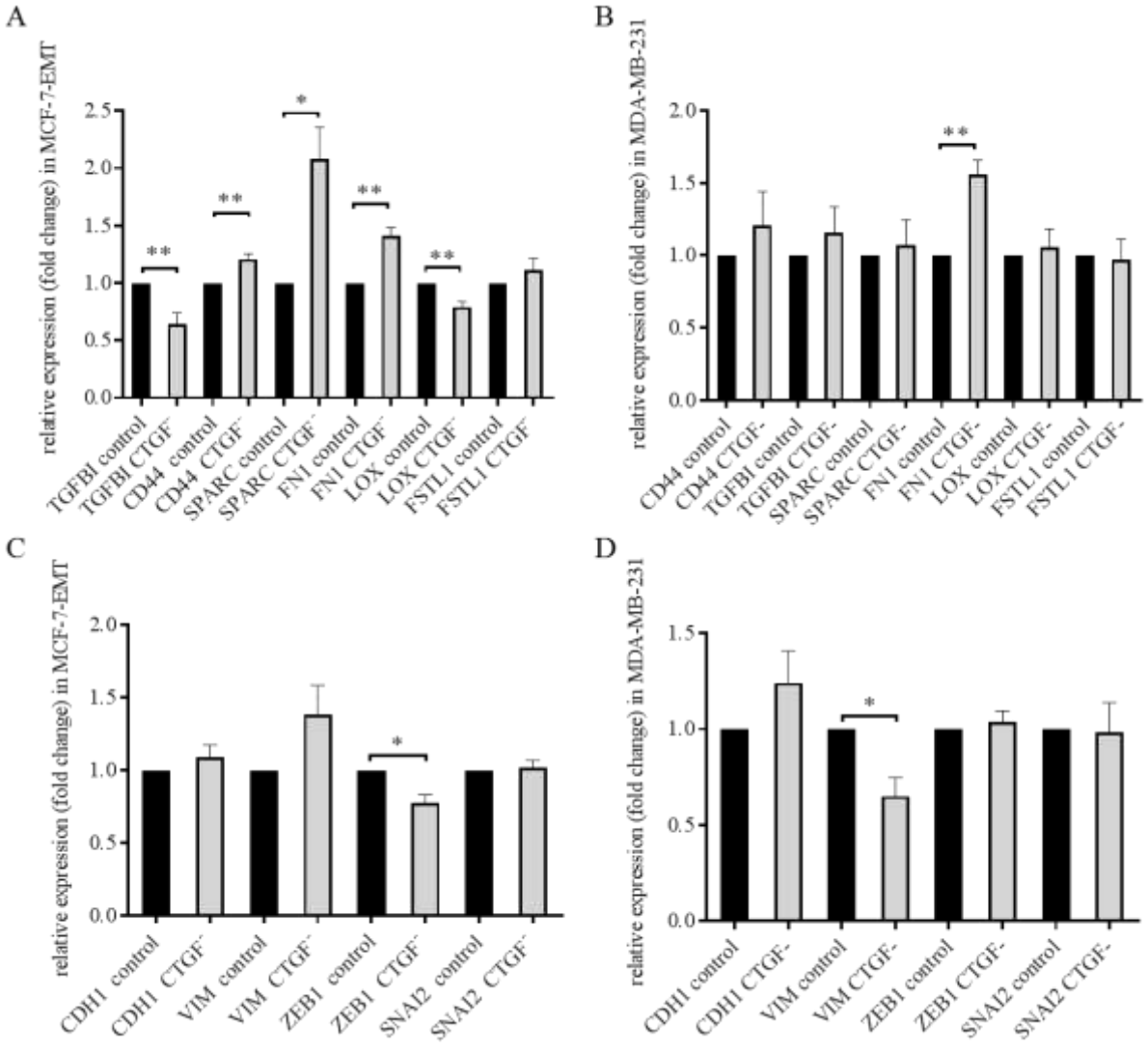

Figure 5 CTGF regulates expression of potential drivers of invasion and EMT-markers. A Relative quantification of TGFBI, CD44, SPARC, FN1, LOX and FSTL1 mRNA expression in mesenchymal transformed breast cancer cells treated transiently with CTGF siRNA for 48 hours. Data represent mean ± SEM. MCF-7-EMT n=3 using unpaired, two-tailed t-test analysis to respective control. * *P< 0.05;*** *P <0.01* **B** Relative quantification of TGFBI, CD44, SPARC, FN1, LOX and FSTL1 mRNA expression in triple negative breast cancer cells treated transiently with CTGF siRNA for 48 hours. Data represent mean ± SEM. MDA-MB-231 n=3 using unpaired, two-tailed t-test analysis to respective control. * *P< 0.05* **C** Relative quantification of EMT markers VIM, CDH1, SNAI2 and ZEB1 mRNA expression in mesenchymal transformed breast cancer cells treated transiently with CTGF siRNA for 48 hours. Data represent mean ± SEM. MCF-7-EMT n=3 using

unpaired, two-tailed t-test analysis to respective control. * *P< 0.05* **D** Relative quantification of EMT markers VIM, CDH1, SNAI2 and ZEB1 mRNA expression in triple negative breast cancer cells treated transiently with CTGF siRNA for 48 hours. Data represent mean ± SEM. MDA-MB-231 n=3 using unpaired, two-tailed t-test analysis to respective control. * *P< 0.05*

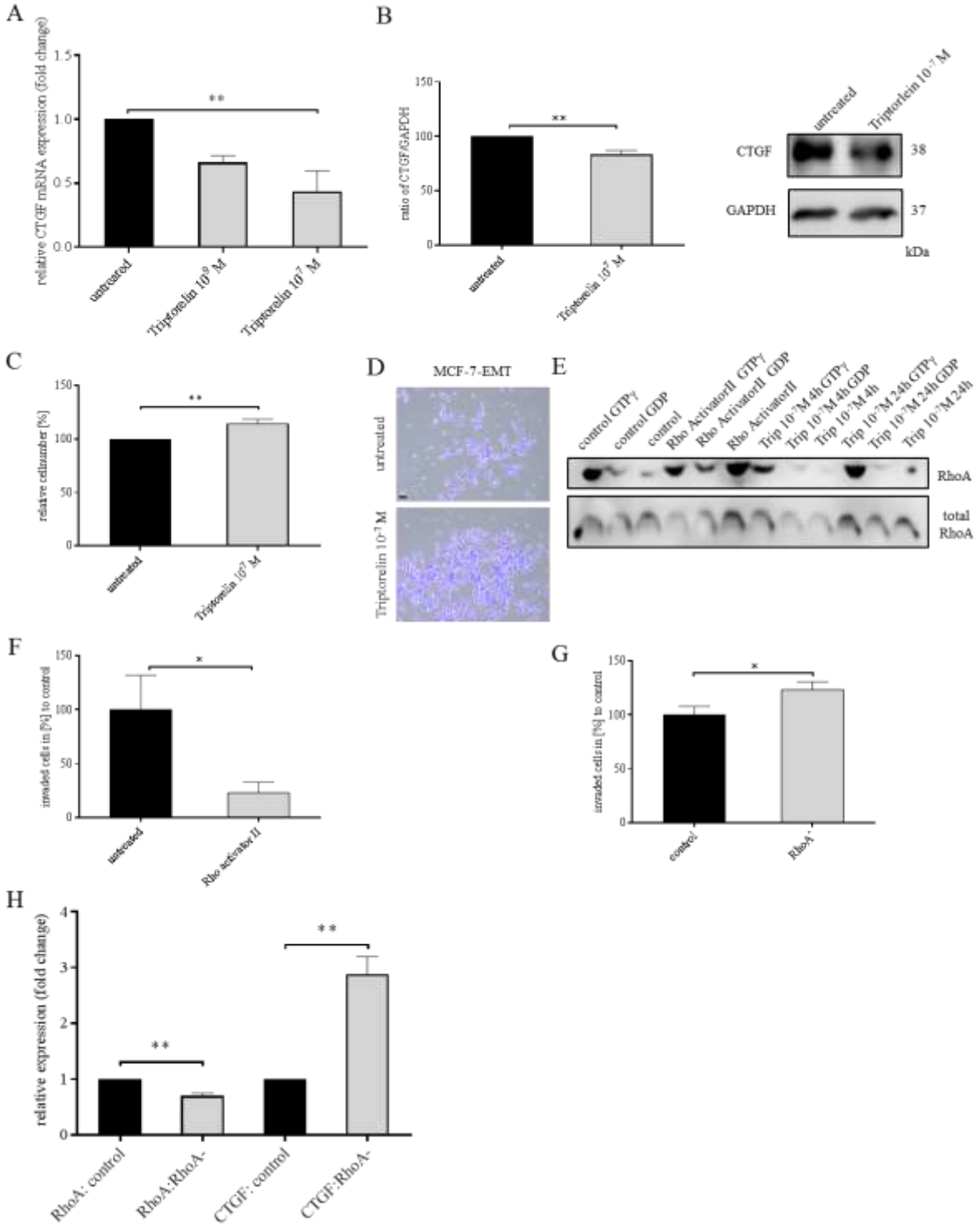

Figure 6 GnRH agonist regulates CTGF through RhoA activity in mesenchymal transformed breast cancer cells. A Relative quantification of CTGF mRNA expression in mesenchymal transformed breast cancer cells (MCF-7-EMT) treated

for 48 hours with 10^{-9} M or 10^{-7} M Triptorelin. Data represent mean ± SEM. MCF-7-EMT n=3 using one-way ANOVA with F= 8.366 and a Dunnett's multiple comparison test with no matching or pairing between groups. ** *P <0.01* **B** Quantification and representative experiment of CTGF protein expression after Triptorelin treatment for 48 hours (10^{-7} M). CTGF band intensity was quantified by densitometry and normalized to GAPDH. Data represent mean ± SEM. MCF-7-EMT n=3 using unpaired, two-tailed t-test analysis to respective control (untreated). ** *P<0.01* (C) Adhesion analysis of mesenchymal transformed breast cancer cells treated with 10^{-7} M Triptorelin. Adhesive cells where counter-stained with crystal violet and absorption was measured at 570nm. Data represent mean ± SEM. MCF-7-EMT n=5 using unpaired, two-tailed t-test analysis to respective control (untreated). ***P<0.01* **D** Representative images corresponding to C. Scale bar gauges 200 µm. **E** RhoA activity pull-down of untreated MCF-7-EMT cells, MCF-7-EMT cells treated 3 hours with an specific Rho activator (1µg/ml) and MCF-7-EMT cells treated with 10^{-7} M Triptorelin for 4 or 24 hours. **F** 2D invasion assay. After 48 hours treatment with or without Rho activator II treatment (1µg/ml) supplement invaded cells under filter were counted in four randomly selected regions. Data represent mean ± SEM. MCF-7-EMT n=7 using unpaired, two-tailed t-test analysis to respective control (untreated). * *P< 0.05* **G** Following transient RhoA siRNA transfection invaded cells under filter was counted in four randomly selected regions. Data represent mean ± SEM. M n=18 using unpaired, two-tailed t-test analysis to respective control. * *P< 0.05* **H** Relative quantification of RhoA and CTGF mRNA expression in MCF-7 cells after transient RhoA transfection (t0h). Data represent mean ± SEM. M n=3 using unpaired, two-tailed t-test analysis to respective control. ** *P <0.01*

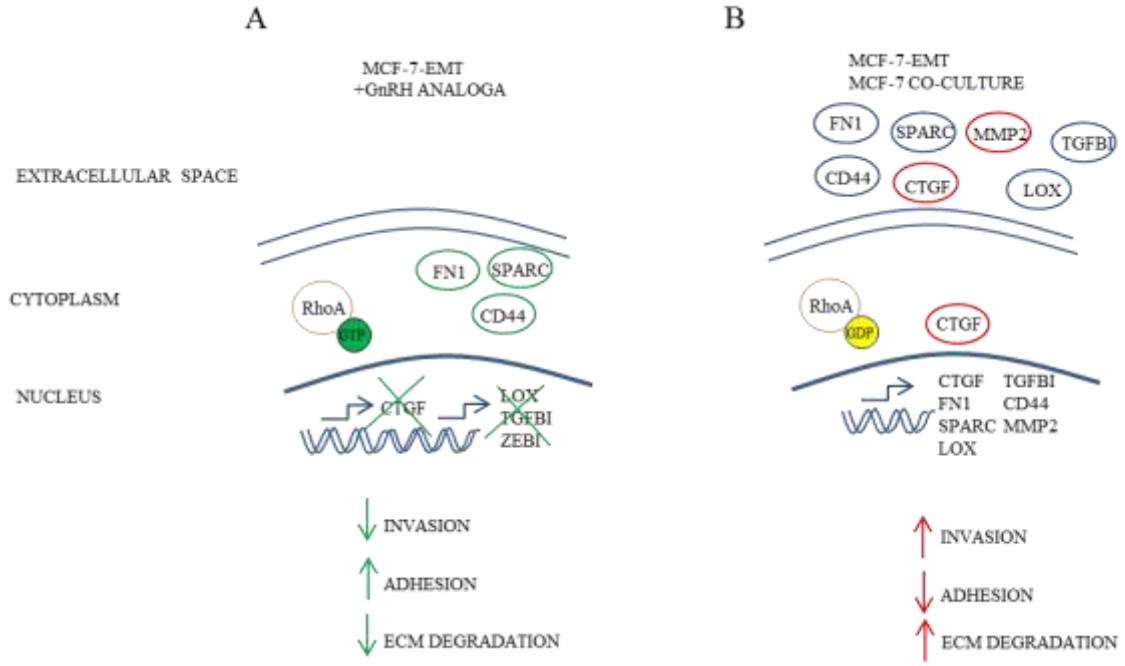

Figure 7 Proposed model of CTGF driven invasion in breast cancer. A Mesenchymal transformed breast cancer cells with Triptorelin treatment, CTGF blocking antibody or transiently suppressed CTGF expression reduces invasiveness, increased cell-ECM adhesion and reduced ECM degradation. On the other hand **B** co-cultured non-invasive MCF-7 breast cancer cells or mesenchymal transformed breast cancer cells exhibit an increased CTGF expression higher invasion, decreased cell-ECM adhesion and increased ECM degradation.

Supplementary Information

Identification of breast cancer invasion drivers by secretome analysis: insight into CTGF signaling

Johanna W. Hellinger [1],Franziska Schömel[1], Christof Lenz [2, 3], Gerd Bauerschmitz [1], Günter Emons [1], Carsten Gründker [1]

Affiliation

[1]Department of Gynecology and Obstetrics, University Medical Center Göttingen, Göttingen, Germany

[2]Bioanalytical Mass Spectrometry Group, Max Planck Institute for Biophysical Chemistry, Göttingen, Germany

[3]Department of Clinical Chemistry, Bioanalytics, University Medical Center Göttingen, Göttingen, Germany

Includes:

Supplementary figures: fig. 1 S4; fig. 2 S8; fig. 3 S10, fig. 6 S11, fig. 6 S12

Supplementary tables: fig. 1 S1; fig. 1 S2; fig. 1 S3; fig. 1 S5; fig. 1 S6; fig. 1 S7; fig. 2 S9

Supplement 1: Protein findings from secretome analysis of co-cultured breast cancer cells with osteosarcoma cells. Information is given about gene symbol/User ID, Ensemble Gene ID, p-value and mean values of co-culture media and MCF-7 control media. List was used to further examine Gene Ontology (GO) enrichment using Shiny GO v06.0.

i	User ID	Ensembl Gene ID	p-value	mean co-culture	mean MCF-7 control
1	HTRA1	ENSG00000166033	0,00021228	28234	6597
2	CD44	ENSG00000026508	0,00037961	12615	1688
3	C1R	ENSG00000159403	0,00033183	61150	8715
4	POSTN	ENSG00000133110	0,0011454	95683	18550
5	HEXA	ENSG00000213614	9,7674E-05	16849	2926
6	B2M	ENSG00000166710	0,00135842	70650	3738
7	LOXL1	ENSG00000129038	3,8422E-10	65281	7724
8	MMP2	ENSG00000087245	0,00146649	4431667	96000
9	COL1A1	ENSG00000108821	0,0002255	3191667	78133
10	NUCB1	ENSG00000104805	0,00158982	120358	12667
11	CNN2	ENSG00000064666	7,0889E-06	81240	7659
12	CAB39	ENSG00000135932	0,00129469	45224	143832
13	SERPINE2	ENSG00000135919	9,9725E-05	7465	1199
14	FN1	ENSG00000115414	0,00127185	2013667	45350
15	FSTL1	ENSG00000163430	0,00158654	77483	11262

16	IGFBP7	ENSG00000163453	4,6509E-05	8350	1784
17	TGFBI	ENSG00000120708	0,00065803	10008	1168
18	SPARC	ENSG00000113140	0,00082713	2172000	116933
19	LOX	ENSG00000113083	0,00111492	18118	5004
20	COL23A1	ENSG00000050767	0,00116807	23983	1270
21	THBS2	ENSG00000186340	0,00035021	59250	8683
22	COL1A2	ENSG00000164692	0,00108052	5150000	31383
23	SERPINE1	ENSG00000106366	0,00054046	37167	7040
24	PCOLCE	ENSG00000106333	8,2456E-05	367167	34500
25	CTSB	ENSG00000164733	0,00064317	827167	82000
26	CLU	ENSG00000120885	0,00071045	130026	51465
27	SVEP1	ENSG00000165124	0,00046555	218000	29017
28	TIMP1	ENSG00000102265	0,00135049	168650	37333

Supplement 2 GO enrichment analysis of findings from secretome analysis. Protein discoveries listed in Fig. 1 S1 were examined for GO enrichment using Shiny GO v06.0. Information is given about enrichment FDR, how many genes within the discovery list are enriched within specific functional category, total number of genes within specific functional category, functional category and genes listed from discoveries which are enriched in specific category.

Enrichment FDR	Genes in list	Total genes	Functional Category	Genes
3,26E-15	14	392	Extracellular matrix organization	COL23A1, MMP2 , COL1A1 , TGFBI , POSTN , COL1A2 , LOX , CD44 , TIMP1 , SERPINE1 , SPARC , FN1 , LOXL1 , HTRA1
1,52E-14	14	460	Extracellular structure organization	COL23A1, MMP2, COL1A1, TGFBI, POSTN, COL1A2, LOX, CD44, TIMP1, SERPINE1, SPARC, FN1, LOXL1, HTRA1
8,92E-09	11	585	Wound healing	SERPINE1, SERPINE2, CNN2, TIMP1, COL1A1, LOX, SPARC, FN1, POSTN, CD44, COL1A2
3,22E-08	11	687	Blood vessel development	COL23A1, COL1A1, THBS2, SPARC, MMP2, LOX, FN1, LOXL1, SERPINE1, TGFBI, COL1A2
3,22E-08	11	716	Response to wounding	SERPINE1, SERPINE2, CNN2, TIMP1, COL1A1, LOX, SPARC, FN1, POSTN, CD44, COL1A2
3,22E-08	11	715	Vasculature development	COL23A1,COL1A1,THBS2,SPARC,MMP2,LOX, FN1,LOXL1,SERPINE1,TGFBI,COL1A2
3,22E-08	18	2983	Cellular response to organic substance	CD44, COL1A2, MMP2, PCOLCE, COL1A1, LOX, SPARC, POSTN, IGFBP7, HTRA1, CTSB, SERPINE1, CLU, CNN2, TIMP1, FN1, FSTL1, B2M
3,22E-08	11	724	Cardiovascular system development	COL23A1, COL1A1, THBS2, SPARC, MMP2, LOX, FN1, LOXL1, SERPINE1, TGFBI, COL1A2
5,11E-08	19	3547	Response to organic substance	TIMP1, CD44, CLU, COL1A2, MMP2, PCOLCE, COL1A1, LOX, SPARC, LOXL1, POSTN, IGFBP7, HTRA1, B2M, CTSB, SERPINE1, CNN2, FN1, FSTL1
3,11E-07	20	4507	Response to stress	CD44, MMP2, SERPINE1, SERPINE2, CAB39, CLU, CNN2, TIMP1, COL1A1, LOX, SPARC, FN1, POSTN, C1R, FSTL1, IGFBP7, HTRA1, COL1A2, CTSB, B2M
4,16E-07	18	3536	Cellular response to chemical stimulus	CD44, POSTN, COL1A2, MMP2, PCOLCE, COL1A1, LOX, SPARC, IGFBP7, HTRA1, B2M, CTSB, SERPINE1, CLU, CNN2, TIMP1, FN1, FSTL1
1,31E-06	12	1372	Response to cytokine	TIMP1, PCOLCE, COL1A1, LOX, SPARC, POSTN, CD44, CNN2, MMP2, FN1, COL1A2, B2M

1,31E-06	11	1077	Circulatory system development	COL23A1, COL1A1, THBS2, SPARC, MMP2, LOX, FN1, LOXL1, SERPINE1, TGFBI, COL1A2
2,76E-06	10	901	Regulated exocytosis	CD44, CNN2, TIMP1, SERPINE1, SPARC, FN1, CLU, CAB39, CTSB, B2M
6,12E-06	15	2785	Anatomical structure morphogenesis	COL23A1, THBS2, SERPINE1, SPARC, FN1, CLU, MMP2, COL1A1, LOX, POSTN, SERPINE2, HTRA1, TGFBI, CD44, COL1A2
6,12E-06	11	1278	Cellular response to cytokine stimulus	PCOLCE, COL1A1, LOX, POSTN, CD44, CNN2, MMP2, TIMP1, FN1, COL1A2, B2M
7,03E-06	10	1023	Exocytosis	CD44, CNN2, TIMP1, SERPINE1, SPARC, FN1, CLU, CAB39, CTSB, B2M
7,03E-06	8	541	Skeletal system development	COL1A1, MMP2, TIMP1, LOX, SPARC, TGFBI, CD44, COL1A2
9,69E-06	12	1704	Response to endogenous stimulus	TIMP1, CD44, COL1A2, MMP2, COL1A1, LOX, SPARC, POSTN, IGFBP7, HTRA1, CTSB, FSTL1
9,87E-06	12	1715	Secretion by cell	FN1, POSTN, SERPINE2, CD44, CNN2, TIMP1, SERPINE1, SPARC, CLU, CAB39, CTSB, B2M
1,35E-05	8	603	Blood vessel morphogenesis	COL23A1, THBS2, SPARC, MMP2, LOX, FN1, SERPINE1, TGFBI
1,39E-05	13	2168	Tissue development	COL23A1, SERPINE1, COL1A1, FN1, TIMP1, LOX, TGFBI, POSTN, SERPINE2, COL1A2, CTSB, CD44, MMP2
1,63E-05	5	135	Platelet degranulation	TIMP1, SERPINE1, SPARC, FN1, CLU
1,94E-05	11	1506	Cell migration	CD44, SERPINE1, COL1A1, SPARC, FN1, CNN2, LOX, POSTN, TIMP1, SERPINE2, COL1A2
1,94E-05	12	1861	Secretion	FN1, POSTN, SERPINE2, CD44, CNN2, TIMP1, SERPINE1, SPARC, CLU, CAB39, CTSB, B2M
3,13E-05	8	694	Cellular response to growth factor stimulus	CD44, COL1A2, COL1A1, LOX, SPARC, POSTN, HTRA1, FSTL1
4,09E-05	8	723	Response to growth factor	CD44, COL1A2, COL1A1, LOX, SPARC, POSTN, HTRA1, FSTL1
4,53E-05	7	511	Angiogenesis	COL23A1, THBS2, SPARC, MMP2, FN1, SERPINE1, TGFBI
4,53E-05	11	1670	Cell motility	CD44, SERPINE1, COL1A1, SPARC, FN1, CNN2, LOX, POSTN, TIMP1, SERPINE2, COL1A2
4,53E-05	11	1670	Localization of cell	CD44, SERPINE1, COL1A1, SPARC, FN1, CNN2, LOX, POSTN, TIMP1, SERPINE2, COL1A2

Supplement 3 GO group enrichment analysis of findings from secretome analysis. Protein discoveries listed in Fig. 1 S1 were examined for GO group enrichment using Shiny GO v06.0.

N	High level GO category	Genes
20	Response to stress	CD44, MMP2, SERPINE1, SERPINE2, CAB39, CLU, CNN2, TIMP1, COL1A1, LOX, SPARC, FN1, POSTN, C1R, FSTL1, IGFBP7, HTRA1, COL1A2, CTSB, B2M
15	Anatomical structure morphogenesis	COL23A1, THBS2, SERPINE1, SPARC, FN1, CLU, MMP2, COL1A1, LOX, POSTN, SERPINE2, HTRA1, TGFBI, CD44, COL1A2
14	Regulation of response to stimulus	CD44, SERPINE1, SERPINE2, COL1A1, FN1, B2M, TIMP1, LOX, CLU, POSTN, C1R, HTRA1, COL1A2, CTSB

13	Immune system process	CD44, CLU, B2M, CNN2, LOX, C1R, HTRA1, SERPINE1, COL1A1, FN1, CAB39, COL1A2, CTSB
13	Response to external stimulus	COL1A1, SERPINE1, SERPINE2, CNN2, POSTN, LOX, SPARC, LOXL1, FSTL1, HTRA1, B2M, CLU, C1R
12	Response to endogenous stimulus	TIMP1, CD44, COL1A2, MMP2, COL1A1, LOX, SPARC, POSTN, IGFBP7, HTRA1, CTSB, FSTL1
12	Regulation of localization	CAB39, SERPINE1, COL1A1, SPARC, FN1, CNN2, NUCB1, POSTN, SERPINE2, CLU, B2M, TIMP1
12	Multi-organism process	FN1, MMP2, SPARC, LOXL1, SERPINE2, IGFBP7, CTSB, HTRA1, B2M, CLU, SERPINE1, TIMP1
11	Locomotion	CD44, SERPINE1, COL1A1, SPARC, FN1, CNN2, LOX, POSTN, TIMP1, SERPINE2, COL1A2
11	Cell motility	CD44, SERPINE1, COL1A1, SPARC, FN1, CNN2, LOX, POSTN, TIMP1, SERPINE2, COL1A2
11	Regulation of developmental process	THBS2, SERPINE1, COL1A1, SPARC, SERPINE2, LOX, FN1, POSTN, B2M, CD44, TIMP1
11	Regulation of multicellular organismal process	THBS2, SERPINE1, SERPINE2, COL1A1, SPARC, FN1, CLU, B2M, LOX, POSTN, TIMP1
11	Localization of cell	CD44, SERPINE1, COL1A1, SPARC, FN1, CNN2, LOX, POSTN, TIMP1, SERPINE2, COL1A2
11	Regulation of biological quality	B2M, SERPINE1, SERPINE2, CLU, LOX, SPARC, FN1, POSTN, THBS2, COL1A2, COL1A1
11	Regulation of molecular function	TIMP1, SERPINE1, SERPINE2, CAB39, CD44, B2M, PCOLCE, LOX, FN1, CTSB, CLU
10	Cell adhesion	CD44, TGFBI, POSTN, SERPINE1, FN1, IGFBP7, COL1A1, SERPINE2, SVEP1, THBS2
10	Cell proliferation	TIMP1, SPARC, FN1, CLU, CNN2, MMP2, TGFBI, SERPINE2, HTRA1, IGFBP7
10	Biological adhesion	CD44, TGFBI, POSTN, SERPINE1, FN1, IGFBP7, COL1A1, SERPINE2, SVEP1, THBS2
10	Regulation of signalling	CD44, SERPINE1, COL1A1, FN1, TIMP1, LOX, POSTN, SERPINE2, HTRA1, CLU
9	Regulation of immune system process	B2M, LOX, CLU, C1R, HTRA1, SERPINE1, COL1A1, COL1A2, CTSB
9	Immune response	B2M, CLU, C1R, CD44, CNN2, COL1A1, CAB39, COL1A2, CTSB
9	Anatomical structure formation involved in morphogenesis	COL23A1, THBS2, SERPINE1, SPARC, FN1, MMP2, COL1A1, HTRA1, TGFBI
8	Immune effector process	B2M, CLU, C1R, HTRA1, CD44, CNN2, CAB39, CTSB
8	Response to abiotic stimulus	MMP2, COL1A1, CAB39, CNN2, SPARC, POSTN, SERPINE2, IGFBP7
8	Regulation of locomotion	SERPINE1, COL1A1, SPARC, FN1, CNN2, POSTN, TIMP1, SERPINE2
7	Catabolic process	MMP2, TIMP1, CLU, CTSB, CD44, SERPINE2, HEXA
7	Regulation of cell adhesion	SERPINE1, FN1, COL1A1, POSTN, SERPINE2, CD44, TGFBI
7	Cellular component biogenesis	CLU, COL1A1, LOX, FN1, CAB39, COL1A2, THBS2
6	Reproduction	MMP2, SERPINE2, IGFBP7, CTSB, HTRA1, TIMP1
6	Response to biotic stimulus	SPARC, LOXL1, HTRA1, B2M, CLU, SERPINE1
6	Reproductive process	MMP2, SERPINE2, IGFBP7, CTSB, HTRA1, TIMP1
6	Leukocyte activation	CD44, CLU, B2M, CNN2, CAB39, CTSB
6	Response to other organism	SPARC, LOXL1, HTRA1, B2M, CLU, SERPINE1
5	System process	TGFBI, POSTN, SERPINE2, COL1A1, COL1A2
5	Macromolecule localization	CLU, COL1A1, FN1, NUCB1, POSTN
5	Multi-organism reproductive process	MMP2, SERPINE2, IGFBP7, CTSB, TIMP1
5	Multi-multicellular organism process	MMP2, SERPINE2, IGFBP7, CTSB, TIMP1
5	Leukocyte migration	SERPINE1, CD44, COL1A1, FN1, COL1A2
4	Cell growth	FN1, POSTN, SERPINE2, IGFBP7
4	Growth	FN1, POSTN, SERPINE2, IGFBP7

3	Activation of immune response	CLU, C1R, CTSB
3	Immune system development	CNN2, LOX, B2M
3	Developmental process involved in reproduction	SERPINE2, CTSB, HTRA1
3	Regulation of growth	FN1, SERPINE2, IGFBP7
3	Interspecies interaction between organisms	FN1, CTSB, B2M
3	Cellular localization ","CLU COL1A1 NUCB1"	CLU, COL1A1, NUCB1
2	Protein folding	CLU, B2M
2	Multicellular organism reproduction	SERPINE2, CTSB
2	Taxis	LOX, SERPINE1
2	Regulation of multi-organism process	HTRA1, TIMP1
2	Regulation of cellular component biogenesis	CLU, THBS2
2	Developmental growth	FN1, POSTN
2	Multicellular organismal reproductive process	SERPINE2, CTSB
2	Protein activation cascade	CLU, C1R
2	Regulation of homeostasis	SERPINE1, SERPINE2

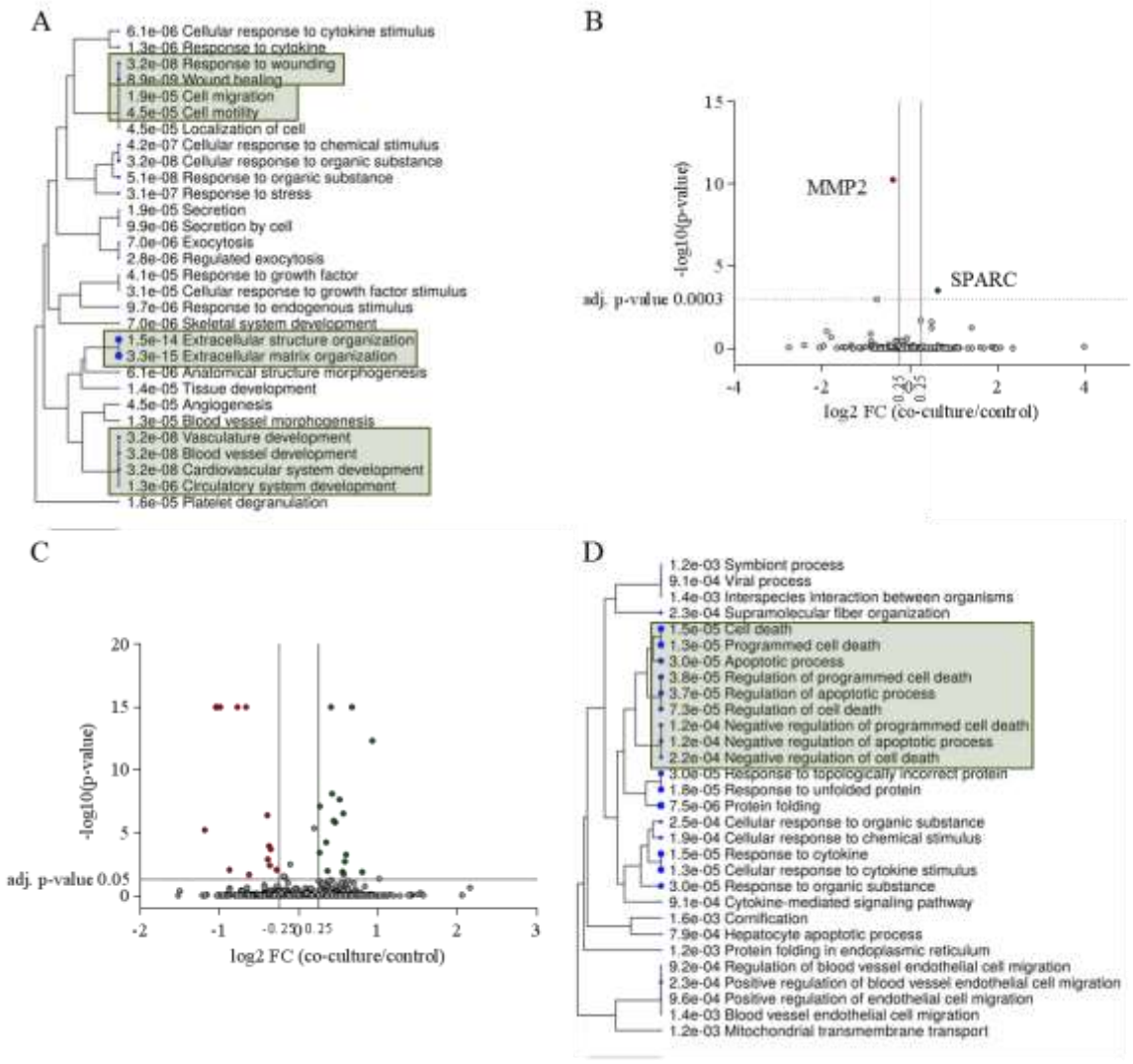

Supplement 4 Functional analysis of detected discoveries from secretome and proteome analysis of co-cultured breast cancer cells. A Hierarchical clustering tree using shiny GO v06.0 Gene ontology enrichment of discoveries from co-culture media with corresponding p-values. **B** Volcano plot demonstrating potential bone-directed breast cancer invasiveness related targets using proteome analysis of media from co-cultures MCF-7 cells vs MG-63 control. Detected target proteins were stated as discovery when adjusted p-value was below 0.03 (dotted line) with a false-discovery rate (FDR) of 5% and a log 2 fold change (FC) higher 0.25 or lower -0.25. Every dot indicates one target, green dots indicate upregulated discoveries and red dot indicates downregulated discoveries. n=6, discovery determined using two-stage linear step-up procedure of Benjamini, Krieger and Yekutieli, with Q = 5%. Each row was analyzed individually, without assuming a consistent SD. **C** Volcano plot demonstrating potential bone-directed breast cancer invasiveness related targets using proteome analysis of lysates from co-cultures MCF-7 cells vs MCF-7 control. Detected target proteins were stated as discovery when adjusted p-value was below 0.05 (dotted line) with a false-discovery rate (FDR) of 1% and a log 2 fold change (FC) higher 0.25 or lower -0.25. Every dot indicates one target, green dots indicate upregulated discoveries and red dot indicates downregulated discoveries. n=6, discovery determined using two-stage linear step-up procedure of Benjamini, Krieger and Yekutieli, with Q = 1%. Each row was analyzed individually, without assuming a consistent SD. **D** Hierarchical clustering tree using shiny GO v06.0 Gene ontology enrichment of discoveries from co-culture lysates with corresponding p-values.

Supplement 5 Protein findings from proteome analysis of cell lysates from co-cultured breast cancer cells with osteosarcoma cells (MG-63) compared to MCF-7 monoculture. Information about gene symbol/User ID, Ensemble Gene ID, Gene Type, Chromosome location (Chr) and genomic position is given. List was used to further examine Gene Ontology (GO) enrichment using Shiny GO v06.0.

i	User ID	Ensembl Gene ID	p-value	mean co-culture	mean MCF-7 control
1	HIST2H3PS2	ENSG00000203818	<0,000000000000001	711875	1418125
2	CFL1	ENSG00000172757	3,995E-07	1362500	1800000

3	SLC3A2	ENSG00000168003	4,69E-13	1318625	694125
4	KRT8	ENSG00000170421	<0,000000000000001	2528750	5233750
5	HSP90B1	ENSG00000166598	<0,000000000000001	3183750	2406250
6	KRT18	ENSG00000111057	<0,000000000000001	1963750	4050125
7	ATP5F1B	ENSG00000110955	1,11105E-06	1610000	1189625
8	PDIA3	ENSG00000167004	1,48704E-06	1531250	1115875
9	KRT19	ENSG00000171345	<0,000000000000001	1441250	2472250
10	FASN	ENSG00000169710	<0,000000000000001	3546250	2232500
11	ATP5F1A	ENSG00000152234	5,68907E-05	1645000	1297625
12	HSPD1	ENSG00000144381	7,80485E-09	1988750	1490500
13	PREX1	ENSG00000124126	6,12649E-06	304250	694500
14	HSPA9	ENSG00000113013	2,96513E-07	1378750	936375
15	HSP90AB1	ENSG00000096384	2,19282E-08	1622500	1139500
16	MDH2	ENSG00000146701	7,73663E-08	2807500	2343750
17	HSPB1	ENSG00000106211	<0,000000000000001	4387500	6976250

Supplement 6 GO enrichment analysis of findings from proteome analysis. Protein discoveries from co-cultured breast cancer cell lysates listed in S5 were examined for GO enrichment using Shiny GO v06.0. Information is given about the enrichment FDR, how many genes with the discovery list are enriched within specific functional category, total number of genes within specific functional category, functional category and genes listed from the discoveries which are enriched in specific category.

Enrichment FDR	Genes in list	Total genes	Functional Category	Genes
7,55E-06	6	245	Protein folding	HSPA9, HSPD1, PDIA3, HSP90AB1, HSP90B1, HSPB1
1,34E-05	11	2257	Programmed cell death	HSPD1, KRT18, HSP90AB1, HSPB1, PDIA3, KRT8, HSP90B1, HSPA9, PREX1, KRT19, CFL1
1,34E-05	9	1278	Cellular response to cytokine stimulus	HSP90AB1, ATP5F1B, KRT18, PDIA3, FASN, KRT8, HSPA9, HSP90B1, CFL1
1,46E-05	11	2415	Cell death	HSPD1, KRT18, HSP90AB1, HSPB1, PDIA3, KRT8, HSP90B1, HSPA9, PREX1, KRT19, CFL1
1,48E-05	9	1372	Response to cytokine	HSP90AB1, ATP5F1B, KRT18, PDIA3, FASN, KRT8, HSPA9, HSP90B1, CFL1
1,82E-05	5	193	Response to unfolded protein	HSPA9, HSPD1, HSP90AB1, HSPB1, HSP90B1
2,97E-05	10	2106	Apoptotic process	HSPD1, KRT18, HSP90AB1, HSPB1, PDIA3, KRT8, HSP90B1, HSPA9, PREX1, CFL1
2,97E-05	12	3547	Response to organic substance	HSPA9, HSP90AB1, HSPD1, HSP90B1, ATP5F1B, KRT18, PDIA3, FASN, KRT8, CFL1, HSPB1, SLC3A2
2,97E-05	5	227	Response to topologically incorrect protein	HSPA9, HSPD1, HSP90AB1, HSPB1, HSP90B1
3,69E-05	9	1657	Regulation of apoptotic process	KRT18, HSPD1, HSP90AB1, HSPB1, PDIA3, HSP90B1, HSPA9, PREX1, CFL1
3,79E-05	9	1681	Regulation of programmed cell death	KRT18, HSPD1, HSP90AB1, HSPB1, PDIA3, HSP90B1, HSPA9, PREX1, CFL1
7,27E-05	9	1835	Regulation of cell death	KRT18, HSPD1, HSP90AB1, HSPB1, PDIA3, HSP90B1, HSPA9, PREX1, CFL1
0,000115066	7	966	Negative regulation of apoptotic process	KRT18, HSP90AB1, HSPB1, HSPD1, HSP90B1, HSPA9, CFL1
0,00012323	7	987	Negative regulation of programmed cell death	KRT18, HSP90AB1, HSPB1, HSPD1, HSP90B1, HSPA9, CFL1
0,000191624	11	3536	Cellular response to chemical stimulus	HSPA9, HSP90AB1, HSP90B1, HSPB1, ATP5F1B, KRT18, PREX1, PDIA3, FASN, KRT8, CFL1
0,000219305	7	1099	Negative regulation of cell death	KRT18, HSP90AB1, HSPB1, HSPD1, HSP90B1, HSPA9, CFL1
0,000225829	6	712	Supramolecular fiber organization	HSP90B1, KRT19, CFL1, PREX1, KRT8, HSP90AB1

0,000225829	3	55	Positive regulation of blood vessel endothelial cell migration	ATP5F1B, ATP5F1A, HSPB1
0,000251526	10	2938	Cellular response to organic substance	HSPA9, HSP90AB1, HSP90B1, ATP5F1B, KRT18, PDIA3, FASN, KRT8, HSPB1, CFL1
0,000790234	2	12	Hepatocyte apoptotic process	KRT18, KRT8
0,000911637	6	951	Viral process	KRT18, HSPD1, KRT8, KRT19, HSP90AB1, CFL1
0,000911637	6	950	Cytokine-mediated signalling pathway	KRT18, KRT8, HSP90AB1, HSPA9, HSP90B1, CFL1
0,000915372	3	95	Regulation of blood vessel endothelial cell migration	ATP5F1B, ATP5F1A, HSPB1
0,000962601	3	98	Positive regulation of endothelial cell migration	ATP5F1B, ATP5F1A, HSPB1
0,001203543	3	109	Mitochondrial transmembrane transport	HSPD1, ATP5F1B, ATP5F1A
0,001203543	2	17	Protein folding in endoplasmic reticulum	HSP90B1, PDIA3
0,001203543	6	1024	Symbiont process	KRT18, HSPD1, KRT8, KRT19, HSP90AB1, CFL1
0,001435777	3	119	Blood vessel endothelial cell migration	ATP5F1B, ATP5F1A, HSPB1
0,001435777	6	1084	Interspecies interaction between organisms	KRT18, HSPD1, KRT8, KRT19, HSP90AB1, CFL1
0,001588854	3	125	Cornification	KRT18, KRT8, KRT19

Supplement 7: GO group enrichment analysis of findings from proteome analysis. Protein discoveries listed in S5 were examined for GO group enrichment using Shiny GO v06.0.

N	High level GO category	Genes
9	Regulation of biological quality	HSPB1, HSP90AB1, PREX1, PDIA3, CFL1, ATP5F1B, HSPA9, HSPD1, HSP90B1
8	Immune system process	HSPD1, HSPA9, PREX1, FASN, HSP90AB1, HSP90B1, PDIA3, SLC3A2
8	Response to stress	HSPB1, HSPA9, ATP5F1A, HSP90B1, PDIA3, HSPD1, HSP90AB1, KRT8
8	Anatomical structure morphogenesis	KRT19, HSP90AB1, PREX1, KRT8, CFL1, HSPB1, ATP5F1B, KRT18
8	Regulation of multicellular organismal process	HSP90AB1, HSPD1, HSPB1, HSPA9, PREX1, ATP5F1B, ATP5F1A, CFL1
8	Cellular localization	HSP90AB1, HSPD1, ATP5F1B, ATP5F1A, KRT18, HSPA9, HSPB1, HSP90B1
7	Cellular component biogenesis	HSP90AB1, HSP90B1, KRT19, HSPA9, PREX1, KRT8, HSPD1
7	Multi-organism process	KRT18, HSPD1, KRT8, KRT19, HSPB1, CFL1, HSP90AB1
6	Protein folding	HSPA9, HSPD1, PDIA3, HSP90AB1, HSP90B1, HSPB1
6	Biological adhesion	HSPB1, HSPD1, ATP5F1B, KRT18, PREX1, HSP90AB1
6	Macromolecule localization	HSP90AB1, HSPD1, KRT18, HSPA9, HSPB1, HSP90B1
6	Locomotion	ATP5F1B, PREX1, CFL1, ATP5F1A, HSPB1, SLC3A2
6	Interspecies interaction between organisms	KRT18, HSPD1, KRT8, KRT19, HSP90AB1, CFL1
6	Regulation of response to stimulus	HSP90AB1, HSPD1, HSPB1, PREX1, PDIA3, HSP90B1
6	Cell motility	ATP5F1B, PREX1, CFL1, ATP5F1A, HSPB1, SLC3A2
6	Localization of cell	ATP5F1B, PREX1, CFL1, ATP5F1A, HSPB1, SLC3A2
5	Cell adhesion	HSPB1, HSPD1, ATP5F1B, KRT18, PREX1
5	Response to external stimulus	HSP90B1, PREX1, KRT8, HSPB1, CFL1

5	Response to abiotic stimulus	HSPA9, HSP90B1, HSP90AB1, KRT8, HSPD1
5	Regulation of localization	HSP90AB1, PREX1, ATP5F1B, ATP5F1A, HSPB1
5	Anatomical structure formation involved in morphogenesis	KRT19, KRT8, CFL1, HSPB1, ATP5F1B
5	Regulation of developmental process	HSPA9, PREX1, HSP90AB1, HSPB1, CFL1
5	Regulation of molecular function	HSP90AB1, HSPD1, HSP90B1, HSPB1, PREX1
4	Immune system development	HSPD1, HSPA9, PREX1, FASN
4	Regulation of immune system process	HSPD1, HSPA9, HSP90AB1, HSP90B1
4	Response to biotic stimulus	HSPD1, KRT8, HSPB1, CFL1
4	Regulation of signalling	HSP90AB1, HSPB1, PREX1, PDIA3
4	Regulation of locomotion	PREX1, ATP5F1B, ATP5F1A, HSPB1
3	Reproduction	HSP90AB1, KRT8, KRT19
3	Activation of immune response	HSPD1, HSP90AB1, HSP90B1
3	Developmental process involved in reproduction	HSP90AB1, KRT8, KRT19
3	Immune response	HSPD1, HSP90AB1, HSP90B1
3	Catabolic process	HSP90AB1, HSP90B1, HSPB1
3	Reproductive process	HSP90AB1, KRT8, KRT19
3	Regulation of cell adhesion	HSPD1, ATP5F1B, PREX1
3	Leukocyte activation	HSPD1, PREX1, HSP90AB1
3	Response to other organism	KRT8, HSPB1, CFL1
2	Immune effector process	HSPD1, HSP90AB1
2	Cell proliferation	HSPD1, ATP5F1A
2	Response to endogenous stimulus	HSP90AB1, HSP90B1
2	Cell cycle process	CFL1, HSP90AB1
2	Taxis	PREX1, HSPB1
2	Leukocyte migration	PREX1, SLC3A2

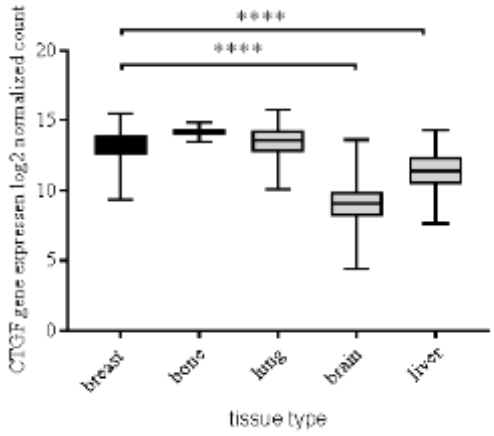

Supplement 8 Tissue expression analysis of CTGF. CTGF expression in human bone (n=2), breast (n=179), lung (n=287) and brain (n=1136) tissue was assessed using xenabrowse with datasets from GTEX, TARGET, and TCGA. One-way ANOVA and a Dunnett‘s multiple comparison test with no matching or pairing between groups was calculated to assess significant differences compared to the untreated control. **** *P <0.0001*

Supplement 9: CTGF expression in invasive ductal carcinoma and normal breast tissue. CTGF expression was assessed in 24 patient samples from biomax tissue array (BR248a). Following information are given: Sex/Age, pathology diagnosis, TNM (Tumor, Node, and Metastasis), Tumor Grading, Stage, Type, Tissue-ID and corresponding detected CTGF expression.

Sex/ Age	Pathology diagnosis	TNM	Grade	Stage	Type	Tissue ID.	CTGF expression
F/34	Invasive ductal carcinoma	T3N0M0	1--2	IIB	malignant	Fmg040048	+
F/37	Invasive ductal carcinoma	T2N0M0	1--2	IIA	malignant	Fmg020357	+
F/60	Invasive ductal carcinoma	T2N0M0	2	IIA	malignant	Fmg040031	+
F/57	Invasive ductal carcinoma	T2N0M0	2	IIA	malignant	Fmg040001	+
F/38	Invasive ductal carcinoma	T1N0M0	2	I	malignant	Fmg040052	++
F/55	Invasive ductal carcinoma	T2N0M0	2	IIA	malignant	Fmg040104	-
F/45	Invasive ductal carcinoma	T2N0M0	2	IIA	malignant	Fmg040113	++
F/48	Invasive ductal carcinoma	T2N0M0	2	IIA	malignant	Fmg040118	+/++
F/58	Invasive ductal carcinoma	T2N0M0	2	IIA	malignant	Fmg040120	++
F/34	Invasive ductal carcinoma	T2N0M0	2	IIA	malignant	Fmg040123	++
F/49	Invasive ductal carcinoma	T2N0M0	2	IIA	malignant	Fmg040125	+
F/58	Invasive ductal carcinoma	T2N0M0	2	IIA	malignant	Fmg040130	++
F/38	Invasive ductal carcinoma	T2N1M0	2	IIB	malignant	Fmg040131	+
F/79	Invasive ductal carcinoma	T2N1M0	3	IIB	malignant	Fmg010491	+
F/43	Invasive ductal carcinoma	T2N0M0	3	IIA	malignant	Fmg040004	-
F/46	Invasive ductal carcinoma	T3N0M0	3	IIB	malignant	Fmg040074	+
F/76	Invasive ductal carcinoma	T4N0M0	3	IIIB	malignant	Fmg010789	+
F/47	Medullary carcinoma	T2N0M0	-	IIA	malignant	Fmg040016	+
F/21	Adenosis	-	-	-	normal	Fmg06N024	-
F/28	Normal breast tissue (fibro fatty tissue and blood vessel)	-	-	-	normal	Fmg11N017	-
F/21	Normal breast tissue	-	-	-	normal	Fmg12N001	+
F/50	Adenosis	-	-	-	normal	Fmg08N034	-
F/50	Normal breast tissue	-	-	-	normal	Fmg12N002	-
F/19	Normal breast tissue	-	-	-	normal	Fmg07N013	-

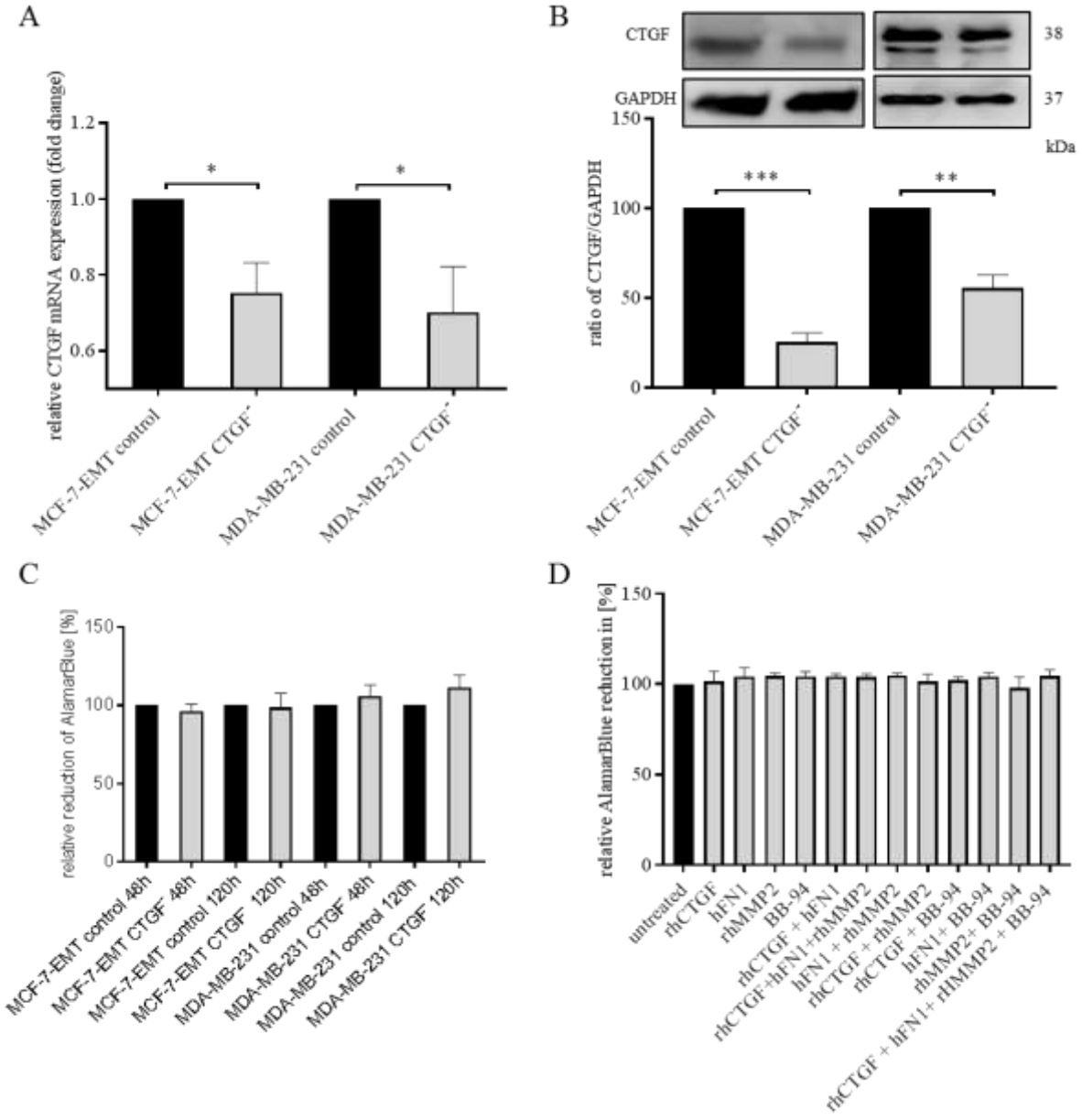

Supplement 10: CTGF expression does not alter proliferation *in vitro*. A CTGF mRNA expression in different breast cancer cell lines 120 hours after siRNA transfection was detected by real-time quantitative PCR. Data represent the mean ± SEM. MCF-7-EMT n=4, MDA-MB-231 n=5 using unpaired, two-tailed t-test analysis compared to respective control. * *P<0.05* **B** CTGF protein expression of different breast cancer cells 48 hours after CTGF siRNA transfection was detected by western blotting. The CTGF band intensity was quantified by densitometry and normalized to GAPDH. Data represent the mean ± SEM. n=3 using unpaired, two-tailed t-test analysis compared to respective control. ** *P<0.01;* *** *P<0.005* **C** Relative AlamarBlue reduction in different breast cancer cell lines 48 and 120 hours after CTGF siRNA transfection at 4 hours AlamarBlue incubation. Data represent the mean ± SEM. MCF-7-EMT t48h n=3, MCF-7-EMT t120h n=4 and MDA-MB-231 n=3 using unpaired, two-tailed t-test analysis compared to respective control. **D** 3D spheroid invasion assay with different compounds supplemented. Spheroids were embedded in Matrigel, after 48 hours AlamarBlue was added and absorption was measured after 4hours incubation. n = 3

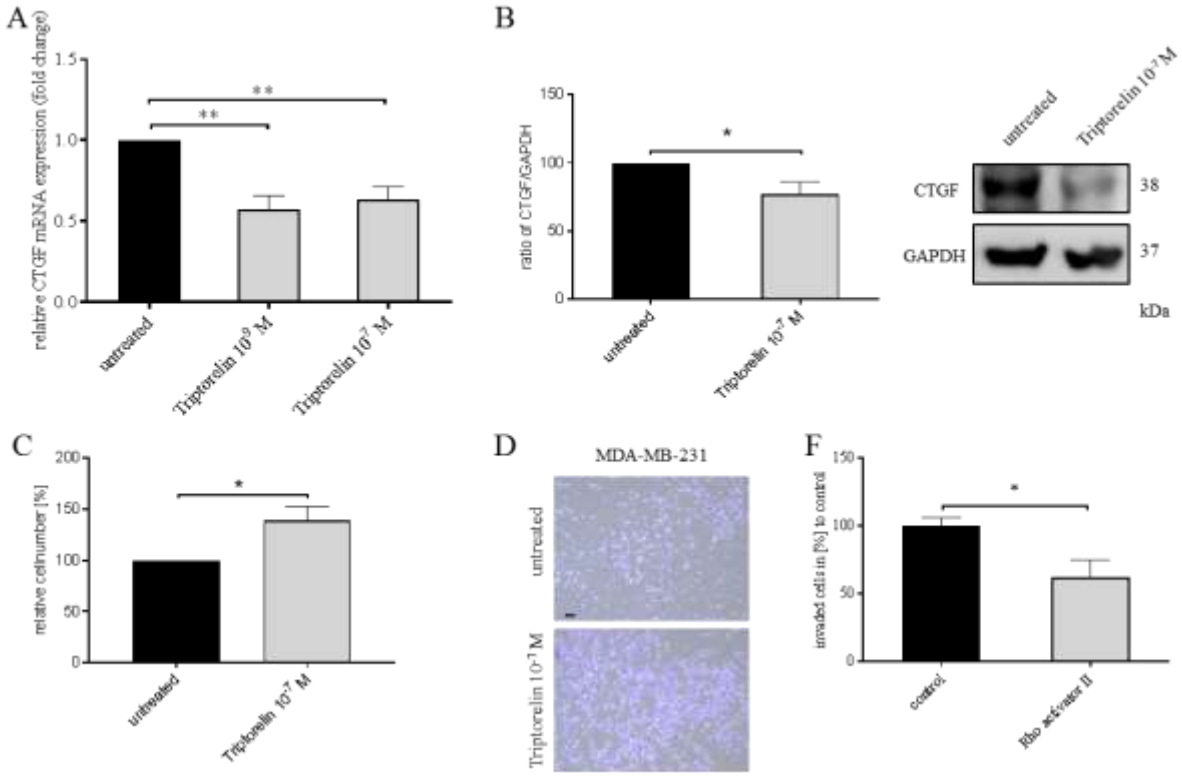

Supplement 11: GnRH agonist regulates CTGF expression in TNBC cells. A Relative quantification of CTGF mRNA expression in TNBC cells (MDA-MB-231) treated for 48 hours with 10^{-9} M or 10^{-7} M Triptorelin. Data represent the mean ± SEM. MDA-MB-231 n=4 using one-way ANOVA with F= 12.29 and a Dunnett's multiple comparison test with no matching or pairing between groups. ** *P <0.01* **B** Quantification and representative experiment of CTGF protein expression after Triptorelin treatment for 48 hours (10^{-7} M). The CTGF band intensity was quantified by densitometry and normalized to GAPDH. Data represent the mean ± SEM. MDA-MB-231 n=7 using unpaired, two-tailed t-test analysis to respective control (untreated). * *P<0.05* **C** Cell-ECM adhesion analysis of TNBC cells treated with 10^{-7} M Triptorelin. Adhesive cells where counter-stained with crystal violet and absorption was measured at 570nm. Data represent the mean ± SEM. MDA-MB-231 n=3 using unpaired, two-tailed t-test analysis to respective control (untreated). **P<0.05* **D** Representative *images corresponding to C. F* Following RhoA activator II treatment (1µg/ml) invaded MDA-MB-231 cells under the filter were counted in four randomly selected regions, using a co-culture Matrigel invasion assay for 48 hours. Data represent the mean ± SEM. n=9 Using unpaired, two-tailed t-test analysis to respective control. * *P< 0.05*

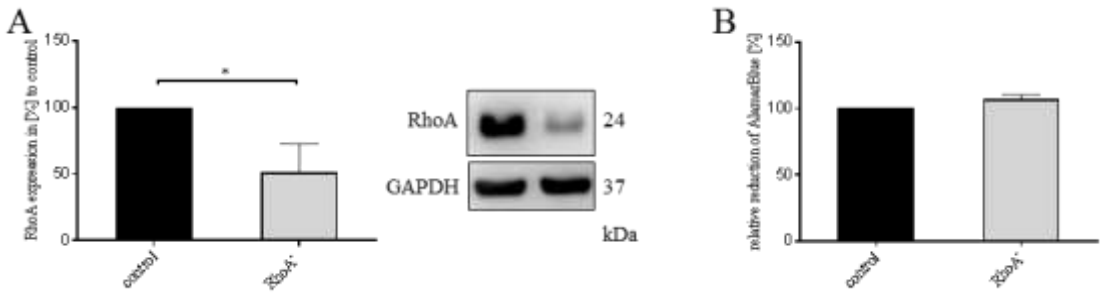

Supplement 12: Reducing RhoA expression does not alter proliferation *in vitro*. (A) RhoA protein expression in MCF-7 breast cancer cells 48 hours after RhoA siRNA transfection was detected by western blotting. The RhoA band intensity was quantified by densitometry and normalized to GAPDH. Data represent the mean ± SEM. n=3 using unpaired, two-tailed t-test analysis compared to respective control. * *P<0.05* (B) Relative AlamarBlue reduction in MCF-7 breast cancer cells 48 hours after RhoA siRNA transfection at 4 hours AlamarBlue incubation. Data represent the mean ± SEM. n=3 using unpaired, two-tailed t-test analysis compared to respective control.

References for this Manuscript are included along with introduction and discussion references at the end of the thesis.

4. DISCUSSION

In this study, we aimed to identify the molecular mechanisms of reduced breast cancer invasion when CYR61 expression was diminished. Additionally, the extracellular drivers of breast cancer bone-directed invasion were identified. Furthermore, the molecular mechanism of reduced breast cancer invasion during reduced CTGF expression was identified. Main findings were as follows:

1) CYR61 expression correlates with invasiveness of TNBC cells (MDA-MB-231, HCC-1806) and mesenchymal-transformed breast cancer cells (MCF-7-EMT, T47D-EMT). Reduced CYR61 expression led to diminished ERK1/2 phosphorylation, thereby reducing S100A4 expression. This signaling cascade could be assured by reduced YAP expression, which led to reduced CYR61 expression, reduced ERK1/2 phosphorylation, and reduced S100A4 expression (Figure 4).
2) CYR61 and S100A4 can be of value as a prognostic marker and therapeutic target for advanced and metastatic breast cancer.
3) We successfully identified 28 drivers of breast cancer bone-directed invasion by combining co-culturing techniques with secretome analysis using mass spectrometry. Additionally, nine identified drivers overlapped with genes upregulated during mesenchymal transition.
4) CTGF is one driver of breast cancer bone-directed invasion and is upregulated during mesenchymal transition. Reduced CTGF expression increased cell-ECM adhesion and decreased proteolytic activity of breast cancer cells. Additionally, CTGF regulates Zeb1, vimentin, LOX, SPARC, CD44, and transforming growth factor beta induced (TGFBI) expression in a cell-specific manner.
5) CTGF can be of value as a therapeutic target for advanced and metastatic breast cancer. Additionally, breast cancer cells treated with gonadotropin- releasing hormone (GnRH) agonist exhibited reduced CTGF expression by induced RhoA activity. These results indicate this agonist may be a possible treatment option.

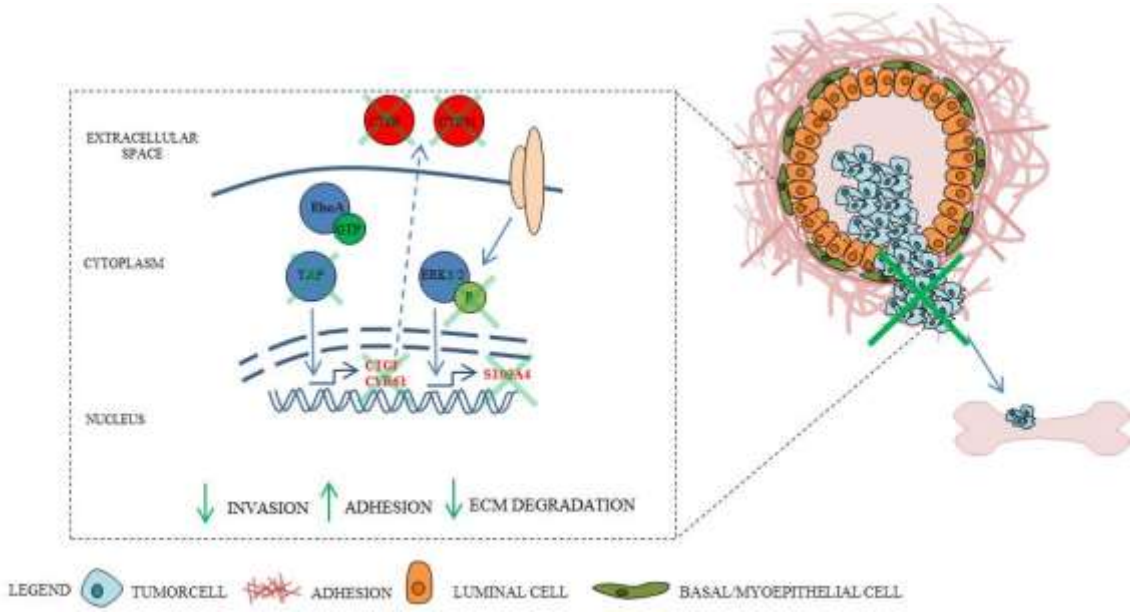

Figure 4 Scheme of signaling, that impedes invasion in highly invasive breast cancer cells. Illustration indicates how reduction of CYR61 or CTGF reduced breast cancer cell invasion.

4.1. IDENTIFICATION OF MOLECULAR MECHANISMS UNDERLYING REDUCED BREAST CANCER INVASIVENESS DUE TO REDUCED CYR61 EXPRESSION

As a matricellular protein, CYR61 acts as link between the ECM and cells within the TME (79). It binds to versatile receptors, thereby influencing manifold cellular processes such as invasion, migration, proliferation, survival, and wound healing (77, 80, 92, 93). Additionally, CYR61 has oncogenic function in several tumor entities including the breast (97, 114, 191, 192). Invasion is the initial step of the invasion-metastatic cascade. Cells unable to invade will not intravasate into the vascular system, extravasate into the distant parenchyma, or form metastases at distant sites (19-22). Bone metastasis is the prominent site for metastases in cancer, accounting for 70% and more of all metastases primarily located in the breast, prostate, and brain (8, 193). Despite having harsh physical environmental circumstances, disseminated tumor cells are able to colonize within the bone microenvironment with features different from the primary site of tumor growth (60). Identifying targets to stage tumor progression and impede invasion of primary breast cancer cells may help to cure currently incurable metastatic breast cancer. Our data suggest higher CYR61 expression in invasive TNBC cells (MDA-MB-231/basal b-like, HCC1806/ basal a-like) and mesenchymal-transformed breast cancer cells (MCF-7-EMT, T47D-EMT), which were generated from non-invasive breast cancer cells from luminal A subtype (MCF-7, T47D) (Manuscript A Figure 1 A). These mesenchymal-transformed breast cancer cells showed increased expression of

TGFBI, vimentin, zinc finger E-box-binding homeobox 1 (Zeb1), Snail family transcriptional repressor 2 (SNAI2), and E-cadherin (Manuscript A Figure S1 A-F). It was previously demonstrated that targeting extracellular CYR61 through specific antibodies led to reduced 2D transwell invasion in co-culture with osteosarcoma cells (7). In our study, transient reduced intracellular CYR61 expression led to reduced 2D transwell invasion in co-culture with osteosarcoma cells and reduced 3D spheroid invaded area growth, which was not due to altered proliferation (Manuscript A Figure 1 C-D + Figure S2 B).

To shed light on the underlying molecular mechanisms of CYR61 related breast cancer invasion, we found S100A4 to be a potential target. S100A4, which was already reported to affect breast cancer invasion, is regulated through integrin $\alpha v\beta_3$ and ERK1/2 (7, 168). Additionally, a previous study demonstrated that CYR61 promotes EMT through $\alpha v\beta_3$ and ERK signaling in osteosarcoma cells (191). In accordance with these findings, we report that reduced CYR61 led to decreased S100A4 expression. Reduced S100A4 expression led to reduced 2D transwell invasion and 3D spheroid invaded area growth, while additional treatment with recombinant CYR61 reversed this effect (Manuscript A Figure 2 D - F). Moreover, reduced CYR61 expression led to reduced ERK1/2 phosphorylation. The blocking of ERK1/2 phosphorylation with U0126 (inhibitor of MEK1/2 kinase) treatment led to reduced S100A4 expression and reduced invasiveness (Manuscript A Figure 3 D, E). In accordance with these results, previous studies have reported that S100A4 induces TGFβ signaling and the EMT and that targeting S100A4 could help to prevent bone metastasis (194-196).

Additionally, we wanted to verify these findings by regulating an upstream target of CYR61: YAP. YAP is a key regulator within Hippo signaling that facilitates organ development and angiogenesis (197-199). Increased YAP expression was reported to increase EMT marker expression (200). In our study, reduced YAP expression led to decreased 3D spheroid invaded area growth of invasive breast cancer cells, decreased CYR61 and S100A4 expression, and reduced ERK1/2 phosphorylation. Additional treatment with recombinant human CYR61 neutralized the effect on 3D spheroid invaded area growth. Interestingly, it was reported that the inhibition of ERK1/2 led to reduced YAP expression, which suggests a feedback loop mechanism (201). Regarding the use of CYR61 as a predictive marker for cancer, it was suggested that increased CYR61 expression correlates with poor prognosis in patients with esophageal squamous cell carcinoma (202). Moreover, CYR61 was proposed to be of clinical relevance regarding hormone receptor–positive early-stage breast cancer (203). Our

observations indicate that CYR61, and to a further extent S100A4, may be of value as a predictive marker and therapeutic target for advanced and metastatic breast cancer (Manuscript A Figure 5, 6). Apart from this, an ongoing prospective trial is aiming to validate expression of different mRNA biomarkers in lung cancer including CCN1/CYR61 (NCT02294578). Another phase I clinical trial indicated a clinical benefit for patients with advanced solid tumors treated with cytostatic drug paclitaxel and cilengitide (antagonist of integrin $\alpha v\beta_3$ and $\alpha v\beta_5$) (204). Regarding S100A4, FDA has already approved niclodamide, which targets S100A4/NFκB/MMP9 signaling. A phase II clinical trial is aiming to test niclodamide for colorectal cancer (NCT02519582), and further applications are suggested for NSCLC (205).

4.2. IDENTIFICATION OF EXTRACELLULAR DRIVERS OF INVASION

Secreted proteins of different cell types prime and alter the constitution of the TME and ECM and drive tumor progression (2). We aimed to identify drivers of breast cancer bone-directed invasion by combining a co-culture model of breast cancer cells with osteosarcoma cells and secretome analysis using mass spectrometry. Identifying key regulators of the TME including the ECM could help to stage tumor progression and impede cancer cell invasion. We successfully detected 28 secreted proteins that are upregulated during the co-culture of non-invasive MCF-7 breast cancer cells and MG-63 osteosarcoma cells, compared with media from MCF-7 cells (Manuscript B figure 3 B-D). Additionally, we analyzed the effect of fibronectin (FN1), MMP2, and CTGF on invaded area growth due to gene ontology enrichment of detected potential drivers of breast cancer bone-directed invasion clustered in, but not restricted to, cell motility and cell migration (Manuscript B Supplement 4 A). Treating MCF-7 spheroids with human recombinant CTGF or MMP2 resulted in increased invaded area growth, whereas treatment with human fibronectin had no effect on the invaded area growth (Manuscript B Figure 5 F). Using BB-94, a MMP inhibitor, invaded area growth was diminished. Treatment of MCF-7 spheroids with FN1 and CTGF or FN1 with MMP2 had no effect on the invaded area growth. Regarding FN1 function in cell invasion and tumor progression, it was proposed that FN1 induced EMT through calpain in MCF-7 cells (206). Apart from this, it was demonstrated that only cleaved FN1 induced metastasis in human melanoma and that autocrine FN1 inhibited breast cancer metastasis (147, 163). Comparing the secretome of co-culture media with the media from osteosarcoma cells identified an upregulation of SPARC and a downregulation of MMP2 (Manuscript B Supplement 4 B). The downregulation of MMP2 may be due to MCF-7 breast cancer cells not expressing MMP2 or MMP9 (207). Furthermore, we analyzed the changed proteome by comparing the

monoculture of MCF-7 and the co-culture of MCF-7 with osteosarcoma cells (MG-63). We found that heat shock proteins are highly dysregulated. Heat shock proteins are upregulated in tumor cells due to higher mutational load, resulting in misfolded proteins. Additionally, there is a great interest in and ongoing clinical trials on the involvement of heat shock proteins in tumor progression (183-185). However, further evaluation is needed to understand how these proteins are regulated with regards to the basal expression of different cell lines. Taken together, we identified potential drivers of breast cancer bone-directed invasion; however, the value of each identified driver needs to be further evaluated. The system we used was a simplified 2 D setup without accounting for fibroblasts, immune cells, or the ECM. Signaling within the TME and at a metastatic niche is very complex, and cell culture techniques have their limitations.

4.3. IDENTIFICATION OF MOLECULAR MECHANISM UNDERLYING REDRUCED BREAST CANCER INVASIVENESS DUE TO REDUCED CTGF EXPRESSION

Mesenchymal transformed breast cancer cells (MCF-7-EMT) exhibit an elevated expression of CTGF (51). In addition, secretome analysis of MCF-7 co-cultured with osteosarcoma cells revealed that CTGF is upregulated. CTGF increased the invaded area growth and proteolytic activity and decreased cell-ECM adhesion (Manuscript B Figure 5 F and Figure 6 E, H). In accordance with these observations, reduced CTGF expression decreased the invaded area growth and increased cell-ECM adhesion (Manuscript B Figure 5 A, B and Figure 6 A-D). The effect of neutralizing CTGF antibodies on cell-ECM adhesion was reported previously, indicating comparable results (116). However, the reduction of CTGF was not sufficient to reduce the proteolytic activity in TNBC cell line MDA-MB-231 (Manuscript B Figure 6 G). This could be due to cell line–specific molecular alterations and would need further evaluation using additional TNBC cell lines. Additionally, it could be a cell line–specific result regarding reduced proteolytic activity in mesenchymal-transformed breast cancer cells after reduced CTGF expression. Therefore, additional experiments should be conducted using at least one more mesenchymal transformed luminal A breast cancer cell line. Nonetheless, Wang et al. reported that CTGF induced the expression of ECM-degrading genes (165). Growing evidence exists that increased expression of one or multiple members of the CCN family correlates with poor prognosis in different tumor entities including the breast, prostate, bone, and pancreas (192, 208-211). In accordance with these results, our data demonstrated that increased CTGF expression correlates with breast cancer invasiveness (Manuscript B Figure 4 C, D). Apart from this, our data suggests that mesenchymal-transformed breast

cancer cells express a combination of integrin αv receptor (CD51) and vascular cell adhesion molecule 1 (VCAM-1/CD106) to a higher extent (Manuscript B Figure 4 E, F). This receptor expression combination may be a possible marker for targeting cells with higher plasticity. Furthermore, several studies found that VCAM-1 activates indolent micrometastases and induces survival signaling in breast cancer cells (58, 167, 212). Previously, Hou et al. demonstrated that due to upregulated VCAM-1 expression, CTGF facilitates osteosarcoma migration and metastasis (166). Nonetheless, further research is indispensable to detect the roles of different integrin β subunits because integrin αv has versatile possible binding β subunits determining the binding of extracellular components (213).

The contribution of EMT to invasiveness and metastasis is still highly debated (24, 43, 214). Therefore, we investigated the effect of CTGF expression on the expression of EMT-TFs and EMT markers. Our results demonstrated a cell line–specific effect, wherein reduced CTGF led to reduced Zeb1 expression in mesenchymal-transformed breast cancer cells. However, in TNBC, reduced CTGF expression led to reduced vimentin expression (Manuscript B Figure 7 C, D). Although SNAI2 did not seem to be regulated through CTGF, a previous study found that SNAI1 and SNAI2 induce the EMT in breast cancer through TGFβ signaling, thereby regulating CTGF and SPARC (170). In mesenchymal-transformed breast cancer cells, we demonstrated that CTFG regulates versatile targets (TGFBI, CD44, SPARC, FN1 and LOX), which we identified previously as secreted potential drivers of breast cancer bone-directed invasion (Manuscript B Figure 7 A). Lysyl oxidase (LOX) facilitates collagen I stabilization, thereby inducing chemo resistance (169). SPARC binds to collagen in a calcium-dependent manner and regulates ECM assembly (215). Moreover, SPARC is associated with anti-cancer effects, inhibits bone metastasis (172, 173). Decreased CTGF expression, led to reduced SPARC expression in mesenchymal-transformed breast cancer cells. Reduced CTGF expression led to increased FN1 expression, which was cell line independent (Manuscript B Figure 7 A, B). After evaluating, which targets are regulated by CTGF, we wanted to shed light on targets regulating CTGF. Moreover, we wanted to investigate a possible treatment option targeting CTGF. Li et al. reported that the activity of GTPase RhoA controls CTGF cleavage and the fate of mesenchymal stem cells (161). Furthermore, Arguilar-Rojas et al. suggested that the treatment with GnRH agonist Busrelin induces RhoA activity in TNBC cells, thereby reducing invasiveness (175). Our data suggest that treatment with a GnRH agonist reduced CTGF expression and increases cell-ECM adhesion in TNBC cells and mesenchymal-transformed breast cancer cells (Manuscript B Figure 8 A-D and Supplement 11). Additionally, treatment with GnRH agonist Triptorelin induced RhoA activity in

mesenchymal-transformed breast cancer cells (Manuscript B Figure 8 E). Induction of RhoA activity led to reduced invasiveness, while reduced RhoA expression led to increased invasion and expression of CTGF (Manuscript B Figure 8 F-H). Previously reported treatment options targeting CTGF include sinomenine, curcumin, caffeine, simvastatin, and DN9693 (216-220). Additionally, monoclonal antibodies targeting CTGF are in use for the treatment of fibrosis and have been proposed to inhibit the migration of human melanoma cells (221, 222). Taken together, CTGF is a promising target regarding invasive breast cancer and metastasis and can be used as a prognostic marker.

4.4. POSSIBLE THERAPEUTIC IMPLEMENTATIONS

Our results suggest that matricellular proteins CYR61 and CTGF regulate the invasiveness of breast cancer cells and can be used as predictive markers and therapeutic targets. As previously indicated, different signaling cascades are involved in CYR61- and CTGF-dependent breast cancer invasion signaling. Different treatment options can be taken into account when targeting CYR61 and CTGF, including GnRH agonist, targeting the ERK1/2 signaling cascade, and targeting the Hippo pathway with key regulators YAP and TAZ.

4.4.1. Treatment with GnRH agonist may help prevent EMT induction and invasiveness of breast cancer cells

Gonadotropin-releasing hormone receptor (GnRH-R) is expressed in different tumor entities dependent or independent of the reproduction system (223). Approximately 50-60% of all human breast cancers and to a further extent 74% of breast cancers diagnosed as TNBC expressing GnRH-R (7, 132, 159). Breast cancer treatment with GnRH agonist resulted in a time- and dose- dependent reduction of *in vitro* invasion and *in vivo* metastasis (132, 160). Binding to GnRH-R resulted in the activation of phosphotyrosine phosphatases, which inhibited G-protein coupled estrogen receptor 1 (GPER)(152). Schubert et al. demonstrated that even the binding of antagonists to GnRH-R induced apoptosis in endometrial, ovarian, and breast cancer (160). Moreover, Gründker et al. reported that GnRH agonist treatment reduced S100A4 and CYR61 expression in mesenchymal-transformed and TNBC cells (7). GnRH agonist Triptorelin was reported to regulate RhoA activity in mesenchymal-transformed breast cancer cells, which was also found for agonist Busrelin in TNBC cells (175). In our study, we demonstrated that a GnRH agonist increases cell-ECM adhesion and reduced CTGF expression. These mechanisms indicate an advantage of patients with GnRH-R expression. We were able to demonstrate a correlation of increased invasion, increased cellular plasticity, and increased expression of matricellular proteins CYR61 and CTGF. In clinical practice, GnRH agonists are used for the suppression of ovarian function of

premenopausal breast cancers of a high grade (151). Clinical trials have identified a benefit of adjuvant chemotherapy ovarian suppression, which reduced distant metastasis free survival and overall survival (8, 224). It would be of high interest to evaluate the effect of GnRH-R agonist on EMT markers and EMT-TFs.

4.4.2. ERK1/2 cascade

In recent years, targeted therapy improved patient survival in different cancer entities and led the way to personalized medicine (225). Molecular alterations of tumors are screened to find treatment options that most benefit patients. Monoclonal antibodies are small molecule inhibitors designed to interfere with known tumorigenic signaling pathways and aim to target tumor cells with special molecular alterations. However, as clonal evolution processes, tumor cells gain resistance that makes them harder to target. Preclinical studies revealed manifold targetable signaling pathways including the MAPK pathway. Versatile clinical trials have aimed to target the kinase Mitogen Activated Protein Kinase Kinase (MEK), which is an upstream regulator of ERK1/2, with inhibitors for different cancer entities including breast cancer, colorectal cancer, and NSCLC (226). Additionally, MEK kinase inhibitors are reported to target cancer with gained resistance to B-Raf proto-oncogene serine/threonine kinase (BRAF). In this study, we demonstrated that treatment of breast cancer spheroid with U0126, which is an inhibitor of MEK1/2, resulted in decreased invaded area growth, reduced S100A4 expression, and decreased proliferation (Manuscript A Figure 3 D-F). ERK1/2 inhibitors appear to be a new treatment option for cancers with gained resistance to MEK kinase inhibitors given its unique position in versatile signaling pathways (176, 177). Furthermore, ERK1/2 phosphorylation is increased in mesenchymal-transformed breast cancer cells and TNBC cells (Manuscript A Figure 3 B). Hou et al. reported that CYR61 targets the MEK-ERK pathway in osteosarcoma cells (191). Breast cancer patients with detected CYR61 or CTGF overexpression may benefit from ERK1/2 targeted therapy. In this study, we demonstrated that reduced CYR61 regulates S100A4 expression through dephosphorylation of ERK1/2. It would be of great interest to evaluate whether targeting CYR61 or CTGF could be used to treat ERK1/2 resistant cancers.

4.4.3. Hippo pathway

The Hippo pathway is evolutionary conserved and regulates key events of development such as organ size and angiogenesis. YAP is negatively regulated through the phosphorylation of Large Tumor Suppressor Kinase 1/2 (LATS1/2), which results in degradation of protein. Dephosphorylation of YAP results in translocation to the nucleus, where it transcriptionally activates different target genes including CYR61 and CTGF (197-199). Regarding breast

cancer, YAP was reported as an oncogene, as well as tumor suppressor (227). Warren et al. reported that increased YAP expression correlates with increased expression of EMT markers (200). We demonstrated that reduced YAP expression led to decreased 3D invaded area growth by suppression of CYR61, p-ERK1/2, and S100A4. In our study, the effect of reduced YAP expression on 3D invasion was restored by extracellular CYR61 addition (Manuscript A Figure 4). Mi et al. observed that breast cancer Hippo signaling induces GGylation-dependent cell proliferation and migration (228). Additionally, breast cancer subtypes that do not express estrogen receptor were more sensitive to the inhibition of GGylation. Moreover, it was reported that taxol resistance is mediated through the Hippo pathway (119). Therefore, it was proposed to target YAP in TNBC with taxol resistance (229). Currently, there is an ongoing clinical trial treating TNBC neoadjuvant with zoledronate and atorvastatin (NCT03358017). Zoledronate, a bisphosphate, was observed to interfere with YAP/TAZ signaling and mevalonate signaling (230). Part of standard treatment regarding early breast cancer is long-term endocrine therapy, leading to decreased estrogen level. Estrogen has a prominent role in skeletal homeostasis (231). To prevent bone damage bisphosphates are added to treatment (232). Different treatment options are necessary to provide patients with different subtypes of breast cancer with appropriate treatment, helping to prolong survival and impede progression. In our study, we demonstrated that CYR61 and CTGF have versatile effects on breast cancer progression and are valuable targets and predictive markers for advanced breast cancer.

5. CONCLUSION

The purpose of this thesis was to target the signaling of invasion to impede breast cancer metastasis. We identified molecular mechanisms through which the reduction of CYR61 led to reduced invasiveness. Additionally, we examined which unique interactions of breast cancer cells with osteosarcoma cells led to increased invasiveness. Furthermore, we evaluated the molecular mechanisms of CTGF, thereby identifying possible treatment strategies to impede breast cancer invasion.

We observed that CYR61 is a key regulator of breast cancer invasion. Reduced CYR61 led to dephosphorylated ERK1/2 and reduced S100A4 expression, thereby reducing 3D spheroid invaded area growth. CYR61 and S100A4 may be utilized as predictive markers and therapeutic target for advanced breast cancer. Moreover, signaling of CYR61 may be impeded by using MEK1/2 inhibitor U0126 or inhibitors of YAP currently under investigation.

Furthermore, we identified versatile potential drivers of breast cancer bone-directed invasion due to secretome analysis of co-culture media from breast cancer cells and osteosarcoma cells. Identification of regulators within TME and ECM, which facilitate tumor initiation, invasion, and tumor progression, would be of benefit for future therapy designs. The TME is crucial for tumor progression, drug delivery, therapy outcome, and drug efficacy. Designing experimental models to better understand the complex interactions appearing in TME would be of great benefit.

Targeting CTGF led to reduced proteolytic activity, decreased 2D transwell invasion and 3D spheroid invaded area growth, and increased cell-ECM invasion. Apart from this, CTGF is regulated by RhoA activity, which can be regulated with GnRH agonist treatment.

6. REFERENCES

1. Bray F, Ferlay J, Soerjomataram I, Siegel RL, Torre LA, Jemal A. Global cancer statistics 2018: GLOBOCAN estimates of incidence and mortality worldwide for 36 cancers in 185 countries. *CA: A Cancer Journal for Clinicians*. 2018;68(6):394-424.
2. Emon B, Bauer J, Jain Y, Jung B, Saif T. Biophysics of Tumor Microenvironment and Cancer Metastasis - A Mini Review. *Computational and Structural Biotechnology Journal*. 2018;16:279-87.
3. Bornstein P. Diversity of function is inherent in matricellular proteins: an appraisal of thrombospondin 1. *The Journal of Cell Biology*. 1995;130(3):503-6.
4. Sage EH, Bornstein P. Extracellular proteins that modulate cell-matrix interactions. SPARC, tenascin, and thrombospondin. *The Journal of Biological Chemistry*. 1991;266(23):14831-4.
5. Dhar A, Ray A. Dhar A, Ray AThe CCN family proteins in carcinogenesis. *Experimental Oncology*. 2010;32:2-9.
6. Wells JE, Howlett M, Cole CH, Kees UR. Deregulated expression of connective tissue growth factor (CTGF/CCN2) is linked to poor outcome in human cancer. *International Journal of Cancer*. 2015;137(3):504-11.
7. Grundker C, Bauerschmitz G, Schubert A, Emons G. Invasion and increased expression of S100A4 and CYR61 in mesenchymal transformed breast cancer cells is downregulated by GnRH. *International Journal of Oncology*. 2016;48(6):2713-21.
8. Harbeck N, Penault-Llorca F, Cortes J, Gnant M, Houssami N, Poortmans P, et al. Breast cancer. *Nature Reviews Disease Primers*. 2019;5(1):66.
9. Perou CM, Sørlie T, Eisen MB, van de Rijn M, Jeffrey SS, Rees CA, et al. Molecular portraits of human breast tumours. *Nature*. 2000;406(6797):747-52.
10. Prat A, Ellis MJ, Perou CM. Practical implications of gene-expression-based assays for breast oncologists. *Nature Reviews Clinical Oncology*. 2012;9(1):48-57.
11. Prat A, Perou CM. Deconstructing the molecular portraits of breast cancer. *Molecular Oncology*. 2011;5(1):5-23.
12. Parker JS, Mullins M, Cheang MCU, Leung S, Voduc D, Vickery T, et al. Supervised Risk Predictor of Breast Cancer Based on Intrinsic Subtypes. *Journal of Clinical Oncology*. 2009;27(8):1160-7.
13. Lehmann BD, Bauer JA, Chen X, Sanders ME, Chakravarthy AB, Shyr Y, et al. Identification of human triple-negative breast cancer subtypes and preclinical models for selection of targeted therapies. *The Journal of Clinical Investigation*. 2011;121(7):2750-67.
14. Burstein MD, Tsimelzon A, Poage GM, Covington KR, Contreras A, Fuqua SAW, et al. Comprehensive Genomic Analysis Identifies Novel Subtypes and Targets of Triple-Negative Breast Cancer. *Clinical Cancer Research*. 2015;21(7):1688-98.
15. Cheang MCU, Martin M, Nielsen TO, Prat A, Voduc D, Rodriguez-Lescure A, et al. Defining Breast Cancer Intrinsic Subtypes by Quantitative Receptor Expression. *The Oncologist*. 2015;20(5):474-82.
16. Bareche Y, Venet D, Ignatiadis M, Aftimos P, Piccart M, Rothe F, et al. Unravelling triple-negative breast cancer molecular heterogeneity using an integrative multiomic analysis. *Annals of Oncology*. 2018;29(4):895-902.
17. Kim HK, Park KH, Kim Y, Park SE, Lee HS, Lim SW, et al. Discordance of the PAM50 Intrinsic Subtypes Compared with Immunohistochemistry-Based Surrogate in Breast Cancer Patients: Potential Implication of Genomic Alterations of Discordance. *Cancer Research and Treatment : Official Journal of Korean Cancer Association*. 2019;51(2):737-47.
18. Lehmann BD, Jovanović B, Chen X, Estrada MV, Johnson KN, Shyr Y, et al. Refinement of Triple-Negative Breast Cancer Molecular Subtypes: Implications for Neoadjuvant Chemotherapy Selection. *PLoS One*. 2016;11(6):e0157368.

19. Lambert AW, Pattabiraman DR, Weinberg RA. Emerging Biological Principles of Metastasis. *Cell*. 2017;168(4):670-91.
20. Fidler IJ. The pathogenesis of cancer metastasis: the 'seed and soil' hypothesis revisited. *Nature Reviews Cancer*. 2003;3(6):453-8.
21. Gupta GP, Massague J. Cancer metastasis: building a framework. *Cell*. 2006;127(4):679-95.
22. Talmadge JE, Fidler IJ. AACR Centennial Series: The Biology of Cancer Metastasis: Historical Perspective. *Cancer Research*. 2010;70(14):5649-69.
23. Craene BD, Berx G. Regulatory networks defining EMT during cancer initiation and progression. *Nature Reviews Cancer*. 2013;13(2):97-110.
24. Nieto MA. Context-specific roles of EMT programmes in cancer cell dissemination. *Nature Cell Biology*. 2017;19(5):416-8.
25. Friedl P, Locker J, Sahai E, Segall JE. Classifying collective cancer cell invasion. *Nature Cell Biology*. 2012;14(8):777-83.
26. Chambers AF, Groom AC, MacDonald IC. Dissemination and growth of cancer cells in metastatic sites. *Nature Reviews Cancer*. 2002;2(8):563-72.
27. Hanahan D, Weinberg RA. Hallmarks of cancer: the next generation. *Cell*. 2011;144(5):646-74.
28. Tahmasebi Birgani M, Carloni V. Tumor Microenvironment, a Paradigm in Hepatocellular Carcinoma Progression and Therapy. *International Journal of Molecular Sciences*. 2017;18(2).
29. De Pascalis C, Etienne-Manneville S. Single and collective cell migration: the mechanics of adhesions. *Molecular Biology of the Cell*. 2017;28(14):1833-46.
30. Roma-Rodrigues C, Mendes R, Baptista PV, Fernandes AR. Targeting Tumor Microenvironment for Cancer Therapy. *International Journal of Molecular Sciences*. 2019;20(4).
31. Hui L, Chen Y. Tumor microenvironment: Sanctuary of the devil. *Cancer Letters*. 2015;368(1):7-13.
32. Willumsen N, Thomsen LB, Bager CL, Jensen C, Karsdal MA. Quantification of altered tissue turnover in a liquid biopsy: a proposed precision medicine tool to assess chronic inflammation and desmoplasia associated with a pro-cancerous niche and response to immuno-therapeutic anti-tumor modalities. *Cancer Immunology, Immunotherapy*. 2018;67(1):1-12.
33. Pickup MW, Mouw JK, Weaver VM. The extracellular matrix modulates the hallmarks of cancer. *EMBO Reports*. 2014;15(12):1243-53.
34. Otranto M, Sarrazy V, Bonté F, Hinz B, Gabbiani G, Desmouliere A. The role of the myofibroblast in tumor stroma remodeling. *Cell Adhesion & Migration*. 2012;6(3):203-19.
35. Sormendi S, Wielockx B. Hypoxia Pathway Proteins As Central Mediators of Metabolism in the Tumor Cells and Their Microenvironment. *Frontiers in Immunology*. 2018;9(40).
36. Coulson R, Liew SH, Connelly AA, Yee NS, Deb S, Kumar B, et al. The angiotensin receptor blocker, Losartan, inhibits mammary tumor development and progression to invasive carcinoma. *Oncotarget*. 2017;8(12).
37. De Pascalis C, Etienne-Manneville S. Single and collective cell migration: the mechanics of adhesions. *Molecular Biology of the Cell*. 2017;28(14):1833-46.
38. Sanz-Moreno V, Gadea G, Ahn J, Paterson H, Marra P, Pinner S, et al. Rac Activation and Inactivation Control Plasticity of Tumor Cell Movement. *Cell*. 2008;135(3):510-23.
39. Giampieri S, Pinner S, Sahai E. Intravital Imaging Illuminates Transforming Growth Factor β Signaling Switches during Metastasis. *Cancer Research*. 2010;70(9):3435-9.
40. Wolf K, Friedl P. Molecular mechanisms of cancer cell invasion and plasticity. *British Journal of Dermatology*. 2006;154(s1):11-5.

41. Kedrin D, Wyckoff J, Sahai E, Condeelis J, Segall JE. Imaging Tumor Cell Movement In Vivo. *Current Protocols in Cell Biology*. 2007;35(1):19.7.1-.7.7.
42. Lamouille S, Xu J, Derynck R. Molecular mechanisms of epithelial-mesenchymal transition. *Nature Reviews Molecular Cell Biology*. 2014;15(3):178-96.
43. Brabletz T, Kalluri R, Nieto MA, Weinberg RA. EMT in cancer. *Nature Reviews Cancer*. 2018;18(2):128-34.
44. Thiery JP. Epithelial–mesenchymal transitions in tumour progression. *Nature Reviews Cancer*. 2002;2(6):442-54.
45. Kurrey NK, Jalgaonkar SP, Joglekar AV, Ghanate AD, Chaskar PD, Doiphode RY, et al. Snail and Slug Mediate Radioresistance and Chemoresistance by Antagonizing p53-Mediated Apoptosis and Acquiring a Stem-Like Phenotype in Ovarian Cancer Cells. *STEM CELLS*. 2009;27(9):2059-68.
46. Gupta PB, Onder TT, Jiang G, Tao K, Kuperwasser C, Weinberg RA, et al. Identification of Selective Inhibitors of Cancer Stem Cells by High-Throughput Screening. *Cell*. 2009;138(4):645-59.
47. Singh A, Settleman J. EMT, cancer stem cells and drug resistance: an emerging axis of evil in the war on cancer. *Oncogene*. 2010;29(34):4741-51.
48. Tsai Jeff H, Donaher Joana L, Murphy Danielle A, Chau S, Yang J. Spatiotemporal Regulation of Epithelial-Mesenchymal Transition Is Essential for Squamous Cell Carcinoma Metastasis. *Cancer Cell*. 2012;22(6):725-36.
49. Ocaña Oscar H, Córcoles R, Fabra Á, Moreno-Bueno G, Acloque H, Vega S, et al. Metastatic Colonization Requires the Repression of the Epithelial-Mesenchymal Transition Inducer Prrx1. *Cancer Cell*. 2012;22(6):709-24.
50. Gaggioli C, Hooper S, Hidalgo-Carcedo C, Grosse R, Marshall JF, Harrington K, et al. Fibroblast-led collective invasion of carcinoma cells with differing roles for RhoGTPases in leading and following cells. *Nature Cell Biology*. 2007;9(12):1392-400.
51. Ziegler E, Hansen MT, Haase M, Emons G, Grundker C. Generation of MCF-7 cells with aggressive metastatic potential in vitro and in vivo. *Breast Cancer Research and Treatment*. 2014;148(2):269-77.
52. Bombonati A, Sgroi DC. The molecular pathology of breast cancer progression. *The Journal of Pathology*. 2011;223(2):308-18.
53. Cheung KJ, Padmanaban V, Silvestri V, Schipper K, Cohen JD, Fairchild AN, et al. Polyclonal breast cancer metastases arise from collective dissemination of keratin 14-expressing tumor cell clusters. *Proceedings of the National Academy of Sciences*. 2016;113(7):E854-E63.
54. Cardoso F, Senkus E, Costa A, Papadopoulos E, Aapro M, André F, et al. 4th ESO–ESMO International Consensus Guidelines for Advanced Breast Cancer (ABC 4)†. Annals of Oncology. 2018;29(8):1634-57.
55. Mariotto AB, Etzioni R, Hurlbert M, Penberthy L, Mayer M. Estimation of the Number of Women Living with Metastatic Breast Cancer in the United States. *Cancer Epidemiology Biomarkers & Prevention*. 2017;26(6):809-15.
56. Gobbini E, Ezzalfani M, Dieras V, Bachelot T, Brain E, Debled M, et al. Time trends of overall survival among metastatic breast cancer patients in the real-life ESME cohort. *European Journal of Cancer*. 2018;96:17-24.
57. Buonomo OC, Caredda E, Portarena I, Vanni G, Orlandi A, Bagni C, et al. New insights into the metastatic behavior after breast cancer surgery, according to well-established clinicopathological variables and molecular subtypes. *PLoS One*. 2017;12(9):e0184680.
58. Croucher PI, McDonald MM, Martin TJ. Bone metastasis: the importance of the neighbourhood. *Nature Reviews Cancer*. 2016;16(6):373-86.
59. Fidler IJ, Kripke ML. The challenge of targeting metastasis. *Cancer and Metastasis Reviews*. 2015;34(4):635-41.

60. Fortunato L, Mascaro A, Baldi A, Farina M, Cortese G, Ventrone M, et al. Positive Bone Marrow Biopsy Is Associated with a Decreased Disease-Free Survival in Patients with Operable Breast Cancer. *Annals of Surgical Oncology*. 2009;16:3010-9.
61. Tjensvoll K, Oltedal S, Heikkilä R, Kvaløy JT, Gilje B, Reuben JM, et al. Persistent tumor cells in bone marrow of non-metastatic breast cancer patients after primary surgery are associated with inferior outcome. *BMC Cancer*. 2012;12(1):190.
62. Domschke C, Diel IJ, Englert S, Kalteisen S, Mayer L, Rom J, et al. Prognostic Value of Disseminated Tumor Cells in the Bone Marrow of Patients with Operable Primary Breast Cancer: A Long-term Follow-up Study. *Annals of Surgical Oncology*. 2013;20(6):1865-71.
63. Butcher DT, Alliston T, Weaver VM. A tense situation: forcing tumour progression. *Nature Reviews Cancer*. 2009;9:108.
64. Paszek MJ, Zahir N, Johnson KR, Lakins JN, Rozenberg GI, Gefen A, et al. Tensional homeostasis and the malignant phenotype. *Cancer Cell*. 2005;8(3):241-54.
65. Ruppender NS, Merkel AR, Martin TJ, Mundy GR, Sterling JA, Guelcher SA. Matrix Rigidity Induces Osteolytic Gene Expression of Metastatic Breast Cancer Cells. *PLoS One*. 2010;5(11):e15451.
66. Johnson RW, Nguyen MP, Padalecki SS, Grubbs BG, Merkel AR, Oyajobi BO, et al. TGF-β Promotion of Gli2-Induced Expression of Parathyroid Hormone-Related Protein, an Important Osteolytic Factor in Bone Metastasis, Is Independent of Canonical Hedgehog Signaling. *Cancer Research*. 2011;71(3):822-31.
67. Müller A, Homey B, Soto H, Ge N, Catron D, Buchanan ME, et al. Involvement of chemokine receptors in breast cancer metastasis. *Nature*. 2001;410(6824):50-6.
68. Taichman RS, Cooper C, Keller ET, Pienta KJ, Taichman NS, McCauley LK. Use of the Stromal Cell-derived Factor-1/CXCR4 Pathway in Prostate Cancer Metastasis to Bone. *Cancer Research*. 2002;62(6):1832-7.
69. Corcoran KE, Trzaska KA, Fernandes H, Bryan M, Taborga M, Srinivas V, et al. Mesenchymal Stem Cells in Early Entry of Breast Cancer into Bone Marrow. *PLoS One*. 2008;3(6):e2563.
70. Gründker C, Bauerschmitz G, Knapp J, Schmidt E, Olbrich T, Emons G. Inhibition of SDF-1/CXCR4-induced epithelial–mesenchymal transition by kisspeptin-10. *Breast Cancer Research and Treatment*. 2015;152(1):41-50.
71. Correa D, Somoza RA, Lin P, Schiemann WP, Caplan AI. Mesenchymal stem cells regulate melanoma cancer cells extravasation to bone and liver at their perivascular niche. *International Journal of Cancer*. 2016;138(2):417-27.
72. Loibl M, Binder A, Herrmann M, Duttenhoefer F, Richards RG, Nerlich M, et al. Direct Cell-Cell Contact between Mesenchymal Stem Cells and Endothelial Progenitor Cells Induces a Pericyte-Like Phenotype In Vitro. *BioMed Research International*. 2014;2014:10.
73. Wong GS, Rustgi AK. Matricellular proteins: priming the tumour microenvironment for cancer development and metastasis. *British Journal of Cancer*. 2013;108(4):755-61.
74. Lu P, Weaver VM, Werb Z. The extracellular matrix: A dynamic niche in cancer progression. *The Journal of Cell Biology*. 2012;196(4):395-406.
75. Christofori G. New signals from the invasive front. *Nature.* 2006;441(7092):444-50.
76. Joyce JA, Pollard JW. Microenvironmental regulation of metastasis. *Nature Reviews Cancer*. 2009;9(4):239-52.
77. Lau LF. CCN1/CYR61: the very model of a modern matricellular protein. *Cellular and Molecular Life Sciences : CMLS*. 2011;68(19):3149-63.
78. Roberts DD. Emerging functions of matricellular proteins. *Cellular and Molecular Life Sciences : CMLS*. 2011;68(19):3133-6.
79. Chiodoni C, Colombo MP, Sangaletti S. Matricellular proteins: from homeostasis to inflammation, cancer, and metastasis. *Cancer and Metastasis Reviews*. 2010;29(2):295-307.

80. Murphy-Ullrich JE, Sage EH. Revisiting the matricellular concept. *Matrix biology : Journal of the International Society for Matrix Biology*. 2014;37:1-14.
81. Sawyer AJ, Kyriakides TR. Matricellular proteins in drug delivery: Therapeutic targets, active agents, and therapeutic localization. *Adv Drug Deliv Rev*. 2016;97:56-68.
82. Brellier F, Martina E, Degen M, Heuzé-Vourc'h N, Petit A, Kryza T, et al. Tenascin-W is a better cancer biomarker than tenascin-C for most human solid tumors. *BMC Clinical Pathology*. 2012;12(1):14.
83. Cao D-X, Li Z-J, Jiang X-O, Lum YL, Khin E, Lee NP, et al. Osteopontin as potential biomarker and therapeutic target in gastric and liver cancers. *World Journal of Gastroenterology*. 2012;18(30):3923-30.
84. Bork P. The modular architecture of a new family of growth regulators related to connective tissue growth factor. *FEBS Letters*. 1993;327(2):125-30.
85. Jones JI, Gockerman A, Busby WH, Camacho-Hubner C, Clemmons DR. Extracellular matrix contains insulin-like growth factor binding protein-5: potentiation of the effects of IGF-I. *The Journal of Cell Biology*. 1993;121(3):679-87.
86. Lau LF. Cell surface receptors for CCN proteins. *Journal of Cell Communication and Signaling*. 2016;10(2):121-7.
87. Kular L, Pakradouni J, Kitabgi P, Laurent M, Martinerie C. The CCN family: A new class of inflammation modulators? *Biochimie*. 2011;93(3):377-88.
88. Zarogoulidis P, Tsakiridis K, Karapantzou C, Lampaki S, Kioumis I, Pitsiou G, et al. Use of Proteins as Biomarkers and Their Role in Carcinogenesis. *Journal of Cancer*. 2015;6(1):9-18.
89. Lin C-C, Chen P-C, Lein M-Y, Tsao C-W, Huang C-C, Wang S-W, et al. WISP-1 promotes VEGF-C-dependent lymphangiogenesis by inhibiting miR-300 in human oral squamous cell carcinoma cells. *Oncotarget*. 2016;7(9):9993-10005.
90. Mo F-E, Muntean AG, Chen C-C, Stolz DB, Watkins SC, Lau LF. CYR61 (CCN1) Is Essential for Placental Development and Vascular Integrity. *Molecular and Cellular Biology*. 2002;22(24):8709-20.
91. Chen C-C, Mo F-E, Lau LF. The Angiogenic Factor Cyr61 Activates a Genetic Program for Wound Healing in Human Skin Fibroblasts. *Journal of Biological Chemistry*. 2001;276(50):47329-37.
92. Todorovic V, Chen CC, Hay N, Lau LF. The matrix protein CCN1 (CYR61) induces apoptosis in fibroblasts. *The Journal of Cell Biology*. 2005;171(3):559-68.
93. Yang G, Lau L. Cyr61, product of a growth factor-inducible immediate early gene, is associated with the extracellular matrix and the cell surface. *Cell Growth Differ*. 1991;2(7):351-7.
94. Barreto S, Ray A, Edgar P. Biological characteristics of CCN proteins in tumor development. *Journal of BUON: Official Journal of the Balkan Union of Oncology*. 2016;21:1359-67.
95. Feng P, Wang B, Ren EC. Cyr61/CCN1 is a tumor suppressor in human hepatocellular carcinoma and involved in DNA damage response. *The International Journal of Biochemistry & Cell Biology*. 2008;40(1):98-109.
96. Tong X, Xie D, O'Kelly J, Miller CW, Muller-Tidow C, Koeffler HP. Cyr61, a member of CCN family, is a tumor suppressor in non-small cell lung cancer. *The Journal of Biological Chemistry*. 2001;276(50):47709-14.
97. Tsai M-S, Bogart DF, Castañeda JM, Li P, Lupu R. Cyr61 promotes breast tumorigenesis and cancer progression. *Oncogene*. 2002;21:8178.
98. Lin M-T, Zuon C-Y, Chang C-C, Chen S-T, Chen C-P, Lin B-R, et al. Cyr61 Induces Gastric Cancer Cell Motility/Invasion via Activation of the Integrin/Nuclear Factor-κB/Cyclooxygenase-2 Signaling Pathway. *Clinical Cancer Research*. 2005;11(16):5809-20.

99. Gery S, Xie D, Yin D, Gabra H, Miller C, Wang H, et al. Ovarian carcinomas: CCN genes are aberrantly expressed and CCN1 promotes proliferation of these cells. *Clinical Cancer Research : an Official Journal of the American Association for Cancer Research*. 2005;11(20):7243-54.
100. Xie D, Yin D, Tong X, O'Kelly J, Mori A, Miller C, et al. Cyr61 Is Overexpressed in Gliomas and Involved in Integrin-Linked Kinase-Mediated Akt and β-Catenin-TCF/Lef Signaling Pathways. *Cancer Research*. 2004;64(6):1987-96.
101. Huang Y-T, Lan Q, Lorusso G, Duffey N, Rüegg C. The matricellular protein CYR61 promotes breast cancer lung metastasis by facilitating tumor cell extravasation and suppressing anoikis. *Oncotarget*. 2016;8(6).
102. Vellon L, Menendez JA, Lupu R. αVβ3 integrin regulates heregulin (HRG)-induced cell proliferation and survival in breast cancer. *Oncogene*. 2005;24(23):3759-73.
103. Kim S-M, Park J-H, Chung S-K, Kim J-Y, Hwang H-Y, Chung K-C, et al. Coxsackievirus B3 infection induces cyr61 activation via JNK to mediate cell death. *J Virol*. 2004;78(24):13479-88.
104. Wiedmaier N, Müller S, Köberle M, Manncke B, Krejci J, Autenrieth IB, et al. Bacteria induce CTGF and CYR61 expression in epithelial cells in a lysophosphatidic acid receptor-dependent manner. International *Journal of Medical Microbiology*. 2008;298(3):231-43.
105. Kurozumi K, Hardcastle J, Thakur R, Shroll J, Nowicki M, Otsuki A, et al. Oncolytic HSV-1 infection of tumors induces angiogenesis and upregulates CYR61. *Molecular Therapy : the Journal of the American Society of Gene Therapy*. 2008;16(8):1382-91.
106. Rivera-Gonzalez R, Petersen DN, Tkalcevic G, Thompson DD, Brown TA. Estrogen-induced genes in the uterus of ovariectomized rats and their regulation by droloxifene and tamoxifen. *The Journal of Steroid Biochemistry and Molecular Biology*. 1998;64(1):13-24.
107. Kim YN, Choe SR, Cho KH, Cho DY, Kang J, Park CG, et al. Resveratrol suppresses breast cancer cell invasion by inactivating a RhoA/YAP signaling axis. *Experimental & Molecular Medicine*. 2017;49(2):e296.
108. Sampath D, Winneker RC, Zhang Z. Cyr61, a Member of the CCN Family, Is Required for MCF-7 Cell Proliferation: Regulation by 17β-Estradiol and Overexpression in Human Breast Cancer. *Endocrinology*. 2001;142(6):2540-8.
109. Xie D, Miller CW, O'Kelly J, Nakachi K, Sakashita A, Said JW, et al. Breast Cancer: Cyr61 is overexpressed, estrogen-inducible, and associated with more advanced disease. *Journal of Biological Chemistry*. 2001;276(17):14187-94.
110. Jiang WG, Watkins G, Fodstad O, Douglas-Jones A, Mokbel K, Mansel RE. Differential expression of the CCN family members Cyr61, CTGF and Nov in human breast cancer. *Endocrine-related Cancer*. 2004;11(4):781-91.
111. Dong Xie KN, Heming Wang, Robert Elashoff, and H. Phillip Koeffler. Elevated Levels of Connective Tissue Growth Factor, WISP-1, and CYR61 in Primary Breast Cancers Associated with More Advanced Features. *Cancer Research*. 2001;61:6.
112. Kleer CG. Dual roles of CCN proteins in breast cancer progression. *Journal of Cell Communication and Signaling*. 2016;10(3):217-22.
113. Sánchez-Bailón MP, Calcabrini A, Mayoral-Varo V, Molinari A, Wagner K-U, Losada JP, et al. Cyr61 as mediator of Src signaling in triple negative breast cancer cells. *Oncotarget*. 2015;6(15).
114. Yu-Ting Huang QL, Girieca Lorusso, Nathalie Duffey, and Curzio Rüegg. The matricellular protein CYR61 promotes breast cancer lung metastasis by facilitating tumor cell extravasation and suppressing anoikis. *Oncotarget*. 2017;8(6):16.
115. Lin B-R, Chang C-C, Chen L-R, Wu M-H, Wang M-Y, Kuo I-H, et al. Cysteine-Rich 61 (CCN1) Enhances Chemotactic Migration, Transendothelial Cell Migration, and

Intravasation by Concomitantly Up-Regulating Chemokine Receptor 1 and 2. Molecular *Cancer Research*. 2007;5(11):1111-23.
116. Ramazani Y, Knops N, Elmonem MA, Nguyen TQ, Arcolino FO, van den Heuvel L, et al. Connective tissue growth factor (CTGF) from basics to clinics. *Matrix Biology*. 2018;68-69:44-66.
117. Chang C-C, Lin B-R, Wu T-S, Jeng Y-M, Kuo M-L. Input of microenvironmental regulation on colorectal cancer: role of the CCN family. *World Journal of Gastroenterology*. 2014;20(22):6826-31.
118. Jia Q, Dong Q, Qin L. CCN: core regulatory proteins in the microenvironment that affect the metastasis of hepatocellular carcinoma? *Oncotarget*. 2016;7(2):1203-14.
119. Lai D, Ho KC, Hao Y, Yang X. Taxol Resistance in Breast Cancer Cells Is Mediated by the Hippo Pathway Component TAZ and Its Downstream Transcriptional Targets Cyr61 and CTGF. *Cancer Research*. 2011;71(7):2728-38.
120. Bartucci M, Dattilo R, Moriconi C, Pagliuca A, Mottolese M, Federici G, et al. TAZ is required for metastatic activity and chemoresistance of breast cancer stem cells. *Oncogene*. 2015;34(6):681-90.
121. Chen Y, Abraham DJ, Shi-Wen X, Pearson JD, Black CM, Lyons KM, et al. CCN2 (connective tissue growth factor) promotes fibroblast adhesion to fibronectin. *Molecular Biology of the Cell*. 2004;15(12):5635-46.
122. Wahab NA, Weston BS, Mason RM. Connective Tissue Growth Factor CCN2 Interacts with and Activates the Tyrosine Kinase Receptor TrkA. *Journal of the American Society of Nephrology*. 2005;16(2):340-51.
123. Segarini PR, Nesbitt JE, Li D, Hays LG, Yates JR, Carmichael DF. The Low Density Lipoprotein Receptor-related Protein/α2-Macroglobulin Receptor Is a Receptor for Connective Tissue Growth Factor. *Journal of Biological Chemistry*. 2001;276(44):40659-67.
124. Mercurio S, Latinkic B, Itasaki N, Krumlauf R, Smith JC. Connective-tissue growth factor modulates WNT signalling and interacts with the WNT receptor complex. *Development*. 2004;131(9):2137-47.
125. Babic AM, Chen C-C, Lau LF. Fisp12/Mouse Connective Tissue Growth Factor Mediates Endothelial Cell Adhesion and Migration through Integrin αvβ3, Promotes Endothelial Cell Survival, and Induces Angiogenesis In Vivo. *Molecular and Cellular Biology*. 1999;19(4):2958-66.
126. Jun JI, Lau LF. Taking aim at the extracellular matrix: CCN proteins as emerging therapeutic targets. *Nature Reviews Drug Discovery*. 2011;10(12):945-63.
127. Kubota S, Takigawa M. Cellular and molecular actions of CCN2/CTGF and its role under physiological and pathological conditions. *Clinical Science*. 2014;128(3):181-96.
128. Van Beek JP, Kennedy L, Rockel JS, Bernier SM, Leask A. The induction of CCN2 by TGFβ1 involves Ets-1. *Arthritis Research & Therapy*. 2006;8(2):R36.
129. Zhu X, Zhong J, Zhao Z, Sheng J, Wang J, Liu J, et al. Epithelial derived CTGF promotes breast tumor progression via inducing EMT and collagen I fibers deposition. *Oncotarget*. 2015;6(28):25320-38.
130. Aguiar DP, de Farias GC, de Sousa EB, de Mattos Coelho-Aguiar J, Lobo JC, Casado PL, et al. New strategy to control cell migration and metastasis regulated by CCN2/CTGF. *Cancer Cell International*. 2014;14:61-.
131. Yeger H, Perbal B. CCN family of proteins: critical modulators of the tumor cell microenvironment. *Journal of Cell Communication and Signaling*. 2016;10(3):229-40.
132. von Alten J, Fister S, Schulz H, Viereck V, Frosch KH, Emons G, et al. GnRH analogs reduce invasiveness of human breast cancer cells. *Breast Cancer Research and Treatment*. 2006;100(1):13-21.

133. Howlader N NA, Krapcho M, Miller D, Bishop K, Kosary CL, Yu M, Ruhl J, Tatalovich Z, Mariotto A, Lewis DR, Chen HS, Feuer EJ, Cronin KA (eds). *SEER Cancer Statistics Review. National Cancer Institute Bethesda, MD*. 1975-2014.
134. Ferlay J, Colombet M, Soerjomataram I, Mathers C, Parkin DM, Pineros M, et al. Estimating the global cancer incidence and mortality in 2018: GLOBOCAN sources and methods. *Int J Cancer*. 2019;144(8):1941-53.
135. Pulido C, Vendrell I, Ferreira AR, Casimiro S, Mansinho A, Alho I, et al. Bone metastasis risk factors in breast cancer. *Ecancermedicalscience*. 2017;11:715-.
136. van Zijl F, Krupitza G, Mikulits W. Initial steps of metastasis: cell invasion and endothelial transmigration. *Mutat Res*. 2011;728(1-2):23-34.
137. Kang Y, Siegel PM, Shu W, Drobnjak M, Kakonen SM, Cordón-Cardo C, et al. A multigenic program mediating breast cancer metastasis to bone. *Cancer Cell*. 2003;3(6):537-49.
138. Weidenfeld K, Barkan D. EMT and Stemness in Tumor Dormancy and Outgrowth: Are They Intertwined Processes? *Frontiers in Oncology*. 2018;8:381-.
139. Reya T, Morrison SJ, Clarke MF, Weissman IL. Stem cells, cancer, and cancer stem cells. *Nature*. 2001;414(6859):105-11.
140. Liede A, Jerzak KJ, Hernandez RK, Wade SW, Sun P, Narod SA. The incidence of bone metastasis after early-stage breast cancer in Canada. *Breast Cancer Research and Treatment*. 2016;156(3):587-95.
141. Moussad EE-DA, Brigstock DR. Connective Tissue Growth Factor: What's in a Name? *Molecular Genetics and Metabolism*. 2000;71(1):276-92.
142. Chen M-T, Sun H-F, Zhao Y, Fu W-Y, Yang L-P, Gao S-P, et al. Comparison of patterns and prognosis among distant metastatic breast cancer patients by age groups: a SEER population-based analysis. *Scientific Reports*. 2017;7(1):9254-.
143. Thompson EW, Nagaraj SH. Transition states that allow cancer to spread. *Nature*. 2018;536:442-4.
144. Lee JY, Chang JK, Dominguez AA, Lee H-p, Nam S, Chang J, et al. YAP-independent mechanotransduction drives breast cancer progression. *Nature Communications*. 2019;10(1):1848.
145. Hashimoto G, Inoki I, Fujii Y, Aoki T, Ikeda E, Okada Y. Matrix Metalloproteinases Cleave Connective Tissue Growth Factor and Reactivate Angiogenic Activity of Vascular Endothelial Growth Factor 165. Journal of Biological Chemistry. 2002;277(39):36288-95.
146. Tsai H-C, Su H-L, Huang C-Y, Fong Y-C, Hsu C-J, Tang C-H. CTGF increases matrix metalloproteinases expression and subsequently promotes tumor metastasis in human osteosarcoma through down-regulating miR-519d. *Oncotarget*. 2014;5(11):3800-12.
147. Jiao Y, Feng X, Zhan Y, Wang R, Zheng S, Liu W, et al. Matrix metalloproteinase-2 Promotes αvβ3 Integrin-Mediated Adhesion and Migration of Human Melanoma Cells by Cleaving Fibronectin. *PLoS One*. 2012;7(7):e41591.
148. Danen EHJ. Integrin Signaling as a Cancer Drug Target. *ISRN Cell Biology*. 2013;2013:14.
149. Jacob A, Prekeris R. The regulation of MMP targeting to invadopodia during cancer metastasis. *Front Cell Dev Biol*. 2015;3:4-.
150. Marc L. Significance, detection and markers of disseminated breast cancer cells. *Endocrine-Related Cancer Endocr Relat Cancer*. 2006;13(4):1033-67.
151. Venturelli M, Guaitoli G, Omarini C, Moscetti L. Spotlight on triptorelin in the treatment of premenopausal women with early-stage breast cancer. *Breast Cancer (Dove Med Press)*. 2018;10:39-49.
152. Gründker C, Emons G. The Role of Gonadotropin-Releasing Hormone in Cancer Cell Proliferation and Metastasis. *Frontiers in Endocrinology*. 2017;8(187).

153. Fekete M, Wittliff JL, Schally AV. Characteristics and distribution of receptors for [d-trp6]- luteinizing hormone-releasing hormone, somatostatin, epidermal growth factor, and sex steroids in 500 biopsy samples of human breast cancer. *Journal of Clinical Laboratory Analysis*. 1989;3(3):137-47.
154. Baumann KH, Kiesel L, Kaufmann M, Bastert G, Runnebaum B. Characterization of binding sites for a GnRH-agonist (buserelin) in human breast cancer biopsies and their distribution in relation to tumor parameters. *Breast Cancer Research and Treatment*. 1993;25(1):37-46.
155. Moriya T, Suzuki T, Pilichowska M, Ariga N, Kimura N, Ouchi N, et al. Immunohistochemical expression of gonadotropin releasing hormone receptor in human breast carcinoma. *Pathology International*. 2001;51(5):333-7.
156. Mangia A, Tommasi S, Reshkin S, Simone G, Stea B, Schittulli F, et al. Gonadotropin releasing hormone receptor expression in primary breast cancer: Comparison of immunohistochemical, radioligand and Western blot analyses. *Oncology Reports*. 2002;9:1127-32.
157. Schneeweiss A, Denkert C, Fasching PA, Fremd C, Gluz O, Kolberg-Liedtke C, et al. Diagnosis and Therapy of Triple-Negative Breast Cancer (TNBC) - Recommendations for Daily Routine Practice. *Geburtshilfe und Frauenheilkunde*. 2019;79(6):605-17.
158. Du Bois A, Schmalfeldt B, Meier W, Sehouli J, Pfisterer J. Arbeitsgemeinschaft Gynäkologische Onkologie (AGO); Kommission OVAR; AGO Study Group Ovarian Cancer (AGO-OVAR); Norddeutsche Gesellschaft für Gynäkologische Onkologie (NOGGO)(2006) Ovarian cancer–can intraperitoneal therapy be regarded as new standard in Germany. *International Journal of Gynecological Cancer : Official Journal of the International Gynecological Cancer Society*. 2006;6(5):1756-60.
159. Fost C, Duwe F, Hellriegel M, Schweyer S, Emons G, Grundker C. Targeted chemotherapy for triple-negative breast cancers via LHRH receptor. *Oncology Reports*. 2011;25(5):1481-7.
160. Schubert A, Hawighorst T, Emons G, Grundker C. Agonists and antagonists of GnRH-I and -II reduce metastasis formation by triple-negative human breast cancer cells in vivo. *Breast Cancer Research and Treatment*. 2011;130(3):783-90.
161. Li C, Zhen G, Chai Y, Xie L, Crane JL, Farber E, et al. RhoA determines lineage fate of mesenchymal stem cells by modulating CTGF–VEGF complex in extracellular matrix. *Nature Communications*. 2016;7:11455.
162. Ren W, Sun X, Wang K, Feng H, Liu Y, Fei C, et al. BMP9 inhibits the bone metastasis of breast cancer cells by downregulating CCN2 (connective tissue growth factor, CTGF) expression. *Molecular Biology Reports*. 2014;41(3):1373-83.
163. Shinde A, Libring S, Alpsoy A, Abdullah A, Schaber JA, Solorio L, et al. Autocrine Fibronectin Inhibits Breast Cancer Metastasis. *Molecular Cancer Research*. 2018;16(10):1579.
164. Abduljauwad SN, Ahmed H-u-R. Enhancing cancer cell adhesion with clay nanoparticles for countering metastasis. *Scientific Reports*. 2019;9(1):5935.
165. Wang X, McLennan SV, Allen TJ, Twigg SM. Regulation of pro-inflammatory and pro-fibrotic factors by CCN2/CTGF in H9c2 cardiomyocytes. *Journal of Cell Communication and Signaling*. 2010;4(1):15-23.
166. Hou C-H, Yang R-s, Tsao Y-T. Connective tissue growth factor stimulates osteosarcoma cell migration and induces osteosarcoma metastasis by upregulating VCAM-1 expression. *Biochemical Pharmacology*. 2018;155:71-81.
167. Lu X, Mu E, Wei Y, Riethdorf S, Yang Q, Yuan M, et al. VCAM-1 Promotes Osteolytic Expansion of Indolent Bone Micrometastasis of Breast Cancer by Engaging α4β1-Positive Osteoclast Progenitors. *Cancer Cell*. 2011;20(6):701-14.

168. Chen P-S, Wang M-Y, Wu S-N, Su J-L, Hong C-C, Chuang S-E, et al. CTGF enhances the motility of breast cancer cells via an integrin-αvβ3–ERK1/2-dependent S100A4-upregulated pathway. *Journal of Cell Science*. 2007;120(12):2053-65.
169. Rossow L, Veitl S, Vorlová S, Wax JK, Kuhn AE, Maltzahn V, et al. LOX-catalyzed collagen stabilization is a proximal cause for intrinsic resistance to chemotherapy. *Oncogene*. 2018;37(36):4921-40.
170. Dhasarathy A, Phadke D, Mav D, Shah RR, Wade PA. The Transcription Factors Snail and Slug Activate the Transforming Growth Factor-Beta Signaling Pathway in Breast Cancer. *PLoS One*. 2011;6(10):e26514.
171. Louderbough JMV, Schroeder JA. Understanding the Dual Nature of CD44 in Breast Cancer Progression. *Molecular Cancer Research*. 2011;9(12):1573.
172. Chlenski A, Guerrero LJ, Yang Q, Tian Y, Peddinti R, Salwen HR, et al. SPARC enhances tumor stroma formation and prevents fibroblast activation. *Oncogene*. 2007;26:4513.
173. Ma J, Lu W, Chen D, Xu B, Li Y. Role of Wnt Co-receptor LRP6 in Triple Negative Breast Cancer Cell Migration and Invasion. *Journal of Cellular Biochemistry*. 2017.
174. Wang JC, Sonnylal S, Arnett FC, De Crombrugghe B, Zhou X. Attenuation of expression of extracellular matrix genes with siRNAs to Sparc and Ctgf in skin fibroblasts of CTGF transgenic mice. *Int J Immunopathol Pharmacol.* 2011;24(3):595-601.
175. Aguilar-Rojas A, Huerta-Reyes M, Maya-Nunez G, Arechavaleta-Velasco F, Conn PM, Ulloa-Aguirre A, et al. Gonadotropin-releasing hormone receptor activates GTPase RhoA and inhibits cell invasion in the breast cancer cell line MDA-MB-231. *BMC Cancer*. 2012;12:550.
176. Sullivan RJ, Infante JR, Janku F, Wong DJL, Sosman JA, Keedy V, et al. First-in-Class ERK1/2 Inhibitor Ulixertinib (BVD-523) in Patients with MAPK Mutant Advanced Solid Tumors: Results of a Phase I Dose-Escalation and Expansion Study. *Cancer Discovery*. 2018;8(2):184.
177. Liu F, Yang X, Geng M, Huang M. Targeting ERK, an Achilles' Heel of the MAPK pathway, in cancer therapy. *Acta Pharmaceutica Sinica B*. 2018;8(4):552-62.
178. Perrone F, De Laurentiis M, de Placido S, Orditura M, Cinieri S, Riccardi F, et al. The HOBOE-2 multicenter randomized phase III trial in premenopausal patients with hormone-receptor positive early breast cancer comparing triptorelin plus either tamoxifen or letrozole or letrozole + zoledronic acid. *Annals of Oncology*. 2018;29.
179. Chatterjee S, Burns TF. Targeting Heat Shock Proteins in Cancer: A Promising Therapeutic Approach. *International Journal of Molecular Sciences*. 2017;18(9):1978.
180. Neckers L, Workman P. Hsp90 molecular chaperone inhibitors: are we there yet? *Clinical Cancer Research : an Official Journal of the American Association for Cancer Research*. 2012;18(1):64-76.
181. KOGA F, KIHARA K, NECKERS L. Inhibition of Cancer Invasion and Metastasis by Targeting the Molecular Chaperone Heat-shock Protein 90. *Anticancer Research*. 2009;29(3):797-807.
182. Huntoon CJ, Nye MD, Geng L, Peterson KL, Flatten KS, Haluska P, et al. Heat Shock Protein 90 Inhibition Depletes LATS1 and LATS2, Two Regulators of the Mammalian Hippo Tumor Suppressor Pathway. *Cancer Research*. 2010;70(21):8642-50.
183. Wang H, Lu M, Yao M, Zhu W. Effects of treatment with an Hsp90 inhibitor in tumors based on 15 phase II clinical trials. *Mol Clin Oncol*. 2016;5(3):326-34.
184. Jhaveri K, Chandarlapaty S, Lake D, Gilewski T, Robson M, Goldfarb S, et al. A Phase II Open-Label Study of Ganetespib, a Novel Heat Shock Protein 90 Inhibitor for Patients With Metastatic Breast Cancer. *Clinical Breast Cancer*. 2014;14(3):154-60.
185. Modi S, Stopeck A, Linden H, Solit D, Chandarlapaty S, Rosen N, et al. HSP90 Inhibition Is Effective in Breast Cancer: A Phase II Trial of Tanespimycin (17-AAG) Plus

Trastuzumab in Patients with HER2-Positive Metastatic Breast Cancer Progressing on Trastuzumab. *Clinical Cancer Research*. 2011;17(15):5132-9.
186. Vinci M, Box C, Eccles SA. Three-dimensional (3D) tumor spheroid invasion assay. *Journal of Visualized Experiments : JoVE*. 2015(99):e52686.
187. Zhang Y, Bilbao A, Bruderer T, Luban J, Strambio-De-Castillia C, Lisacek F, et al. The Use of Variable Q1 Isolation Windows Improves Selectivity in LC–SWATH–MS Acquisition. *Journal of Proteome Research*. 2015;14(10):4359-71.
188. Lambert J-P, Ivosev G, Couzens AL, Larsen B, Taipale M, Lin Z-Y, et al. Mapping differential interactomes by affinity purification coupled with data-independent mass spectrometry acquisition. *Nature Methods*. 2013;10:1239.
189. Ge SX, Jung D. ShinyGO: a graphical enrichment tool for ani-mals and plants. *bioRxiv*. 2018:315150.
190. Goldman M, Craft B, Hastie M, Repečka K, Kamath A, McDade F, et al. The UCSC Xena platform for public and private cancer genomics data visualization and interpretation. *bioRxiv*. 2019:326470.
191. Chun-Han Hou F-LL, Sheng-Mon Hou and Ju-Fang Liu. Cyr61 promotes epithelial-mesenchymal transitionand tumor metastasis of osteosarcoma byRaf-1/MEK/ERK/Elk-1/TWIST-1 signaling pathway. *Molecular Cancer*. 2014;13(1):13.
192. Haque I, Mehta S, Majumder M, Dhar K, De A, McGregor D, et al. Cyr61/CCN1 signaling is critical for epithelial-mesenchymal transition and stemness and promotes pancreatic carcinogenesis. *Molecular Cancer*. 2011;10:8.
193. Coleman RE. Metastatic bone disease: clinical features, pathophysiology and treatment strategies. *Cancer Treatment Reviews*. 2001;27(3):165-76.
194. Chen A, Wang L, Li BY, Sherman J, Ryu JE, Hamamura K, et al. Reduction in Migratory Phenotype in a Metastasized Breast Cancer Cell Line via Downregulation of S100A4 and GRM3. *Scientific Reports*. 2017;7(1):3459.
195. Ning Q, Li F, Wang L, Li H, Yao Y, Hu T, et al. S100A4 amplifies TGF-β-induced epithelial–mesenchymal transition in a pleural mesothelial cell line. *Journal of Investigative Medicine*. 2018;66(2):334-9.
196. Li F, Shi J, Xu Z, Yao X, Mou T, Yu J, et al. S100A4-MYH9 Axis Promote Migration and Invasion of Gastric Cancer Cells by Inducing TGF-beta-Mediated Epithelial-Mesenchymal Transition. *Journal of Cancer*. 2018;9(21):3839-49.
197. Boopathy GTK, Hong W. Role of Hippo Pathway-YAP/TAZ Signaling in Angiogenesis. *Front Cell Dev Biol*. 2019;7(49).
198. Halder G, Johnson RL. Hippo signaling: growth control and beyond. *Development*. 2011;138(1):9-22.
199. Pan D. The Hippo Signaling Pathway in Development and Cancer. *Developmental Cell*. 2010;19(4):491-505.
200. Warren JSA, Xiao Y, Lamar JM. YAP/TAZ Activation as a Target for Treating Metastatic Cancer. *Cancers*. 2018;10(4).
201. You B, Yang Y-L, Xu Z, Dai Y, Liu S, Mao J-H, et al. Inhibition of ERK1/2 down-regulates the Hippo/YAP signaling pathway in human NSCLC cells. *Oncotarget*. 2015;6(6).
202. Xie JJ, Xu LY, Wu ZY, Li LY, Xu XE, Wu JY, et al. Expression of cysteine-rich 61 is correlated with poor prognosis in patients with esophageal squamous cell carcinoma. *European Journal of Surgical Oncology (EJSO)*. 2011;37(8):669-74.
203. Mayer S, Gabriel B, Erbes T, Timme-Bronsert S, Jager M, Rucker G, et al. Cyr61 Expression Pattern and Association with Clinicopathological Factors in Patients with Cervical Cancer. *Anticancer Research*. 2017;37(5):2451-6.
204. Haddad T, Qin R, Lupu R, Satele D, Eadens M, Goetz MP, et al. A phase I study of cilengitide and paclitaxel in patients with advanced solid tumors. *Cancer Chemotherapy and Pharmacology*. 2017;79(6):1221-7.

205. Stewart RL, Carpenter BL, West DS, Knifley T, Liu L, Wang C, et al. S100A4 drives non-small cell lung cancer invasion, associates with poor prognosis, and is effectively targeted by the FDA-approved anti-helminthic agent niclosamide. *Oncotarget*. 2016;7(23).
206. Li C-L, Yang D, Cao X, Wang F, Hong D-Y, Wang J, et al. Fibronectin induces epithelial-mesenchymal transition in human breast cancer MCF-7 cells via activation of calpain. *Oncology Letters*. 2017;13(5):3889-95.
207. Singer CF, Kronsteiner N, Marton E, Kubista M, Cullen KJ, Hirtenlehner K, et al. MMP-2 and MMP-9 Expression in Breast Cancer-Derived Human Fibroblasts is Differentially Regulated by Stromal-Epithelial Interactions. *Breast Cancer Research and Treatment.* 2002;72(1):69-77.
208. Bleau A-M, Planque N, Perbal B. CCN proteins and cancer: two to tango. *Frontiers in Bioscience : a Journal and Virtual Library*. 2005;10:998-1009.
209. Menendez JA, Vellon L, Mehmi I, Teng PK, Griggs DW, Lupu R. A novel CYR61-triggered 'CYR61-αvβ3 integrin loop' regulates breast cancer cell survival and chemosensitivity through activation of ERK1/ERK2 MAPK signaling pathway. *Oncogene.* 2005;24(5):761-79.
210. Menendez JA, Mehmi I, Griggs DW, Lupu R. The angiogenic factor CYR61 in breast cancer: molecular pathology and therapeutic perspectives. *Endocrine-related Cancer*. 2003;10(2):141-52.
211. Kok SH, Chang HH, Tsai JY, Hung HC, Lin CY, Chiang CP, et al. Expression of Cyr61 (CCN1) in human oral squamous cell carcinoma: An independent marker for poor prognosis. *Head & Neck*. 2010;32(12):1665-73.
212. Chen Q, Zhang Xiang HF, Massagué J. Macrophage Binding to Receptor VCAM-1 Transmits Survival Signals in Breast Cancer Cells that Invade the Lungs. *Cancer Cell*. 2011;20(4):538-49.
213. Schneider JG, Amend SR, Weilbaecher KN. Integrins and bone metastasis: integrating tumor cell and stromal cell interactions. *Bone*. 2011;48(1):54-65.
214. Ye X, Brabletz T, Kang Y, Longmore GD, Nieto MA, Stanger BZ, et al. Upholding a role for EMT in breast cancer metastasis. *Nature*. 2017;547(7661):E1-E3.
215. Bradshaw AD. The role of SPARC in extracellular matrix assembly. *Journal of Cell Communication and Signaling*. 2009;3(3-4):239-46.
216. Bao H-R, Liu X-J, Li Y-L, Men X, Zeng X-L. Sinomenine attenuates airway inflammation and remodeling in a mouse model of asthma. *Molecular Medicine Reports*. 2016;13(3):2415-22.
217. Yang WH, Kuo MYP, Liu CM, Deng YT, Chang HH, Chang JZC. Curcumin Inhibits TGFβ1-induced CCN2 via Src, JNK, and Smad3 in Gingiva. *Journal of Dental Research*. 2013;92(7):629-34.
218. Fehrholz M, Glaser K, Speer CP, Seidenspinner S, Ottensmeier B, Kunzmann S. Caffeine modulates glucocorticoid-induced expression of CTGF in lung epithelial cells and fibroblasts. *Respiratory Research*. 2017;18(1):51.
219. Mun J-H, Kim Y-M, Kim B-S, Kim J-H, Kim M-B, Ko H-C. Simvastatin inhibits transforming growth factor-β1-induced expression of type I collagen, CTGF, and α-SMA in keloid fibroblasts. *Wound Repair and Regeneration*. 2014;22(1):125-33.
220. Kondo S, Tanaka N, Kubota S, Mukudai Y, Yosimichi G, Sugahara T, et al. Novel angiogenic inhibitor DN-9693 that inhibits post-transcriptional induction of connective tissue growth factor (CTGF/CCN2) by vascular endothelial growth factor in human endothelial cells. *Molecular Cancer Therapeutics.* 2006;5(1):129.
221. Canalis E, Zanotti S, Beamer WG, Economides AN, Smerdel-Ramoya A. Connective Tissue Growth Factor Is Required for Skeletal Development and Postnatal Skeletal Homeostasis in Male Mice. *Endocrinology*. 2010;151(8):3490-501.

222. Finger EC, Cheng CF, Williams TR, Rankin EB, Bedogni B, Tachiki L, et al. CTGF is a therapeutic target for metastatic melanoma. *Oncogene*. 2014;33(9):1093-100.
223. Limonta P, Montagnani Marelli M, Mai S, Motta M, Martini L, Moretti RM. GnRH receptors in cancer: from cell biology to novel targeted therapeutic strategies. *Endocrine Reviews*. 2012;33(5):784-811.
224. Francis PA, Pagani O, Fleming GF, Walley BA, Colleoni M, Láng I, et al. Tailoring Adjuvant Endocrine Therapy for Premenopausal Breast Cancer. *New England Journal of Medicine*. 2018;379(2):122-37.
225. Troy AB. Targeted Cancer Therapy: The Next Generation of Cancer Treatment. *Current Drug Discovery Technologies*. 2015;12(1):3-20.
226. Cheng Y, Tian H. Current Development Status of MEK Inhibitors. *Molecules*. 2017;22(10).
227. Cao L, Sun PL, Yao M, Jia M, Gao H. Expression of YES-associated protein (YAP) and its clinical significance in breast cancer tissues. *Human Pathology*. 2017;68:166-74.
228. Mi W, Lin Q, Childress C, Sudol M, Robishaw J, Berlot CH, et al. Geranylgeranylation signals to the Hippo pathway for breast cancer cell proliferation and migration. *Oncogene.* 2015;34(24):3095-106.
229. Li Y, Wang S, Wei X, Zhang S, Song Z, Chen X, et al. Role of inhibitor of yes-associated protein 1 in triple-negative breast cancer with taxol-based chemoresistance. *Cancer Science*. 2019;110(2):561-7.
230. Di Agostino S, Sorrentino G, Ingallina E, Valenti F, Ferraiuolo M, Bicciato S, et al. YAP enhances the pro-proliferative transcriptional activity of mutant p53 proteins. *EMBO Reports*. 2016;17(2):188-201.
231. Streicher C, Heyny A, Andrukhova O, Haigl B, Slavic S, Schüler C, et al. Estrogen Regulates Bone Turnover by Targeting RANKL Expression in Bone Lining Cells. *Scientific Reports*. 2017;7(1):6460.
232. Gnant M, Mlineritsch B, Stoeger H, Luschin-Ebengreuth G, Knauer M, Moik M, et al. Zoledronic acid combined with adjuvant endocrine therapy of tamoxifen versus anastrozol plus ovarian function suppression in premenopausal early breast cancer: final analysis of the Austrian Breast and Colorectal Cancer Study Group Trial 12. *Annals of Oncology*. 2014;26(2):313-20.

7. APPENDIX

7.1. LIST OF ABBREVIATIONS

%	percentage
µg	microgram
µL	microliter
µM	micro molar
BRAF	B-Raf Proto-Oncogene, Serine/Threonine Kinase
BRCA	Breast Cancer 1, early onset
CCN	CYR61, CTGF, NOV protein family
CD44	CD44 molecule (Indian Blood Group)
CTGF	Connective Tissue Growth Factor
CXCL12	C-X-C Motif Chemokine Ligand 12
CXCR4	C-X-C Motif Chemokine Receptor 4
CYR61	Cysteine- Rich Angiogenic Inducer 61
DCIS	ductal carcinoma *in situ*
DFS	distant-metastasis free survival
ECM	extracellular matrix
EMT	epithelial-mesenchymal transition
ER	estrogen receptor
ErbB2	Erb-B2 Receptors Tyrosine Kinase 2
ErbB3	Erb-B2 Receptors Tyrosine Kinase 3
ERK1/2	Extracellular Signaling Related Kinase 1 / 2
ESR1	Estrogen Receptor 1

ETS1	ETS proto-oncogene 1
FN1	Fibronectin 1
GnRH	Gonadotropin Releasing Hormone
GnRH-R	Gonadotropin Releasing Hormone Receptor
GPER	G-protein coupled estrogen receptor 1
GRB7	Growth Factor Receptor Bound Protein 7
HER2	Erb-B2 Receptors Tyrosine Kinase 2
HSPGs	Heparan Sulfate Proteoglycans
IDC	invasive ductal carcinoma
IHC	immunohistochemistry
ILC	invasive lobular carcinoma
IM	immunomodulatory
Ki-67	proliferation marker in clinical practice
LAR	Luminal Androgen Receptor
LATS1/2	Large Tumor Suppressor Kinase 1/2
LOX	Lysyl Oxidase
LRPs	Low-Density Receptor Related Protein
M	mesenchymal
MAP3K1	Mitogen-Activated Protein Kinase Kinase Kinase 1
MEK	Mitogen-Activated Protein Kinase Kinase 1
MET	mesenchymal-epithelial transition
MMP2	Matrix Metallopeptidase 2
MSL	mesenchymal/stem-like

MYC	MYC Proto-Oncogene
NOV	Nephroblastoma Overexpressed
PI3KCA	Phosphatidylinositol-4, 5-Bisphosphate-3 Kinase Catalytic Subunit α
PR	progesterone receptor
RFS	remission-free survival
SDC4	Syndecan 4
SNAI1	Snail Family Transcriptional Repressor 1
SNAI2	Snail family transcriptional repressor 2
SPARC	Secreted protein acidic and cysteine rich
TAZ	Transcriptional Coactivator with PDZ-Binding Motif
TEAD	Transcriptional Enhancer Factor TEF-1
TGFβ	Transforming growth factor β
TGFBI	Transforming Growth Factor Beta Induced
TME	tumor micro environment
TNBC	triple negative breast cancer
TN-C	Tenascin C
TOP2A	DNA Topoisomerase II α
TP53	Tumor-Suppressor P53
TSP-1	Thrombospondine 1
VCAM-1	Vascular Cell Adhesion Molecule 1
VEGF	Vascular Endothelial Growth Factor
VWC	Von Willebrand Factor Type C
WISP	WNT1-Inducible-Signaling Pathway Protein

YAP	Yes Associated Protein
Zeb1	Zinc finger E box binding home box 1

7.2. LIST OF FIGURES

8. PUBLICATIONS

Hellinger, J.W., Schömel, F., Lenz, C., Bauerschmitz, G., Emons, G. & Gründker, C.

Identification of invasion drivers by secretome analysis: Insight into CTGF signaling. (under revision in *Communication Biology*)

Hellinger, J.W., Hüchel, S.,Goetz, L., Bauerschmitz, G., Emons, G. & Gründker, C. (2019)

Inhibition of CYR61-S100A4 axis Limitis Breast Cancer Invasion. *Front Oncol 9,* (1074). doi: 10.3389/fonc.2019.01074

Gründker, C., Läsche M., **Hellinger, J.W.**, Emons, G. (2019).

Mechanisms of metastais and cell Mobility- The Role of Metabolism. *Geburtshilfe und Frauenheilkd, 79* (2), 184-188. doi: 10.1055/a-0805-9113

Hellinger, J.W., Bauerschmitz, G., Emons, G. & Gründker, C. (2018a)

CTGF knock-out reduziert Invasivität von mesenchymal transformierten Mammakarzinomzellen. *Geburtshilfe und Frauenheilkd, 78* (10), P126. doi: 10.1055/s-0038-1671037

Hellinger, J.W., Bauerschmitz, G., Emons, G. & Gründker, C. (2018b)

Reduzierte RhoC Expression in mesenchymal tranformierten Mammakarzinomzellen durch Behandlung mit GnRH Agonist Triptorelin beeinflusst Tumorinvasivität. *Geburtshilfe und Frauenheilkd, 78* (10), P127. doi: 10.1055/s-0038-1671038

9. ACKNOWLEDEMENT

I thank Prof. Dr. Carsten Gründker and Prof. Dr. Günter Emons for the opportunity to pursue my doctoral thesis at the Laboratory of Molecular Gynecology, and Prof. Dr. Hubertus Jarry for being my supervisor.

I am grateful for the chance to be enrolled at the Göttinger Graduate Scholl of Neuroscience, Biophysics and Molecular Bioscience (GGNB) and the manifold opportunities for personal and professional continuing education offered here. I would like to thank the Deutsche Krebshilfe- Dr. Mildred Scheel Stiftung for funding this interesting and promising project, I was allowed to work on.

I would like to thank my thesis advisory committee members Prof. Dr. Heidi Hahn and Prof. Dr. Dieter Kube for the valuable discussions.

I am grateful for the support and company of the working group of Prof. Dr. Gründker. A special thanks to Prof. Carsten Gründker for his supervision and the confidence to implement my own ideas. And I thank Sonja Blume for her excellent technical assistance. I learned a lot from and enjoyed the supervision of different medical thesis projects.

I am thankful, that I had the possibility to join the lab meetings of the working group of Dr. Florian Wegwitz and for the help, support and feedback I received here.

I am grateful for the support and appreciation of my family and friends, especially from my inspiring sister and caring mom.

My heartfelt gratitude to my boyfriend Marc, who supported me, encouraged me and believed in my strength of purpose and power of endurance throughout this whole journey.